Phenomenological approach to spin fluctuations in itinerant magnets and superconductors from *ab initio* calculations

Von der Fakultät Mathematik und Physik der Universität Stuttgart
zur Erlangung der Würde eines Doktors der Naturwissenschaften
(Dr. rer. nat.) genehmigte Abhandlung

vorgelegt von

Luciano Ortenzi
aus Rom (Italien)

Hauptberichter: Prof. Dr. Ole Krogh Andersen
Mitberichter: Prof. Dr. Alejandro Muramatsu
Mitberichterin: Dr. Lilia Boeri

Tag der mündlichen Prüfung: 17. Oktober 2013

Max-Planck-Institut für Festkörperforschung

Stuttgart 2013

"Ex uno Verbo omnia et unum loquuntur omnia, et hoc est *Principium quod et loquitur nobis* (Ioann. 8, 25). Nemo sine illo intelligit, aut recte judicat. Cui omnia unam sunt et omnia ad unum trahit et omnia in uno videt potest stabilis corde esse et in Deo pacificus permanere. O veritas Deus, fac me unum tecum in caritate perpetua!"

De imitatione Christi Lib. I Cap. III, "De doctrina veritatis".

Contents

Abbreviations

DFT	density functional theory
DOS	density of states
GGA	generalized gradient approximation
LAPW	linear augmented plane wave
LDA	local density approximation
LSDA	local spin density approximation
SDW	spin-density wave
ARPES	angle-resolved photoemission spectroscopy
SQUID	superconducting quantum Interference device
BCS	Bardeen, Cooper, Schrieffer
RPA	random phase approximation
EDM	extended Drude Model
VBM	valence band maximum
SCR	self-consistent renormalization
EST	extended Stoner theory
RST	reduced Stoner theory
RBA	rigid band approximation

Introduction

The discovery of superconductivity in a Fe compound by Kamihara *et al.* [1] and the following success in improving the critical temperature T_c up to 26 K by partial chemical substitution of O with F in the antiferromagnetic metal LaOFeAs, [2, 3] aroused the interest on itinerant magnetism in connection to superconductivity. Indeed early electron-phonon calculations [4] on this compound found the electron-phonon mechanism to be inadequate for reproducing T_c. For this reason, a mechanism for superconductivity based on the exchange of antiferromagnetic spin fluctuations was proposed. [5, 6]

In contrast to the electron-phonon superconductors, for which a well defined procedure for calculating the critical temperature starting from first-principles has been established, [7–16] for spin fluctuations-mediated superconductors this is not yet the case. The reason resides in the fact that spin fluctuations are a purely electronic degree of freedom, and therefore their description requires a good approximation for the electron-electron interaction, over a large energy scale. In itinerant systems spin fluctuations affect in a crucial way also the magnetic properties since the spin susceptibility gets selfconsistently renormalized. [17] On the other hand, since in itinerant systems local correlations are usually negligible, ground-state properties such as total energies and electronic structures, in the paramagnetic state are usually well described by mean-field approximations like the

local density approximation (LDA) within the density functional theory (DFT).

As a result a completely *ab-initio* description of real materials is possible for electron-phonon superconductors and for weakly correlated metals. For itinerant magnets and spin fluctuations superconductors *ad hoc* approximations must be applied, and phenomenological models chosen.

The approach I adopted during my PhD activity, and presented in this thesis, uses the discrepancies (whenever present) between DFT calculations and the experiments in order to construct phenomenological models which explain the magnetic, superconducting and optical properties of four representative systems of superconductors and itinerant magnets. In particular I will focus my attention on the superconducting and normal state properties of the recently discovered $A\mathrm{Pt}_3\mathrm{P}$ superconductors, on the interplay between magnetism and superconductivity of hole-doped CuBiSO, on the optical properties of LaFePO and finally on the ferromagnetic-paramagnetic transition of $\mathrm{Ni}_3\mathrm{Al}$ under pressure.

In the following, I will give a brief historical overview of the two main physical phenomena investigated in the present thesis, itinerant electron magnetism and superconductivity, introducing the aspects that are of particular interest for this work.

Itinerant electron magnetism

The first attempt to explain the macroscopic magnetic properties of real materials dates back to the end of the 19th century with the experimental work done by Pierre Curie [18] and formalized by Langevin. [19] Assuming that every atom (or molecule) in a given ensemble of N atoms behaves like a "small" magnet with fixed magnetic moment $\mathbf{m}$, whose absolute value is given by $|\mathbf{m}| = m$, the interaction of the atom with an external magnetic field $\mathbf{H} = h\hat{\mathbf{z}}$ is given by $\mathbf{m}\cdot\mathbf{H} = mh\cos(\theta)$ where θ is the angle between the magnetic moment $\mathbf{m}$ and the vector $\hat{\mathbf{z}}$. The average value of the magnetization component parallel to $\hat{\mathbf{z}}$, $\langle m_z \rangle$ is given by the integral over the solid angle Ω of $m\cos(\theta)$ times the Boltzmann factor $e^{\frac{mh\cos(\theta)}{k_B T}}$,

where k_B is the Boltzmann constant and T is the temperature. Dividing $\langle m_z \rangle$ by h and sending h to zero, Langevin [19] reproduced the experimental data for the magnetic susceptibility χ measured by Curie [18] obtaining the following formula:

$$\chi^{-1} = 3k_B T/Nm^2 = T/C$$

where C is the Curie constant. Afterwards Weiss [20] considered the interactions among the atomic magnetic moments as an additional contribution $\tilde{h} = \Gamma m$ to the external field, proportional by the factor Γ to the magnetization m. This is the so-called Weiss *mean field*. [20] In this way he obtained a self-consistent equation for the magnetization and a slightly modified form for the susceptibility:

$$\chi^{-1} = (T - T_c)/C.$$

This is the Curie-Weiss law for the uniform susceptibility and it is obeyed by almost all ferromagnets. The quantity $T_c = m^2\Gamma/3k_B$ is the Curie temperature. Despite the success of the theory in explaining the temperature dependence of χ and m, the phenomenological assumption of atomic magnetic moment was hard to justify. Indeed van Leeuwen [21] demonstrated the impossibility for a system to have constant magnetization within classical statistical mechanics. Since in classical electromagnetism every magnetic moment is associated with a moving charged particle, assuming "pre-formed" magnetic moments and then averaging over the solid angle corresponds to integrating over all the phase space with a particular condition. The assumption is that some relevant part of the energy associated with the degrees of freedom of the charged particles remains finite (even constant) while the coordinates go to infinity. This restriction is not justified in classical mechanics, but it is natural in quantum mechanics which assumes discrete occupation numbers for the degrees of freedom of the charged particles. [22]

In quantum mechanics, [22] at low temperature, the atoms can actually be regarded as having quantized and fixed magnetic moment and the electrons in the atoms are governed by the Hund's rules coupling. [23] The states with largest total spin quantum number S have the lowest energy and, among these states, the state

with the largest orbital quantum number L has the lowest energy. The result by Heitler and London on the H_2 molecule gave also a quantum mechanical origin to the Weiss molecular field. [24] The two electrons in this molecule interact via the Coulomb integral which is the quantum mechanical equivalent of the Coulomb energy for two charged particles, plus a term which has no classical analog and takes into account the fermionic nature of electrons. The latter is the exchange integral J defined as the energy difference between the triplet and singlet configuration. If J is positive, the spins align with respect to each other and the field felt by a spin is the magnetic moment of the nearby electron plus the external field. If J is negative the second electron screens the external field being antiparallel to the first one. In the ground state of the H_2 molecule J is negative and the electrons are in the singlet state. Heisenberg pointed out that for some critical value of the interatomic distance, the sign of J changes leading to the triplet state.

These concepts led to the first quantum mechanical model for ferromagnetism: the Heisenberg model. [25] This model describes spins sitting on a lattice in d dimensions interacting via the exchange mechanism. The exchange integral is shown to be directly connected to the Weiss field. The Heisenberg model, depending on the value of J, can describe both ferromagnetism and antiferromagnetism and describes a new kind of elementary excitations emerging at finite temperature called **magnons**. The most simplified version of the Heisenberg model is the Ising model [26] which considered only spin 1/2 electrons with spins collinear to a given direction $\hat{\mathbf{z}}$. The first microscopically description of antiferromagnetism was done by Néel [27] who considered two sublattices where an electron on one sublattice interacts both with spins on the same sublattice and spins sitting on the other sublattices.

All the models briefly reviewed up to now suppose the existence of well defined local moment given by local spins or angular momenta. This physical picture is realized in free atoms and molecules or in highly localized f electrons in solids.

In this thesis however I will treat metallic systems where electrons come from the d shell (Cu, Ni, Fe, Pt) and may be hybridized with s or p electrons. In these systems the measured magnetic moment are not integer numbers, *i.e.* they are *quenched*.

A classical example of "quenched" magnetic moment is the experimental value of the magnetic moment of bcc Fe $m_{\mathrm{Fe}} = 2.2\mu_B$. For these systems an itinerant model must be considered. A big step towards an itinerant electron theory of magnetism was given by the band model of Bloch. [28] In this model indeed the relevant quantum numbers are the quasi-momentum $\mathbf{k}$ and the spin σ of the electrons. For free electrons Pauli derived a formula for the susceptibility which appears to be proportional to the density of states at the Fermi level N_0. The idea of the metallic state described as a gas of free electrons was developed by Slater, [29, 30] Mott, [31] and finally by Stoner. [32, 33] He derived a model where the electrons are defined by energy bands and the disproportion between spin up and spin down is created in the reciprocal space (k-space) and not in real space. Under the effect of an external magnetic field the spin up and spin down bands split by a quantity Δ which is equivalent to the Weiss field. This model explains non integer magnetic moment in terms of the filling of d bands interacting with the s or p electrons. The paramagnetic susceptibility is enhanced with respect to the Pauli (non interacting) one by the factor $\Sigma = (1 - N_0 I)^{-1}$ where I is the Stoner parameter which is the analog of the exchange integral J.[1] The Stoner enhancement factor Σ allows to extract a microscopic criterion for ferromagnetism. If $\Sigma < 0$ indeed, the susceptibility is negative and the paramagnetic state is a maximum of the energy.

In order to clarify the role of the exchange parameter and the one of the exchange potential in metallic systems in general, many attempts were made using tight binding and Hartree-fock calculations for the free electron gas. On this subject see for example Ref. [34]. A step forward in this sense was made by Slater [35] who proposed to approximate the exchange interaction by a local potential resulting from an average over the occupied states of an homogeneous electron gas. This potential v_x depends only on the electron density n at position $\mathbf{r}$:

$$v_x(\mathbf{r}) = -3e\mathrm{e}^2 \left(\frac{3}{8\pi}\right)^{\frac{1}{3}} n^{\frac{1}{3}}(\mathbf{r}),$$

[1] The Stoner enhancement factor is usually indicated with $S^{-1} = (1-\alpha)^{-1} = (1 - N_0 I)^{-1}$. For avoiding confusion here I will refer to it as Σ, indeed I used S for indicating the total spin quantum number.

where e is the Neper number. A significant improvement to the Slater potential came by Schwarz [36] whose X_α-potential is constructed by multiplying the Slater potential for a factor α fixed by the condition that the total energy of an isolated atom must be equal to its Hartree-Fock value.

The definitive step towards the present way of treating the problem of itinerant electron magnetism was given by the development of density functional theory DFT by Hohenberg and Kohn. [37] In their original work they showed that for an interacting electron system the total energy is a unique functional of the density, and that this functional is minimum if the density is the ground state density. In a second paper Kohn and Sham [38] reformulated the problem in such a way that the total energy functional is expressed as the sum of the kinetic energy of a non interacting system plus the electron-electron interaction term plus an exchange-correlation potential v_{xc}. Minimizing the total energy functional, Kohn and Sham arrived at a set of single particle Schrödinger equations for a fictitious system having the same ground state density as the full interacting one. [39] Kohn and Sham proposed for v_{xc} a local form which depends only on the density at position $\mathbf{r}$: the so-called local density approximation (LDA). The extension to a spin polarized electron gas is called local spin density approximation (LSDA) and it is commonly used in actual DFT calculations. [40–44]

Within LSDA the Stoner parameter can be evaluated as the average over the ground state $|\,\Phi\rangle$ of the difference between the exchange-correlation potential for spin up and spin down electrons: [45]

$$\Delta = mI = \langle \Phi \mid v_{xc}^{\uparrow} - v_{xc}^{\downarrow} \mid \Phi \rangle,$$

where Δ is the Weiss mean field, m is the total magnetization and I is the Stoner parameter.

Despite their *mean field* nature, LDA and LSDA are quite successful in reproducing the ground state properties of real materials. [46] This is proved by the amount of papers which use these approximations for interpreting the ARPES or de Haas-van Alphen experimental data, or use total energy minimization for predicting

new crystal structures, or even use the LDA band structure for constructing low-energy model Hamiltonians. The reason for this was found by Gunnarsson and Lundqvist [40] who showed that these approximations satisfy the sum rule for the exchange and correlation hole.[2]

In some cases, however, non local correlations are important. Their effect becomes dramatic in systems close to a quantum critical point (QCP) which recently came back into interest. [47–49] In these circumstances the system develops spatial correlations over distances comparable with the volume of the sample. As a consequence, in itinerant systems such as FeAl, [50] Pd, [51] Ni_3Al [52] or the superconducting Fe pnictides, [53–56] LDA gives a very good description of the high temperature paramagnetic properties, but as soon as a QCP is approached, the disagreement becomes dramatic, causing a large overestimation of the tendency to magnetism. [57] The reason for this overestimation was found by Moriya: [17] the interaction of electrons with spin fluctuations is mediated by the spin susceptibility which gets self-consistently renormalized by the interaction. Such a renormalization of the susceptibility, with respect to the LSDA (mean-field) one, was observed for example in Pd, [58] $SrRu_2O_3$, [59] $Sr_2Ru_2O_4$ [60] and in $BaCo_2As_2$. [61] However up to now it was taken into account only phenomenologically. [51, 61–63]

The present relevance of this problem is due to the fact that a correct description of the magnetic properties close to a QCP can shed light on the relevant interaction channels leading to spin fluctuations-mediated superconductivity. For this reason indeed, a lot of research activity was recently dedicated to a correct description of magnetism in Fe pnictides. [64–69] In these systems LSDA gives an almost material-independent magnetic moment $\sim 2\ \mu_B$/Fe atom while the experimental magnetic moment is smaller than $1\ \mu_B$/Fe atom. [53, 54, 57, 61, 68] This can be also seen from a different point of view saying that LSDA gives good local moments but underestimates the bondlengths. [57, 70]

[2] The fact that an electron sits at position $\mathbf{r}$ automatically reduces the probability of finding another electron at point $\mathbf{r}'$. This can be seen as an interaction between an electron and its exchange-correlation hole and the interaction energy is given by the exchange-correlation energy. LDA and LSDA satisfy the sum rule according to which the pair correlation function $g(\mathbf{r}, \mathbf{r}')$ integrates to $-1 \forall \mathbf{r}$. [40]

A general argument is that fluctuations beyond *mean field* should go in the right direction by suppressing the ordered moment. Ferber *et al.* [65] have shown that it is possible to bring the LSDA magnetic moment in agreement with the experimental value, using the $LDA + U$ method [71] with a negative value of the Hubbard U parameter. However the physical interpretation of such an approach is quite questionable. The effect of dynamical fluctuations on the magnetic properties were also taken into account within LDA+DMFT by Yin *et al.* [68] and by Hansmann *et al.* [66]. These works revealed the presence of high local moment of about $\sim 2\ \mu_B$/Fe and fluctuating moment whose amplitude is strongly material dependent. The Gutzwiller [69] approximation applied on a two-dimensional eight-band Hubbard model model, [72] showed that the magnetic properties of LaOFeAs could be easily explained within a Stoner picture.

However the fluctuations considered in these kind of approaches are local, therefore adopting local correlations *à la* Hubbard for correcting an effect coming from near critical fluctuations appears hardly justified. [73] Moreover the computational load in these methods is many times larger than a normal LSDA $+U$ calculation.

In chapter 3 I will take into account near critical fluctuations by means of a phenomenological reduction of the LSDA Stoner parameter, in order to describe the superconductivity in hole-doped CuBiSO. In chapter 5 I will go towards an *ab-initio* description of this effect by including the renormalization of the susceptibility inside the LSDA functional. This method is complementary to the one adopted by Ferber *et al.* but it has a much transparent physical meaning due to its connection to Moriya's theory.

Superconductivity

A superconductor is a material which, below a critical temperature T_c, has zero electrical resistivity and behaves like a perfect diamagnet *i.e.* it expels completely the magnetic field (Meissner-Ochsenfeld effect). These effects were phenomenologically explained by Ginzburg and Landau [74] assuming the presence of a charged order

parameter which obeys a modified Schrödinger equation and is associated with a non dissipative current for $T < T_c$. Seven years later Bardeen Cooper and Schrieffer (BCS) [75] constructed a microscopic theory which explains the Meissner–Ochsenfeld effect. [76] The theory is based on the fact that a Fermi gas in the presence of an arbitrary small attractive potential is unstable against the formation of bound states with energy $E_c < E_F$ which involve electrons with opposite spin and momentum, where E_F is the Fermi energy. This fact was demonstrated for the first time by Cooper and the bound states are called *Cooper pairs*. [77] Below the critical temperature the bound states extend to the entire Brillouin zone and a gap is opened in the band dispersion.[3] Gor'kov demonstrated that the amplitude of the gap is proportional to the complex Ginzburg-Landau order parameter. [78] In the BCS theory the attractive potential mimics the effect of phonons, however no retardation effects were taken into account. Therefore the theory is valid only for values of the gap functions which are small compared with the Debye frequency.

Retardation effects were considered by Migdal and Eliashberg and Scalapino, Schrieffer and Wilkins [7, 79–81] who extended the BCS/electron-phonon theory to the case of a frequency dependent interaction parameterized by the so-called Eliashberg function which can be obtained by neutron scattering or by the inversion of the tunneling data. [10] The central concept was in this case the possibility of calculating the electronic self-energy up to an accuracy $\sqrt{m/M}$ taking into account only first order Feynman diagrams, being the parameter m/M the ratio between the electronic and ionic mass. This result is the famous Migdal theorem. [79] Since the expansion is valid for small m/M, and does not depend on the strength of the interaction, this theory is called strong coupling theory for electron-phonon superconductivity or Migdal- Eliashberg theory.

The strong coupling theory for electron-phonon superconductors turned out to be very accurate when applied to real materials. [8–11] As a consequence, this allows also to classify the superconductors into conventional and the unconven-

[3] This phenomenon is usually called condensation of the Cooper pairs, however I would like to avoid this definition since the Cooper pairs are not bosons.

tional superconductors.[4] The most famous example of conventional superconductor is magnesium diboride (MgB_2), discovered by Nagamatsu *et al.* [83] which has a superconducting critical temperature $T_c = 39$ K. This compound shows multiband superconductivity. Different electronic states couple to specific phonon modes causing the existence of multiple gaps in this material. [15, 16, 84] Evidences for this kind of pairing symmetry in MgB_2 [85] were collected from specific heat measurements, [86–88] point contact spectroscopy, [89] Raman scattering measurement, [90] angle resolved photoemission spectroscopy (ARPES) [91, 92] and magnetic susceptibility measurements. [88] The gap structure of MgB_2 calculated by Choi *et al.* is shown on the left panel of Fig. 1.

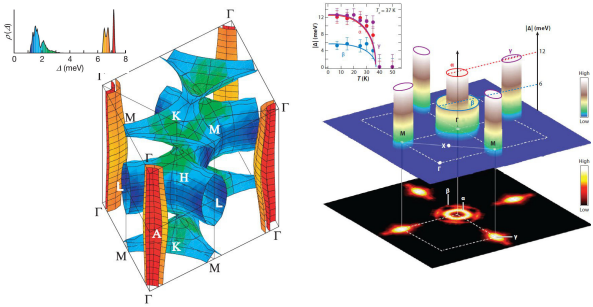

Figure 1: *Left*: Gap structure of MgB_2 as calculated from Ref. [84]. The two gaps are associated with specific phonon modes identified by the different colors.*Right*: Multigap structure of optimally doped pnictide $Ba_{0.6}$ $K_{0.4}Fe_2$ As_2 and Fermi surface as measured by angle resolved photoemission spectroscopy in Ref. [93]. The hole and electro sheets are connected by the nesting vector $\mathbf{Q} = M = (\pi, \pi, 0)$ associated with the stripe antiferromagnetic instability. The inset shows the temperature dependence of the different gaps associated with different colors.

In 1966, the same year the paper by Scalapino *et al.* [81] appeared, the effect

[4] More exactly unconventional superconductors are the ones whose order parameter has a different symmetry with respect to the $s-$wave one obtained within the BCS theory. [82]

of itinerant magnetism on strong-coupling electron-phonon superconductivity was taken into account by Berk and Schrieffer. [94] They showed that itinerant magnetism can have a detrimental effect on superconductivity, through the exchange of spin fluctuations. They treated this effect within the random phase approximation (RPA). [95] In this approximation, at finite momentum **q** a broad peak appears in the imaginary part of the susceptibility. These resonances are physical and called **paramagnons**. This effect was used to explain the absence of superconductivity in Pd and the overestimation of the critical temperature in calculations made for other transition metal compounds. [96–98]

Later on, Fay and Appel [99] made a very interesting observation: paramagnons can couple electrons with the same spin in a nearly ferromagnetic metal and lead to triplet superconductivity. In this case, the gap has *p*-wave symmetry. The possibility of having gaps with exotic symmetry (different from the *s*- wave emerging from the BCS theory) is indeed characteristic of spin fluctuations. The authors proposed this kind of pairing for superconductivity in Ni and $ZrZn_2$. However none of these compounds showed reproducible superconductivity. The electron-phonon and spin fluctuations superconductivity, having different symmetry of the order parameter, compete with each other and against the incipient ferromagnetic state, rendering these materials non superconducting.

Later on several unconventional superconductors were discovered. The list is very long and goes from the heavy fermion superconductors like $CeCu_2Si_2$, [100] $CeRhIn_5$,$CeCoIn_5$ [101, 102] UPt_3 [103] and URu_2Si_2, [104] including the $CePt_3Si$ non centrosymmetric superconductor, [105] to the strontium ruthenates. [60] In $CePt_3Si$ the large spin orbit coupling of Pt together with the lack of inversion symmetry lifts the spin degeneracy leading to exotic superconductivity. [105, 106] The importance of spin orbit coupling in Sr_2RuO_4 has also been recently considered. [107, 108]

Finally, the most famous exotic superconductors because of their critical temperature, are the cuprates (Cu oxides) discovered by Bednorz and Müller in 1986 [109] and the more recent Fe pnictides. [1] In most exotic superconductors, superconductivity emerges in the vicinity of a magnetic instability that can be ferromagnetic, [62,

110–112] antiferromagnetic, [101–105] characterized by local [113] or itinerant magnetism. [68, 114] A sketch of a representative phase diagram for heavy fermion materials, Cu-oxide superconductors and Fe-based superconductors is shown in Fig. 2.

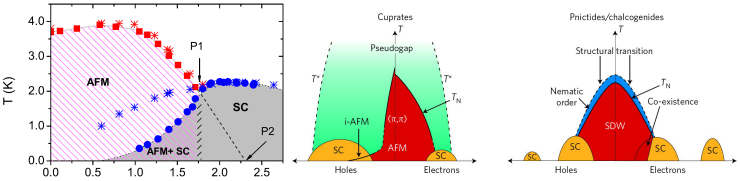

Figure 2: Phase diagram of some unconventional superconductors where superconductivity sets in at the border with antiferromagnetism. *From left to right*: Phase diagram of $CeRhIn_5$ heavy fermion compound under pressure from specific heat (filled symbols) and electrical resistivity measurements (crosses) of the superconducting T_c (blue symbols) and Néel temperature T_N (red symbols). The figure is taken from Ref. [102]. Schematic phase diagram of cuprate and Fe pnictides superconductors describing the transitions from an antiferromagnetic (AFM) or spin-density wave (SDW) state, to superconductivity (SC) with hole or electron doping. T_N is the Néel temperature, T^* is the onset of the pseudogap state (figure from Ref. [115]).

As representative of heavy fermions, the phase diagram of $CeRhIn_5$ under pressure P, extracted from specific heat and electrical resistivity measurements is shown in panel a) of the figure. At zero pressure the system shows an antiferromagnetic order whose Néel temperature T_N decreases up to a pressure P_1, where it equals the superconducting critical temperature at zero applied magnetic field and a first QCP appears. The second QCP appears at $P = P_2$. In Cu oxide superconductors the undoped compound is usually an antiferromagnetic Mott insulator. Doping with holes and electrons, superconductivity emerges and above T_c a pseudogap phase appears with an onset temperature T^* and whose origin is still controversial. For small hole doping superconductivity coexists with antiferromagnetism. In Fe pnictides the undoped system is metallic and in most cases shows antiferromagnetic stripe order *i. e.* the spins are aligned ferromagnetically in one direction of the

squared Fe plane and antiferromagnetically along the other.[5] This magnetic order is described by the vector $\mathbf{Q} = M = (\pi, \pi, 0)$ in the three dimensional Brillouin zone. For T equal or larger than the Néel temperature T_N a structural phase transition happens. Superconductivity coexists with antiferromagnetism in the hole doped part of the phase diagram and appears also for very strong doping regime.

In order to understand the nature of the superconducting state in unconventional superconductors, several experiments were done in order to extract the pairing symmetry and trace back the nature and the momentum dependence of the interaction. For heavy fermion compounds the situation is still controversial concerning both the pairing symmetry and the pairing mechanism. [116] In strontium ruthenates the spin-triplet symmetry for the order parameter, which seemed to be well established up to now, [62, 110–112] was recently questioned by scanning superconducting quantum Interference device (SQUID) microscopy [117] and ARPES experiment, [108] after being questioned by Haverkort et al. [107][6]

Up to now, the most studied family of unconventional superconductors is the one of cuprates. The SQUID microscopy was used for the first time in these materials to probe the pairing symmetry of the order parameter which was found to have $d_{x^2-y^2}$ symmetry. [119–122] The $d_{x^2-y^2}$ symmetry of the order parameter alone cannot exclude the participations of phonon in the pairing mechanism, [123] but together with the linear behavior of the resistivity above T_c [124] reduces the probability for this pairing channel to dominate.

A strong rearrangement of the states near the Fermi level below T_c leads to a resonance peak in the inelastic neutron scattering measurements in Cu oxides superconductors. [125–129] This mode was found to be compatible with the $d_{x^2-y^2}$ symmetry for the order parameter in Cu oxides superconductors. [130] The gap anisotropy in cuprates was also confirmed by ARPES measurements, [131] a technique largely employed later on to investigate the low-energy bandstructure of

[5] This is actually the most common case but there are systems where the magnetic order is different from the stripe one or even absent.

[6] For an update review about the superconductivity in strontium ruthenate compounds see for example [118]

these materials. [132]

In order to explore the nature of the bosonic mode involved in superconductivity, optical spectroscopy was also used. [133] This technique gives indeed informations on the low-energy excitations and charge dynamics in correlated materials. The degree of correlation is parameterized by an effective mass m^* and an effective scattering time τ^* which enter the Drude formula for the optical conductivity of metals. [133–135] In correlated materials, close to a Mott transitions these quantities get strongly renormalized due to local interaction. In superconductors, below the critical temperature the Drude peak disappears and a gap 2Δ (being Δ the superconducting gap) in the optical spectrum reveals the formation of the superconducting order parameter built up by the rearrangement of the states in a range 2Δ around the Fermi level. A schematic example of the change in the real part of the optical conductivity above and below T_c is shown in Fig. 3.

All the experimental techniques mentioned up to now were applied also to Fe pnictides in order to investigate the pairing mechanism and the symmetry of the order parameter. Early comparison between DFT calculations and ARPES measurements revealed the multiband nature of these materials with a Fermi surface composed by hole and electron sheets located around different points of the Brillouin zone, as shown in Fig. 1, and connected by the nesting vector $\mathbf{Q} = M$ associated with the stripe antiferromagnetic instability experimentally observed. [3, 93, 136] Given the topology of the Fermi surface, [136] the vicinity with the antiferromagnetic instability, [3] and the small value of the electron-phonon coupling constant, [4, 137] Mazin and coworkers [5] and Kuroki *et al.* [6] proposed the $s_{\pm}$ symmetry for the order parameter. This proposal has been slightly extended for taking into account the possibility of accidental nodes on the order parameter due to the different orbital character of the states involved in the pairing, [138] which could lead to $d_{x^2-y^2}$ [6] pairing symmetry.

Experimentally, multiband superconductivity in Fe pnictides was observed by early ARPES measurements [139, 140] and specific heat measurements. [141] Nodes in the order parameter were observed in LaFePO [142, 143] and were defi-

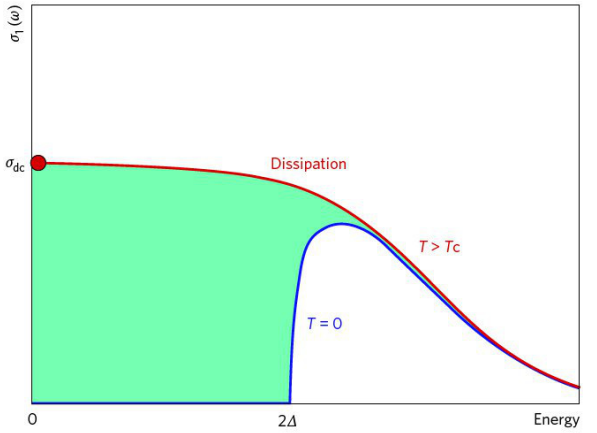

Figure 3: Schematics of the change in the real part of the optical conductivity due to the condensate formation in a superconductor. The green shaded area represents the superfluid density whose formation involves an energy scale of 2Δ around the Fermi level. The green area in $\sigma_1(\omega)$ can be estimated by $\sigma_{dc} \times 2\Delta$. [115]

nitely excluded in $NdFeAsO_{0.88}F_{0.12}$. [144] For $BaKFe_2As_2$ [145] and $BaCoFe_2As_2$ [146] the experiments are compatible with *s*-wave symmetry, while line nodes are present in $BaFe_2(As_{1-x}P_x)_2$ system. [147] Finally, a remarkable experiment by Hanaguri, *et al.* [148] showed that the Fe selenides and tellurides are most-likely $s_{\pm}$ superconductors. The gap structure of optimally doped $Ba_{0.6}$ $K_{0.4}Fe_2$ As_2 pnictide measured by Ding *et al.* is shown on the right of Fig. 1. Two larger gaps are located on the hole and electron Fermi surface sheets located respectively at Γ and M while a smaller gap is located on the second hole Fermi surface around Γ.

Concerning the spin fluctuations modes involved in superconductivity, inelastic neutron scattering (INS) experiments were also performed on pure and doped $BaFe_2As_2$ and in LaFePO samples, [149–152] shedding light on the nature and

on the energy scale of the bosonic mode involved in the coupling. A paramagnon resonance was indeed found with characteristic energy scale ω_0 evolving with temperature like $\omega_0(T) = \omega_{00}(T + \theta)$, with $\omega_{00} = 0.14 \pm 0.004$ meV/K and $\theta = 30 \pm 10$ K. This resonance broadens with temperature until it disappears above T_c. The optical properties were also widely explored in these materials, but in the following I will refer only to the works relevant for the present thesis. [153–159]

Unfortunately, despite a large theoretical effort, at the moment theory does not permit to reach the same level of precision as experiments, but only to suggest the main interaction channel. Therefore a corresponding theoretical image for the gap structure of $Ba_{0.6}$ $K_{0.4}Fe_2$ As_2 as calculated for MgB_2 and shown in Fig. 1 is not yet available. The situation is the same for heavy fermion materials, strontium ruthenates and cuprate superconductors. This is due to the complicated interplay between magnetic and orbital degrees of freedom of the electrons (and holes) involved in the superconductivity of these materials. In the following I briefly review the most common theoretical methods employed in literature.

The first thing to notice is that, like a detailed theory of electron-phonon superconductivity needs a detailed description of the phonon spectrum, an accurate description of the Fermi surface, and a well controlled approximation on the interaction kernel (like the Migdal theorem [79]), in the same way a detailed theory for spin fluctuations mediated superconductivity needs an accurate description of the spin fluctuations modes observed by neutron scattering. However this is strictly connected with the magnetic properties of the system. [17]

The spin susceptibility was first approximated within the random phase approximation. [95, 160–162] In this approximation all the ladder and bubble diagrams are summed up under the assumption that no other diagrams are relevant. The first model for superconductivity due to antiferromagnetic (zero range) correlations is the spin-bag model by Schrieffer, Wen, and Zhang. [163, 164] This model aimed to reproduce superconductivity experimentally observed by hole-doping an antiferromagnetic insulator (see the schematic phase diagram in Fig. 2). In this model, if the Coulomb repulsion U is smaller than the bandwidth W, a hole is introduced in an antiferromagnetically ordered two dimensional lattice. The hole locally suppresses

the magnetic order and consequently also the pseudogap Δ_{SDW} associated with it. This suppression forms a bag where the hole remains self-consistently trapped. Moreover if two trapped holes get close to each other an attractive potential is generated among two sharing bag holes. In the opposite limit $U \gg W$ it can be shown that a similar result is obtained. Unfortunately Schrieffer *et al.* performed calculations in the weak coupling regime, using simple model susceptibility and ignoring the details of the Fermi surface topology. This yielded to nodeless p and d-wave pairing in disagreement with the experiment. At the same time, Bickers, Scalapino, and White developed a new technique for going beyond RPA in the Bethe-Salpeter equation [165] and applied it to the Hubbard model: the so-called fluctuations exchange (FLEX) approximation.

In 1992 Monthoux and Pines pointed out that for the description of spin fluctuations-induced superconductivity it is crucial to take into account the momentum and frequency dependence of the interaction. [166, 167] Since the pairing interaction for spin fluctuations involves the spin susceptibility, this led to several efforts to model in a proper way this quantity which acts as a propagator of the collective modes seen as the boson which mediates the interaction (boson mediator).

A phenomenological model for the spin susceptibility was first proposed by Millis *et al.* [168] then by Monthoux, Balatsky, and Pines [169, 170] and finally generalized by Millis, [171] who applied a Migdal Eliashberg approach to spin fluctuations-mediated superconductivity using a model $\chi(\mathbf{q}, \omega)$. This was meant to reproduce a broadened resonance seen in neutron scattering rather than the spin waves as thought originally by Schrieffer, Wen, and Zhang. In this way Millis ascribed the origin of superconductivity in non local correlations more then in the local ones. The extreme consequence of this is represented by the spin-fermion model, [172, 173] which is a microscopic model describing the interaction of low-energy fermions with their own collective spin degrees of freedom. The latter are described by bosonic operator whose spectrum is given by the bare susceptibility $\chi_0(\mathbf{q})$ which is supposed to have the Ornstein-Zernike form. In chapter 4 I will use the Millis-Eliashberg phenomenological approach to describe the normal state properties of LaFePO. [171] For a review on the non-phonon mediated superconductivity see Ref. [174].

On the other hand the problem of correlation was also simplified by the work on the Hubbard model in infinite dimensions by Metzner and Vollhardt, [175] and Georges and Kotliar. [176] These discoveries led to dynamical mean field theory (DMFT) [177, 178] which is still one of the more successful techniques for taking into account local correlations in real materials. [177, 178] Finally, 20 years ago, concepts coming from the renormalization group approach and the formalism of functional integrals were put together by Wetterich [179] and brought to condensed matter physics by Honerkamp *et al.* [180] in such a way that a new approach to correlated systems came out: the functional renormalization group approach (f-RG). [181]

With the advent of Fe pnictides, the phenomenological Eliashberg approach as well as RPA, FLEX approximations and f-RG were combined with *ab-initio* methods (in particular, with realistic models of the electronic structure derived *ab-initio*). [182–194] Indeed, since for many of these materials correlation effects are less important than in cuprates, the bandstructure and Fermi surface obtained by means of DFT calculations was found in decent agreement with ARPES and de Haas-van Alphen measurements. Therefore the LDA or GGA band structure was considered to be a good starting point for constructing low energy models for the normal and superconducting state. [182, 183, 186, 194, 195] These works led to important informations and understanding both on the normal state properties and on the superconducting ones.

For example, this approach permitted to understand that the presence or absence of nodes in the order parameter, and the variation of T_c between different classes of compounds, was related to the changes in the electronic structure induced by the change in pnictogen height. [186, 192]

However, the DFT starting point in its common implementations (LDA and GGA), has some problems which makes it impossible to completely reproduce the experimental data or predict new superconductors. In particular the usual DFT implementations do not describe the contribution of local correlations to the magnetic and non magnetic properties and, at the same time underestimate the contribution to the local magnetic moment coming from near critical spin

fluctuations in itinerant systems. The first kind of fluctuations are well taken into account within $LDA+U$ [50] or $LDA+DMFT$ [67, 68, 196] approaches. The non local spin fluctuations should be instead accessible within DFT itself by modifying the exchange and correlation functional in an appropriate way.

The present thesis deals with electron-phonon superconductivity (chapter 2) and spin fluctuations-mediated interaction concerning the superconducting properties (chapter 3) as well as the paramagnetic (chapter 4) and magnetic ones (chapter 5) of weakly correlated electron systems. In chapter 5 a method for correcting the LSDA overestimation of the tendency to magnetism in these systems is also presented.

Investigated compounds: an overview

In the present thesis I use both *ab-initio* calculations and many-body techniques such as Migdal Eliashberg theory and random phase approximation (RPA) in order to describe the electronic, electron-phonon, magnetic and optical properties of four systems, which present interesting problems in magnetism, superconductivity and their interplay. They are the recently discovered $A\mathrm{Pt_3P}$ compounds, the hole-doped CuBiSO, superconducting LaFePO, and $\mathrm{Ni_3Al}$ itinerant ferromagnet.

The $A\mathrm{Pt_3P}$ compounds and the hole-doped CuBiSO, are recently discovered superconductors, in which the origin of superconductivity was controversial. [197–200] In APt3P compounds, an exotic pairing mechanism, standard electron-phonon coupling, and charge density waves were proposed to play a role in superconductivity. The optical properties of LaFePO seem to be experimentally dominated by the spin fluctuations dynamics, [153] however the role of interband transition was unclear. [154–157] Finally $\mathrm{Ni_3Al}$ undergoes a ferromagnetic-paramagnetic transition under pressure [201] which is qualitatively reproduced by LSDA. However, both the zero-pressure magnetic moment and the critical pressure are highly overestimated. [52]

In all these compounds, I used DFT calculations as a starting point to investigate the electronic properties, phonon density of states and electron-phonon coupling.

Indeed, DFT is usually a good starting point for understanding the low-energy properties of itinerant systems. [46] Moreover, due to the high accuracy reached in actual electron-phonon calculations, [12, 202] this technique can actually be used to "probe" the electron-phonon coupling and used, together with the experiment, to understand the physics of real materials. Spin fluctuations are taken into account phenomenologically even if in chapter 5 a new method for suppressing the magnetic moment in itinerant systems, within the LSDA functional, is discussed. In the following I briefly introduce the systems I studied in the present thesis giving the motivation of the work.

The new APt_3P superconductors

The success in synthesizing new superconductors by substituting Fe for other transition metals in pnictide superconductors, [53–56] together with the renewed interest in the effect of spin-orbit coupling on the superconductivity of Ru-based compounds, [107, 108, 117] recently led to the discovery of several superconductors based on Pt, Fe and As, [203–205] such as the 122 Pt-doped Fe pnictides. [206–208] The large spin orbit coupling in Pt might lead to unconventional superconductivity, it has been speculated. Due to the lack of local inversion symmetry, exotic superconductivity has been discussed in the hexagonal SrPtAs superconductor, for example. [209–211] On the other hand, the $ThCr_2Si_2$-type of structure, [212] of the 122 Fe pnictides recently offered interesting examples of emerging quantum criticality by isoelectronic substitution of As with P, [47–49] and doping Fe with Co, [213] or by substituting Ge with P in the $SrCo_2(Ge_{1-x}P_x)_2$ system. [214] Finally, the large spin orbit coupling of Pt in crystals without inversion symmetry like $CePt_3Si$, lifts the spin degeneracy of the states at the Fermi level leading to exotic pairing. [105, 215, 216]

In trying to synthesize the isoelectronic counterpart of the $SrPt_2As_2$ superconductor, Takayama *et al.* [197] discovered the new family of APt_3P (A = Sr, Ca, La) superconductors while the desired $SrPt_2P_2$ phase was observed only in a minimal part. [217]

The $A\mathrm{Pt_3P}$ family immediately attracted the interest of the scientific community due to their relatively high critical temperatures ($T_c = 8.4$ K in $\mathrm{SrPt_3P}$, $T_c = 6.6$ K in $\mathrm{CaPt_3P}$ and $T_c = 1.5$ K in $\mathrm{LaPt_3P}$) and to their crystal structure which is the centrosymmetric counterpart of the $\mathrm{CePt_3Si}$ one. [198, 199, 218] In the paper reporting the discovery of the $A\mathrm{Pt_3P}$'s, [197] the authors indeed suggested that the synthesis of these compounds could lead to new insight on superconductivity in non centrosymmetric crystals, by studying isoelectronic compounds both in the centrosymmetric and non centrosymmetric structural phase.

Moreover, for $\mathrm{SrPt_3P}$ a very large value of the α ratio, *i. e.* the ratio between the specific heat jump ΔC at T_c and the critical temperature, was experimentally reported and for this reason superconductivity was proposed to be of multiband character. [197] This proposal was also supported by the presence of multiple Fermi surface pockets inferred from the Hall resistivity measurements and effectively found in DFT calculations. [197, 198] Furthermore, due to the large spin orbit coupling of Pt, the possibility of unconventional superconductivity could not be a priori excluded and it was indeed proposed in Ref. [199] for $\mathrm{LaPt_3P}$.

Finally, even considering electron-phonon coupling as pairing mechanism, it was not clear why $\mathrm{SrPt_3P}$ shows a specific heat jump ΔC at T_c which is twice as large as in $\mathrm{CaPt_3P}$, an isoelectronic compound belonging to the same family and having a very similar critical temperature ($T_c = 8.4$ K in $\mathrm{SrPt_3P}$ and $T_c = 6.6$ K in $\mathrm{CaPt_3P}$). I will address these points by calculating *ab-initio* the electronic, vibrational and electron-phonon properties of these materials and show that all these findings are compatible with standard strong-coupling, single-band Midgdal Eliashberg theory of electron-phonon superconductivity. Interestingly, I will also show that it might be possible to realize the original proposal of Takayama, *et al.* [197] of synthesizing centro and non-centro symmetric variants of electronically equivalent compounds.

Superconductivity in $\mathrm{Cu_{1-x}BiSO}$

At present, the highest superconducting critical temperature ever was observed in copper oxides (highest $T_c = 153$ K in $\mathrm{HgBa_2Ca_2Cu_3O_{8+\delta}}$ at high pressures [219])

and in the Fe pnictides (highest $T_c = 56$ K in $Gd_{1-x}Th_xFeAsO$ [220] and $Sr_{1-x}Sm_xFeAsF$ [221]) superconductors. [1, 109] In particular Fe superconductors, despite the lower critical temperatures, can be synthesized in many different structures, and doped and modified in many different ways. [53–56] For example, doping can be done into the FePn planes (Pn =As,P, N, Sb), substituting Fe with other transition metals, [206, 222, 223] or the Pn atom with another pnictogen atoms, or even chalchogen. [224]

Following this track, Ubaldini and coworkers synthesized a new superconductor by substituting Fe and Pn with irespectively Cu and S in the ReOFePn (Re = rare earth) structure of the 1111 Fe pnictides. [225] Other experiments did not confirm superconductivity, [226, 227] on the contrary, optical conductivity measurements found CuBiSO to be an insulator with a band gap of ~ 1.1 eV. [226] Superconductivity in CuBiSO, was indeed found by doping with holes *i. e.* introducing vacancies into the Cu planes. The nominal doping level was $\sim 10\%$ but the sample was rather dirty. [225] Hole-doped CuBiSO has a relatively high $T_c = 5.8$ K (in LaFePO, the first Fe-based superconductor discovered, $T_c = 7$ K [1]). For this material early calculations by Mazin [200] showed a weak ferromagnetic instability and for this reason spin fluctuations were proposed as the most likely pairing interaction with p-wave symmetry. However no electron-phonon calculations were done and experiment did not see any trace of magnetism. Moreover triplet p-wave superconductivity is usually characterized by a much smaller critical temperature than 5.8 K. [105, 112] CuBiSO has a bandstructure which is very similar to that of the Fe pnictides such as LaFePO, but the Fermi level is shifted up by ~ 1.5 eV due to the different electron count of Cu d^{10} with respect to Fe d^6. Therefore the Fermi level of $Cu_{0.9}$BiSO sits in a region of the bandstructure governed by a strong Cu d-S p antibonding hybridization. This is in contrast to Fe pnictides where the Fermi level sits in the non bonding region of the bandstructure dominated by the Fe d orbitals. [72] In the latter compounds this is associated also with a depression of the density of states and the nesting condition favors the stripe antiferromagnetic instability. [72] In CuBiSO the Fermi level sits on a peak of the density of states which favors the ferromagnetic instability found by Mazin. [200]

I will perform paramagnetic, spin polarized and electron-phonon calculations in

order to "probe" the magnetic and superconducting properties of CuBiSO. Afterwards I will phenomenologically take into account the effect of spin fluctuations and draw a phase diagram describing the interplay between magnetism and superconductivity in this material.

Optical spectrum of LaFePO

As shown in the schematic phase diagram of Fig. 2 superconductivity in Fe pnictides usually occurs in the vicinity of an antiferromagnetic instability. For this reason and due to the small value of the electron-phonon coupling, [4, 70, 137, 228] superconductivity is most likely driven by spin fluctuations. [5, 6] Since this kind of pairing interaction is coupled to the electronic degrees of freedom, a general procedure for obtaining the coupling constant starting from the low energy band structure has not yet been developed. Experimental techniques like infrared optical spectroscopy for probing the electronic properties are quite useful in understanding the nature of superconductivity and the strength of the interaction. [133–135]

This is done by analyzing the experimental data of the optical conductivity within the extended Drude model (EDM). In this model the electron-boson interaction is parameterized in terms of a frequency dependent renormalization of the scattering life time τ and of the effective mass m^* of the quasiparticles, which enter a modified Drude formula for the intraband optical conductivity.

Optical conductivity measurements on LaFePO analyzed using the EDM found a surprisingly large inverse time scattering rate $\tau^{-1}(\omega)$ with a significant frequency dependence. [153] This was interpreted as an indication for strong many body effects, due to a retarded interaction. However other experiments and theoretical studies based on the derivation of low-energy Hamiltonian by down-folding the LDA bandstructure, [194] agree in viewing LaFePO as a weakly correlated, compensated metal. [136, 229–231] Moreover, both the superconducting T_c and the low-energy properties of this material can be easily explained by using a frequency dependent interaction in the weak coupling regime. [195]

This discrepancy could be due to the presence of interband optical transitions in

the low-energy spectrum of LaFePO. Indeed, the underlying assumption of the EDM analysis is that coherent electronic excitations, *i. e.* optical interband transitions, are on an energy scale much larger than the width of the Drude peak.

However, in pnictides this assumption could be quite questionable as clearly indicated by the experimental ellipsometry data by Charnukha et al. [158, 159] In order to clarify the role of interband transitions on the optical spectrum of LaFePO I will calculate both the interband and the intraband optical conductivity. The former will be calculated using a low-energy model solved in the Migdal Eliashberg approximation. [195] The latter will be estimated using DFT and modeled in a phenomenological way in order to include correlation effects. My calculations clearly show that the strong frequency dependence of $\tau^{-1}(\omega)$ for LaFePO comes from the spurious contribution of low-energy interband transitions on the optical spectrum rather than from spin fluctuations retarded interaction.

Accounting for spin fluctuations suppression of magnetic properties in itinerant magnets

DFT is in principle the only way of accessing the ground state in real materials. This is due to the reformulation of the many-body problem in terms of the ground state electronic density, which is a three-dimensional variable, together with the connection with the variational principle.

However, in order to perform the calculations, some approximations must be applied, and this reduces the predictive power of the theory which, nevertheless, offers a good starting point for understanding the material properties. The most common implementations of DFT are the local (spin) density approximation -L(S)DA- and the generalized gradient approximation (GGA). The drawback of the mean-field nature of these approximations emerges in a special way when facing magnetism. In localized systems indeed LSDA and GGA underestimate the tendency to magnetism. This is due to an underestimation of the effect of correlations.

Considering for example LSDA, the superexchange mechanism for magnetism is for example not included. [232] The origin of magnetism in LSDA has indeed an itin-

erant nature as for the Stoner model. [45] On the other hand long-wavelength spin fluctuations, happening for example in near critical systems, are also not included in LSDA. In these systems indeed, the spin susceptibility gets self consistently renormalized by the interaction as suggested by Moriya, [17] and this renormalization is not taken into account in LSDA.

For correcting the underestimation of the tendency to local magnetism, the Hubbard U parameter has been efficiently included in the exchange and correlation functional in the so called LDA+U method. [50, 71]

In itinerant systems, the renormalization of the spin susceptibility has been taken into account in a phenomenological way, by reducing the static susceptibility calculated in LSDA in order to reproduce the experiments. This method has been applied for correcting the calculated magnetic properties in systems close to a quantum critical point. [51, 52, 233, 234]

Recently, the overestimation of the tendency to magnetism revealed its importance in connections to the Fe-pnictides, where this is reflected in a underestimation of the bondlengths if magnetism is suppressed. [57, 61, 64, 70]

In order to suppress the magnetic moment in pnictides, LDA+U with a negative Hubbard parameter U has been also used [65] with the argument that negative U should correct the overestimated Coulomb interaction in LDA and bring the theoretical results in agreement with the experiments, by mimicking the effect of long wavelength fluctuations. Although mimicking the effect of long wavelength fluctuations by suppressing the local ones implies non trivial physical assumptions, and the presence of an attractive local interaction is hard to justify, the fact of including the suppression of the magnetic moment and susceptibility inside the LSDA functional is a good idea. This could open the root towards a new method for accounting for spin fluctuations beyond LSDA within density functional theory, which will be actually presented in chapter 5.

A possible system for testing the method should be a nearly ferromagnetic metal close to a phase transition. Indeed, given the connection between the local spin density approximation and the Stoner theory, corrections made to the LSDA functional can be compared with modifications of the Stoner model. Moreover the

presence of a phase transition makes the effect of near critical fluctuations to be important.

The perfect candidate for such a study is the Ni_3Al itinerant ferromagnet under pressure. [201] This system, indeed undergoes a ferromagnetic paramagnetic transition and LSDA overestimates both the magnetic moment at zero pressure and the critical pressure. [52]

In order to reconcile the LSDA calculation and the experiment about the ferromagnetic-paramagnetic transition in Ni_3Al, I will apply a simple method for suppressing the tendency to magnetism within the LSDA. The method consists in scaling the spin polarized part of the exchange-correlation potential by a constant factor s. This factor mimics the effect of long wavelength fluctuations in reducing the Stoner parameter I and it is demonstrated to be the ratio between the renormalized Stoner parameter and the bare one. For this reason I call this method Reduced Stoner Theory (RST). The quantity s can be in principle calculated via the fluctuation dissipation theorem rendering the method equivalent to the self-consistent renormalization theory by Moriya. [17] In Ni_3Al, due to a peculiar scaling property of the bandstructure it is possible to obtain the pressure dependence of s *ab initio*. The obtained phase diagram gives a pressure dependent Curie temperature in good agreement with the experiment. The method is easy to implement and does not carry any additional computational load with respect to a normal spin polarized calculation.

Organization of the thesis

The following chapters describe in more details the topics mentioned above. From chapter 2 on, the properties of the investigated materials are studied in comparison with the experiment and, if necessary, the quantities calculated *ab-initio* are corrected by suitable models. This is what I called phenomenological approach from *ab-initio* calculations.

In chapter 1 a theoretical overview of magnetism and superconductivity is of-

fered. These are indeed the topics around which the whole thesis is constructed. The approaches to localized and itinerant magnetism are described together with the main approximations, their limitations and successes. A short presentation of density functional theory is included with particular attention to its connection with the Stoner model. The self-consistent renormalization theory by Moriya [17] is presented as a renormalization of the Landau functional as reported by Ref. [235]. Some recent developments of the spin fluctuations theory are also mentioned. The Ginzburg and Landau [74] phenomenological model for superconductivity is illustrated together with a short discussion on the BCS wave function and the Migdal-Eliashberg theory for strong coupling superconductors. The theory of unconventional superconductors is also briefly mentioned.

In chapter 2 I present my theoretical results on the $A\mathrm{Pt_3P}$ (A=Sr, Ca, La) compounds, recently discovered by Takayama *et al.* [197] The structural, electronic and electron-phonon properties are studied using first-principles calculations. The thermodynamical properties in the normal and superconducting states are accessed by Migdal-Eliashberg theory and compared with the experiment. Given the remarkable agreement with the experiment, some conclusive statements are possible and the classifications of this new family of electron-phonon superconductors, along the lines of Marsiglio and Carbotte is done. [236] Multiband superconductivity, [197, 198] exotic pairing, [199] and dynamical instabilities are excluded. [199] Moreover the conjecture by Takayama *et al.* about the possibility of synthesizing the $A\mathrm{Pt_3P}$ compounds in the non centrosymmetric structure of $\mathrm{CePt_3Si}$ is supported, being the energy barrier between the two structure of ~ 20 meV.

In chapter 3 the superconducting pairing mechanism of hole-doped CuBiSO is studied. In order to examine the ferromagnetic instability found in Ref. [200] the paramagnetic and ferromagnetic electronic properties of this material are calculated. The ferromagnetic instability is reproduced and is due to a peak in the density of states (DOS) which gets populated when the system is doped with holes (the stoichiometric compound is indeed a band insulator). The phonon DOS and electron-phonon coupling are then calculated and the obtained T_c is 5 times larger than the experimental one. For this reason the effect of ferromagnetic fluctuations on

superconductivity must be also considered. Through a suitable parameterization of the interacting spin susceptibility at the RPA level, and the use of an appropriate formula for T_c triplet superconductivity is also explored. The effect of fluctuations is simulated by reducing phenomenologically the LSDA Stoner parameter. Due to the uncertainty on the experimental doping level, this variable is considered in the calculations in the rigid band approximation. As a result a phase diagram is obtained, as a function of doping x and Stoner parameter I. At experimental doping the critical temperature associated with triplet, spin fluctuations-mediated, superconductivity and the one associated with singlet, spin fluctuations-suppressed, superconductivity are found to be the same.

In chapter 4 the optical properties of LaFePO are studied by calculating both the intraband and the interband contributions to optical conductivity. The former is obtained from the low-energy model of Ref. [195] while the latter is calculated *ab-initio* from DFT. After having recalled the general assumption of the extended Drude model, experimentally used for interpreting the data, [153] the low-energy model used for calculating the optical properties is described. After having shown that the intraband contribution alone does not explain the experimental data, the interband optical conductivity are calculated and their origin investigated. Afterwards the optical conductivity is modeled in order to include the intraband contribution, the interband one and the effect of local correlations, which is not included in the *ab-initio* calculations. This analysis shows that low-energy interband transitions dominate the optical spectrum of LaFePO, showing in this way the inadequacy of the EDM analysis.

In chapter 5 a simple method for suppressing the magnetic properties of itinerant systems is presented. The method aims to mimic the effect of long wavelength fluctuations in reducing the tendency to magnetism. The magnetic and paramagnetic results for Ni_3Al under pressure are presented and, consistently with previous calculations, [52] it is found that LSDA overestimates both the magnetic moment at zero pressure and the critical pressure. It is found that the paramagnetic density of states shows a particular scaling property with pressure. Afterwards it is shown that the effect of spin fluctuations on the mean field magnetic properties is to renormalize

the Stoner parameter I by a quantity $s = \tilde{I}/I$ that can be obtained by applying the fluctuation dissipation theorem. Finally the method for including s inside the exchange and correlation functional as a phenomenological factor is shown. Closing the equations for s by calculating the interacting spin susceptibility would render the method completely *ab-initio* on the same lines by the self-consistent renormalization theory by Moriya. [17] In Ni_3Al under pressure this is possible due to the scaling property of the density of states. The obtained phase diagram is in good agreement with the experiment.

Conclusions and Outlook are given at the end.

Chapter 1

Theoretical overview

In this chapter I review the basic theoretical concepts used in the whole thesis. First of all, I introduce the problem of magnetism and two viewpoints corresponding to the localized and itinerant limits. I describe these two different approaches, their main approximations, limitations and their successes. After that I shortly introduce the Density Functional Theory and the approximations used in the present thesis. In particular I show the link between the local spin density approximation and Stoner theory of magnetism. At this point the role of spin fluctuations in suppressing the tendency to magnetism in itinerant systems is elucidated by means of the Shimizu-Moriya theory and some recent developments on the theory of paramagnons is also shortly reviewed. Finally I give a very basic introduction to the theory of superconductivity. Without entering too much into the details of the formalism, I describe the most important quantities in the theory, what is the effect of electron-phonon coupling and paramagnons. In the end I shortly present an extension of the BCS theory to the case of the spin fluctuations-mediated superconductors.

1.1 Localized and itinerant electron magnetism

Despite almost two hundred years of systematic studies on magnetism, the magnetic properties of metallic systems are still an open challenge. This is due to an apparent duality of the d electrons in these systems: they are described by band theory in their ground state, while at finite temperature they show temperature dependence of the physical properties coming from the physics of local moment.

In this section I will review the most successful theories of magnetism starting from the localized model in which the spins interact in real space and continue to the Stoner model in which the electrons are described by bands, and therefore the disproportion between spin up and spin down giving rise to the magnetization takes place in reciprocal space.

1.1.1 Heisenberg model

The Heisenberg model is the first quantum mechanical formulation of the interaction between two spins leading to magnetic order. In this model, two spins sitting on a lattice in d dimensions interact with each other and with an external magnetic field $\mathbf{H}$ according to the following Hamiltonian: [25]

$$H = -\frac{1}{2}\sum_{i,j} J_{ij}\mathbf{s}_i \cdot \mathbf{s}_j - \sum_i \mathbf{H}\cdot\mathbf{s}_i \tag{1.1}$$

where the spin operator $\mathbf{s}_{i(j)}$ acts on site $i(j)$ and $J_{ij} > 0$ for ferromagnetic (FM) coupling and $J_{ij} < 0$ for antiferromagnetic (AFM) coupling. I will first focus on the FM case, and I will shortly treat the AFM one at the end of the present subsection.

Ferromagnetism

The Heisenberg model for ferromagnetism can be easily solved assuming a mean field decoupling between the spin operators $\mathbf{s}_i$ and $\mathbf{s}_j$ acting respectively on site i and on site j, *i.e.* neglecting the second order term $(\mathbf{s}_i - \langle\mathbf{s}_i\rangle)(\mathbf{s}_j - \langle\mathbf{s}_j\rangle)$ in the

product $\mathbf{s}_i \cdot \mathbf{s}_j$:

$$\mathbf{s}_i \cdot \mathbf{s}_j \simeq \mathbf{s}_i \cdot \langle \mathbf{s}_j \rangle + \langle \mathbf{s}_i \rangle \cdot \mathbf{s}_j - \langle \mathbf{s}_i \rangle \cdot \langle \mathbf{s}_j \rangle + \cancel{(\mathbf{s}_i - \langle \mathbf{s}_i \rangle)(\mathbf{s}_j - \langle \mathbf{s}_j \rangle)} \tag{1.2}$$

where $\langle\rangle$ indicates the ensamble statistical average. The **mean field decoupling** (1.2) corresponds then to neglecting the statistical fluctuation of the quantity $\mathbf{s}_i(\mathbf{s}_j)$ around its mean value. The substitution (1.2) leads to the following mean field effective Hamiltonian:

$$H_{eff} = \frac{1}{2} \sum_{i,j} J_{ij} m^2 - \sum_i \tilde{h} s_{zi} \tag{1.3}$$

where $\langle \mathbf{s}_i \rangle = m\hat{\mathbf{z}}$, $\mathbf{H} = h\hat{\mathbf{z}}$, and s_{zi} is the z component of the spin operator $\mathbf{s}_i$. The quantity

$$\tilde{h} = h + \sum_j J_{ij} m \tag{1.4}$$

is the **Weiss mean field** acting on the spin s_{zi} due to the presence of the external field and to the presence of the other $N-1$ spins. Since at this level of the mean field approximation only the z component of the spins plays a role, it is possible to introduce a simpler model where the spins have unitary value and can be only parallel or antiparallel to the external field. This is the **Ising model**, described by the following Hamiltonian:

$$H = -\frac{1}{2} \sum_{i,j} J_{ij} \sigma_i \sigma_j - \sum_i h_i \sigma_i. \tag{1.5}$$

The spin σ_i sitting on the site i gains energy h_i if it is aligned with the external field, and energy J_{ij} if it is aligned with the spin σ_j sitting on the site j. At zero temperature the system is ordered. The direction of the total magnetization is parallel to $\hat{\mathbf{z}}$ and the system remains polarized even if $h \to 0$. At finite temperature the thermal energy tends to destroy the order increasing the entropy. Solving the model in the mean field approximation leads to a selfconsistent equation for the magnetization:

$$m(T) = \tanh\left[\beta h + \beta j_0 m(T)\right], \tag{1.6}$$

where $\beta = (k_B T)^{-1}$ and k_B is the Boltzmann constant. This is the Curie-Weiss law and $N j_0 = \sum_{ij} J_{ij}$ is, by definition, N times the Fourier transform at $\mathbf{q} = \mathbf{0}$ of the coupling constant J_{ij}. [1]

Eq. (1.6) can be obtained applying the mean field decoupling (1.2) to the Ising Hamiltonian (1.5), calculating the partition function: [237]

$$Z = \sum_{\{\sigma\}} e^{-\beta H_{MF}} = \sum_{\{\sigma\}} \left\{ e^{-\beta [\frac{NJ_0 m^2}{2} - \tilde{h} \sum_i \sigma_i]} \right\} = e^{-\beta \frac{NJ_0 m^2}{2}} \prod_{i=1}^{N} \left(e^{-\beta \tilde{h}} + e^{\beta \tilde{h}} \right) =$$

$$= e^{-\beta \frac{NJ_0 m^2}{2}} \left[2\cosh(\beta h + \beta J_0 m) \right]^N , \tag{1.7}$$

then minimizing the free energy

$$\bar{F}(T,h) = -k_B T \log Z = \frac{N}{\beta} \left\{ \frac{J_0 \beta m^2}{2} - \log \left[2\cosh(\beta h + \beta J_0 m) \right] \right\}. \tag{1.8}$$

[1] Assuming translational invariance, $J_{ij} = J(\mathbf{r}_i - \mathbf{r}_j)$ and the Fourier transform of the coupling constant J_{ij} is defined as $j_{\mathbf{q}} = \frac{1}{N} \sum_i \exp^{i\mathbf{q}\cdot(\mathbf{r}_i - \mathbf{r}_j)} J_{ij}$

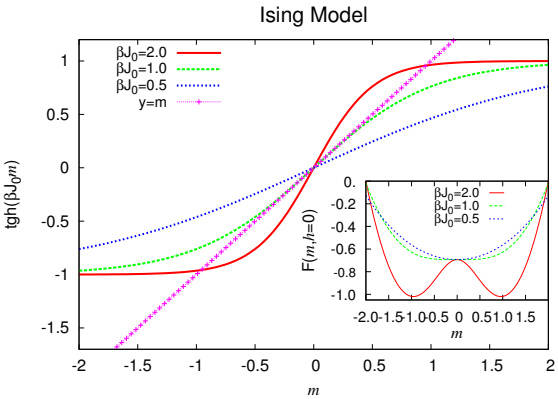

Figure 1.1: Graphical solution of the eq. (1.6). For a given temperature (corresponding to a given β), the solution is given by the intersection between the straight line $y(m) = m$ (magenta line) and the function $\Gamma(m) = \tanh(\beta J_0 m)$ (different colors). The figure shows three cases, corresponding to three possible choices of the parameter βJ_0. For $\beta J_0 < 1$ the function $\Gamma(m)$ is represented by the blue line and only the trivial solution $m = 0$ is possible. For $\beta J_0 > 1$ the function $\Gamma(m)$ is represented by the red line and the three solutions $m = 0$, $m = \pm m_0 \neq 0$ are possible. For $\beta J_0 = 1$ the three solutions collapse on the trivial one since $m_0 = 0$. *Inset*: Free energy at zero magnetic field $F(m, h = 0)$ for the Ising model for different values of temperature $k_B T = 1/\beta$. For $\beta J_0 > 1$ the function $F(m, h = 0)$ has two minima at $\pm m_0 \neq 0$ separated by a maximum at $m = 0$. For $\beta J_0 > 1$ only one minimum is present. The condition $\beta J_0 = 1$ marks the critical point where the two minima at $\pm m_0$ collapse into $m_0 = 0$.

For $h = 0$ the solution of eq. (1.6) can be graphically found by the intersection between the straight line $y = m(T)$ and the function $y' = \tanh(\beta J_0 m(T))$. From Fig. 1.1 one sees that for $\beta J_0 < 1$ y intersects y' only at the trivial solution $m(T) = 0$. This solution is associated with the paramagnetic state. For $\beta J_0 > 1$ eq. (1.6) has three intersections with y': $m(T) = \pm m_0(T)$ and $m(T) = 0$. $\beta J_0 = 1$ is the critical point which separates the regimes with three solutions from the regime with only one solution. The temperature T_c associated with $\beta_c = 1/J_0$ is the Curie temperature. The free energy (1.8) reported in the inset of Fig. 1.1 has only one minimum at $m(T) = 0$ for $T \geq T_c$ and two minima at $\pm m_0(T)$ for $T \leq T_c$. The two minima are separated by a maximum, and the energy $\bar{F}(m_0, 0)$ gives the energy necessary to rotate all the spins for inverting the magnetization (from $m(T) = m_0$ to $m(T) = -m_0$). The shape of the free energy in Fig. 1.1 it is actually quite general and it occurs whenever the system is close to a second order phase transition.

Antiferromagnetism

If $J_{ij} < 0$ the spins in (1.5) prefer to be antialigned. The Ising model can be easily solved by using a **bipartite lattice**.

Definition 1. *A bipartite lattice is a lattice which can be divided into two sublattices, called A and B, such that a site in the sublattice A is surrounded only by sites of sublattice B and vice versa.*

Assuming that the magnetization in the sublattice A is opposite to the magnetization of lattice B *i. e.* $m_A = -m_B$, one gets:

$$m_i(T) = \tanh\left[\beta h + \beta j_0 m_j(T)\right] \tag{1.9}$$

with $j = A, B$.

By means of a gaussian transformation it can be shown that the Ising model, treated at the mean field level, becomes equivalent to the Landau model for the second order phase transitions. [238]

Therefore, in the next subsection I introduce the Landau model and obtain the temperature dependence of the physical observables, like the magnetization or the susceptibility, in the vicinity of T_c. In this way I will collocate the phenomenon of ferromagnetism in the broader and more natural landscape of second order phase transitions to which also superconductivity belongs. At the same time I will also introduce a compact formalism and the concept of order parameter that will be used later on in the thesis.

1.1.2 Landau theory of second order phase transitions

The Ising model can be represented in terms of functional integrals. [238] Using this representation it can be shown that, at the mean field level, the behavior of the thermodynamic quantities close to the critical temperature, characterized by the so-called **critical exponents**, is the same as for the Landau model of second order phase transitions. [239] In this respect the Landau theory is a mean field theory in the sense of eq. (1.2) *i. e.* it neglects spatial correlations.

By means of a Legendre transformation applied to the free energy $\bar{F}(T,h)$ it is possible to introduce the **order parameter** $\phi(\mathbf{r})$ with respect to which the quantity

$$F[T,\phi] = \bar{F}(T,h) + \int d^3\mathbf{r}\ h(\mathbf{r})\phi(\mathbf{r}) = \int d^3\mathbf{r}\, f(T,\phi(\mathbf{r})) \tag{1.10}$$

is minimum. The quantity $h(\mathbf{r})$ in eq. (1.10) is the **conjugated field** to the order parameter $\phi(\mathbf{r})$. [240]

The **order parameter** for the paramagnetic-ferromagnetic transition driven by temperature is the magnetization $m(T)$ while for the antiferromagnetic case is the **staggered magnetization** $m = m_A - m_B$, where m_A and m_B are the magnetization on the two A and B sublattices. For a general second order phase transition the order parameter is defined by its properties which are repeated in the following from Ref. [240]:

(a) It may vanish above the critical point but it must be non-zero in the region just below T_c.

(b) It can approach zero continuously at $T \to T_c$, from below (for example, at zero applied field the magnetization vanishes as the temperature is raised to the Curie temperature). This condition ensures that the transition is not of the first order.

(c) Below the phase transition, the order parameter is not fully determined by the external conditions, but it can assume two or more different values under physically identical conditions. For example, at zero applied magnetic field, the magnetization may point in the plus or minus z direction with equal facility below T_c. Similarly, in the liquid - gas phase transition, the appropriate order parameter is the density minus the critical density: $\rho - \rho_c$. When the liquid is in contact with the vapor, this order parameter takes two values: positive value appropriate to the liquid phase and negative value appropriate to the gaseous phase.

From points (a) and (b), Landau supposes that near the critical temperature T_c, $\phi(\mathbf{r})$ is small, so that it is possible to expand $f(T, \phi(\mathbf{r}))$ around T_c in the following way:[2] [239]

$$f(T, \phi(\mathbf{r})) = \frac{a_2}{2}\phi^2(\mathbf{r}) + \frac{a_4}{4}\phi^4(\mathbf{r}) + \frac{c'}{2} \mid \nabla\phi(\mathbf{r}) \mid^2, \tag{1.11}$$

where a_4 is positive otherwise the transition becomes of the first order and $c' > 0$ because to curl the order parameter must cost energy. [240]

By taking now the functional derivative to the left and to the right of eq. (1.10),

[2] Actually this assumption is not valid if the order parameter is a non trivial function of $\mathbf{r}$ since the word "small" becomes meaningless. On the other hand the modern theory of critical phenomena justifies this assumption *a posteriori*. Indeed the n-order coefficient of the expansion scales with negative exponent approaching the critical point for $n \geq 6$. [237, 241]

and using eq. (1.11), the following equation of state is obtained: [3]

$$\frac{\delta F[T,\phi]}{\delta \phi(\mathbf{r})} = a_2\phi(\mathbf{r}) + a_4\phi^3(\mathbf{r}) - c'\nabla^2\phi(\mathbf{r}) = h(\mathbf{r}). \tag{1.12}$$

The homogeneous limit

In the limit of small spatial fluctuations and zero external field $h(\mathbf{r})$, the condition of minimum for $F[T,\phi]$ gives:

$$a_2 + 3a_4\phi_0^2 > 0, \tag{1.13}$$

where $\phi_0 = \lim_{h\to 0}\phi(\mathbf{r})$. Given the definition of order parameter, [240] the condition (1.13) implies that $a_2 = r_0(T - T_c)$ and

$$\phi_0 = \sqrt{\frac{-r_0(T-T_c)}{a_4}} \approx \mid T_c - T \mid^{\beta} \tag{1.14}$$

with r_0 constant and $\beta = 1/2$.

In the same limit ($c' = 0$), deriving eq. (1.12) again with respect to $\phi(\mathbf{r})$ at $h = 0$ one obtains the uniform spin susceptibility:

$$\chi_0 = \left.\frac{\partial\phi}{\partial h}\right|_{h=0} = \frac{1}{a_2 + 3a_4\phi_0^2} \begin{cases} = \frac{1}{a_2} & \text{for } T > T_c \\ = \frac{1}{-2a_2} & \text{for } T < T_c \end{cases} \tag{1.15}$$

which implies:

$$\chi_0 \approx \mid T - T_c \mid^{-\gamma} \tag{1.16}$$

with $\gamma = 1$.

For a ferromagnet eq. (1.14) describes how the spontaneous magnetization vanishes as the temperature increases, and eq. (1.16) reflects the linear behavior

[3] Eq. (1.12) is obtained by considering $F[\phi + \delta\phi] - F[\phi] = \int d^3\mathbf{r}\left[a_2\phi(\mathbf{r}) + a_4\phi^3(\mathbf{r})\right]\delta\phi + \int d^3\mathbf{r}\left(c' \mid \nabla\phi \mid \nabla\delta\phi\right)$ and integrating by part the last term. The underlying assumption is that $\delta\phi$ goes to zero at infinity, so $\int d^3\mathbf{r}\left(c' \mid \nabla\phi \mid \nabla\delta\phi\right) = c'\nabla\phi\delta\phi\Big|_{-\infty}^{+\infty} - c'\int d^3\mathbf{r}\nabla^2\phi\delta\phi = -c'\int d^3\mathbf{r}\nabla^2\phi\delta\phi$.

of the **Curie law** for the susceptibility which is found to hold in a big variety of compounds.

Approaching the transition the specific heat C, which is the second derivative of the free energy with respect to the temperature, has a jump. This is the biggest evidence that a second order phase transition is happening in the bulk. On the other hand from the analysis of the specific heat jump is possible to deduce the volume fraction of the sample involved in the transition.

From eq. (1.11) the expression of the specific heat below the transition $C = -T\frac{\partial^2 f(\phi_0)}{\partial T^2} \propto T$ can be easily obtained, while above the transition C vanishes since the order parameter vanishes as well. Therefore:

$$\Delta C(T) = C(T \to T_c^+) - C(T \to T_c^-) = \mid T - T_c \mid^{-\alpha} \tag{1.17}$$

with $\alpha = 0$.

The inhomogeneous case

Introducing now spatial fluctuations it is possible to calculate the correlation function and the correlation length. Indeed the **correlation function**: [237]

$$\Gamma(\mathbf{R}, \mathbf{R}') = \langle \phi(\mathbf{R})\phi(\mathbf{R}')\rangle - \langle \phi(\mathbf{R})\rangle\langle \phi(\mathbf{R}')\rangle \tag{1.18}$$

gives the probability of finding a given value of the order parameter at $\mathbf{R}$ given a certain value of the order parameter at $\mathbf{R}'$. In case of translational invariance, $\Gamma(\mathbf{R}, \mathbf{R}') = \Gamma(\mathbf{R} - \mathbf{R}') = \Gamma(\mathbf{r})$. The quantity $\Gamma(\mathbf{r})$ can be related to the uniform magnetic susceptibility χ by the **fluctuation dissipation theorem**[4]: [238, 242]

$$\chi = \beta \int d\mathbf{r}\Gamma(\mathbf{r}). \tag{1.19}$$

In the linear response theory, the relation $\delta\phi(\mathbf{R}) = \beta \int d^3R'\Gamma(\mathbf{R} - \mathbf{R}')\delta h(\mathbf{R}')$ holds and allows us to calculate $\Gamma(\mathbf{r})$ differentiating $h(\mathbf{r})$ in eq. (1.12) and calculating the

[4] If $h(\mathbf{R}) \to 0$ translation invariance is restored and $\Gamma(\mathbf{R}, \mathbf{R}') = \Gamma(\mathbf{R} - \mathbf{R}') = \Gamma(\mathbf{r})$.

following functional derivative:[5]

$$\frac{\delta h[\phi]}{\delta h} = \delta(\mathbf{R}' - \mathbf{R}) = \beta\Gamma(\mathbf{R}, \mathbf{R}')[a_2 + 3a_4\phi^2(\mathbf{R}) - c'\nabla^2].$$

Sending $h(\mathbf{R}) \to 0$ and doing the Fourier transformation, the **Ornstein-Zernike** form for the correlation function is obtained:

$$\Gamma(\mathbf{q}) = \frac{1/\beta}{a_2 + 3a_4\phi_0^2 + c'\mathbf{q}^2} = \frac{1}{\beta c'}\frac{1}{\xi^{-2} + \mathbf{q}^{2-\eta}} \tag{1.20}$$

with $\eta = 0$. The quantity ξ is the **correlation length** defined by the Fourier transform of eq. (1.20) in d dimensions:

$$\Gamma(\mathbf{r}) \sim |\ \mathbf{r}\ |^{2-d}\ e^{-|\mathbf{r}|/\xi} \tag{1.21}$$

that diverges close to T_c as:

$$\xi = \sqrt{\frac{c'}{a_2 + 3a_4\phi_0^2}} = \sqrt{c'\chi_0} \sim \sqrt{\frac{c'}{r_0}}\ |\ T_c - T\ |^{-\nu} \tag{1.22}$$

with $\nu = 1/2$.

This indicates that the mean-field approximation in the form of eq. (1.2) breaks down close to the critical point. In this respect, a cryterion on the applicability of the mean-field approximation involving the temperature T can be obtained by choosing $c' = 1$ and evaluating the ratio $\Gamma(\xi(T))/\phi_0^2(T) = -a_4\xi^{2-d}/a_2$, which is the ratio between the average fluctuations and the square of the mean value of the order parameter. The mean field approximation in the sense of eq. (1.2) is a good approximation as soon as this ratio is small, *i. e.* when:

$$a_4[r_0(T_c - T)]^{\frac{d-4}{2}} \ll 1. \tag{1.23}$$

[5] The result follows from the fact that

$$h(\phi + \delta\phi) - h(\phi) = a_2\delta\phi(\mathbf{R}) + 3a_4\phi^2(\mathbf{R})\delta\phi(\mathbf{R}) - c'\nabla^2\delta\phi(\mathbf{R}) =$$

$$= \int \left(a_2 + 3a_4\phi^2(\mathbf{R}') - c'\nabla^2\right)\delta\phi(\mathbf{R}')\frac{\delta h(\mathbf{R}')}{\delta h(\mathbf{R})}d\mathbf{R}'$$

Eq. (1.23) is the **Ginzburg criterion** and gives the temperature range called **critical region**, within which the mean-field approximation is applicable in terms of the microscopic parameters of the model. The exponents α, β, γ, ν and η which define the behavior of the macroscopic observables of the system close to the critical point in eqs. (1.14), (1.16), (1.17), (1.20) and (1.22) respectively, are called **critical exponents**.[6] Experimentally these quantities were found to depend only on the dimensionality of the problem d and on the number of components of the order parameter n. [240] From the theoretical point of view they also depend on the approximations made on the model and in this way they can be used for classifying also the approximations made. The critical exponents that I have obtained here are the critical exponents corresponding to d= 4 and n= 1 in the gaussian approximation for the Wilson action. [237, 238, 241] These are the values of d and n characterizing the collinear ferromagnetic transition and the liquid-gas transition. For a superconductor n=2, indeed the superconducting order parameter is a complex number characterized by an amplitude and a phase.

Up to now I treated models in which the presence of local moments was an explicit (Heisenberg and Ising model) or implicit (Landau theory) assumption. Approaching the critical point, thermal fluctuations make the local moments more and more correlated. As a consequence, the mean field approximation becomes more and more questionable up to a point where the entire system is correlated over distances comparable with the coherence length of the electrons, and the order is destroyed (created) coming from below (above) T_c.

In the next section I will introduce a model in which the formation of local moment is instead linked to a condition on the non magnetic density of states at the Fermi level.

[6] The additional critical exponent δ defines the behavior of the order parameter at $T = T_c$ as a function of the magnetic field: $\phi_0 \sim h^{1/\delta}$ with $\delta = 3$.

1.1.3 The Stoner-Wohlfarth model

The Stoner model considers electrons moving in a periodic potential $V(\mathbf{r}+\mathbf{R}) = V(\mathbf{r})$ under a uniform magnetic field $\mathbf{H} = h\hat{\mathbf{z}}$ along the $\hat{\mathbf{z}}$ direction. If $h = 0$ the energy bands are degenerate for spin up and spin down electrons, therefore the spin index in the single particle energy can be dropped. Under the effect of the magnetic field the one-particle energy $\varepsilon^n_{\mathbf{k}}$ associated with wave vector $\mathbf{k}$ in the $n-th$ band acquires spin dependency and if the additional potential due to the spin polarization of the other $N-1$ electrons (Weiss field) is $\mathbf{k}$ independent, as Stoner assumes, the spin up and spin down energy bands shift rigidly in opposite directions with respect to the Fermi level:

$$\varepsilon^n_{\mathbf{k}} \rightarrow E_{\mathbf{k}\sigma} = \varepsilon^n_{\mathbf{k}} + \sigma\frac{\Delta}{2} \tag{1.24}$$

where $\sigma = \pm 1$ is the electron spin orientation (up or down) with respect to the $\hat{\mathbf{z}}$ direction and the wave vector independent quantity Δ is defined as:

$$\Delta = Im + 2\mu_B h \tag{1.25}$$

and it is the total band splitting. The quantity m in eq. 1.25 is the total magnetization, $\mu_B = e\hbar/(2mc)$ is the Bohr magneton (being the gyromagnetic factor $g = 2.0023$) and I is the so-called **Stoner parameter**. The kinetic energy of an electron system increases with increasing magnetization, owing to splitting of the energy bands for up and down spin electrons.

The quantity Δ is equivalent to the Weiss field (1.4). In practice each electron "feels" the effect of the external magnetic field h plus the mean field Im due to the polarization of the other $N-1$ electrons.

At finite temperature T the total number of electrons and the total magnetization m are given respectively by:

$$N = \int d\varepsilon N(\varepsilon)[f(\varepsilon-\Delta) + f(\varepsilon+\Delta)] \tag{1.26}$$

and

$$m = \int d\varepsilon N(\varepsilon)[f(\varepsilon-\Delta) - f(\varepsilon+\Delta)] \tag{1.27}$$

where $N(\varepsilon)=\sum_{\mathbf{k}}\delta(E_{\mathbf{k}\sigma}-\varepsilon)$ is the paramagnetic density of states per spin, $f(\varepsilon)=1/[e^{\frac{(\varepsilon-\mu)}{k_BT}}+1]$ is the Fermi function, and μ is the chemical potential.

The free energy for such a system can be written as:[7]

$$F(T,m)=\Omega_0(\mu,T,m)+\mu N(T,m)-Im^2-hm, \tag{1.28}$$

where the grand canonical potential $\Omega_0(\mu,T,m)$ in eq. (1.28) is given by:

$$\Omega_0(\mu,T,m)=-k_BT\sum_{\sigma}\int d\varepsilon N(\varepsilon)\ln[1+e^{-\frac{(\varepsilon+\sigma\frac{\Delta}{2}-\mu)}{k_BT}}]+\Delta m \tag{1.29}$$

whose derivatives with respect to μ and Δ, given eqs. (1.26) and (1.27), are respectively: $-\partial\Omega_0/\partial\mu=N$ and $\partial\Omega_0/\partial\Delta=0$.

For small m the following expression for $F(T,m)$ can be obtained from eqs. (1.28-1.29): [17]

$$F(T,m)=F(T,0)+\left(\frac{1}{2\chi_0(T)}-I\right)\frac{m^2}{2}+g(T)\frac{m^4}{4}+\ldots-hm \tag{1.30}$$

with

$$\chi_0(T)=\frac{1}{2}N_0\left(1-\frac{\pi^2}{6}RT^2+\ldots\right)$$

and

$$g(T)=\frac{F_1}{N_0^3}\left(1+\frac{\pi^2}{6}R_1T^2+\ldots\right),$$

where the coefficients R, R_1 and F_1 depend on the density of states at the Fermi level $N(0)\equiv N_0$ and on its derivatives. [17] In the following I consider the $T=0$ limit, for which eq. (1.30) reduces to the expression:

$$F(0,m)=F(0,0)+\left(\frac{1}{N_0}-I\right)\frac{m^2}{2}+\frac{F_1}{N_0^3}\frac{m^4}{4}+\ldots-hm. \tag{1.31}$$

[7] See for example Ref. [17]

If $\alpha \equiv N_0 I > 1$ the **Stoner criterion** is realized, and if $F_1 > 0$ a finite magnetization appears also in the limit $h \to 0$:

$$m = \sqrt{-\left(\frac{1}{N_0} - I\right)\frac{N_0^3}{F_1}}. \tag{1.32}$$

If $\alpha < 1$, although ferromagnetism is not realized, the magnetic susceptibility is enhanced with respect to its Pauli value:

$$\chi = \frac{\chi_0}{1 - I\chi_0}. \tag{1.33}$$

The denominator of eq. (1.33) is called **Stoner enhancement factor**. When combined with *ab-initio* calculations, the Stoner model gives a deep insight of the zero-temperature properties of real materials. This will be shown better in the next section.

However, at finite temperature the Stoner theory turned out to be unsatisfactory. The most important disagreement with the experiments are listed below:

- The temperature dependence of the inverse magnetic susceptibility: $\chi^{-1}(T) \propto T^2 - T_c^2$ instead of $\chi^{-1}(T) \propto T$ predicted by the Curie law and experimentally observed.

- The Curie temperatures for $3d$ metals like Fe Co and Ni, calculated using realistic density of states, [45] resulted to be overestimated from 3 to 5 times with respect to the experiments.

- The low temperature dependence of the magnetization $m(0) - m(T) \propto T^2$ instead of $m(0) - m(T) \propto T^{3/2}$ experimentally observed.

These discrepancies appear because the Stoner theory does not take into account the thermal excitation of the quantum degrees of freedom such as spin density waves (SDW) and neglects quantum fluctuations beyond the Hartree Fock approximation.

Antiferromagnetism and nesting condition

The uniform non-interacting susceptibility χ_0 in (1.33), defined as the derivative of the magnetization m with respect to the uniform magnetic field h in the $m \to 0$ limit, can be generalized to the case of a non uniform magnetic field $h(\mathbf{r}) = \sum_{\mathbf{q}} h(\mathbf{q}) e^{i\mathbf{q}\cdot\mathbf{r}}$ by means of its Fourier component $\chi_0(\mathbf{q}) = \delta m(\mathbf{q})/\delta h(\mathbf{q}) \mid_{m(\mathbf{q})\to 0}$. Equation (1.33) can be then written in the following way:

$$\chi(\mathbf{q}) = \frac{\chi_0(\mathbf{q})}{1 - I(\mathbf{q})\chi_0(\mathbf{q})}. \tag{1.34}$$

Assuming translational invariance, $\chi_0(\mathbf{q})$ can be expressed as:

$$\chi_0(\mathbf{q}) = \sum_{\mathbf{k},\mu,\nu} \frac{[f(\varepsilon_{\mathbf{k},\nu}) - f(\varepsilon_{\mathbf{k}-\mathbf{q},\mu})]}{\varepsilon_{\mathbf{k}-\mathbf{q},\mu} - \varepsilon_{\mathbf{k},\nu} + i\delta} \cdot \langle \mid \mathbf{k},\nu \mid e^{i\mathbf{q}\cdot\mathbf{r}} \mid \mathbf{k}-\mathbf{q},\mu \rangle \mid^2, \tag{1.35}$$

where $\mid \mathbf{k},\nu \rangle$ is the Bloch state with band index ν, wave vector $\mathbf{k}$ and energy $\varepsilon_{\mathbf{k},\nu}$ and $f(\varepsilon_{\mathbf{k},\nu}) = 1/(e^{(\varepsilon_{\mathbf{k},\nu} - E_F)/k_B T} + 1)$ is the Fermi function. For non interacting fermions and small momentum $\mathbf{q}$, eq. (1.35) coincides with the Lindhard function and has a logarithmic divergence when $\mid \mathbf{q} \mid$ equals twice the Fermi vector k_F. Actually, Lomer [243] showed that this is the case also in three dimensions whenever the Fermi surface has portions that can be superimposed by a translation vector $\mathbf{Q}$ called **nesting vector**. This can be easily realized looking at eq. (1.35). At low temperatures indeed, if $\varepsilon_{\mathbf{k}-\mathbf{Q},\mu} \approx \varepsilon_{\mathbf{k},\nu} = E_F$ the denominator is close to zero while the numerator is close to one (it is zero if and only if $\varepsilon_{\mathbf{k},\nu} = \varepsilon_{\mathbf{k}-\mathbf{Q},\mu}$). In this case the **generalized Stoner criterion** $I(\mathbf{q})\chi_0(\mathbf{q}) \geq 1$ is fulfilled even for arbitrary small values of $I(\mathbf{q})$, and $\chi(\mathbf{Q})$ is unstable.

1.2 Density functional theory and its approximations

Up to now I analyzed the general properties of a phenomenological model (the Landau theory) and two microscopic ones without specifying the parameters involved in those models. In this section I briefly introduce density functional theory

(DFT) which gives a well defined procedure for obtaining the exact ground state of a many-body problem in terms of single particle Schrödinger equations. In the present thesis I will use this powerful tool for obtaining microscopic parameters like band mass, band dispersion and density of states.

Let us consider the Hamiltonian of N electrons moving in a time independent external potential $V_{\text{ext}}(\mathbf{r})$ (Born-Oppenheimer approximation) in Rydberg units:

$$H = T + U + V = \sum_i (-\nabla_i^2) + \sum_{i \neq j} r_{ij}^{-1} + \sum_i V_{\text{ext}}(\mathbf{r}_i), \tag{1.36}$$

The three terms in the Hamiltonian (1.36) represent respectively the kinetic energy of the electrons, the electron-electron interaction and the interaction of the electrons with an external potential which includes the electrostatic potential of the (fixed) nuclei. The ground state wave function $\Phi(\mathbf{r}_1\sigma_1, \ldots, \mathbf{r}_N\sigma_N)$ is defined by the secular equation $H\Phi(\mathbf{r}_1\sigma_1, \ldots, \mathbf{r}_N\sigma_N) = E\Phi(\mathbf{r}_1\sigma_1, \ldots, \mathbf{r}_N\sigma_N)$. Before presenting the density functional theory is useful to define the ground state density of the system represented by the Hamiltonian (1.36) as $n(\mathbf{r}) = N \sum_{\sigma_1} \sum_{\sigma_2} \ldots \int d^3r_2 \ldots \int d^3r_N \times |$ $\Phi(\mathbf{r}_1\sigma_1, \ldots, \mathbf{r}_N\sigma_N)\,|^2$ and to report here the basic lemma on which DFT hinges on: [37, 39]

Lemma 1. *The ground state density $n(\mathbf{r})$ of a bound system of interacting electrons in some external potential V_{ext} determines this potential uniquely.*

In stating the Lemma 1 additional remark are needed:

- the potential V_{ext} is uniquely determined up to a constant,
- in case of degenerate ground state the lemma refers to any density $n(\mathbf{r})$.

The proof of the lemma is easy and can be found in Refs. [37, 39].

1.2.1 Density functional theory

Density functional theory is based on the two **Hohenberg-Kohn theorems**:[8] [37]

[8] A compact and useful presentation of the following arguments can be found in Refs. [39, 46] and [244]

Theorem 1. *For any system of interacting particles in an external potential V_{ext}, for specified operators T and U in (1.36) the ground state wave function $\Phi(\mathbf{r}_1\sigma_1,\ldots,\mathbf{r}_N\sigma_N)$ is a unique functional of the ground-state electron density only.*

The proof is based on lemma 1 which states that the density uniquely specifies the external potential V_{ext} and hence the Hamiltonian, and consequently $\Phi(\mathbf{r}_1\sigma_1,\ldots,\mathbf{r}_N\sigma_N)$, too.

Since theorem 1 holds, the functional $F[n(\mathbf{r})] = \langle\Phi \mid T+U \mid \Phi\rangle$ is an universal functional valid for any external potential and any number of particles.

The second theorem states that:

Theorem 2. *The functional $E[n(\mathbf{r})] = \langle\Phi \mid T+U \mid \Phi\rangle + \int d^3r\, V_{\text{ext}}(\mathbf{r})n(\mathbf{r})$ is minimum if $n(\mathbf{r})$ is the ground state electron density. The minimum of $E[n(\mathbf{r})]$ is the ground state electron energy.*

From theorems 1 and 2 follows that once the universal functional $F[n(\mathbf{r})]$ is known, the system is specified only by the external potential $V_{\text{ext}}(\mathbf{r})$ and the ground state wave function can be found by applying the variational principle.

Unfortunately $F[n(\mathbf{r})]$ is not known and the complexity of the solution of the many-body Hamiltonian (1.36) is reflected in an accurate determination of $F[n(\mathbf{r})]$. However the density functional scheme instead of using, as a basic variable, the three-N dimensional quantity $\Phi(\mathbf{r}_1\sigma_1,\ldots,\mathbf{r}_N\sigma_N)$ uses as a basic variable the three-dimensional quantity $n(\mathbf{r})$, notably reducing the computational complexity.

What permits to compute the total energy of the interacting system (1.36) in practice, using DFT by minimizing the functional $E[n(\mathbf{r})]$, is the **Kohn-Sham scheme**. [37] Kohn and Sham showed indeed that the stationary property $\delta E[n(\mathbf{r})]/\delta n(\mathbf{r}) = 0$ could lead to a set of one particle Schrödinger equations to be solved self-consistently.

The result is obtained by considering, together with the real system (1.36), a fictitious non interacting system whose Hamiltonian is given by:

$$H' = \sum_i(-\nabla_i^2) + \sum_i v(\mathbf{r}_i). \tag{1.37}$$

The potential $v(\mathbf{r})$ in eq. (1.37) is determined in such a way that the ground-state density of the system described by (1.37) is the same as the density of the real system (1.36). Since according to lemma 1 the potential is uniquely determined by the density, the Hamiltonian (1.37) is uniquely defined by $n(\mathbf{r})$. The ground state wave function of the non interacting system (1.37) is given by the Slater determinant obtained by occupying the lowest lying one electron states labeled by $\mathbf{k}$ and defined by the Schrödinger equation:

$$[(-\nabla^2) + v(\mathbf{r})]\psi(\mathbf{k},\mathbf{r}) = \varepsilon_{\mathbf{k}}\psi(\mathbf{k},\mathbf{r}) \tag{1.38}$$

whose density is given by:

$$n(\mathbf{r}) = \sum_{\mathbf{k}} f(E_F - \varepsilon_{\mathbf{k}}) \mid \psi(\mathbf{k},\mathbf{r}) \mid^2 \tag{1.39}$$

and the potential $v(\mathbf{r})$ is determined in such a way that the density (1.39) is the ground state density of the real system:

$$v(\mathbf{r}) = 2\int d^3r' \frac{n(\mathbf{r}')}{\mid \mathbf{r}-\mathbf{r}' \mid} + V_{\text{ext}}(\mathbf{r}) + v_{\text{xc}}, \tag{1.40}$$

where v_{xc} is the unknown **exchange-correlation potential** that will be defined in the following. The Kohn-Sham scheme consists of solving eqs. (1.38)-(1.40) self-consistently. The procedure for obtaininng eq. (1.40) is the following. As first step the energy functional $E[n(\mathbf{r})]$ in theorem 2 is rewritten in the following way:

$$E[n(\mathbf{r})] \equiv \langle \Phi \mid H \mid \Phi \rangle =$$

$$= \langle \Phi' \mid T \mid \Phi' \rangle + \int\int d^3r d^3r' \frac{n(\mathbf{r})n(\mathbf{r}')}{\mid \mathbf{r}-\mathbf{r}' \mid} + E_{\text{xc}}[n(\mathbf{r})] + \int d^3r\ V_{\text{ext}}(\mathbf{r})n(\mathbf{r}). \tag{1.41}$$

In the same way the energy functional $E'[n(\mathbf{r})]$ associated with the non interacting system described by the Hamiltonian H' (1.37) is given by:

$$E'[n(\mathbf{r})] = \langle \Phi' \mid T \mid \Phi' \rangle + \int d^3r\ v(\mathbf{r})n(\mathbf{r}). \tag{1.42}$$

The term $\langle \Phi' \mid T \mid \Phi' \rangle = \sum_{\mathbf{k}} \int d^3r \ \psi^*(\mathbf{k},\mathbf{r})(-\nabla^2)\psi(\mathbf{k},\mathbf{r})$ in eqs. (1.41) and (1.42) is the kinetic energy of the non interacting system. The second term in eq. (1.41) is the Coulomb energy of the electronic charge cloud. The third term is the **exchange-correlation energy**: the difference between the true kinetic energy and that of the non-interacting system, plus the difference between the true interaction energy and that of the electronic charge cloud. This term is in principle rather small, [46] and contains all the unknown part of the information about the many-body interaction. Eq. (1.40) for $v(\mathbf{r})$ is obtained by requiring that both the interacting system (1.41) and the non interacting one (1.42), attain their respective minima for the same ground-state density $n_0(\mathbf{r})$. This leads to the condition $v(\mathbf{r}) = \frac{\delta}{\delta n(\mathbf{r})}\{E[n(\mathbf{r})] - \langle \Phi' \mid T \mid \Phi' \rangle\}$. Eq. (1.40) is obtained straightforwardly by defining the exchange and correlation potential as:

$$v_{\text{xc}} = \frac{\delta E_{\text{xc}}[n(\mathbf{r})]}{\delta n(\mathbf{r})}. \tag{1.43}$$

The total energy (1.41) and the corresponding density $n(\mathbf{r})$ obtained by applying the Kohn-Sham scheme (1.38)-(1.40) are in principle exact, while the eigenvalues of the single particle equations (1.38), the so-called Kohn-Sham eigenvalues, have no particular physical meaning. Indeed, in order to describe the quasi-particle excitations, the self-energy $\Sigma(\mathbf{r},\mathbf{r}',\varepsilon_{\mathbf{k}})$ should be used. However, since $\Sigma(\mathbf{r},\mathbf{r}',\varepsilon_{\mathbf{k}})$ is a ground state property, it can be expressed as a function of the density and, close to the Fermi level it becomes equivalent to v_{xc}. [46, 245] This grants that the obtained Fermi surface is the correct one. Several approximations exist of v_{xc} and in the following subsection I will present the ones employed in the present thesis.

1.2.2 LDA, LSDA and GGA Functionals

Local density approximation and generalized gradient approximation

For paramagnetic calculations, I will use mainly the **local density approximation** (LDA). This approximation consists of writing:

$$E_{\text{xc}}^{\text{LDA}}[n(\mathbf{r})] \approx \int d^3r \varepsilon_{xc}[n(\mathbf{r})]n(\mathbf{r}) \tag{1.44}$$

where $\varepsilon_{xc}[n]$ is the exchange-correlation energy per particle of a homogeneous electron gas with density n. [38] Kohn and Sham showed that this form of $E_{\rm xc}[n(\mathbf{r})]$ becomes exact in the limit of slowly varying density. Moreover, in contrast to the Thomas-Fermi approximation, [246, 247] the kinetic energy of the non-interacting system is treated exactly, therefore the approximation (1.44) remains good also in the limit of high density. [46]

Eq. (1.44) for $E_{\rm xc}[n(\mathbf{r})]$ leads to the following expression for the exchange-correlation potential:

$$v_{\rm xc} \approx \frac{d[n\varepsilon_{xc}(n)]}{dn} \equiv \mu_{\rm xc}[n(\mathbf{r})], \tag{1.45}$$

which is a local potential and coincides with the exchange-correlation part of the chemical potential in a homogeneous electron gas. The exchange part of the potential (1.45) is given by: [38, 41]

$$\mu_{\rm x}(n) = \frac{4}{3}\varepsilon_{\rm x}(n) = -2(3\pi^{-1}n)^{\frac{1}{3}} \tag{1.46}$$

with $n \equiv n(\mathbf{r})$.

Hedin and Lundqvist have shown that the exchange-correlation potential (1.45) may be expressed as: [42]

$$v_{\rm xc} \approx \frac{3}{2}\alpha(n)\mu_{\rm x}(n) \tag{1.47}$$

where $\alpha(n) = \frac{2}{3}$ in the high density limit (where correlation effects can be neglected) and ~ 0.85 for $(4/3\pi n)^{-1/3} \equiv r_s = 4$ (which corresponds to a value of the density typical of the interatomic region in metals).

In actual calculations the functional form of the correlation part of $v_{\rm xc}$, first estimated by Wigner, [248] is accessed via Montecarlo simulations. [249, 250] As specified earlier, LDA becomes exact in the limit of slowly varying density, the only source of error comes therefore form regions where the density varies rapidly. In order to correct this behavior, gradient corrections in $n(\mathbf{r})$ can be considered.

When gradient correction in $n(\mathbf{r})$ are taken into account in eq. (1.44) the **generalized gradient approximation** for the exchange-correlation energy is obtained:

$$E_{\rm xc}^{\rm GGA}[n(\mathbf{r}),\mid \nabla n(\mathbf{r}) \mid] \approx \int d^3 r f_{xc}[n(\mathbf{r}),\mid \nabla n(\mathbf{r}) \mid] n(\mathbf{r}) \tag{1.48}$$

In order to have access to eq. (1.44) the density $n(\mathbf{r})$ needs to be calculated, while eq. (1.48) requires to calculate independently $n(\mathbf{r})$ and its gradient $\mid \nabla n(\mathbf{r}) \mid$. In the following I will use the expression for $E_{\rm xc}^{\rm GGA}[n(\mathbf{r}),\mid \nabla n(\mathbf{r}) \mid]$ given by Perdew, Burke, and Ernzerhof. [251]

The Local spin density approximation

Although DFT can in principle lead to a spin polarized ground state, LDA cannot describe spin polarized systems since it cannot generate a spin disparity. However a rather simple generalization of eqs. (1.44) can be obtained by considering as independent variable the space-diagonal matrix element of the first-order density matrix, $n(\mathbf{r}\sigma,\mathbf{r}\sigma')$. In the following I will restrict the discussion to *collinear magnetism*, [252] therefore I assume that the quantization axis for the spin operator is fixed and the variable σ can assume only two values: $+1 \equiv \uparrow$ *parallel* or $-1 \equiv \downarrow$ *antiparallel* to the quantization axis z. As a consequence $n(\mathbf{r}\sigma,\mathbf{r}\sigma')$ can be considered as a Pauli matrix:

$$\begin{pmatrix} n_{\uparrow\uparrow}(\mathbf{r}) & n_{\uparrow\downarrow}(\mathbf{r}) \\ n_{\downarrow\uparrow}(\mathbf{r}) & n_{\downarrow\downarrow}(\mathbf{r}) \end{pmatrix} \tag{1.49}$$

and the off-diagonal elements $n_{\sigma\sigma'}(\mathbf{r})$ can be neglected. The quantity $n(\mathbf{r}\sigma,\mathbf{r}\sigma')$ is therefore expressed in terms of the electron density

$$n(\mathbf{r}) = \sum_{\sigma} n(\mathbf{r}\sigma,\mathbf{r}\sigma) = n_{\uparrow}(\mathbf{r}) + n_{\downarrow}(\mathbf{r}) \tag{1.50}$$

and spin density

$$m(\mathbf{r}) = \sum_{\sigma} \mathrm{sign}(\sigma) n(\mathbf{r}\sigma,\mathbf{r}\sigma) = n_{\uparrow}(\mathbf{r}) - n_{\downarrow}(\mathbf{r}), \tag{1.51}$$

where I used the abbreviation $n_{\sigma\sigma} \equiv n_\sigma$.

The generalization of eqs. (1.38)-(1.40) follows then as: [40]

$$\sum_{\sigma'}[(-\nabla^2) + v(\mathbf{r}\sigma, \mathbf{r}\sigma')]\psi_{\mathbf{k}}(\mathbf{r}\sigma') = \varepsilon_{\mathbf{k}}\psi_{\mathbf{k}}(\mathbf{r}\sigma) \tag{1.52}$$

$$n(\mathbf{r}\sigma, \mathbf{r}\sigma') = \sum_{\mathbf{k}} f(E_F - \varepsilon_{\mathbf{k}})\psi^*_{\mathbf{k}}(\mathbf{r}\sigma)\psi_{\mathbf{k}}(\mathbf{r}\sigma') \tag{1.53}$$

$$v(\mathbf{r}\sigma, \mathbf{r}\sigma') = 2\int d^3r' \frac{n(\mathbf{r}')}{\mid \mathbf{r} - \mathbf{r}' \mid} + V_{\text{ext}}(\mathbf{r}\sigma, \mathbf{r}\sigma') + v_{\text{xc}}[n(\mathbf{r}\sigma, \mathbf{r}\sigma')]. \tag{1.54}$$

In **local spin density approximation** (LSDA), the expression (1.44) for $E_{\text{xc}}[n(\mathbf{r})]$ is generalized in the following way: [40]

$$E_{\text{xc}}^{\text{LSDA}}[n(\mathbf{r}\sigma, \mathbf{r}\sigma')] \approx \sum_{\sigma}\int \varepsilon_{xc}[n_\uparrow(\mathbf{r}), n_\downarrow(\mathbf{r})]n(\mathbf{r}\sigma, \mathbf{r}\sigma')d^3r =$$

$$= \int \varepsilon_{xc}[n_\uparrow(\mathbf{r}), n_\downarrow(\mathbf{r})]n(\mathbf{r})d^3r, \tag{1.55}$$

where $\varepsilon_{xc}[n_\uparrow, n_\downarrow]$ is the exchange-correlation energy per electron for a homogeneous electron gas with density $n = n_\uparrow + n_\downarrow$ and spin density $m = n_\uparrow - n_\downarrow$, the latter being created by an external magnetic field. In this approximation the exchange-correlation potential is diagonal in spin:

$$\delta E_{\text{xc}}^{\text{LSDA}}[n(\mathbf{r}\sigma, \mathbf{r}\sigma')]/\delta n_{\uparrow\downarrow}(\mathbf{r}) = \delta E_{\text{xc}}^{\text{LSDA}}[n(\mathbf{r}\sigma, \mathbf{r}\sigma')]/\delta n_{\downarrow\uparrow}(\mathbf{r}) = 0$$

and

$$\frac{\delta E_{\text{xc}}^{\text{LSDA}}[n(\mathbf{r}\sigma, \mathbf{r}\sigma')]}{\delta n_\sigma(\mathbf{r})} = \frac{\partial \varepsilon_{xc}(n_\uparrow, n_\downarrow)(n_\uparrow + n_\downarrow)}{\partial n_\sigma(\mathbf{r})} \equiv \mu_{\text{xc}\sigma}[n_\uparrow(\mathbf{r}), n_\downarrow(\mathbf{r})]. \tag{1.56}$$

Expanding to the first order in m, one obtains:

$$\mu_{\mathrm{xc}\sigma}[n_\uparrow(\mathbf{r}), n_\downarrow(\mathbf{r})] = \mu_{\mathrm{xc}}(n) + \mathrm{sign}(\sigma)\frac{1}{3}\delta(n)\mu_{\mathrm{x}}(n)\frac{m}{n} \tag{1.57}$$

where $\delta(n)$ is 1 in the high density limit and gets reduced by correlation to ~ 0.55 for $r_s = 4$. Clearly eq. (1.57) reduces to eq. (1.45) when $m(\mathbf{r}) = 0$, therefore it is possible to use only one functional while performing DFT calculations in LDA or LSDA. In particular von Barth and Hedin obtained the following form for $\varepsilon_{xc}(n_\uparrow, n_\downarrow)$: [43]

$$\varepsilon_{xc}(n,\zeta) \quad = \quad \varepsilon_{xc}^{P}(n) + f(\zeta)\Delta\varepsilon_{xc}(n), \tag{1.58}$$

where $\zeta(\mathbf{r}) = m(\mathbf{r})/n(\mathbf{r})$. In eq. (1.58) $\varepsilon_{xc}^{P}(n)$ and $\Delta\varepsilon_{xc}(n)$ do not depend on m, while $f(\zeta)$ is a known function of ζ. Therefore the response to magnetism is entirely defined by the $\Delta\varepsilon_{xc}(n)$ functional, as the energy difference between the fully polarized and unpolarized electron gas. I will use this result in chapter 5 while in the rest of the thesis, when I will use LDA or LSDA, I will adopt the expression for $E_{\mathrm{xc}}^{\mathrm{LSDA}}[n(\mathbf{r}\sigma, \mathbf{r}\sigma')]$ obtained by Perdew and Wang. [44]

1.2.3 Extended Stoner theory for ferromagnetism

The local spin density approximation may be approximated by a Stoner formalism. This can be done for example treating the spin polarized part of the potential (1.57) by first order perturbation theory. [45, 253, 254] In this approximation the exchange splitting is given by:

$$\Delta \equiv E_{\mathbf{k}\uparrow} - E_{\mathbf{k}\downarrow} = 2\mu_B h + m\left\langle \psi(\mathbf{k},\mathbf{r}) \left| \frac{4}{(9\pi)^{\frac{1}{3}}} \frac{\delta[n(\mathbf{r})]}{n^{\frac{2}{3}}(\mathbf{r})} \frac{m(\mathbf{r})}{m} \right| \psi(\mathbf{k},\mathbf{r}) \right\rangle =$$

$$= 2\mu_B h + mI \tag{1.59}$$

which is equivalent to eq. (1.25), *i. e.* I and Δ are strictly $\mathbf{k}$-independent if both the charge and spin density $n(\mathbf{r})$ and $m(\mathbf{r})$ are spherically symmetric. [45, 244, 253, 255]

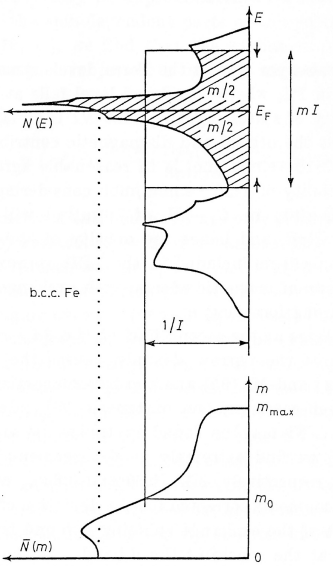

Figure 1.2: Stoner criterion for ferromagnetism illustrated for bcc Fe. Figure from Ref [255].

Based on the correspondence between LSDA and Stoner model, one can think of describing the magnetic properties of metallic systems like bcc Fe by considering the (LDA) paramagnetic density of states $N(\varepsilon)$ (per spin) and then moving the spin up and spin down Fermi level by a quantity $\Delta = 2\mu_B h + mI$, where I is the Stoner parameter as coming from LSDA (1.59). In other words, under the effect of the magnetic field a disparity between spin up and spin down is created by moving the relative Fermi levels $E_F^{\uparrow}$ and $E_F^{\downarrow}$. Selfconsistency requires that the integral over a range Δ around the Fermi level of the paramagnetic density of states equals the

magnetization m. If one considers a function $\tilde{N}(n,m)$ defined as the density of sates averaged over the Fermi level corresponding to an occupancy of $n/2$ spins over a range of m spins, the selfconsistency condition requires that $\tilde{N}(n,m) = \frac{m}{\Delta}$ and by considering eq. (1.59) this leads to: [244, 253, 254]

$$(I + 2\mu_B h/m)\tilde{N}(m) = 1, \tag{1.60}$$

where I dropped the dependence on n, since I will consider always fixed occupation when using this formalism (chapter 5). The function $\tilde{N}(m)$ defines the full material dependent ferromagnetic response in terms of the paramagnetic bandstructure. An example of how to construct the function $\tilde{N}(m)$ is shown for bcc Fe in Fig. 1.2.

Eq. (1.60) represents the magnetic equation of state of a ferromagnet from which the Stoner uniform susceptibility can be obtained as:

$$\mu_B \frac{dm}{dh}\Big|_{m=0} = \chi = \frac{2\mu_B^2 \tilde{N}(0)}{1 - I\tilde{N}(0)}. \tag{1.61}$$

The equilibrium magnetization m fulfills the condition $dE(m)/dm - \mu_B h = 0$, therefore

$$E(m) = \int_0^m \mu_B h dm' = \frac{1}{2}\int_0^m \frac{m'}{\tilde{N}(m')} dm' - \frac{I}{4}m^2. \tag{1.62}$$

This is the expression for the magnetic energy. From eqs. (1.61) and (1.62) the **extended Stoner criterion** for ferromagnetism is obtained:

$$\tilde{N}(m)I \geq 1, \tag{1.63}$$

which gives the condition for the realization of a spin polarized state with magnetization m in terms of the paramagnetic DOS of the real system calculated in LDA.

1.3 Effect of spin fluctuations on the magnetic properties

Spin fluctuations in itinerant systems are known, since long time, for being important in influencing the low-energy properties [256, 257] and the thermodynamic quantities like specific heat, [258] electrical resistivity [201] and Curie temperature. [17] Moreover they can be responsible also for the complete suppression of s-wave superconductivity like in Pd, [94] or for exotic pairing alternative to phonons. [5, 6, 62, 105, 123, 174, 215, 259, 260] Here I will analyze the basics of the underlying theoretical concepts while at the end of next section I will describe the interplay with superconductivity.

1.3.1 Failure of the mean-field description

The approaches to magnetism described up to now, can be all associated with a mean-field decoupling like in (1.2). In other words, the interaction among the spins is described as the interaction of a single spin with an external potential, like the Weiss field in (1.4), given by the sum of the external potential plus the polarization of the other $N-1$ spins. For the Landau theory this is shown by comparing the critical exponents in eqs. (1.14), (1.16), (1.17), (1.20) and (1.22) with the gaussian approximation for the Wilson action. [237, 238, 241] The mean field decoupling corresponds to truncating the expansion for the action to quadratic terms. [238]

The Stoner model presented in section 1.1.3 is equivalent to the Hartree-Fock approximation (HFA) applied to the four-body Hamiltonian: [17]

$$H = H_0 + V = \sum_{\mathbf{k}} \sum_{\sigma} \varepsilon(\mathbf{k}) a^{\dagger}_{\mathbf{k}\sigma} a_{\mathbf{k}\sigma} + \sum_{\mathbf{k}} \sum_{\mathbf{k}'} \sum_{\mathbf{q}} V(\mathbf{q}) a^{\dagger}_{\mathbf{k}+\mathbf{q}\uparrow} a^{\dagger}_{\mathbf{k}'-\mathbf{q}\downarrow} a_{\mathbf{k}'\downarrow} a_{\mathbf{k}\uparrow}, \quad (1.64)$$

where $a^{\dagger}_{\mathbf{k}\sigma}(a_{\mathbf{k}\sigma})$ creates (destroys) a Bloch state with momentum $\mathbf{k}$ and spin σ (for simplicity only one band is considered). In this sense the Stoner model can be viewed as a *mean field* approximation and the equivalent of the Weiss field is given by $\Delta(m)$ in eq. (1.25).

For the LSDA I showed in section 1.2.1 that, in case of spherically symmetric spin density $n(\mathbf{r})$ and magnetization $m(\mathbf{r})$, this approximation can be mapped into a Stoner model, elucidating in this way its *mean field* nature.[9] The mean field $\Delta(m)$ in this case is given by eq. (1.59).

Close to the critical region defined by the Ginzburg criterion (1.23) presented in section 1.1.2, the mean field approximation breaks down. This is due to the fact that the system starts to correlate over a distance ξ which is comparable with the volume of the sample and, for magnetic systems, spin fluctuations over distances of the order of ξ start to dominate the dynamics of the system. In section 1.1.2 I have shown by this introducing the Ornstein-Zernike form for the correlation function (1.20). Actually I did this for the static case in classical phase transitions but the argument used there can be generalized to quantum phase transitions by using the argument by Hertz, Millis and Abanov and Chubukov. [172, 261, 262]

The break-down of the mean-field approach shows up as an overestimation of the tendency to magnetism close to the transition. For the Stoner model, calculations done using realistic density of states have indeed shown an overestimation of the Curie temperature in 3 d metals by a factor which goes from 3 to 5 times, [45] and LSDA usually overestimates the susceptibility and magnetic moment of system close to a QCP. [51, 52, 263] In the Stoner model this is due to an underestimations of thermal fluctuations, like in the gaussian approximation for the Wilson action or for the Landau theory of second order phase transitions (see section 1.1.2). In LSDA the effect is due to quantum and dynamical fluctuations which are important within the critical region.

[9] This doesn't mean however that the Hartree-Fock approximation is equivalent to LSDA. The Stoner parameter obtained in HFA is indeed substantially larger than the one estimated in LSDA. One reason for this difference is the underestimation of correlation in HFA. In this approximation indeed, electrons with equal spin are kept apart, while unequal spin electrons are not. This results in a large Stoner parameter. If correlation effects are included, also unequal spin electrons are kept apart, although less efficiently. The correlation of unequal spin electrons causes a reduction of the Stoner parameter. For a better understanding of the difference between HFA and LSDA see for example [45, 46] and reference therein.

1.3.2 Dynamical susceptibility and spin fluctuations

In order to describe the effect of spin fluctuations, I start considering here the case of a nearly ferromagnetic metal. An electron at position $\mathbf{r}$ and time t with spin $\mathbf{S}(\mathbf{r},t)$ polarizes the surrounding electrons acting as a local magnetic field $\mathbf{H}(\mathbf{r},t)$ which has the following form:

$$\mathbf{H}(\mathbf{r},t) = -\frac{I}{\hbar\mu_B}\mathbf{S}(\mathbf{r},t). \tag{1.65}$$

In eq. (1.65), the coupling constant I corresponds to a local exchange interaction in (1.64) and is defined by the exchange integral:

$$H_{exch} = \Omega \int d^3r\, d^3r' I\delta(\mathbf{r}-\mathbf{r}')n_{\uparrow}(\mathbf{r})n_{\downarrow}(\mathbf{r}') \tag{1.66}$$

where $n_\sigma(\mathbf{r})$ is the electron density with spin σ and Ω is the volume of the system. In linear response theory the magnetization $\mathbf{m}$ at a point $\mathbf{r}'$ and time t' caused by a magnetic field at $(\mathbf{r},t)$ is given by:

$$\mathbf{m}(\mathbf{r}',t') = \mu_B \int d^3r\, dt\, \chi(\mathbf{r}'-\mathbf{r},t'-t)\mathbf{H}(\mathbf{r},t). \tag{1.67}$$

where $\chi(\mathbf{r}-\mathbf{r}',t-t')$ is the isotropic dynamical susceptibility.[10] The molecular field at $(\mathbf{r}',t')$ is proportional to $\mathbf{m}(\mathbf{r}',t')$. Therefore the gain in energy of one spin $\mathbf{S}(\mathbf{r}',t')$ due to the presence of the molecular field $\mathbf{H}(\mathbf{r}',t')$ is given by: [260, 264]

$$\begin{aligned}\Delta E &= -\mu_B\mathbf{S}(\mathbf{r}',t')\cdot\mathbf{H}(\mathbf{r}',t') = \\ &= \frac{I}{\hbar}\mathbf{S}(\mathbf{r}',t')\mu_B\int d^3r\, dt\,\chi(\mathbf{r}'-\mathbf{r},t'-t)\mathbf{H}(\mathbf{r},t) = \\ &= \frac{I}{\hbar}\mathbf{S}(\mathbf{r}',t')\mu_B\int d^3r\, dt\,\chi(\mathbf{r}'-\mathbf{r},t'-t)\left(-\frac{I}{\hbar\mu_B}\right)\mathbf{S}(\mathbf{r},t).\end{aligned} \tag{1.68}$$

[10] I assume here time and spatial invariance such that $\chi(\mathbf{r},\mathbf{r}',t,t') = \chi(\mathbf{r}-\mathbf{r}',t-t')$

Integrating over all the possible $(\mathbf{r}', t')$, eq. (1.68) can be written in Fourier space as:

$$V = H_{SF} =$$
$$= -\frac{I^2}{4V}\int d\omega \sum_{\mathbf{k},\mathbf{k}',\mathbf{q}} \mathrm{Re}[\chi(\mathbf{q},\omega)]\times$$
$$\times \sum_{S_1S_2S_3S_4} \left\{c^{\dagger}_{\mathbf{k}+\mathbf{q},S_1}\vec{\sigma}_{S_1S_2}c_{\mathbf{k},S_2}\right\}\cdot\left\{c^{\dagger}_{-\mathbf{k}'-\mathbf{q}S_3}\vec{\sigma}_{S_3S_4}c_{\mathbf{k}',S_4}\right\}. \tag{1.69}$$

The Hamiltonian (1.69) represents the scattering process characterized by the exchange of spin fluctuations, being $\vec{\sigma}_{S_iS_j}$ the spin operator whose components are the Pauli matrices. Finding a reliable approximation for $\chi(\mathbf{q},\omega)$ is still an open problem. Indeed this quantity involves energy scales comparable with the characteristic energy scale of electrons for which no "small" parameter can be individuated, therefore the perturbative approach is not appropriate.

1.3.3 Random phase approximation and paramagnons

The first attempt in this sense is given by the **random phase approximation** [95, 160–162] (RPA) where a diagrammatic expansion is applied to the four legs vertex and, summing up all the cross (Fock) and ladder (Hartree) diagrams, the following approximated expression for $\chi(\mathbf{q},\omega)$ was found:

$$\chi(\mathbf{q},\omega) \approx \chi^{\mathrm{RPA}}(\mathbf{q},\omega) = \frac{\chi_0(\mathbf{q},\omega)}{1 - I\chi_0(\mathbf{q},\omega)}. \tag{1.70}$$

Here $\chi_0(\mathbf{q},\omega) = \sum_{\mathbf{k}} \frac{f(\varepsilon_{\mathbf{k}}) - f(\varepsilon_{\mathbf{k}-\mathbf{q}})}{\varepsilon_{\mathbf{k}-\mathbf{q}} - \varepsilon_{\mathbf{k}} - \omega}$ is the bare dynamical susceptibility of the isotropic electron gas. For $|\,\mathbf{q}\,| \ll k_F$ and $\omega \ll \varepsilon_F$ an approximated form for $\chi_0(\mathbf{q},\omega)$ leads to:

$$\chi_0(\mathbf{q},\omega) \approx N_0\left(1 - \frac{|\,\mathbf{q}\,|}{12k_F^2} + i\frac{\pi}{2}\frac{\omega}{v_F\,|\,\mathbf{q}\,|}\right). \tag{1.71}$$

For a parabolic band (no nesting features) the static susceptibility $\chi(\mathbf{q},\omega=0)$ has its maximum for $\mathbf{q}=0$ where the divergence happens for $N_0 I = 1$ and recovers the

Stoner criterion for ferromagnetism. The imaginary part of $\chi(\mathbf{q},\omega)$ in eq. (1.70) at fixed $\mathbf{q}$ has instead a broad peak indicating the presence of a resonance called **paramagnon** whose dispersion for small $|\,\mathbf{q}\,|$ is given by:

$$\omega_{\mathbf{q}} = \frac{2}{\pi N_0 I}(1 - N_0 I) v_F \,|\,\mathbf{q}\,| \tag{1.72}$$

Although the RPA represents a step forward with respect to the mean field level, close to the transition temperature this approximation fails since the effect of spin fluctuations to the thermal equilibrium is neglected. This effect is important when the Curie temperature is very small and the transition is driven by pressure or doping. At this point a further renormalization of the susceptibility must be taken into account. In practice electrons interact via spin fluctuations exchange and the susceptibility gets self-consistently renormalized by the interaction.

1.3.4 Self-consistent renormalization theory

This effect has been discussed within the self-consistent renormalization (SCR) theory by Moriya, [17] where a self-consistent scheme for $\chi(\mathbf{q},\omega)$ is described. Here I discuss this approach as considered by Shimizu [235] since this will be the starting point for the new approach developed in chapter 5. The Moriya-Shimizu approach to spin fluctuations starts with expanding the free energy in terms of the square of the uniform magnetization $m^2 = \sum_i^n m_i^2$ where the index $i = x, y, z$.

$$F(m) = \frac{a_2}{2} m^2 + \frac{a_4}{4} m^4 + \frac{a_6}{6} m^6 \ldots$$

Here $a_2 = \partial^2 F / \partial m^2 \,|_{m=0}$ is the bare uniform susceptibility. Under the effect of spin correlations the average magnetization fluctuates around its mean value and the free energy functional gets renormalized by the fluctuations. If $\xi^2_{i\mathbf{q}} = \langle \delta m_{i\mathbf{q}} \delta m_{i-\mathbf{q}} \rangle$ is the average value of the spin fluctuations amplitude and $m_{i\mathbf{q}}$ is the Fourier component of the fluctuating magnetization, the renormalized free energy functional can be

expressed as:

$$\tilde{F} = F_0 + \frac{1}{2}\sum_{i,\mathbf{q}} c'\mathbf{q}^2 \xi_{i\mathbf{q}}^2 + \frac{1}{2}\tilde{a}_2 m^2 + \frac{1}{4}\tilde{a}_4 m^4 + \frac{1}{6}\tilde{a}_6 m^6 + \ldots \tag{1.73}$$

The bare coefficients and the renormalized ones are related by the following recursive relations:

$$\tilde{a}_2 = a_2 + (n+2)n^{-1}[a_4\xi^2 + (n+4)n^{-1}a_6\xi^4 + (n+4)(n+6)n^{-2}a_8\xi^6 + \ldots]$$

$$\tilde{a}_4 = a_4 + 2(n+4)n^{-1}a_6\xi^2 + (n+4)(n+6)n^{-2}a_8\xi^4 + \ldots$$

$$\tilde{a}_6 = a_6 + 3(n+6)n^{-1}a_8\xi^2 + \ldots$$

$$\vdots$$

with $\xi^2 = \sum_{i,\mathbf{q}} \xi_{i\mathbf{q}}^2$, and for $n = 3$ this leads to:

$$\tilde{a}_2 = a_2 + \frac{5}{3}a_4\xi^2 + \frac{35}{9}a_6\xi^4 + \frac{35}{3}a_8\xi^6 + \ldots \tag{1.74}$$

$$\tilde{a}_4 = a_4 + \frac{14}{3}a_6\xi^2 + 21a_8\xi^4 + \ldots$$

$$\tilde{a}_6 = a_6 + 9a_8\xi^2 + \ldots$$

and the quantity ξ^2 can be calculated by the quantum formulation of the fluctuation dissipation theorem (1.19):

$$\xi^2 = \frac{3\hbar}{\Omega}\int d\mathbf{q}\int \frac{d\omega}{2\pi}\frac{1}{2} Im\chi(\mathbf{q},\omega),$$

following the lines suggested by Moriya [17] and elaborated by other authors. [265–267] In the broken symmetry phase both $a_2 < 0$ and $\tilde{a}_2 < 0$, while $a_4 > 0$; therefore eq. (1.74) leads to a net reduction of the uniform susceptibility. Although the connection between ξ and the microscopic band parameters is well defined, calculating $\chi(\mathbf{q},\omega)$ is very complicated since it involves large energy scales. For this reason

in the past the approach described up to now was applied either approximating χ with the non interacting spin susceptibility or assuming ξ as a phenomenological parameter. [51, 52, 268] Moreover, as I will show in chapter 5 the spin fluctuations parameterized by ξ act as a detrimental agent on the Stoner parameter I as estimated in LSDA. Therefore the renormalization of the uniform susceptibility was sometimes achieved by reducing I phenomenologically. [62]

1.3.5 Recent developments on the spin fluctuations theory in itinerant systems

As I stressed more than once, the difficulty of evaluating the full interacting $\chi(\mathbf{q},\omega)$ *ab-initio*, resides in the fact that it involves large energy scales. The DFT scheme that I have shown in the previous subsection is a ground state, time-independent approach and does not allow to treat frequency dependent phenomena, unless by calculating the transition rate among states connected by the exchange of quantized normal modes like phonons or magnons. Since the energy range involved is very large, the calculations become prohibitive apart from some simple cases. [269] Moreover, due to the approximation made on the exchange and correlation potential $E_{xc}[n_\uparrow(\mathbf{r}), n_\downarrow(\mathbf{r})]$, some part of the spin fluctuations are already included, and the consequent approximation on $\chi(\mathbf{q},\omega)$ is not transparent. A first attempt to go beyond the DFT approach in order to include the time dependence in $E_{xc}[n_\uparrow(\mathbf{r}), n_\downarrow(\mathbf{r})]$ was made by Savrasov [270] who used the time dependent density functional theory (TD-DFT) developed by Runge and Gross [271] within the adiabatic local density approximation (ALDA) by Gross and Kohn. [272] However the calculations are very demanding and for a long time they were restricted to simple bulk systems. [270, 273] Recently, Lounis *et al.* [274, 275] used the Korringa-Kohn-Rostoker (KKR) method [276, 277] for calculating the dynamical susceptibility starting from an empirical tight-binding scheme and making several simplifications like neglecting the energy dependence of the electronic wave functions and restricting the analysis only to the d electron states.

In the meanwhile also the approximation made on the ω-dependent exchange

and correlation energy functional and the approach on the two-body problem via TD-DFT were substantially improved, [278–281] and a new method for calculating $\chi(\mathbf{q},\omega)$ by means of the KKR Green's function was implemented by Buczek *et al.* [282–285] This developed and efficient computational scheme allowed to calculate the paramagnon spectrum of FeSe opening new perspectives towards the understanding of superconductivity in this material. [286] Although, up to now I implicitly considered only the particle-hole channel for the Hamiltonian (1.68), which in RPA leads to particle-hole excitations via paramagnon exchange (1.72), one could consider also the particle-particle or Cooper channel for which, under certain conditions an effective attractive potential can be obtained. Therefore the lack of accuracy in determining the spin fluctuations interaction in the normal (nearly magnetic) state is reflected in the inaccuracy in evaluating the superconducting gap Δ and the critical temperature T_c.

1.4 Superconductivity

1.4.1 Ginzburg-Landau phenomenological theory

Superconductivity is characterized essentially by two phenomena happening at the same time below a certain critical temperature T_c:

- the expulsion of the magnetic field called **Meissner-Ochsenfeld effect**,
- zero electrical resistivity.

Moreover the superconducting transition is a second order phase transition, it is therefore accompanied also by a divergence in the second order thermodynamic derivative of the free energy as I showed in section 1.1.2. In order to account for all these effects, Ginzburg and Landau [74, 287] generalized the theory of second order phase transitions to the case of a complex order parameter $\psi(\mathbf{r})$. When $\psi(\mathbf{r}) \neq 0$ both the effects listed above are present, when $\psi(\mathbf{r}) = 0$ they vanish as well. Close to T_c the order parameter is small and the free energy can be expanded in terms of

$\psi(\mathbf{r})$.[11]

$$F(T,\psi) = F_n + \int d^3r \left\{ \alpha \mid \psi(\mathbf{r}) \mid^2 + \frac{\beta}{2} \mid \psi(\mathbf{r}) \mid^4 + \right.$$

$$\left. + \frac{1}{2m^*} \left| \left(-i\hbar\nabla - \frac{e^*}{c}\mathbf{A} \right) \psi(\mathbf{r}) \right|^2 + \frac{h^2}{8\pi} \right\}. \tag{1.76}$$

In eq. (1.76) F_n is the free energy in the normal state, the coefficient c is the velocity of light and $\mathbf{A}$ is the vector potential, defined in terms of the magnetic field $\mathbf{H} = h\tilde{\mathbf{z}}$ as $\mathbf{H} = \nabla \times \mathbf{A}$.

By minimizing the difference $F(T,\psi) - F_n$ between the free energy in the superconducting state and that in the normal state, the **Ginzburg-Landau equations for superconductivity** can be derived:

$$\frac{1}{2m^*} \left(-i\hbar\nabla - \frac{e^*}{c}\mathbf{A} \right) \psi(\mathbf{r}) + \beta \mid \psi(\mathbf{r}) \mid^2 \psi(\mathbf{r}) = -\alpha(T)\psi(\mathbf{r})$$

$$\mathbf{J}_s = \frac{e^*\hbar}{i2m^*} [(\psi^*(\mathbf{r})\nabla\psi(\mathbf{r}) - \psi(\mathbf{r})\nabla\psi^*(\mathbf{r})] - \frac{e^{*2}}{m^*c} \mid \psi(\mathbf{r}) \mid^2 \mathbf{A}. \tag{1.77}$$

These two equations represent respectively the equation of motion of the order parameter $\psi(\mathbf{r})$ and the non dissipating current $\mathbf{J}_s$ associated with it. The order parameter has a charge e^* and mass m^*. From eq. (1.77) two characteristic length scale, called respectively the **coherence length** ξ and the **penetration depth** λ, can be obtained. They represent respectively the length associated with the spatial fluctuations of the order parameter and the length of the region, inside the superconductor, where the magnetic field is still finite. As the temperature $T \to T_c$, $\lambda \to \infty$ and the Meissner-Ochsenfeld effect disappears. At the same time the order parameter vanishes and the non dissipative current vanishes as well.

[11] The minimal substitution

$$\frac{c'}{2}\nabla \to \frac{1}{2m^*} \left(-i\hbar\nabla - \frac{e^*}{c}\mathbf{A} \right) \tag{1.75}$$

in eq. (1.11) is necessary since the order parameter ψ is assumed to be charged.

The superconductors can be classified in the following way according to their values of the ratio $k = \lambda/\xi$ called **Ginzburg landau parameter**. The classification is the following:

- type I superconductors: $0 < k < 1/\sqrt{2}$,
- type II superconductors: $k > 1/\sqrt{2}$.

For the type I superconductors the superconducting transition is of first order in the magnetic field **H**, in the type II superconductors the transition is anticipated by a regime called **Shubnikov phase** in which the magnetic field penetrates into the superconductor by means of non superconducting domains. [288]

1.4.2 Microscopic theory of superconductivity

Seven years after the Ginzburg-Landau theory for superconductors, Bardeen Cooper and Schrieffer (BCS) [75] constructed the ground state wave function for a superconductor $\mid \Phi_G\rangle$ by making use of the result by Cooper. [77] Cooper indeed found that the Fermi gas, in the presence of an attractive potential $V_{\mathbf{kl}}$, no matters how weak, is unstable against the formation of bound states with energy E below the Fermi level. The quantities $\mathbf{k}$ and $\mathbf{l}$ are the momenta of the fermions (having opposite spins) involved in the bound state called **Cooper pair**.

The **BCS wave function** has the following form:

$$\mid \Phi_G\rangle = \prod_{\mathbf{k}=\mathbf{k}_1,..,\mathbf{k}_N} (u_{\mathbf{k}} + v_{\mathbf{k}} c^{\dagger}_{\mathbf{k}\uparrow} c^{\dagger}_{-\mathbf{k}\downarrow}) \mid \Phi_0\rangle \tag{1.78}$$

with the normalization constraint $\mid u_{\mathbf{k}} \mid^2 + \mid v_{\mathbf{k}} \mid^2 = 1$.

Averaging the two-body Hamiltonian

$$H = \sum_{\mathbf{k}\sigma} \varepsilon_{\mathbf{k}} n_{\mathbf{k}\sigma} + \sum_{\mathbf{kl}} V_{\mathbf{kl}} c^{\dagger}_{\mathbf{k}\uparrow} c^{\dagger}_{-\mathbf{k}\downarrow} c_{-\mathbf{l}\downarrow} c_{\mathbf{l}\uparrow} \tag{1.79}$$

with the wave function (1.78) and applying the minimal principle, the following self-consistent equation was obtained:

$$\Delta_{\mathbf{k}} = -\frac{1}{2}\sum_{\mathbf{l}} \frac{V_{\mathbf{kl}}\Delta_{\mathbf{l}}}{E_{\mathbf{l}}} = -\frac{1}{2}\sum_{\mathbf{l}} \frac{V_{\mathbf{kl}}\Delta_{\mathbf{l}}}{\sqrt{\xi_{\mathbf{l}}^2 + \Delta_{\mathbf{l}}^2}} \tag{1.80}$$

provided the definition of $\Delta_{\mathbf{k}}$ and $\xi_{\mathbf{k}}$ to be: $\Delta_{\mathbf{k}} = -\sum_{\mathbf{l}} V_{\mathbf{kl}} u_{\mathbf{l}} v_{\mathbf{l}}$ and $\xi_{\mathbf{k}} = \varepsilon_{\mathbf{k}} - \mu$, where μ is the chemical potential and $\varepsilon_{\mathbf{k}}$ is the bare fermionic energy. $E_{\mathbf{k}}$ is indeed the quasi-particle energy and $\Delta_{\mathbf{k}}$ is the minimal excitation energy or zero-temperature energy gap that can be observed, for example, by low temperature optical spectroscopy measurements. In 1959 (two years later the BCS paper appeared) Gor'kov [78] finally showed the connection between the Ginzburg-Landau phenomenological theory and the BCS theory. The Ginzburg-Landau theory is indeed the limit of the BCS theory for $T \approx T_c$ and the order parameter $\psi(\mathbf{r})$ is proportional by a factor $e^{i\phi}$ to the gap Δ. The phase ϕ is a phase factor hidden in (1.78) which characterizes the superconductor. The coefficient $u_{\mathbf{k}}$ and $v_{\mathbf{k}}$ are indeed complex and ϕ is their phase difference: $u_{\mathbf{k}} v_{\mathbf{k}} = \mid u_{\mathbf{k}} \mid\mid v_{\mathbf{k}} \mid e^{i\phi}$. The value of e^* and m^* where found to be twice the electron charge and electron mass respectively.

At finite temperature eq. (1.80) becomes: [289]

$$\Delta_{\mathbf{k}} = -\frac{1}{2}\sum_{\mathbf{l}} \frac{V_{\mathbf{kl}}\Delta_{\mathbf{l}}}{E_{\mathbf{l}}} \tanh\left(\frac{E_{\mathbf{l}}}{2k_B T}\right). \tag{1.81}$$

An approximate solution of eq. (1.81) can be found by choosing a particular form for the potential $V_{\mathbf{kl}}$:

$$V_{\mathbf{kl}} = -V \quad \text{for} \quad \mid \xi_{\mathbf{k}} \mid \leq \hbar\omega_c \text{ and } \mid \xi_{\mathbf{l}} \mid \leq \hbar\omega_c$$

$$V_{\mathbf{kl}} = 0 \quad \text{otherwise.} \tag{1.82}$$

Here $V > 0$ and $\hbar\omega_c$ is an energy cut-off representing the energy scale of the attracting potential V. The condition (1.82) implies:

$$\Delta_{\mathbf{k}} = \Delta \quad \text{for} \quad \mid \xi_{\mathbf{k}} \mid \leq \hbar\omega_c$$

$$\Delta_{\mathbf{k}} = 0 \qquad \text{otherwise.} \tag{1.83}$$

Therefore eq. (1.81) reduces to $1/V = 1/2\sum_{\mathbf{k}} \tanh(E_{\mathbf{k}}/2k_BT)/E_{\mathbf{k}}$. Transforming the sum over $\mathbf{k}$ in an integral over $\xi_{\mathbf{k}}$ ($\sum_{\mathbf{k}} \to \int_0^{\hbar\omega_c} N(\xi)d\xi$) and assuming that the density of states $N(\xi)$ doesn't change much within the range of integration, an approximate expression for Δ and for T_c can be easily obtained:[12]

$$\Delta \approx 2\hbar\omega_c e^{-1/N_0V} \tag{1.84}$$

$$k_BT_c = 1.13\hbar\omega_c e^{-1/N_0V} \tag{1.85}$$

where N_0 is the density of states at the Fermi level. From eqs. (1.84) and (1.85) the universal ratio

$$\alpha = \frac{\Delta}{k_BT_c} = 1.77 \tag{1.86}$$

is obtained.

Notice that eq. (1.84) is valid only in the **weak coupling regime** when $N_0V \ll 1$. In the BCS approximation another universal ratio can be obtained and is the ratio between the specific heat jump ΔC at the critical temperature and the normal state specific heat $C(T_c)$, namely:

$$\frac{\Delta C(T_c)}{C(T_c)} = 1.43. \tag{1.87}$$

If the weak coupling approximation is not valid these two ratios change and therefore the measure of these ratios gives an indication about the strength of the coupling constant $\lambda = N_0V$. In chapter 2 I will analyze the case of the recently discovered APt_3P superconductor where the ratios (1.86) and (1.87) will be analyzed.

1.4.3 Migdal-Eliashberg theory for electron-phonon superconductivity

Up to now I showed that in the presence of an attractive potential, a macroscopic quantum state leading to the Meissner-Ochsenfeld effect and to the loss of electrical

[12] One has to take into account that at $\Delta(T = T_c) = 0$

resistivity can be realized at finite temperature $T < T_c$. However I have not specified anything about the potential and I only showed the link between some microscopic parameters and a phenomenological theory close to T_c. On the other hand, the BCS theory implicitly assumes the coupling due to phonons but completely neglects retardation effects. As I will show in chapter 2 retardation effects can be sometimes crucial in understanding material properties.

The Migdal-Eliashberg theory, [79, 80] accurately treats the electron-phonon interaction and offers a way to calculate the critical temperature. The equation for the gap Δ appears as a generalization of eq. (1.81):

$$\phi(\omega_n) = \pi T \sum_m [\lambda_{\rm ep}(\omega_n - \omega_m) - \mu^*] \times$$

$$\times \frac{\phi(\omega_m)}{\sqrt{\omega_m^2 Z^2(\omega_m) + \phi^2(\omega_m)}} \tag{1.88}$$

$$Z(\omega_n)\omega_n = \omega_n + \pi T \sum_m \lambda_{\rm ep}(\omega_n - \omega_m) \times$$

$$\frac{Z(\omega_m)\omega_m}{\sqrt{\omega_m^2 Z^2(\omega_m) + \phi^2(\omega_m)}} \tag{1.89}$$

$$\lambda_{\rm ep}(\omega_n - \omega_m) \quad = \quad 2\int_0^\infty \frac{\Omega \alpha^2 F(\Omega) d\Omega}{(\omega_n - \omega_m)^2 + \Omega^2}, \tag{1.90}$$

where $\phi(\omega_n) = \Delta(\omega_n)Z(\omega_n)$, $\Delta(\omega_n)$ is the superconducting order parameter, $Z(\omega_n)$ is the mass enhancement factor and ω_n are the Matsubara frequencies; here and in the following $\Delta(0) = \Delta$. The quantity μ^* is the Coulomb pseudopotential which accounts for the Coulomb repulsion among the electrons and acts as a pair-braking potential. Since evaluating this term requires to solve the electron-electron interaction problem, this term is usually fixed phenomenologically and its typical value varies from 0.1 to ~ 0.13. Eq. (1.90) defines the kernel of the interaction and if $\lambda_{\rm ep}(\omega_n - \omega_m) \to 0$, the retardation effects are neglected, $Z(\omega_n) \to 1$ and eqs. (1.88) reduces to eq. (1.81).

The quantity $\alpha^2F(\Omega)$ is the **Eliashberg function** and represents the spectrum of the interaction. It can be experimentally accessed by neutron scattering or via the inversion of the tunneling data. [10] This quantity is obtained by evaluating the electron-phonon matrix element $g^{\nu,n,m}_{\mathbf{k},\mathbf{k}+\mathbf{q}}$ between the Bloch states $\psi_{\mathbf{k},n}(\mathbf{r})$ and $\psi_{\mathbf{k}+\mathbf{q},m}(\mathbf{r})$, and then summing the transition rate $\mid g^{\nu,n,m}_{\mathbf{k},\mathbf{k}+\mathbf{q}} \mid^2$ over the exchanged momentum $\mathbf{q}$ associated with the phonon frequencies $\omega^{\nu}_{\mathbf{q}}$, the electron momentum $\mathbf{k}$ and the phonon and electron band indeces ν, n and m respectively, provided the Fermi golden rule. The final expression for $\alpha^2F(\Omega)$ is:

$$\alpha^2F(\Omega) = \frac{1}{N_0}\sum_{\mathbf{k},\mathbf{q},\nu,n,m} \delta(\epsilon^n_{\mathbf{k}})\delta(\epsilon^m_{\mathbf{k}+\mathbf{q}})|g^{\nu,n,m}_{\mathbf{k},\mathbf{k}+\mathbf{q}}|^2\delta(\Omega-\omega^{\nu}_{\mathbf{q}}). \tag{1.91}$$

The electron-phonon matrix element $g^{\nu,n,m}_{\mathbf{k},\mathbf{k}+\mathbf{q}}$ can be calculated *ab-initio* by means of the Kohn-Sham orbitals obtained from the solution of eqs. (1.38)-(1.40). The quantity $\alpha^2F(\Omega)$ completely defines the microscopic properties of electron-phonon superconductors also at finite temperature, indeed eqs. (1.88)-(1.90) are still valid above T_c where $\Delta = 0$. The self-consistent eqs. (1.88)-(1.90) where obtained perturbatively by Eliashberg [80] by using the Migdal theorem [79] which states that if the parameter $\lambda_{\rm ep}(0)/\omega_D E_F \ll 1$, *i.e.* the ratio between the typical phonon energy scale ω_D and the Fermi energy E_F times the coupling constant $\lambda_{\rm ep} \equiv \lambda_{\rm ep}(0)$ is small, and the contributions coming from the second (and higher) order diagrams can be neglected. The Migdal-Eliashberg theory for electron-phonon superconductors turned out to be very accurate when applied to real materials. [8–11] This together with the large degree of accuracy reached in actual calculation for the phonon spectrum $F(\omega) = \sum_{\mathbf{q},\nu}\delta(\Omega-\omega^{\nu}_{\mathbf{q}})$ and the Eliashberg function, [12] allows to consider the problem of electron-phonon superconductivity solvable in most of the cases. [7, 12–16, 236, 290] In this respect I will show in chapter 2 my results on the superconducting properties of the $A\mathrm{Pt_3P}$ compounds (A = Sr, Ca, La) where the agreement with the experiment concerning the thermodynamic properties is really remarkable. As a step further toward a completely *ab-initio* description of electron-phonon-mediated superconductivity there is the development of a DFT for the superconducting order parameter where the basic variable is not the electron

density $n(\mathbf{r})$ but is the order parameter $\psi(\mathbf{r})$. As a consequence the electron-electron interaction enters the theory on the same footing as electron-phonon one with no need for its parameterization via μ^*. For further details and results see Refs. [291–297]

As I showed in the previous subsection, such a well defined approximation like the Migdal-Eliashberg approximation is not yet available for spin fluctuations-mediated interaction (1.69). As a consequence, evaluating the full interacting susceptibility $\chi(\mathbf{q},\omega)$ which enters in the Hamiltonian (1.69) and gets self-consistently renormalized by the interaction is still a challenge. The same difficulty is then reflected in the calculation of the kernel (1.90) for spin fluctuations-mediated superconductors for which suitable approximations must be found.

1.4.4 Paramagnons and unconventional superconductivity

The BCS interaction only takes into account the coupling between antiparallel spins. Moreover $\Delta_{\mathbf{q}}$ in eq. (1.81), in the form (1.83), is basically $\mathbf{q} = \mathbf{k} - \mathbf{l}$ independent. This is usually valid for electron-phonon coupling which is implicitly assumed to be the "glue" of the cooper pairs and is explicitly parameterized in the Migdal-Eliashberg formulation (1.88)-(1.90).

Superconductivity suppressed by paramagnons

Early calculations on d metals, tended to overestimate the critical temperature. [96–98] The problem was individuated in the fact that some of these materials have a substantial tendency to ferromagnetism and at low temperatures medium-range spin order with moderate time scale act as an attractive potential for electrons with aligned spins and as a repulsive potential for electrons with antialigned spins. [96] In other words, in nearly ferromagnetic metals the interaction (1.69) in the particle-hole channel works against the electron-phonon coupling in the particle-particle channel. Within RPA (1.70) electrons interact via paramagnon exchange (1.72) in the particle-hole channel and the spectrum of the interaction (the corresponding

$\alpha^2F(\Omega)$) is given by the interacting spin susceptibility $\chi^{\mathrm{RPA}}(\mathbf{q},\omega)$. The detrimental effect on superconductivity was pointed out by Berk and Schrieffer, [94] who modified the Migdal-Eliashberg equations (1.88)-(1.90), by adding a term $K_s(\omega_n - \omega_m)$ to the electron-phonon kernel $\lambda_{\mathrm{ep}}(\omega_n - \omega_m)$. Neglecting retardation effects and considering a spherical Fermi surface, the authors evaluated the electron-paramagnon coupling constant in the singlet channel as given by:

$$\lambda_{SF} = N_0 K_s(0,0) = (2k_F^2)^{-1} \int_0^{2k_F} q\,dq\; I^2 \chi^{\mathrm{RPA}}(q,0), \tag{1.92}$$

where

$$I^2\chi^{\mathrm{RPA}}(q,0) = \frac{I^2 N_0 u(q)}{1 - I N_0 u(q)}. \tag{1.93}$$

Here N_0 is the electronic DOS at the Fermi level, $u(q)$ is the Lindhard function in three dimensions and $q = \mid \mathbf{q} \mid$. In this way they found that superconductivity in the singlet channel could occur only if the electron-phonon coupling constant $\lambda_{\mathrm{ep}} \equiv \lambda_{\mathrm{ep}}(0)$ exceeds the coupling to spin fluctuations λ_{SF}. The RPA form of the spin susceptibility and the assumption of spherical Fermi surface can be considered satisfactory for getting the rough physical picture about the competition between magnetism and electron-phonon superconductivity. Moreover it can be regarded as a reasonable degree of approximation if the electron-phonon coupling is considered to involve an Einstein phonon as done by the author of Ref. [94]. However the above approximations for λ_{SF} result to be extremely poor if compared with the degree of accuracy that can be obtained in actual electron-phonon calculations. [12] In chapter 3 I will try to overcome this problem by making the $\mathbf{q}$ average of $\chi(\mathbf{q},0)$ in a suitable way, being aware that further improvement are needed.

Ferromagnetic spin fluctuations and triplet superconductivity

After the work by Berk and Schrieffer, Fay and Appel [99] realized that since the paramagnons act as an attracting potential for spin parallel electrons, they could favor the formation of a superconducting order parameter with different symmetry

with respect to the one expected by BCS: the *p*-**wave triplet order parameter**. Indeed the Hamiltonian (1.69) for the electron-paramagnon interaction limited to the Cooper (particle-particle) channel can be rewritten as: [260]

$$H_{SF} = \sum_{\mathbf{k},\mathbf{l}} \sum_{S_1 S_2 S_3 S_4} V_{\mathbf{k}\mathbf{l}S_1S_2S_3S_4} c^{\dagger}_{\mathbf{k}S_1} c^{\dagger}_{-\mathbf{k}S_2} c_{-\mathbf{l}S_3} c_{\mathbf{l}S_4} \tag{1.94}$$

$$\text{where} \quad V_{\mathbf{k}\mathbf{l}S_1S_2S_3S_4} = -\frac{I^2}{4}\mathrm{Re}\chi(\mathbf{q}=\mathbf{k}-\mathbf{l},\omega=\varepsilon_{\mathbf{k}}-\varepsilon_{\mathbf{l}})\vec{\sigma}_{S_1S_4}\cdot\vec{\sigma}_{S_2S_3},$$

and $\vec{\sigma}_{S_1S_4}$ is the spin operator whose components are the Pauli matrices and I is a coupling constant. In RPA approximation (1.70) (consistent with paramagnon exchange) I can be taken as the Stoner parameter.

Due to the spin dependency of $V_{\mathbf{k}\mathbf{l}S_1S_2S_3S_4}$ different values for spin singlet and spin triplet configurations are obtained:

$$V^S_{\mathbf{k}\mathbf{l}} = \frac{3I^2}{4}\mathrm{Re}\chi(\mathbf{q}=\mathbf{k}-\mathbf{l},\omega=\varepsilon_{\mathbf{k}}-\varepsilon_{\mathbf{l}}) \quad \text{for} \quad S=0$$

$$V^t_{\mathbf{k}\mathbf{l}} = -\frac{I^2}{4}\mathrm{Re}\chi(\mathbf{q}=\mathbf{k}-\mathbf{l},\omega=\varepsilon_{\mathbf{k}}-\varepsilon_{\mathbf{l}}) \quad \text{for} \quad S=1. \tag{1.95}$$

The spin fluctuations interaction is repulsive in the singlet channel ($S=0$) and attractive in the triplet channel ($S=1$). Moreover it gets weakened by a factor of 3 going from one channel to the other. For the gap function $\Delta_{\mathbf{k}}$ a similar form like (1.81) can be obtained and it is easy to see that the order parameter has *p*-wave ($l=1$) symmetry. Due to the factor of 3 of reduction in (1.95) the triplet superconductors have usually lower critical temperature than singlet ones.

As I already explained at the end of section 1.3, the effect of spin fluctuations is to renormalize the susceptibility in a self-consistent way. Indeed the spin fluctuations interaction is governed by the spin susceptibility which gets self-consistently renormalized by the interaction. Since the magnetic properties and the superconducting ones are governed by the same kind of interaction but in different channels (particle-particle and particle-hole respectively), the uncertainty on $\chi(\mathbf{q},\omega)$ affects at the same time both the predictions of the magnetic properties (magnetization and

Curie temperature) and those on the superconducting ones (superconducting gap Δ and critical temperature). A transparent example of this will be offered in chapter 3. There I will show that in order to get a consistent physical understanding of the system a renormalization of the spin susceptibility is needed both in the particle-hole channel, in order to avoid the ferromagnetic instability, and in the particle-particle (singlet and triplet) channel in order to reproduce the critical temperature. One of the most important cases where magnetic degrees of freedom are highly entangled with the superconducting ones is the case of Fe pnictides. I will briefly introduce the problem in the following.

Antiferromagnetic spin fluctuations and $s_{\pm}$ superconductivity

The first model for superconductivity driven by antiferromagnetic correlations was introduced by Schrieffer, Wen, and Zhang [163, 164] for explaining the superconductivity in hole-doped antiferromagnetic insulators like some cuprate superconductors. This model is called the spin bag model since it considers an hole introduced in an antiferromagnetically ordered two dimensional lattice which remains trapped into a bag given by a depression of the nearby staggered magnetization. If two trapped holes get close enough, an attractive potential can be generated leading to a kind of Cooper phenomenon. Schrieffer *et al.*, however did not succeed in explaining the superconductivity in Cu oxide superconductors which is still an open challenge. Moreover their model was thought for system close to a Mott transition, therefore dominated by short range correlations, while the present thesis is focused on itinerant systems. Itinerant models were introduced later on after Monthoux and Pines pointed out that for the description of spin fluctuations induced superconductivity it is crucial to take into account the momentum and frequency dependence of the interaction. [166, 167]

Due to the momentum dependence of the pairing potential, additional symmetries with respect to s and p can emerge. In subsection 1.1.3 I showed that some portions of the Fermi surface can be sometimes brought into overlap by a translational vector $\mathbf{Q}$ called nesting vector. If this is the case, the susceptibility at

$\mathbf{q} = \mathbf{Q}$ is enhanced. If electron-phonon coupling can be neglected and the pairing can be supposed to be mediated only by spin fluctuations (1.94), a solution for the BCS equation for the order parameter can still be found if the order parameter has opposite sign in the two portions of the Fermi surface connected by $\mathbf{Q}$. The simplest form for the order parameter fulfilling eq. (1.80) that can be found is the $d_{x^2-y^2}$ symmetry, [123] with

$$\Delta(\mathbf{k}) = \frac{\Delta_0}{2}\left[\cos(k_x) - \cos(k_y)\right].$$

Notice that an *s*-wave order parameter, possibly with nodes, never satisfies eq. (1.80) with repulsive (spin fluctuations-mediated) interaction *i. e.* the order parameter needs to change from one portion of the Fermi surface to the other connected by the vector $\mathbf{Q}$ (see [82, 123] and reference therein).

An interesting case, of present interest, is however represented by the extended *s*-wave symmetry of the order parameter realized in Fe pnictides and chalcogenides: [144–146, 148] the so-called $s_{\pm}$ symmetry. The Fermi surface of these materials is formed by several portions connected by the nesting vector $\mathbf{Q}$ associated with the antiferromagnetic stripe instability. [53–56]

In such a situation a solution of eq. (1.80) in the single channel can be found, provided that the coupling is purely interband -*i.e* in $V^S_{\mathbf{kl}}$ $\mathbf{l}$ and $\mathbf{k}$ belong to two different portions of the Fermi surface- and the order parameter on the two portions of the Fermi surface has opposite sign.

In this way eq. (1.81) is decomposed as follows: [298]

$$\Delta_1 = -\frac{1}{2}\sum_{\mathbf{k}} \frac{V\Delta_2}{E_{2,\mathbf{k}}} \tanh(\frac{E_{2,\mathbf{k}}}{2k_B T})$$

$$\Delta_2 = -\frac{1}{2}\sum_{\mathbf{k}} \frac{V\Delta_1}{E_{1,\mathbf{k}}} \tanh(\frac{E_{1,\mathbf{k}}}{2k_B T}) \tag{1.96}$$

where $E_{i,\mathbf{k}} = \sqrt{\xi_{i,\mathbf{k}} + \Delta_i}$ is the quasiparticle energy in the band i giving rise to the $i-th$ portion of the Fermi surface. Such a model was suggested for the first time by Mazin *et al.* [5] for the superconductivity in Fe pnictides and chalcogenides.

This proposal has been slightly extended for taking into account the possibility of accidental nodes on the order parameter due to the different orbital character of the states involved in the pairing, [138] which could lead to $d_{x^2-y^2}$ [6] pairing symmetry. This case is realized in LaFePO, [142, 143] the first discovered Fe compound whose optical properties I will analyze in chapter 4.

Chapter 2

Electron-phonon superconductivity in $A\mathrm{Pt_3P}$ (A = Sr, Ca, La) compounds

In this chapter I report the results of Ref. [299] where the Pt phosphides APt_3P (A =Sr, Ca, La), recently discovered by T. Takayama et al., [197] *are studied using first-principles calculations and Migdal-Eliashberg theory. The agreement is so remarkable that I can draw several definitive conclusions about the superconductivity in these materials. In particular, I can rule out the charge-density wave (CDW) scenario proposed by Ref. [199]. Also spin orbit coupling has a minor effect on the electronic states at the Fermi level, ruling out exotic effects on superconductivity. Migdal Eliashberg Theory for single gap s-wave superconductors describes the three compounds; the large differences in T_c (8.4 K in $SrPt_3P$, 6.6 K in $CaPt_3P$ and 1.5 K in $LaPt_3P$), come from changes in the electron-phonon matrix elements and phonon softening. Preliminary total energy calculations further show that this class of compounds could open new perspectives towards the understanding of unconventional superconductivity.*

Introduction

Having introduced the methods that I will use along the whole thesis, in this and in the following chapters I will describe the topics which my PhD activity was dedicated to.

I start with the APt$_3$P (A =Sr, Ca, La) superconductors recently discovered by T. Takayama *et al.* [197] This class of materials immediately attracted the interest of the scientific community for their relatively high critical temperatures ($T_c = 8.4,\ 6.6,\ 1.5\ K$ for SrPt$_3$P, CaPt$_3$P and LaPt$_3$P respectively), but also for the peculiarity of their crystal structure and for the presence of Pt with a high spin orbit coupling (SOC). Indeed the crystal structure of these compounds is the centrosymmetric counterpart of the structure of CePt$_3$Si heavy fermion superconductor, where the high spin orbit coupling of Pt together with the lack of inversion symmetry lifts the spin degeneracy leading to exotic superconductivity. [105, 106] In this respect the APt$_3$P series is important because, as proposed by the author of Ref. [197], the possibility of synthesizing them both in the centrosymmetric and in the non centrosymmetric variants could allow to study the effect of the lack of inversion symmetry on superconductivity in electronically equivalent compounds.

Concerning the origin of superconductivity, the analysis of the specific heat data revealed the presence of low-energy phonons in these materials, focusing the attention on the electron-phonon mechanism in the strong coupling regime. However the presence of multiple Fermi surface pockets inferred from Hall resistivity measurements and effectively found in DFT calculations [197, 198] left also some room for multiband superconductivity. The main experimental argument in favor of multiband superconductivity was the very large ratio of ~ 2.5 between the superconducting gap Δ and the critical temperature T_c (1.4 times larger than the BCS value). [197]

A previous density functional theory (DFT) study [199] found a dynamical instability in the phonon dispersion of SrPt$_3$P. The authors argued that superconductivity in this compound could have an exotic origin and could be enhanced by the presence of charge density wave. The same authors also proposed that the large difference

in the critical temperatures between $LaPt_3P$ and the other two compounds could be due to the different electron count - La^{+3} instead of Sr^{+2} and Ca^{+2} - which changes the nature of the bands at the Fermi level (E_F). According to the authors of Ref. [199] indeed, in $LaPt_3P$ these bands get split by the SOC of Pt and the spin symmetry is broken. As a consequence the pairing strength of the electrons is reduced. [199]

In this chapter I present first-principles calculations of the electronic structure, phonon dispersions and electron-phonon coupling on the APt_3P compounds. Thermodynamical properties (superconducting gap, specific heat jump, T_c) are then calculated within Migdal-Eliashberg theory for a direct comparison with the experiment. The superconducting gap, the critical temperature and the specific heat jump are in very good agreement with the experiment, and this allows to give some definitive conclusions about the APt_3P series and exclude any route for multiband or exotic superconductivity. These compounds indeed turn out to be a textbook example of electron-phonon superconductors in which the electron phonon coupling varies from strong coupling in the Sr compound ($SrPt_3P$) to weak coupling in the La compound ($LaPt_3P$) through the moderate regime in the Ca one ($CaPt_3P$). The variation from strong/moderate to weak coupling is due to the change in the electron count going from Sr^{+2} and Ca^{+2} to La^{+3}. In the A^{+2} compounds, albeit the similar critical temperatures -$T_c = 8.4$ K in $SrPt_3P$ and $T_c = 6.6$ K in $CaPt_3P$- the ratio between the specific heat jump and T_c and the ratio between the superconducting gap Δ and T_c are very different and place the two compounds in the strong and in the moderate coupling regime respectively. This is due to a shift towards lower frequencies of the phonon modes involved in superconductivity of $SrPt_3P$ with respect to $CaPt_3P$. As a result the electron-phonon coupling increases and the thermodynamic observables (specific heat jump and superconducting gap) increase as well. However, in the formula for the critical temperature the increase of the coupling is compensated by the decrease of the characteristic frequency associated with the bosonic mode involved, therefore it is less affected. Indeed, the critical temperature of $CaPt_3P$ and $SrPt_3P$ are very close to each other. The shift towards lower frequency from the Ca to Sr compound, turns out to be almost entirely a structural

effect. Indeed, in the two compounds the electron-phonon matrix element is very similar, whereas the frequency of the breathing modes involved in superconductivity increases (decreases) with decreasing (increasing) the in-plane lattice constant.

The structure of the chapter is the following. In section 2.1 I present in detail the crystal structure of the APt$_3$P superconductors and describe its relation with its non-centrosymmetric variant, the CePt$_3$Si structure. Both structures are tetragonal antiperovskites, which contain distorted octahedra formed by the Pt atoms occupying two inequivalent positions (4e and 2c) in the unit cell. I will call Pt(1) the Pt atoms sitting in the basal plane and Pt(2) the atoms sitting in the apical edges of the octahedra. The two structures differ for the in-plane arrangement of the octahedra. A polar arrangement gives rise to a non-centrosymmetric structure (CePt$_3$Si), an antipolar arrangement gives rise to the centrosymmetric variant (APt$_3$P). With total energy calculations I show that the proposal by Takayama, *et al.* [197] of synthesizing the APt$_3$P compounds in both crystal structures could likely be realized.

In section 2.2 I discuss the electronic structure of the APt$_3$P compounds with a particular focus on the energies around the Fermi level. The electron count is different in SrPt$_3$P, CaPt$_3$P and LaPt$_3$P. The Fermi surface is modified by the change in the electron count from Sr and Ca to La. In the first two compounds the Fermi surface is indeed formed by two different sheets with different character and the Pt(1) $d_{x^2-y^2}$ character is the dominant one. The Fermi surface of LaPt$_3$P is instead composed of highly dispersive sheets with strongly mixed characters. The difference in electronic states contributing to the Fermi surface has important consequences on the electron-phonon coupling. In all compounds, the effect of SOC is negligible.

In section 2.3 I present the results for phonon dispersions and electron-phonon coupling. The phonon dispersions appear to be stable at ambient pressure and very similar among the three compounds. In-plane breathing motions of the Pt(1) atoms form low-energy branches. These branches couple mostly to Pt in-plane electronic states. Their presence or absence at the Fermi level results in an enhanced/decreased electron-phonon coupling.

In section 2.4 I use the calculated phonon DOSs (PDOS) and Eliashberg functions to calculate the thermodynamic quantities to compare them with the experiment. I

find a perfect agreement between the theoretical results and the experimental data and in section 2.5 I draw my conclusions.

Technical details are listed at the end of the chapter in section 2.6.

2.1 Crystal structure

The three $A\mathrm{Pt_3P}$ compounds ($A =$ Sr, Ca, La) crystallize in the antiperovskite tetragonal structure (space group $P4/nmm$). The antiperovskite or inverse perovskite is commonly defined as a perovskite structure with cations replaced by anions and vice versa.

The simplest example of perovskite structure is the cubic one with chemical formula BCX_3 where B and C are cations and X is an anion. In this structure, C is a small cation such as Ti^{+4} and sits in the center of an octahedron formed by the X anion like O^{-2}, while the bigger cations B (e.g Sr^{+2}) enclose the octahedron sitting at the edges of a cube as shown on the left panel of in Fig. 2.1.

The antiperovskite structure is obtained from this by exchanging the anions with cations and vice versa and has chemical formula B_3XA or AB_3X, where A can be an anion or a cation which sits at the edge of a cube (or parallelepiped) and encloses the XB_6 corner-sharing octahedra. A typical example is the structure of $\mathrm{Na_3OCl}$ [300] made by $\mathrm{ONa_6}$ oxocentered corner-sharing octahedra with cavities occupied by large Cl^- anions. The Cl^- anion at the edge of the cube can be replaced by a cation as in $\mathrm{CePt_3Si}$.

In this material, since the Pt cation and the Si anion have comparable size, Si moves out of the Pt plane and gets close to one of the two apical Pt's as shown in the right panel of Fig. 2.1. Finally the other apical Pt cation gets closer to the basal plane to ensure closer packing. This causes a distortion of the octahedron which loses inversion symmetry. Indeed the apical Pt cation and the basal ones are not equivalent anymore and occupy the $2c$ and $1a$ inequivalent Wyckoff positions respectively. The space group of such a structure is $P4mm$.

If the unit cell contains only one octahedron, as in the case of $\mathrm{CePt_3Si}$, the

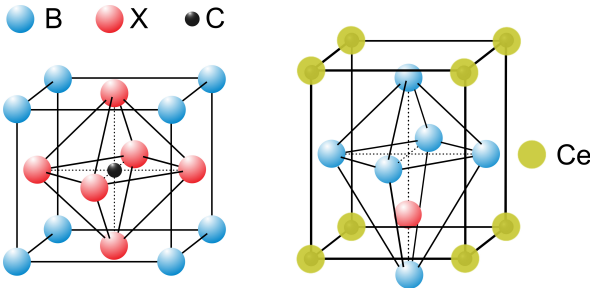

Figure 2.1: *Left*:unit cell of a cubic perovskite structure like $CaTiO_3$ having chemical formula BCX_3. B is the bigger cation, C is the smaller one and X is the anion (see text). The antiperovskites have chemical formula B_3XA as for Na_3OCl or AB_3X, where A sits at the edge of a cube (or parallelepiped) enclosing the XB_6 corner-sharing octahedra. A can be either a cation, as for $CePt_3Si$ or an anion as for Na_3OCl. *Right*: tetragonal antiperovskite structure with the octahedral distortion causing the lack of inversion symmetry in $CePt_3Si$.

local lack of inversion symmetry is transferred from the octahedron to the whole solid. We call this a *polar* arrangement. Hovever, if the unit cell contains an even number of octahedra, arranged in an antipolar fashion (*i.e* with the X anion in the right panel of Fig. 2.1 sitting above and below the octahedral basal plane in two corner-sharing octahedra), the global inversion symmetry is recovered. This situation is the one actually realized in the APt_3P compounds whose crystal structure is shown in Fig. 2.2(a). In the phosphides the distorted octahedra shown in Fig. 2.2(b) point alternatingly up and down and are arranged in a checkerboard fashion. As a consequence, the in-plane lattice parameter is $\sqrt{2}$ times larger than the Pt(1)-Pt(1) distance and the unit cell contains two formula units. The A atoms sit in the 2a Wyckoff position while the P atoms sit in the 2c one and occupy the central position of the distorted Pt_6P octahedra. Pt atoms occupy two inequivalent Wyckoff positions (4e) and (2c), corresponding to in-plane and apical positions. As anticipated before, the in plane arrangement of the distorted octahedra makes

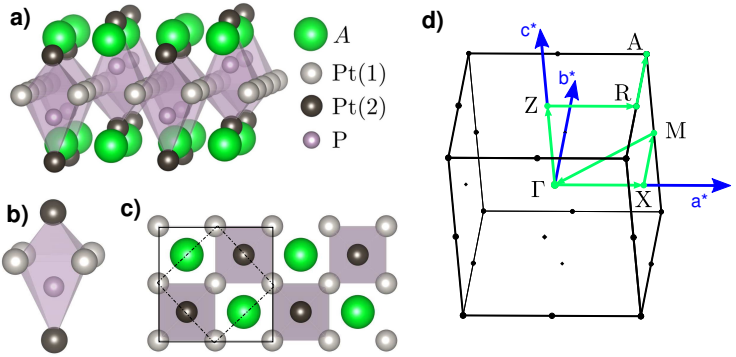

Figure 2.2: Figure adapted from Ref. [299]. (*a*) Crystal structure of $A\mathrm{Pt_3P}$, space group $P4/nmm$. The $\sqrt{2} \times \sqrt{2}$ in-plane arrangement of the distorted $X\mathrm{Pt_6}$ octahedra (*b*) distinguishes the $A\mathrm{Pt_3P}$ compounds from the non-centrosymmetric $\mathrm{CePt_3Si}$ superconductor (space group $P4mm$); the corresponding unit cells are shown as full and dashed lines in panel (*c*).(*d*) Brillouin zone used to plot the band structure in Figs. 2.4 and 2.5. The reciprocal lattice vectors are also shown (blue arrows).

the difference between this structure and the one of the tetragonal antiperovskites $\mathrm{CePt_3Si}$ non-centrosymmetric superconductor. In this sense both the phosphides and the silicides can be seen as two different variants of a more general $A\mathrm{Pt_3}X$ type of structure. Note that the antipolar structure was reported for the first time in the work of Takayama *et al.*, who proposed that this could be used as a viable way to study the effect of inversion symmetry on superconductivity in non-centrosymmetric crystals. [197]

The unit cell of the $A\mathrm{Pt_3}X$ type of structure for both the $P4/nmm$ and $P4mm$ space groups is plotted in Fig. 2.2 (*c*). Both the phosphides with antipolar centrosymmetic structure and the silicides with polar non centrosymmetic structure are superconductors and, as stated by the authors of Ref. [197], it would be interesting to synthesize the $A\mathrm{Pt_3P}$ compounds in the noncentrosymmetric polar structure to

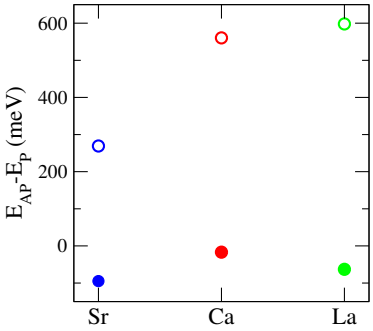

Figure 2.3: Figure from Ref. [299]. Total energy difference between the antipolar and polar structure for phosphides APt$_3$P (full symbols) and silicides APt$_3$Si (empty symbols) superconductors, with A =Sr, Ca, La. The fully relaxed GGA structure at zero pressure were used.

study the effect of the inversion symmetry on superconductivity in electronically equivalent systems. Therefore it is important to see whether this would be possible.

For this reason, I present in Fig. 2.3 total energy calculations for the APt$_3$P compounds both in the antipolar and in the polar structure. The same total energy differences were also-calculated for the corresponding silicides (APt$_3$Si). Actually, among all the 12 possible structures -APt$_3X$ with A = Sr, Ca, La and X =P, Si both in the $P4/nmm$ and $P4mm$ space groups- analyzed here, only 4 were experimentally synthesized. Only for La indeed, both a non-centrosymmetric silicide and a centrosymmetric phosphide have been synthesized.

In our calculations, the structures were fully relaxed in the generalized gradient approximation (GGA) -see section 2.6 for technical details- and, for the existing compounds, the agreement between the calculated structural parameters and the experimental ones was within $\sim 2\%$. The relaxed parameters are given in table 2.1 and the results of the calculations are plotted in Fig. 2.3.

The difference in total energies between the antipolar and polar structures

Table 2.1: Fully relaxed structural parameters (GGA) for the $A\mathrm{Pt_3P}$ compounds in the experimental $P4/nmm$ structure from Ref. [299].

	$a(\AA)$	$c(\AA)$	z_{Pt2}	z_P
$\mathrm{SrPt_3P}$	5.898	5.470	0.1362	0.7227
$\mathrm{CaPt_3P}$	5.758	5.494	0.1357	0.7303
$\mathrm{LaPt_3P}$	5.838	5.553	0.1418	0.7719

$(E_{AP} - E_P)$ is negative for phosphides (full symbols), and positive for silicides (empty symbols). Its absolute value varies, between the two cases, approximately by one order of magnitude.

The calculations indicate that while the silicides strongly favor a *polar* arrangement, which allows neighboring Si atoms to form partly covalent bonds, the phosphides prefer an *antipolar* arrangement. For the phosphides, the energy differences between the centro and non-centro symmetric structures are small ($\sim 20 - 100$ meV) and it might also be possible to tune the polar arrangement of the octahedra, choosing appropriate synthesis conditions. This is very unlikely, in turn, for the silicides.

2.2 Electronic structure

After having analyzed the structural properties of the $A\mathrm{Pt_3P}$ series both in the centrosymmetric and non centrosymmetric variants, I now focus on the centrosymmetric experimental crystal structure and analyze the electronic properties of all three compounds. Since I'm interested in explaining the origin and nature of superconductivity in this class of materials, my analysis will be particularly focused on energies around the Fermi level.

The electronic structure calculations presented here are in very good agreement with previous calculations. [198, 199, 218] For all three $A\mathrm{Pt_3P}$ compounds, the bandstructure from -8 eV to 2 eV around the Fermi level E_F originates from the

Pt(1) and Pt(2) d orbitals hybridized with the P p ones, which form bonding states around -7 eV below the Fermi level and partially occupied antibonding states around E_F. [218] Since La^{+3} has a different oxidation number with respect to Sr^{+2} and Ca^{+2}, the electron count of $LaPt_3P$ is different from the other two compounds and its Fermi level is shifted up by ~ 0.5 eV. As a consequence, the band in Fig. 2.4 which is flat along the $M - \Gamma$ direction is completely full and the double degenerate electron band around the M point is partially occupied.

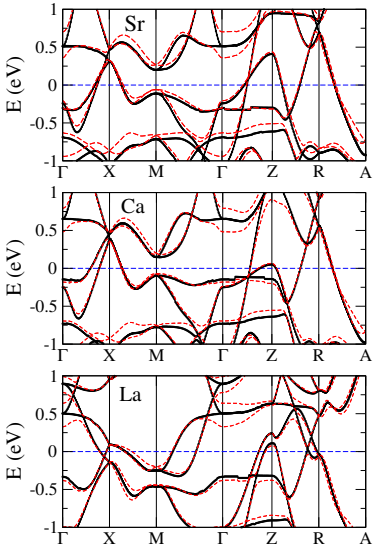

Figure 2.4: Figure adapted from Ref. [299]. Electronic structure of APt_3P in an energy range of 2 eV around the Fermi level E_F. With red, dashed line (black, solid line) is indicated the band structure with (without) spin orbit coupling; the zero of the energy is the Fermi level.

In Fig. 2.4 a blow-up of the bandstructure about 2 eV around the Fermi level is

shown and, as it can been clearly seen, the band splitting caused by the SOC of Pt is negligible both in the Sr and in Ca compounds and it vanishes at the Fermi level. This means that the SOC is not relevant for superconductivity, as supposed instead in Ref. [199]. For the La compound a small splitting at E_F is present, however it does not lift the spin degeneracy. This is in contrast to what was claimed by the authors of Ref. [199]. The densities of states (DOS) at E_F are $N_0 \sim 2.36$ st/eV f.u. in Sr, 2.37 st/eV f.u. in Ca, and 1.94 st/eV f.u. in La, and the SOC changes them by less than 5 %. Since the SOC plays only a marginal role on the electronic states near E_F, I will neglect it in the following.

Fig. 2.5 shows the "fat" bands without the SOC of the three APt$_3$P compounds, highlighting the orbital characters which give the highest contribution to the electronic states at the Fermi surface. The axes are oriented along the shortest in-plane Pt-Pt distance. The bands at the Fermi level have mainly $pd\pi$ antibonding character while the pair of Pt(2) d_{z^2} and P p_z orbitals and that of Pt(1) d_{xy} and P $p_{x,y}$ orbitals form $pd\sigma$ bonding states and therefore are located far below E_F. [218] The $pd\pi$ antibonding bands can be grouped in two:

- the bands that originate from the Pt(1) $d_{x^2-y^2}$ and Pt(2) $d_{xz,yz}$ orbitals hybridized with the P $p_{x,y}$ ones: among these bands a low dispersive band along the $\Gamma - Z$ direction is present,

- the bands that originate from the Pt(1) d_{yz} hybridized with P p_y ones.

As shown in Fig. 2.5 (the P character is not shown), in the A^{+2} compounds ($SrPt_3P$, $CaPt_3P$) only the first group of bands is partially filled while the second one is empty. In $LaPt_3P$ instead the first group of bands is completely filled and the second one gets partially occupied.

The Fermi surface in the A^{+2} compounds is formed by the Pt(1) $d_{x^2-y^2}$ hole pocket around the X point and two other free electron-like bands with prevalent Pt(2) and interstitial character. These bands cross E_F along the $Z - R - A$ line and form two more dispersive pockets, *i.e.* a large, flat, structure centered around the Γ point, and a small cigar-shaped hole pocket around the Z point. [199] This

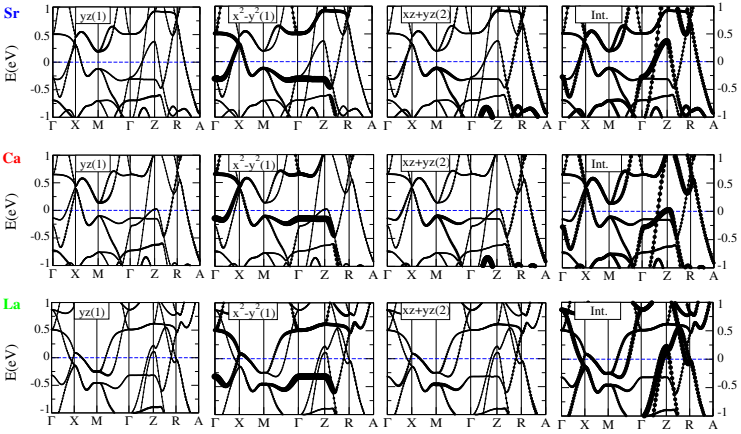

Figure 2.5: "Fat bands" of APt$_3$P from Ref. [299], decorated with partial orbital characters. $x^2-y^2(1)$ and $yz(1)$ stand for in-plane Pt (Pt(1)) $d_{x^2-y^2}$ and d_{yz} partial characters; $xz+yz(2)$ refers to Pt apical (Pt(2)) atomic d_{xz+yz} character; Int. stands for interstitial.

unequal distribution of orbital characters on the Fermi surface suggests that the superconducting gap may be anisotropic.

Given the presence of one more electron per formula unit, the Fermi level of LaPt$_3$P is shifted up by ~ 0.5 eV with respect to the other compounds. Therefore this compound has two electron pockets around the M point with mixed Pt(1) d_{yz} and $d_{x^2-y^2}$ characters, while the band with low dispersion along $M-\Gamma$ direction is completely full. The Fermi surface is composed of highly dispersive sheets, with strongly mixed orbital contributions of Pt(2), P and Pt(1) characters. [198]

The different band character at the Fermi level influences the way in which the electrons couple to the phonon modes. I will focus on this point in the next section.

2.3 Phonon dispersions and electron-phonon coupling

The moderate critical temperature and the experimental analysis of the magnetic susceptibility and the specific heat suggested, since the beginning, that superconductivity in $A\mathrm{Pt_3P}$ compounds is most likely due to electron-phonon mechanism. [197] However some questions remained open. In particular $\mathrm{CaPt_3P}$ and $\mathrm{SrPt_3P}$, despite having similar critical temperatures T_c (8.4 K in $\mathrm{SrPt_3P}$ and 6.6 K in $\mathrm{CaPt_3P}$), show very different $\Delta C/\gamma T_c$ ratios, where ΔC is the specific heat jump at the superconducting transition and γT_c is the linear contribution to the normal state specific heat at T_c. This quantity and the ratio $\alpha = \Delta/k_B T_c$ are associated with the entropy and energy gain relative to the transition respectively, and can be used to characterize the coupling regime (strong or weak) of electron-phonon superconductors. [236]

The experimental value of α, extracted by fitting the data using the α model, [301] is $\alpha \sim 2.55$ in $\mathrm{SrPt_3P}$ and the corresponding value of $\Delta C/\gamma T_c$ is larger than 2: both quantities are well beyond their weak coupling BCS values of 1.76 and 1.42 respectively. For the $\mathrm{CaPt_3P}$ compound, the value of $\Delta C/\gamma T_c$ appears sensibly smaller than in $\mathrm{SrPt_3P}$, also because the experimental estimate of γ suffers the poorer homogeneity of the sample which tends to overestimate it.[1] [197]

Takayama *et al.* [197] suggested that the strong coupling regime, manifested in $\mathrm{SrPt_3P}$ by the large value of the α ratio, could be due to the presence of low energy phonons which enhance the electron-phonon coupling λ in the same way discussed for $\mathrm{KOs_2O_6}$, [302] and the Chevrel compounds. [303] Indeed, being N_0 the DOS at the Fermi level, ω the frequency of the phonons involved in superconductivity and M its mass, the electron-phonon coupling constant can be expressed as $\lambda = N_0\langle g^2\rangle/\langle M\omega^2\rangle$ where $\langle g^2\rangle$ is the average of the square of the electronic matrix element over the Fermi surface and $\langle\rangle$ in the denominator indicates an appropriate average. [8, 304] Therefore λ is large if the characteristic frequency of the phonons involved in superconductivity is small. The experimental evidence for these kind of modes in $\mathrm{SrPt_3P}$ comes from the linear temperature behavior of the resistivity and from the non linear behavior of the C/T vs T^2 plot. [197] In particular, the

[1] The calculated value of γ shown in table 2.3 is indeed significantly smaller.

linear temperature behavior of the resistivity down to 20 K indicates the presence of modes, in this energy range (tenth of cm^{-1}), responsible for the scattering. The non-linear behaviour in C/T vs T^2 indicates the presence of low-energy Einstein modes in the phonon spectrum. According to the same authors, the large value of α could be also due to multiband effects which affect this ratio already at the BCS level. [305] Indeed the Hall conductivity shows contributions from both positive and negative carriers, indicating the presence of both hole and electron bands at the Fermi level. This argument together with the large value of α are the strongest experimental argument fo multiband superconductivity in $SrPt_3P$.

$LaPt_3P$ is instead a weak coupling superconductor and this is due to the different electron count which modifies the Fermi surface and therefore the electron-phonon coupling. [197]

The presence of low energy phonon branches was also found in previous calculations [199, 218] and in Ref. [199] a charge density wave (CDW) instability with wave vector $X = (\pi, \pi, 0)$ in the phonon branches was also found. The same authors argued that the different T_c's in the A^{+2} compounds ($SrPt_3P$ and $CaPt_3P$) with respect to $LaPt_3P$, could be due to the effect of the SOC of Pt which splits the Pt bands populated in $LaPt_3P$ and empty in the $A^{+2}Pt_3P$. [199]

In oder to check the presence of low-lying phonons, [197, 199] possible dynamical instabilities, [199] and understand the differences in the electron-phonon coupling in the three compounds, I present here *ab initio* calculations of the phonon dispersions and the electron-phonon coupling for the APt_3P series. A direct comparison with the experiment based on these calculations will be presented in the next section.

The calculated phonon dispersions of the APt_3P compounds are shown in the left panel of Fig. 2.6. The first thing to notice is that they are stable. The convergence of the phonon spectra were indeed carefully checked, in particular at the X-point, where the authors of Ref. [199] found a dynamical instability at ambient pressure. However no indications of instabilities were found. [2]

[2] The difference most likely stems from the different pseudopotentials employed in that work (See technical details summarized in section 2.6).

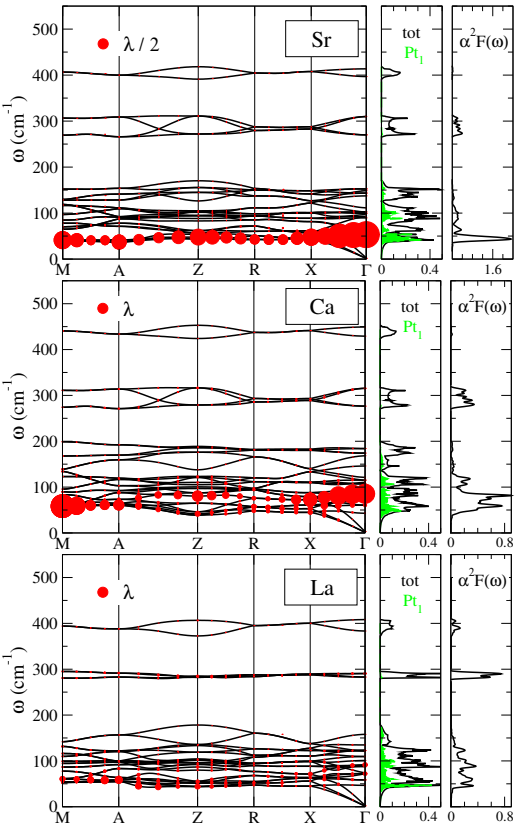

Figure 2.6: Figure from Ref. [299]. Phonon dispersions, densities of states and Eliashberg functions $\alpha^2F(\omega)$ of the APt_3P (A = Sr, Ca, La) compounds. The phonon dispersions are decorated with symbols, proportional to the partial EP coupling $\lambda_{\mathbf{q}\nu}$; for readability, the λ's for Sr have been rescaled by a factor of 2. The logarithmically averaged phonon frequencies $\omega_{\ln}$, the EP coupling constants λ, and the corresponding critical temperatures T_c's are given in Table 2.3.

The phonon bands are very similar for all the three compounds and are formed by thirty phonon branches extending up to ∼450 cm^{-1}. These branches can be easily grouped in three sets as done in the following:

- two upper branches originated mostly by the out-of-plane P vibrations,
- four intermediate branches at ∼300 cm^{-1} mostly coming from the in-plane vibration of P,
- a lower manyfold of the remaining twenty-four strongly intertwined branches, with mixed *A*, Pt(1) and Pt(2) character at lower energy.

The phonon dispersions are decorated with red symbols which indicate the intensity of the EP coupling $\lambda^{\nu}_{\mathbf{q}}$ associated with the phonon band ν and momentum $\mathbf{q}$. The figure shows that, while the coupling is uniform in $LaPt_3P$, in the two A^{2+} compounds it is strongly enhanced at low frequencies and is more $\mathbf{q}$ dependent. The phonon density of states at low frequencies is dominated by the Pt(1) (mainly in plane) character. The breathing modes of Pt couple more strongly to Pt(1) in-plane electronic states, and less to other characters.

Since the phonon dispersions are very similar among the three APt_3P compounds, the coarse difference in $\lambda^{\nu}_{\mathbf{q}}$ must come from the different electronic states at the Fermi level. In particular the Pt(1) in-plane character contributes to a large part of the $A^{2+}Pt_3P$ Fermi surface but not in a uniform way. On the other hand, due to the different electron count, in the Fermi surface of $LaPt_3P$ the Pt(1) d_{yz} character is also present. This character can couple to out-of-plane vibrations of the atoms which involve higher phonon frequencies.

As a result, the coupling in $LaPt_3P$ is smaller and more uniform while in the $A^{2+}Pt_3P$ is larger and more anisotropic. The total electron-phonon coupling (EPC), $\lambda = \sum_{\mathbf{q},\nu} \lambda^{\nu}_{\mathbf{q}}$, is large in $SrPt_3P$, intermediate in $CaPt_3P$ and small in $LaPt_3P$ (see table 2.2).

In order to better explain the similarities and differences among the APt_3P compounds, and to clarify the role of the electron count and the importance of the

	N_0	λ	$\omega_{\ln}$	$\omega^{\rm br}$	$\lambda^{\rm br}$	$I^{\rm br}$	$a(\AA)$
$SrPt_3P$	2.36	1.33	77	53.0	1.90	5337	5.898
$CaPt_3P$	2.37	0.85	110	85.5	0.63	4605	5.758
$LaPt_3P$	1.94	0.57	118	91.5	0.14	1172	5.838

Table 2.2: Some calculated results for $A\mathrm{Pt_3P}$: Electronic density of states at the Fermi level N_0 in states/eV/spin/unit cell; $\omega_{\ln}$ in K; frequency $\omega^{\rm br}$ in cm^{-1}, e-ph coupling $\lambda^{\rm br}$, and e-ph coupling strength $I^{\rm br}$ in cm^{-2} for the in-plane Pt(1) breathing mode at Γ. In the last column the values of the in plane lattice constants are also reported.

Pt(1) breathing modes for the superconductivity of these compounds, it is useful to analyze the Eliashberg functions defined as follows:

$$\alpha^2F(\omega)=\frac{1}{N_0}\sum_{\mathbf{k},\mathbf{q},\nu,n,m}\delta(\epsilon^n_{\mathbf{k}})\delta(\epsilon^m_{\mathbf{k+q}})|g^{\nu,n,m}_{\mathbf{k},\mathbf{k+q}}|^2\delta(\omega-\omega^\nu_{\mathbf{q}}), \tag{2.1}$$

where $\omega^\nu_{\mathbf{q}}$ are phonon frequencies, $\epsilon^n_{\mathbf{k}}$ electronic energies, and $g^{\nu,n,m}_{\mathbf{k},\mathbf{k+q}}$ are the EP matrix elements. Due to their structure, the $\alpha^2F(\omega)$ yield indeed informations on the nature of the bonding and on the character of the superconducting state. In general, an $\alpha^2F(\omega)$ roughly proportional to the PDOS is characteristic of metals with a weak to moderate total coupling and low $T_c's \lesssim 5$ K. The best EP superconductors, such as MgB_2 and A15's, are instead characterized by $\alpha^2F(\omega)$ which display sharp peaks only at specific parts of the phonon spectrum, reflecting a strong coupling between specific electron and phonon states. This characteristic requires (partly) covalent bonding. Concerning the Eliashberg functions of the three $A\mathrm{Pt_3P}$ compounds (plotted on the right panel of Fig. 2.6) there is a substantial difference: for the $SrPt_3P$ indeed $\alpha^2F(\omega)$ has only one large peak around $\sim 50\ \mathrm{cm}^{-1}$, while in $LaPt_3P$ the shape of that function resembles the PDOS. The Ca compound is in a intermediate situation where $\alpha^2F(\omega)$ has two broad features at ~ 300 and $\sim 100\ \mathrm{cm}^{-1}$. This simple analysis already gives an insight about the different regime in $LaPt_3P$ (weak coupling) with respect to the A^{+2} compounds (strong/intermediate coupling).

While in the La and Sr compounds the change in λ is explained with the change

in the electron count from La to Sr, the reason why the total EPC increases by $\sim 50\%$ from $CaPt_3P$ to $SrPt_3P$ needs instead a more detailed analysis.

As already pointed out, for the A^{+2} compounds the EPC is not only larger than in $LaPt_3P$, but also almost entirely concentrated in the low-lying phonon branches of the phonon dispersion. These branches have substantial Pt(1) in-plane breathing character (green color in Fig. 2.6) and the most coupled mode has B_{2u} symmetry at the Γ point; I will refer to these modes as $\omega_{\mathbf{q}}^{\mathrm{br}}$ in the following. [199, 218]

In $SrPt_3P$ the energy of these modes is very low and their dispersion almost flat, in $CaPt_3P$ their energy sightly increases and their dispersion extends up to $\sim$100 cm^{-1}. The evolution of these modes from one compound to the other can be captured by following the largest red circles in the left panel of Fig. 2.6 or the green line in the central panel of the same figure. The red dots represent indeed the value of $\lambda_{\mathbf{q}}^{\nu}$ and the green line in the phonon DOS highlights the Pt(1) character.

The total EPC constant can be written in terms of the Eliashberg function as $\lambda = 2\int_0^{\infty} \frac{\alpha^2 F(\omega)}{\omega} d\omega$. In $SrPt_3P$ $\alpha^2 F(\omega)$ has a very sharp peak at ~ 50 cm^{-1} which in $CaPt_3P$ broadens and shifts up by ~ 50 cm^{-1}. Therefore, due to the $1/\omega$ factor, the EPC is strongly enhanced in $SrPt_3P$ with respect to $CaPt_3P$. A similar softening of the breathing branch is discussed by Chen *et al.* [199] In that case this softening brings even a dynamical instability which is absent in the phonon dispersion presented here.

In order to understand where this softening of the phonon frequencies comes from, I now focus on the differences between the two A^{+2} compounds in the Pt(1) breathing modes. If $\omega_{\mathbf{q}}^{\mathrm{br}}$ is the frequency of the breathing mode associated with a given $\mathbf{q}$ point, the EPC constant associated with that particular mode acquires a simple form which gives the $\mathbf{q}$ distribution of the coupling of the electrons with the breathing modes, over the phonon Brillouin zone: $\lambda_{\mathbf{q}}^{\mathrm{br}} = const \times I_{\mathbf{q}}^{\mathrm{br}}/(\omega_{\mathbf{q}}^{\mathrm{br}})^2$ where $I_{\mathbf{q}}^{\mathrm{br}}$ is the electron-phonon matrix element. Graphically, the quantity $\lambda_{\mathbf{q}}^{\mathrm{br}}$ can be individuated by looking at the largest red dots in the right panel of Fig. 2.6 while the values at the Γ point are given in table 2.2 for all three APt_3P compounds together with the values of $I_{\mathbf{q}}^{\mathrm{br}}$ and $\omega_{\mathbf{q}}^{\mathrm{br}}$. Going from $SrPt_3P$ to $CaPt_3P$, the value of $\lambda_{\mathbf{q}}^{\mathrm{br}}$ decreases by about a factor of three despite a difference of about 10% in $I_{\mathbf{q}}^{\mathrm{br}}$.

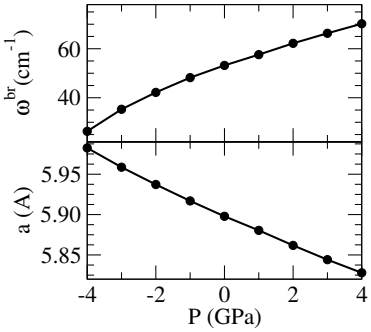

Figure 2.7: Calculated frequency of the B_{2u} mode of $SrPt_3P$ (top) and in-plane lattice constant (bottom) as a function of pressure.

Indeed the electronic states involved in superconductivity are the same while the characteristic frequency of the modes involved increases by$\sim$ 40%.

Adding one electron to the electron count changes the nature of the electronic states selected by the two δ functions in eq. (2.1) and reduces drastically $I^{\rm br}_{\mathbf{q}}$. This together with the hardening of $\omega^{\rm br}_{\mathbf{q}}$, makes $\lambda^{\rm br}_{\mathbf{q}}$ more than ten times smaller in $LaPt_3P$ than in $SrPt_3P$.

Since among the A^{+2} compounds the difference in the EP matrix elements is small, the lowering of the breathing mode frequencies in Sr with respect to Ca is not due to an increase in the EP coupling. Rather this could be due to a structural effect. In fact, as shown in table 2.2, decreasing the in plane lattice constant a, $\omega^{\rm br}_{\mathbf{q}}$ increases and the coupling $\lambda^{\rm br}_{\mathbf{q}}$ decreases. In order to verify this hypothesis the phonon frequencies at the Γ point for $SrPt_3P$ were calculated under hydrostatic pressure using the theoretical structures and the results for the B_{2u} mode are shown in Fig. 2.7 The pressure dependence of a is also shown. For pressures $-4 \leq P \leq 4$ GPa, the frequency $\omega^{\rm br}(P)$ of the B_{2u} mode shows a linear dependence and the slope can be estimated to be 5 $\rm cm^{-1}$/GPa. Since a scales also linearly with pressure

with a slope ~ -0.019 Å/GPa, the relation $\omega^{\mathrm{br}}(a) \approx (-260\ \mathrm{cm}^{-1}/\text{Å})\ a(\text{Å})$ can be extracted. The latter relation is in very good agreement with the 33 cm^{-1} shift in ω^{br} going from $SrPt_3P$ to $CaPt_3P$ whose in plane lattice constants differ by 0.14 Å.

2.3.1 Strong coupling and weak coupling superconductivity in APt$_3$P compounds

From the experimental point of view $SrPt_3P$ and $CaPt_3P$, despite having very similar critical temperature T_c, show very different thermodynamic properties. In particular the specific heat jump appears to be much larger in the former compound than in the latter. Moreover, by fitting the specific heat of $SrPt_3P$ with the so called α model, [301] the author of Ref. [197] extracted a value of the ratio $2\Delta/k_BT_c \sim 5$ well beyond the BCS value of 3.53. For this reason they propose that multiband effects could be important in this material. Indeed for multiband systems the $2\Delta/k_BT_c$ is increased already at the BCS level.[3] [305] From the analysis of the resistivity they also proposed the presence of low energy phonons that are supposed to enhance the coupling in $SrPt_3P$. Previous calculations by H. Chen *et al.* [199] proposed that the difference in the critical temperature and between $SrPt_3P$ and $CaPt_3P$ are given by a CDW instability present in the first compound and absent in the latter one. They argued that superconductivity could benefit of this instability and consequently T_c could be enhanced. [199]

In the phonon dispersion I have presented this instability is not seen, while low energy phonons are present and I have shown that they affect significantly the coupling constant. The reason why they also affect the $\Delta C(T_c)/\gamma T_c$ and the $2\Delta/k_BT_c$ but leave T_c almost unchanged is explained in the following. By fitting the numerical solution of the Eliashberg equations [7], Marsiglio and Carbotte obtained the following expressions for the BCS ratios of strong-coupling superconductors: [236]

$$2\alpha = \frac{2\Delta}{k_BT_c} = 3.53\left[1 + 12.5\left(\frac{T_c}{\omega_{\ln}}\right)^2 \log\left(\frac{\omega_{\ln}}{2T_c}\right)\right] \tag{2.2}$$

[3] This phenomenon doesn't involve all the gaps in the same way. In a two band system for example the larger gap is increased with respect to the single band case while the smaller gets reduced.

$$\alpha_1 = \frac{\Delta C(T_c)}{\gamma T_c} = 1.43 \left[1 + 53 \left(\frac{T_c}{\omega_{\ln}} \right)^2 \log \left(\frac{\omega_{\ln}}{3T_c} \right) \right] \tag{2.3}$$

where $\omega_{\ln} = \exp\left(\frac{2}{\lambda} \int_0^\infty d\omega/\omega \alpha^2 F(\omega) \ln \omega \right)$, *i.e.* the strong-coupling corrections to the BCS value depend on the ratio $T_c/\omega_{\ln}$.

Strong-coupling electron-phonon superconductors can thus be classified according to the value of the parameter $T_c/\omega_{\ln}$, into strong ($T_c/\omega_{\ln} \gg 1$), weak ($T_c/\omega_{\ln} \ll 1$), or intermediate ($T_c/\omega_{\ln} \approx 1$) coupling superconductors. This is done in the Marsiglio-Carbotte plots. [236] However, by plotting these ratios as a function of $\omega_{\ln}/T_c$, a characteristic of these quantities emerges which is particularly important for the $A\mathrm{Pt_3P}$ series. Indeed the two $A^{+2}\mathrm{Pt_3P}$ have almost the same T_c but quite different and relatively low $\omega_{\ln}$ (see table 2.2). For small values of $\omega_{\ln}$ compared to T_c these ratios have a larger value with respect to the BCS one. Moreover a softening of the phonons involved in superconductivity has big consequences on these ratios. On the other hand, if the phonons involved in superconductivity are at larger energies compared to T_c, the quantities in eqs. (2.2) and (2.3) approach the BCS value and do not depend on $\omega_{\ln}/T_c$ anymore.

Eqs. (2.2) and (2.3) are plotted in Fig. 2.8 as a function of $\omega_{\ln}/T_c$. The values of 2α and α_1 for the $A\mathrm{Pt_3P}$ compounds where obtained using the calculated values of $\omega_{\ln}$ reported in table 2.2 and the experimental critical temperatures.

As it can be easily seen, due to their small $\omega_{\ln}$, $\mathrm{SrPt_3P}$ and $\mathrm{CaPt_3P}$ sit in the most sensitive region of the parameter space and even if the critical temperatures are very similar a small shift in the frequency of the phonons involved in superconductivity affects the value of α and α_1 a lot. Note that the value of $2\alpha = 4.33$ found in this way for $\mathrm{SrPt_3P}$ is smaller than 5.1 experimentally claimed. [197] However the comparison should be done using the calculated values of Δ, $\Delta C(T_c)$ and T_c obtained from the Eliashberg function, and density of states calculated before. I will do this in the next section.

$\mathrm{LaPt_3P}$ has a larger $\omega_{\ln}/T_c$ ratio and therefore is located in the weak coupling regime region where a change in $\omega_{\ln}$ doesn't affect the values of α and α_1 rations,

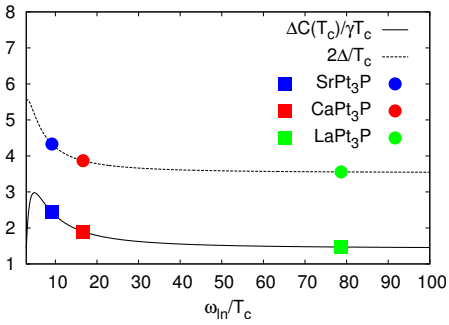

Figure 2.8: $\frac{2\Delta}{k_B T_c}$ (black dotted line) and $\frac{\Delta C(T_c)}{\gamma T_c}$ (black continuous line) extracted from eqs.(2.2) and (2.3) plotted as a function of $\omega_{\ln}/T_c$. The values of $\omega_{\ln}$ for $SrPt_3P$ (blue dots), $CaPt_3P$ (red dots) and $LaPt_3P$ (green dots) are the calculated ones while the values of T_c are the experimental values taken from Ref. [197].

whose values are close to the BCS one.

Concerning the dependence of the critical temperature on the spectrum of the phonons involved in superconductivity, I showed that a shift towards lower frequencies of $\alpha^2F(\omega)$ causes a substantial increase in the electron-phonon coupling constant λ. However this makes also $\omega_{\ln}$ to decrease and, since $\omega_{\ln}$ appears as a prefactor in the Allen-Dynes expression for T_c:

$$T_c = \frac{\omega_{\ln}}{1.20} \exp\left(-\frac{1.04(1+\lambda)}{\lambda - \mu^* - 0.62\lambda\mu^*}\right),$$

one can see that the increase in λ does not correspond to an increase in T_c.

2.4 Migdal-Eliashberg Theory

As seen in the last part of the previous section, in order to define the type of superconducting regime *i.e.* weak or strong coupling, one has to look at the α and α_1 ratios between the superconducting gap Δ and T_c or between the specific heat jump at T_c, $\Delta C(T_c)$ over the critical temperature. However in the previous analysis I used the calculated values of $\omega_{\ln}$ and the experimental values of T_c to extract the α and α_1 ratios, finding a value for α smaller than the one experimentally found.

Indeed, superconductivity in the $A\mathrm{Pt_3P}$ series was experimentally claimed and characterized by measuring the specific heat and fitting the data with the α model [301] in order to infer the superconducting gap magnitude which in $\mathrm{SrPt_3P}$ was found to be $\Delta \sim 1.85$ meV corresponding to $\alpha \sim 2.55$. [197] This was the strongest experimental argument towards multiband superconductivity.

For these reasons the direct comparison with the experiment must be done by comparing the theoretical results with the thermodynamical quantities Δ, $\Delta C(T_c)$ and T_c. In order to access these quantities I solved the Migdal Eliashberg equations in the single-band approximation: [7]

$$\phi(\omega_n) = \pi T \sum_{m=-M}^{m=M} [\lambda(\omega_n - \omega_m) - \mu^*] \frac{\phi(\omega_m)}{\sqrt{\omega_m^2 Z^2(\omega_m) + \phi^2(\omega_m)}} \tag{2.4}$$

$$Z(\omega_n)\omega_n = \omega_n + \pi T \sum_{m=-M}^{m=M} \lambda(\omega_n - \omega_m) \frac{Z(\omega_m)\omega_m}{\sqrt{\omega_m^2 Z^2(\omega_m) + \phi^2(\omega_m)}} \tag{2.5}$$

$$\lambda(\omega_n - \omega_m) = 2\int_0^\infty \frac{\Omega\alpha^2 F(\Omega) d\Omega}{(\omega_n - \omega_m)^2 + \Omega^2},$$

where $\phi(\omega_n) = \Delta(\omega_n)Z(\omega_n)$, $\Delta(\omega_n)$ is the superconducting order parameter, $Z(\omega_n)$ is the mass enhancement factor and M is the number of Matsubara frequencies ω_n used in the calculations; here and in the following $\Delta(0) = \Delta$. As input parameters I used the electronic density of states calculated in section 2.2 and listed

in table 2.2 and the Eliashberg functions coming from the same calculations and plotted in Fig. 2.6. The value of μ^* was chosen in order to reproduce the experimental T_c and kept fixed in the calculations of the specific heat jump and superconducting gap. Its values are listed in table 2.3 and vary about 10% around $\mu^* = 0.1$ for all three compounds. To obtain the specific heat, I calculated numerically the difference $\Delta F(T)$ between the normal state (N) and superconducting (S) free energy in the Migdal Eliashberg approximation: [86]

$$\begin{aligned}\Delta F(T) &= -\pi T \sum_{m=-M}^{m=M} \Big\{ |\omega_n| (Z_N(\omega_n) - 1) \\ &- \frac{2\omega_n^2 [Z_S^2(\omega_n) - 1] + 2\phi^2(\omega_n)}{|\omega_n| + \sqrt{\omega_n^2 Z_S^2(\omega_n) + \phi^2(\omega_n)}} \\ &+ \frac{\omega_n^2 Z_S(\omega_n)(Z_S(\omega_n - 1)) + \phi^2(\omega_n)}{\sqrt{\omega_n^2 Z_S^2(\omega_n) + \phi^2(\omega_n)}} \Big\}.\end{aligned}$$

After fitting the obtained numerical curve with a 12^{th} order polynomial expansion, I extracted the difference between the normal and superconducting specific heat from the second derivative of the free energy. The phonon contribution to the normal state specific heat was obtained by integrating the phonon density of states, weighted with the Einstein factor $x^2 e^x/(e^x - 1)^2$, where x is the ratio between the phonon frequency ω and the temperature T. [306]

The linear coefficient of the normal state specific heat, the BCS ratio and the critical temperature of the three $A\mathrm{Pt_3P}$ compounds are reported in table 2.3 and Fig. 2.9 shows the comparison between the calculated electronic specific heat (continuous lines) and the experimental one (symbols) from Ref. [197].

One can appreciate the almost perfect agreement for $\mathrm{SrPt_3P}$ and $\mathrm{CaPt_3P}$. For $\mathrm{LaPt_3P}$ instead, even if the agreement for T_c and the normal state properties was found to be pretty good, the experimental data for the jump in the specific heat are too noisy for a meaningful comparison. The inset of Fig. 2.9 shows the normal state

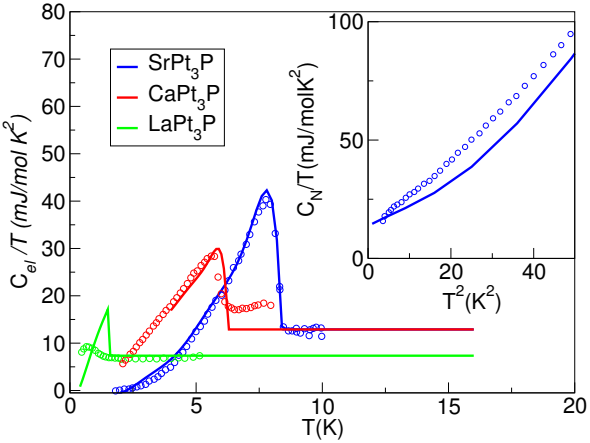

Figure 2.9: Figure from Ref. [299] Comparison between experimental data from Ref. [197] (colored dots) and Migdal Eliashberg theory (colored lines) for the heat capacities of APt_3P (A = Sr, Ca and La). Inset: Comparison between experimental data from Ref. [197] (blue dots) and first-principles calculations (blue line) for the normal state specific heat of $SrPt_3P$.

specific heat of $SrPt_3P$. The lattice specific heat is fitted with a fifth order polynomial $C_{ph}(T) = bT^3 + dT^5$, b = 1.29(1.26) mJ/mol K^4, d=8.9(13.0) mJ/mol K^6 for theoretical (experimental) data, respectively. For this compound the remarkable agreement between the theoretical curves and the experimental data, reflects the agreement between the calculated phonon spectra and the measured ones. This allow to definitely exclude any possibility of structural instability like the one found in Ref. [199].

For the superconducting specific heat of $SrPt_3P$, the single band analysis gives already a perfect agreement with the experiment, leaving in this way no route for exotic pairing as proposed by Ref. [198], unconventional superconductivity as proposed by Ref. [199] or multiband superconductivity as proposed by Ref. [197].

	γ_N (mJ/mol K^2)	T_c (K)	$2\Delta/k_B T_c$
Sr	12.9 (12.7)	8.5 (8.4)	4.06
Ca	10.3 (17.4)	6.34 (6.6)	3.66
La	7.18 (6.7)	1.56 (1.5)	3.53

	$T_c/\omega_{\ln}$	μ^*	$\Delta\ C/T_c$ (mJ/mol K^2)
Sr	0.110	0.11	29.0 (28)
Ca	0.058	0.09	16.8 (11)
La	0.013	0.11	10.5 (2)

Table 2.3: Superconducting properties of $A\mathrm{Pt_3P}$ from first-principles calculations and Migdal-Eliashberg theory; γ_N is the electronic normal-state specific heat, Δ is the value of the superconducting gap measured in K, ΔC is the specific heat jump at T_c. Experimental data from Ref. [197] are in parentheses. The Coulomb pseudopotential μ^* was fixed to reproduce the experimental T_c.

Strong coupling superconductivity is instead found in this compound as indicated by the large value of ratio $\frac{2\Delta}{k_B T_c} \sim 4.06$ but still lower than 5 as proposed by Takayama *et al.* [197] This was their strongest argument for multiband superconductivity in $\mathrm{SrPt_3P}$ and I will come back later on this point.

The agreement is also very good for $\mathrm{CaPt_3P}$ but the mass enhancement factor in the normal state results to be 1.7 times larger than the calculated one. This is probably due to the presence of additional superconducting phases during the measurement. All the other quantities are instead in very good agreement with the experiment.

For all three compounds the critical temperature was obtained by the condition $\Delta(T_c) = 0$ in eqs. (2.4) and (2.5) and a very good agreement was found for $\mu^* \sim 0.1$, which confirms the reliability of the single band analysis and gives therefore a strong indication of conventional superconductivity in these compounds.

The remarkable agreement with the experiment allows to make some conclusive statement concerning the nature of superconductivity in the $A\mathrm{Pt_3P}$ compounds. In particular, by using the α and α_1 ratios it is possible to classify these materials

and place them in the wide class of EP superconductors according to their weak moderate or strong coupling regime. In Ref. [236] Marsiglio and Carbotte have indeed shown that these ratios, for all known EP superconductors, fall on a universal curve when plotted as a function of $T_c/\omega_{\ln}$. It is then possible to better characterize the $A\mathrm{Pt_3P}$ superconductors, by comparing their α and α_1 ratios with the ones already known for other EP superconductors. I do this using the Marsiglio-Carbotte plot reported in Fig. 2.10 where the dotted and continuous lines are 2α and α_1 extracted from eqs. (2.2) and (2.3) plotted as a function of $T_c/\omega_{\ln}$.

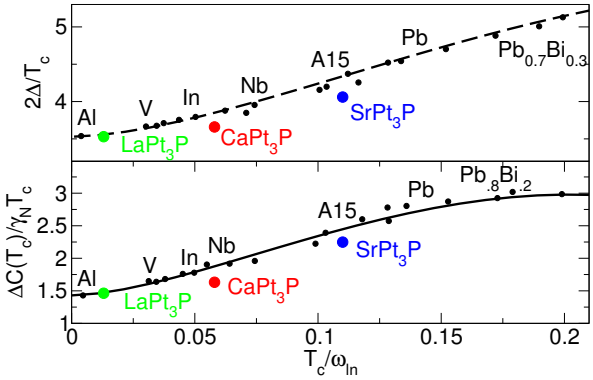

Figure 2.10: Figure from Ref. [299]. Location of the $A\mathrm{Pt_3P}$ compounds on the Marsiglio-Carbotte plots for strong-coupling superconductors. Δ is the superconducting gap at zero temperature, T_c is the critical temperature, $\Delta C(T_c)$ is the jump in the electronic specific heat at T_c, γ is the linear coefficient of the normal-state specific heat, obtained from DFT and single-band Migdal-Eliashberg theory and $\omega_{\ln}$ is the logarithmic averaged phonon frequency (see text). Lines are obtained by fitting the numerical solution of the Migdal-Eliashberg equations. In increasing order the black points correspond to the following systems: Al, V, Ta, Sn, Tl, In, Nb (Butler), Nb (Arnold), Nb (Robinson), $Nb_{0.75}Zr_{0.25}$, V_3Ga,Nb_3Al, Nb_3Ge, Pb, $Pb_{0.8}Tl_{0.2}$, $Pb_{0.9}Bi_{0.1}$, $Pb_{0.8}Bi_{0.2}$, $Pb_{0.7}Bi_{0.3}$ and $Pb_{0.65}Bi_{0.35}$. Data taken from Ref. [236] and references cited therein.

Fig. 2.10 clearly shows that the theoretical α and α_1 values obtained for all three APt$_3$P compounds are fully in line with other *EP* superconductors. In this plot LaPt$_3$P and CaPt$_3$P, with $T_c/\omega_{\ln}$=0.013 and 0.058, respectively, lie together with elemental metals, while SrPt$_3$P ($T_c/\omega_{\ln} = 0.110$) sits, together with the A15 and Chevrel compounds, at the lower end of a broad class of low-phonon, strong-coupling superconductors. At this point the very large ratio $2\Delta/k_B T_c = 5.0$ reported from Takayama *et al.*[197] can be definitely excluded for SrPt$_3$P. This value indeed definitely lies out of the general trend. More precisely, from Fig. 2.10 one sees that $2\alpha = 5.0$ corresponds to $T_c/\omega_{\ln} \sim 0.18$. Given the calculated $\omega_{\ln}$, this value leads to a $T_c \sim 14$ K and $\lambda \sim 3$ which is clearly inconsistent with the experiment. Since in Ref. [197] the value $2\alpha = 5.1$ is one of the strongest arguments for multiband superconductivity, one could think that this inconsistency comes form not having taken into account multi band effects in the calculations. However, given the very good agreement between the single band Migdal Eliashberg calculations and the experiment shown in Fig. 2.9 one has to conclude that the α model is inaccurate and retarded interaction effects must be taken into account rather than multiband effects.

2.5 Conclusions

In this chapter I presented the results of Ref. [299] about the electronic structure, phonon dispersion, electron-phonon properties and superconductivity in the recently discovered APt$_3$P superconductors. The total energy calculations presented in section 2.1 showed that these compounds are potentially very interesting since, given the small energy difference between the polar and antipolar version of their structure, they could be synthesized in both configurations realizing in this way the idea of Takayama *et al.*, [197] of studying the effect of the lack of inversion symmetry on superconductivity in a *controlled* way. The electronic structure presented in section 2.2 showed that the effect of the SOC of Pt can be neglected in studying superconductivity and the Fermi surface is significatively different in the A^{+2} (Ca^{+2},

Sr^{+2}) compounds with respect to $LaPt_3P$ due to the different electron count. This has consequences on the electron-phonon properties examined in section 2.3. I showed that the phonon dispersions are very similar among the three compounds and in contrast to what was found in Ref. [199], they are stable. The Eliashberg functions instead change sensibly going from $SrPt_3P$ to $LaPt_3P$ and the drop in the critical temperature is not given by the effect of the SOC of Pt, as proposed by Chen *et al.*, [199] but is simply due to the different electronic states involved in the expression of the Eliashberg function (different electron count). The change in the critical temperature among the A^{+2} compound is instead demonstrated to be a structural effect due to the softening of the phonon frequencies with increasing the in-plane lattice parameter. The stability of the phonon dispersions and the negligible effect of the SOC of Pt rules definitely out any possible route for unconventional superconductivity. An *a posteriori* test of the validity of this analysis is given in section 2.4 where I used the calculated phonon DOSs and Eliashberg functions to calculate thermodynamical observables to be compared with the experiment. I did this in the single band Migdal Eliashberg approximation. The perfect agreement between the experimental data and the calculated curves rules out also the possibility of multiband superconductivity and allows to classify all the three APt_3P compounds according to their different superconducting regime. In conclusion the APt_3P superconductor result to be a textbook example of electron-phonon superconductors. The electron-phonon coupling is weak in $LaPt_3P$ with respect to $SrPt_3P$ and $CaPt_3P$ because of different electron count. In the A^{+2} compounds superconductivity originates from the coupling of the Pt(1) in-plane breathing modes with the Pt(1) mainly in plane electronic states and the frequency of these breathing modes changes by changing the in plane lattice constant. This suggests that in this case the EP coupling can be tuned by applying pressure while in the former case it can be increased by doping. Moreover it is important to stress that changing in an appropriate way the synthesis conditions or partial replacement of P with Si, one could synthesize these compounds in the $CePt_3Si$ kind of structure with dramatic consequences on the symmetry of the order parameter.

While an extensive study of this effect for these materials is beyond the scope of

the thesis, in the next chapter I will analyze the case of hole doped CuBiSO. In this material the presence of a ferromagnetic instability near by conventional $s-$wave EP superconductivity, breaks the inversion symmetry and can tune the superconducting order parameter from singlet to triplet p-wave type.

2.6 Technical details

The electron-phonon calculations presented in this chapter employ density functional perturbation theory,[202] within the generalized gradient approximation (GGA) as implemented in the Quantum-ESPRESSO package, [251, 307] while the band structure shown in Figs. 2.4 and 2.5 were obtained with the linearly augmented plane wave methods, [308] as implemented in the Wien2K code. [309] The structures were fully relaxed in GGA such that the force on each atom is less than 10^{-5} Ry/Bohr, and the results of the structural relaxation were tested with the all-electron code Wien2k, which employs the full potential linear augmented plane wave method. [308, 309] The electron-phonon calculations in section 2.3 were done using ultrasoft pseudopotentials [310] and basis set cutoffs of 40 Ry and 400 Ry for wave function and charge density, respectively. The Brillouin zone integration was done by using an $8 \times 8 \times 8$ grid in the self-consistent calculations, while a denser $16 \times 16 \times 16$ grid was used in the electron-phonon coupling calculations. The dynamical matrices were calculated on an $8 \times 8 \times 8$ grid, and phonon dispersions and DOS were then obtained by Fourier interpolation.

Chapter 3

Spin fluctuations and electron-phonon coupling in superconducting $Cu_{1-x}BiSO$

In this chapter I report the results of Ref. [311] on the interplay between magnetism and superconductivity in hole-doped CuBiSO. For this material ab-initio *calculations predict a ground state characterized by weak ferromagnetism and electron-phonon superconductivity with a high critical temperature $T_c = 33$ K. The experimental sample is instead non magnetic and its $T_c = 5.8$ K. In order to bring the theoretical results in agreement with experiment, ferromagnetic spin fluctuations must be taken into account by modeling the electron paramagnon interaction in a semi-phenomenological way. The ad-hoc model I derive treats both doping and the Stoner parameter as adjustable parameters to study the competition of magnetism, singlet and triplet superconductivity in the phase diagram.*

Introduction

In the previous chapter, I studied the superconducting properties of a textbook example of electron-phonon (EP) superconductors. In this way I could show how effective is DFT in reproducing the experiment and how extremely reliable is density functional perturbation theory (DFPT) within the Migdal Eliashberg approximation in describing EP superconductivity. [7]

However, while for EP superconductors such a detailed first-principles theory, albeit computational expensive, has been developed in the last 20 years, [12] for spin fluctuations (SF) superconductors, even if the earliest works date back to the 60's, [94, 99] the state of the art is far less advanced. [270] Therefore SF are usually taken into account as a phenomenological detrimental agent against EP superconductivity. [312] In fact in itinerant systems close to a quantum critical point (QCP), like Pd or ZrZn, [51, 234, 313] ferromagnetic SF (paramagnons) compete against EP coupling in the singlet channel, making the material non superconducting or reducing substantially the superconducting T_c. [233, 312, 314] On the other hand, since in the triplet channel EP coupling cancels out, strong ferromagnetic SF could also be responsible for triplet superconductivity, as it was proposed for Sr_2RuO_4. [62] In any case a quantitative theory is still missing.

As for the case of SF superconductivity, also the problem of itinerant magnetism, where spin fluctuations tend to reduce the tendency to static magnetism, has not yet been completely clarified. [17]

In this chapter I show the results of Ref. [311] concerning the specific case of hole-doped CuBiSO (HCBSO). This compound was synthesized for the first time by Hiramatsu *et al.* [226] and superconductivity with a $T_c = 5.8$ K was reported by Ubaldini *et al.* [225] under 10 % of Cu vacancies. Due to the vicinity to a ferromagnetic instability, superconductivity was conjectured to be driven by spin fluctuations and being of unconventional triplet p-wave type. [200] However this proposal was not supported by any quantitative studies and the electron-phonon coupling was never calculated for this material. Moreover, the relatively high experimental T_c and the strong Cu-d S-p hybridization which characterizes the band

structure could be, in principle, compatible also with EP mediated superconductivity.

In the following I present the calculated electron-phonon coupling and a quantitative theory for the effect of spin fluctuations on superconductivity both in the singlet channel, where they compete against phonons, and in the triplet channel, were they are responsible for superconductivity. Due to the importance of doping in inducing superconductivity, I take into account this variable within the rigid band approximation (RBA) in order to make the EP calculations feasible. The effect of SF is evaluated using a spin density functional version of the random phase approximation (RPA).

This is the first quantitative approach for the competition between EP coupling and spin fluctuations in superconducting HCBSO.

The chapter is structured in the following way. In section 3.1 I analyze the electronic structure in relation to both the tendency to magnetism and the possibility of having EP superconductivity in Cu_{1-x}BiSO. Since introducing Cu vacancies into the system is equivalent to dope it with holes, in the following I will use indifferently the acronym HCBSO and Cu_{1-x}BiSO. Concerning the magnetic properties of this material, I also give an estimate of the Cu-*d* S-*p* hybridization contribution in reducing the Stoner parameter of atomic Cu. However this effect is not sufficient to bring the doped material out of the ferromagnetic instability, therefore SF must be invoked in order to justify the absence of magnetism in the experiment.

In section 3.2, I calculate *ab-initio* the EP properties of Cu_{1-x}BiSO. Because of the importance of hole doping in turning CuBiSO into the metallic phase and, the experimental uncertainty about the doping level, I take into account the doping in the RBA. The EP coupling is found to be overestimated with respect to the experiment. Indeed the calculated critical temperature is found to be 6 times larger than the experimental one. This calls again for an important role of ferromagnetic SF in reducing the critical temperature in the singlet channel. The EP matrix element is found to be almost doping-independent and this allows to obtain a simplified expression for the doping dependence of the EP coupling constant.

Given the important role of SF in reducing both the tendency to static magnetism and to EP superconductivity, in section 3.3 I give an approximate expression for

the electron paramagnon coupling constant in the singlet channel as a function of doping and Stoner parameter.

Finally in section 3.4, I study the phase diagram of $Cu_{1-x}BiSO$ as a function of doping and Stoner parameter. In this way I can draw some conclusions, in section 3.5, about the competition between magnetism and superconductivity in HCBSO. Technical details are presented in section 3.6.

3.1 Electronic structure and weak ferromagnetism

The crystal structure of CuBiSO is the ZrCuAsSi-type one (space group $P4/nmm$). The $\left[Cu^{+1}S^{-2}\right]^{-1}$ and $\left[Bi^{+3}O^{-2}\right]^{+1}$ layers alternate along the c axis and play the role to the Fe-Pn and Re-O one in Fe pnictides, where Re is rare earth and Pn is a pnictogen atom (As, P). Cu(O) atoms form a square lattice surrounded by distorted S(Bi) tetrahedra as shown in Fig. 3.1 (a).

The unit cell is tetragonal and contains two formula units - see Fig. 3.1 (b). The lattice parameters are $a = 3.8726\ \mathring{A}$ and $c = 8.5878\ \mathring{A}$. [225] Since Ref. [225] reports superconductivity but does not give the internal parameters, in the following calculations I use the internal coordinates given by Ref. [226]: $Z_S = 0.6710$ and $Z_{Bi} = 14829$. On the other hand the sensitivity of the bandstructure to these parameters is very small in comparison to the approximations I will adopt later on in this chapter. [1]

The electron count of CuBiSO can be understood from a simple chemical point of view, by looking at the electronic configurations and oxidation numbers in table 3.1.

S and O take two electrons each for closing their p shells. These electrons are provided from 4s and 6p orbitals of Cu and Bi respectively. In this way all the d orbitals of Cu are completely filled and the p orbitals of Bi remain empty.

A sketch of the calculated electronic structure and electronic DOS of CuBiSO, along the path indicated in Fig. 3.1 (c), is shown in Fig. 3.2 for a wide energy

[1] This can be seen by comparing the bandstructure obtained in literature for this compound. [200, 226, 315] with the one presented in section 3.1.

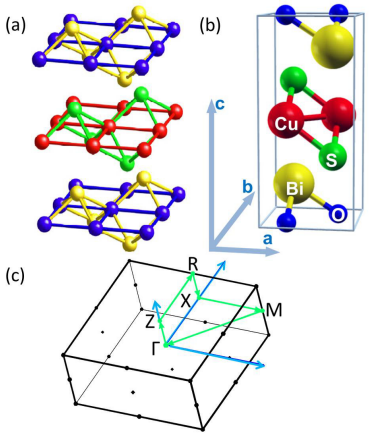

Figure 3.1: ZrCuAsSi-type crystal structure of CuBiSO. (a) The Cu(red)-S(green) layers and Bi(yellow)-O(Blue) ones alternate along the c axis. The Cu (O) atoms form square lattice in which the Cu(O) atoms are tetrahedrally coordinated with the S(Bi) ones. (b) The unit cell of CuBiSO contains two formula units per unit cell. (c) Path (green line) in the Brillouin zone along with the band structure is plotted. The reciprocal lattice vectors (blue arrows) are also marked.

range around the valence band maximum (VBM). The stoichiometric compound is indeed found to be a band insulator with an indirect band gap $\Delta \approx 0.5$ eV. This is in agreement with previous calculations. [200, 226, 315] The VBM occurs along the $\Gamma - M$ line and this is chosen as the zero of the energy in the following.

As expected from the simple chemical analysis, the O p orbitals are all below the Fermi level (all filled) while the Bi ones form the conduction band (all empty). Below the VBM the band structure of CuBiSO is very similar to that of the Fe pnictides. 16

Element	Electronic configuration	Oxidation number
Cu	$3d^{10}\ 4s^1$	+1
Bi	$6s^2\ 6p^3$	+3
S	$2s^2\ 2p^4$	-2
O	$3s^2\ 3p^4$	-2

Table 3.1: Electronic configuration and oxidation numbers of Cu, Bi, S and O in stoichiometric CuBiSO.

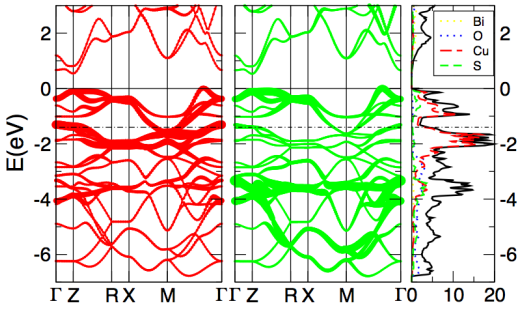

Figure 3.2: GGA band structure of CuBiSO from Ref. [311], plotted along the path shown in Fig. 3.1 (c) and shaded according to the partial Cu d_{xz+yz} (*left*) and S p_{x+y} (*right*) characters: the continuous and dashed-dotted lines mark respectively the position of the Fermi level in the undoped compound and that corresponding to the filling d^6 of Fe pnictides (*see text*); the corresponding DOS is also shown.

bands, completely derived by the Cu d and S p states, can be identified and grouped into three main regions: a low-lying region, centered around -5 eV, where 6 bands have essentially S p character; an intermediate region, from -3 eV to -1. eV, where 6 Cu d bands are located and are separated by a pseudogap from the last region,

where the remaining 4 bands with mixed S p Cu d character sit.

From the DOS plotted for several atomic characters in Fig. 3.2 it appears indeed that, for a wide energy range ($\sim$ 7 eV) below the VBM, the bandstructure is completely derived from the Cu d and S p states. They strongly hybridize and form bonding and antibonding states at energy $E \sim -3.5$ eV and $E \sim -1$ eV respectively.

The antibonding states originate mainly from the S p_{x+y} orbitals hybridized with Cu d_{xz+yz} and $d_{x^2-y^2}$ ones, and from S p_z orbitals hybridized with Cu d_{xz+yz} and d_{xy} ones. The bonding states are instead mainly originated from the S p_z orbitals hybridized with the Cu d_{xy} orbitals and from the S p_{x+y} orbitals hybridized with Cu d_{xz+yz} ones. Finally the non bonding states of Cu are centered at $E \sim -2$ eV and are mainly derived from the Cu d_{xz+yz}, d_{xy} and d_{z^2} orbitals.

I describe now the whole band structure, and the expected physical properties, within a rigid band scheme. Where the Cu d-S p hybridization is strong one expects strong EP coupling while, whenever the Cu d character is predominant, a strong tendency to magnetism is expected. [200] Starting from zero energy and imagining to move "rigidly" the Fermi level along the band structure and DOS for $x \leq 0$, the reader would meet a region, close to the VBM, where the states are strongly antibonding and the DOS has a pronounced peak due to the flat band along the $\Gamma - M$ line. This region would be then characterized by both a large electron lattice susceptibility and a possible tendency to ferromagnetism. Indeed, due to the large Stoner parameter of Cu ($I_{Cu} \approx 0.9$ eV), magnetism is favored through the entire Cu d bands. However, pure CuBiSO is an insulator and Cu is in a nominal d^{10} state (thus non magnetic), therefore doping is crucial to drive the system into the magnetic (and the superconducting) instability. Moving E_{F} further down, the electron lattice susceptibility will be substantially decreased due to the reduced degree of p-d hybridization, and ferromagnetism will be suppressed by the vicinity to the pseudogap which separate the Cu-S antibonding states from the Cu d non bonding ones. In this range of energies antiferromagnetism is more favored. At $E \sim -1.4$ eV indeed, the electron filling, marked by the dashed-dotted line in Fig. 3.2, is d^6 and the low-energy band structure of Fe pnictides can be individuated. [72] The Cu d_{xz} and Cu d_{yz} bands -degenerate due to the tetragonal

symmetry- are highlighted in the left panel of Fig. 3.2 as "fat bands". These bands, in the energy range marked by the dashed-dotted line, form two almost degenerate electron pockets around the M point nested with the two hole-like pockets located around the Γ point. This kind of nesting favors the antiferromagnetic stripe order with the spins ferromagnetically aligned along the a axis and antiferromagnetically aligned along the b axis. This is, actually, the same kind of instability that the reader will encounter in chapter 4 when talking about LaFePO. [53, 54] Shifting even further down the Fermi level, the electron lattice coupling would be enhanced again due to the bonding character of the states around $E \sim -3$ eV.

Since experimentally the superconducting instability appears in $Cu_{1-x}BiSO$ under Cu vacancies ($x = 0.1$), and there is a certain degree of uncertainty about the doping level in the experimental sample, [225] in the following I will realize this idea of shifting the Fermi level by making calculations in RBA for $0 < x \leq 0.5$ (doping up to 1 hole per unit cell). This approximation is justified because the considered levels of doping are very small, and the Fermi level moves within a single, doubly-degenerate band, whose character does not change appreciably in the energy range explored. Since the character of the band doesn't change, both the magnetic and the EP properties stay constant as a function of doping. [2]

I focus the discussion first on the magnetic properties and then, in the next section, on the electron-phonon coupling.

The top of Fig. 3.3 shows a blow-up of the band structure of CuBiSO around zero energy. Increasing x in RBA corresponds to move the Fermi level towards negative energies. The stoichiometric compound, as already said, appears to be a band insulator and is therefore non magnetic. Increasing x, also the DOS at the Fermi level $N_0(x)$ increases, up to the peak ($N_0(0.1) = 1.93$ states/eV/spin) caused by the flat band located at energy corresponding to hole doping $x = 0.1$ and marked by the red dotted line. Increasing the doping further, $N_0(x)$ decreases again. The red dashed line marks the energy corresponding to the lowest filling ($x = 0.5$) considered in my calculations.

[2] An "*a posteriori*" test will be given later in the chapter when considering the doping dependence of the Stoner parameter I and of the EP matrix element V_{ep}.

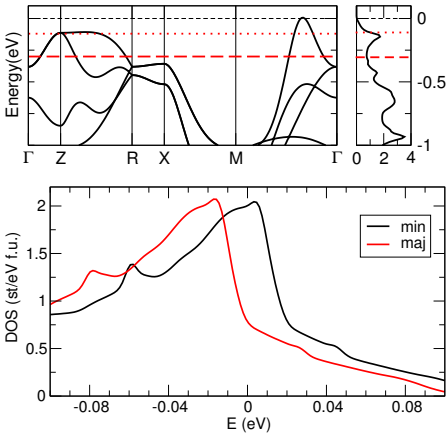

Figure 3.3: *top*: A blow-up of the low-energy band structure of CuBiSO; the dotted and dashed red lines mark the position of the Fermi level, corresponding to a hole doping $x = 0.1$ and $x = 0.5$ respectively, in RBA. *bottom*: GGA Majority (red) and minority (black) spin DOS in the ferromagnetic state for Cu_{1-x}BiSO for the experimental value of $x = 0.1$, calculated in virtual crystal approximation (VCA). The magnetic moment for this value of x is $m = 0.03\ \mu_B$/ Cu and the splitting between majority and minority DOS is $\Delta E \approx 20$ meV. The Stoner parameter is obtained by the relation $I = \Delta E/m = 0.67$ eV.

Under hole doping the Cu state is reduced from d^{10} to d^9, it is therefore magnetic and its large Stoner parameter in the atomic configuration ($I_{Cu} = 0.9$ eV) would bring the system well above the Stoner criterion for ferromagnetism $N_0(0.1) * I_{Cu} = 1.74$. For $x \geq 0.1$ the ground state of the system is indeed ferromagnetic both in GGA and in LSDA, while $Cu_{0.9}$BiSO experimentally doesn't show instability against any kind of commensurate antiferromagnetism. [200] On the other hand, for $x = 0.1$ the magnetic moment in GGA is $m = 0.03\ \mu_B$ and the gain in energy calculated from fixed spin moment calculations was found to be very small. [200] Moreover,

as it was pointed out before, the bandstructure is characterized by a strong Cu d-S p hybridization which points toward a dilution of the Stoner parameter. Indeed if several atoms contribute to the states at the Fermi level, each one with a partial DOS ν_i, the total Stoner parameter is $I = \sum_i I_i \nu_i^2$ where I_i is the individual (quasiatomic) Stoner parameter. [52, 63] It is therefore important, in order to understand the magnetic properties of HCBSO, to give a more reliable estimate of I, also because this compound was suggested to be a new spin fluctuations superconductor. [200]

The effect of hybridization in reducing the Stoner parameter I can be estimated by calculating it from the split between the majority and minority bands in the ferromagnetic state. The GGA splitting in VCA is shown for $x = 0.1$ at the bottom of Fig. 3.3. When the magnetic interaction is turned on, the bands spin polarize and split by a quantity ΔE which, for small values of the self-consistent magnetic moment m, is proportional to m and the proportionality constant is the Stoner parameter I. In my calculations the GGA Stoner parameter is $I = 0.67$ eV, larger than the LSDA one $I = 0.53$ eV, as expected for itinerant magnetism [51, 52, 57]. In both cases $I < I_{Cu}$ which confirms the expected importance of the role played the Cu-d S-p hybridization in affecting the magnetic properties of HCBSO. Moreover in virtual crystal approximation I is found to be doping independent and this gives an "*a posteriori*" test of the validity of RBA.

Both the LSDA and GGA values of the Stoner parameter are overestimated with respect to experiments. Indeed the experimental sample is non magnetic. This is typically observed in compounds close to a magnetic quantum critical point (QCP), where long wavelength (spin) fluctuations are strong and suppress the value of the magnetic moment. [263]

These spin fluctuations can couple to electrons and provide a mechanism for superconductivity, alternative to phonons. In fact SF near a ferromagnetic instability are in general pair-breaking in the singlet channel, *i.e.* they suppress the attractive coupling to phonons, and pairing in the triplet channel. This mechanism for the origin of superconductivity in HCBSO was conjectured in Ref. [200] and in this respect my calculations confirm the importance of a mechanism, beyond mean-field, necessary to explain the magnetic properties of this material but they are not suf-

ficient to answer the most important question: **Is $Cu_{0.9}$BiSO a spin fluctuations mediated superconductor?** In order to answer this question indeed, one has to calculate the electron paramagnon coupling constant. Even if there is not yet a standard theory for calculating it, in section 3.3 I will use the spin density functional version of the RPA in order to give an approximate expression for this quantity. In the next section I will instead focus the attention on the EP properties. Indeed the important role played by the Cu-d S-p hybridization and the relatively high experimental T_c make the EP properties worth exploring.

In this section I showed that DFT calculations found stoichiometric CuBiSO to be a band insulator whose band structure is characterized by a strong Cu d-S p hybridization. When holes are introduced into the system the Fermi level moves into a double degenerate flat band with mixed Cu d_{xz+yz} and S p_{x+y} character. This causes a peak in the DOS at E_F at the experimental doping $x = 0.1$ which makes the system slightly unstable against ferromagnetism, even if the Stoner parameter is reduced by the hybridization. The fact that so far experiment have not shown any trace of static magnetism calls for a significant role of spin fluctuations in reducing the tendency to magnetism. I will come back later to this point in the next sections. Moreover the problem of finding a reliable description of magnetism in itinerant magnets close to a QCP will be the focus of chapter 5.

3.2 Phonons and electron-phonon properties

In order to have a clear idea of the ground state properties of superconducting HCBSO I analyzed, in the previous section, the electronic properties, and I found that spin fluctuations could play an important role in this material, above all in reducing the tendency to magnetism and, may be also, in driving superconductivity. [200]

On the other hand, the relatively high experimental T_c of $Cu_{0.9}$BiSO, the fact that EP superconductivity was excluded only by means of qualitative arguments [200] and the strong Cu d-S p hybridization found in the previous section, make the

phonon and electron-phonon (EP) properties of HCBSO worth calculating *ab-initio*. Furthermore, given the doping uncertainty in the experiment, is also important to take into account the doping dependence of these quantities. Therefore in this section I show the results of Ref. [311] concerning the vibrational properties of $Cu_{1-x}BiSO$ as a function of doping x in RBA. For the reasons explained in the previous section -*i.e.* the doping value is small and the band character remains constant under hole doping-, indeed, I suppose the RBA to be valid.

Note that calculating the EP coupling selfconsistently for each doping, would be computationally prohibitive. Indeed, as explained below, the calculations imply an integration over the Fermi surface and a double δ function is also involved. Since the Fermi level moves into a flat band, the calculations could become strongly dependent on the electron filling and the resolution needed in $\mathbf{k}$ space could make the computational load too large also for an high-performance computer. In order to make the calculations feasible I assume the RBA to be valid and I verify *a posteriori* that this is the case by looking at the ratio between the EP coupling constant and the DOS at the Fermi level as a function of doping. This gives indeed an indication of the doping dependence of the EP matrix element.

Within RBA the partial phonon density of states (PDOS) used to calculate the EP properties is calculated only for the stoichiometric compound while the doping dependent EP coupling constant $\lambda_{\rm ep}(x)$ is computed from the integral of the first inverse moment of the Eliashberg function $\alpha^2F(\omega,x)$ obtained by averaging the EP matrix element $g^{\nu,n,m}_{\mathbf{k},\mathbf{k}+\mathbf{q}}(x)$, which in principle depends on x, over the doping dependent Fermi surface $\delta(\epsilon^n_{\mathbf{k}},x)$ obtained by a rigid-band shift corresponding to the doping level. Namely:

$$\alpha^2F(\omega,x)=\frac{1}{N_0(x)}\sum_{\mathbf{k},\mathbf{q},\nu,n,m}\delta(\epsilon^n_{\mathbf{k}},x)\delta(\epsilon^m_{\mathbf{k}+\mathbf{q}},x)|g^{\nu,n,m}_{\mathbf{k},\mathbf{k}+\mathbf{q}}(x)|^2\delta(\omega-\omega_{\nu\mathbf{q}}) \qquad (3.1)$$

and $\lambda_{\rm ep}(x)=2\int_0^\infty d\Omega\alpha^2F(\Omega,x)/\Omega$.

The electron-phonon properties of $Cu_{1-x}BiSO$ are summed up in Fig. 3.4. The upper panel shows the PDOS of the undoped compound. The spectrum extends

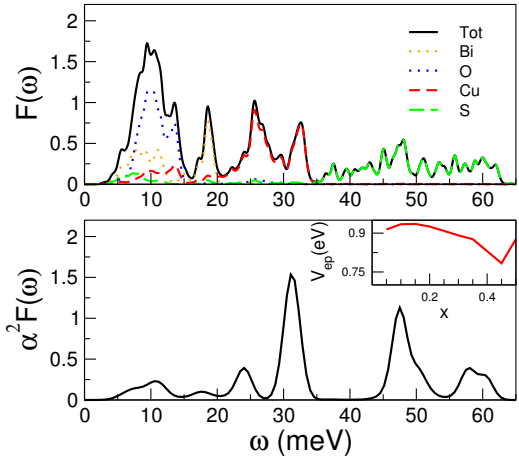

Figure 3.4: From top to bottom: Partial phonon density of states (PDOS), Eliashberg spectral function for $x = 0.1$, in RBA, and (inset) ratio between the coupling constant and $N_0(x)$ as a function of doping.

up to 65 meV; modes involving vibrations of the Bi-O layers are concentrated at energies $\leq$ 20 meV, while modes involving the Cu-S layers are found at higher energies. The light S atoms give rise to a very broad feature in the DOS, from 35 to 65 meV.

For all values of doping, I found that only two groups of phonon modes, corresponding to the out-of-plane vibrations of the Cu-S layers, have sizable EP matrix elements $g^{\nu,n,m}_{\mathbf{k},\mathbf{k}+\mathbf{q}}(x)$: these give rise to two narrow peaks in $\alpha^2F(\omega)$, centered at 32 meV and 48 meV. As an example, the $\alpha^2F(\omega, x = 0.1)$ is shown at the bottom panel of Fig. 3.4. In my calculations I found that the shape of the Eliashberg function, and hence the spectral distribution of the EP coupling, does not depend on doping for $x \leq 0.5$. Therefore the total EP coupling constant $\lambda_{\text{ep}}(x)$ depends on doping

only through the value of the DOS at E_F $N_0(x)$. In the inset of the bottom panel of Fig. 3.4 I plotted the ratio $V_{ep}(x)$, between $\lambda_{ep}(x)$, numerically calculated from eq. (3.1), and $N_0(x)$. V_{ep} appears to be constant and ~ 0.9 eV spin f.u. in the entire range of doping considered ($x \leq 0.5$). Together with a simplified expression for the EP coupling constant, this gives also a further confirmation of the validity of the RBA. I thus rewrite $\lambda_{ep}(x)$ as:

$$\lambda_{ep}(x) = N_0(x) V_{ep}. \tag{3.2}$$

For $x = 0.1$, $N_0(x = 0.1) = N_0 = 1.93$ *st/eV spin f.u.*, $\lambda_{ep}(x = 0.1) = \lambda_{ep} = 1.74$, $\omega_{ln} = 263$ K and T_c, estimated from Mc Millan's formula (with $\mu^* = 0.1$):

$$T_c^{McM} = \frac{\omega_{ln}}{1.2} \exp \frac{-1.04(1+\lambda_{ep})}{\lambda_{ep} - (1+0.62\lambda_{ep})\mu^*} = 33 \text{ K}. \tag{3.3}$$

This value is sensibly larger than the experimental value $T_c = 5.8$ K, therefore a deeper understanding is needed. Indeed this discrepancy is much larger than the typical uncertainity of T_c in similar calculations, coming from the computational uncertainity on λ_{ep} - typically 10 %, or from the arbitrary value of μ^* in the McMillan formula. In fact, keeping all the parameters in eq. (3.3) the same, I would have to use $\lambda_{ep} = 0.6$ to reproduce the experimental T_c.

The *ab-initio* parameters involved in formula (3.3) are the coupling constant λ_{ep} and the logarithmic average of the phonon frequencies ω_{ln}. Using eq. (3.2) end eq. (3.3) it is possible to separate the contribution to the critical temperature coming from phonons (by means of ω_{ln}), electrons (via N_0) and the interaction among them (through V_{ep}). Therefore in table 3.2 I report the material trend involving the mentioned parameters for several materials. From top to bottom I start with magnetic materials like LaOFeAs and Pd. In these materials SF play against EP superconductivity, and the EP coupling is very weak due to the small value of V_{ep}. Then come Al, Nb and Pb which are "classical" example of EP superconductors respectively in the weak, moderate and strong coupling regime. Finally I examine CuBiSO and then MgB_2 which is the EP superconductor with the highest critical

material	λ_{ep}	N_0	V_{ep}	$\omega_{\ln}(K)$	μ^*	$T_c^{McM}(K)$
LaOFeAs [4]	0.21	2.100	0.1	206	0.00	< 0.4
Pd [12]	0.35	1.255	0.3	180	0.10	0.3
Al [12]	0.44	0.202	2.2	270	0.12	1.2
Pb [12]	1.68	0.253	6.6	65	0.17	6.2
Nb [12]	1.26	0.750	1.7	185	0.21	10.5
CuBiSO	1.74	1.93	0.9	263	0.10	33.0
MgB_2[15]	0.87	0.355	2.5	719	0.10	39.7

Table 3.2: Different values of the quantities involved in the McMillan formula (3.3) for different materials listed with respect the critical temperature. N_0 is the DOS at E_F expressed in (*st./eV spin f. u.*), V_{ep} is the ratio betweenλ_{ep} and N_0 and is expressed in (*eV spin f.u./st.*)

temperature. In magnetic materials, the major contribution to the EP coupling comes from the DOS at the Fermi level. However this is a *fictitious* contribution. Indeed an high value of N_0 makes the material highly sensitive to several interaction channels (*e.g.* EP superconductivity, magnetism and, as I will show later on, interaction with SF) sometimes also competing against each other. For EP superconductors like Al, Nb and Pb instead, even if there are few electrons at the Fermi level available for the interaction, the values of V_{ep} are at least one order of magnitude larger than the previous ones.

Once the instability channel is selected, $\omega_{\ln}$ enters as a prefactor in the formula for the critical temperature. For this reason Pb has a lower T_c then Nb even if λ_{ep} is $\sim 30\%$ larger. In this respect, the quite substantial value of V_{ep} and the very large value of $\omega_{\ln}$ make MgB_2 to have the highest T_c among the EP superconductors.

CuBiSO has the smallest V_{ep} among the EP superconductors, while it has the highest value of N_0. This means that is very likely unstable but the EP channel may be or may not be the favored one. For this reason, even if its T_c associated with EP superconductivity is almost the highest among the considered compounds, SF driven superconductivity cannot been yet excluded for this material.

This can be rationalized *a posteriori* thinking about the nature of the bonds involved. In MgB_2, like in B-doped diamond, the bands involved in superconductivity are indeed the bonding $p-p$ σ bands which have a large EP matrix element and no tendency to magnetism. [14, 15] While the p-d bands involved in the superconductivity of CuBiSO have quite substantial V_{ep} but bring also the tendency to magnetism. For these reasons in HCBSO the SF origin of superconductivity cannot be completely excluded.

In this section I showed that the EP properties of HCBSO are dominated by the Cu-S out-of-plane vibrational modes. These modes are indeed sensibly coupled to the electrons and hardly doping dependent. The Eliashberg function is indeed characterized by two high peaks in correspondence of the out-of-plane vibrations of the Cu-S layer and is doping independent. This allows to write the doping dependence of the EP coupling constant in a particularly simple way. The critical temperature, calculated using the *ab-initio* parameters, is ~ 6 times larger than the experimental one and the biggest contribution to λ_{ep} comes from the large value of the DOS at the Fermi level.

This, together with the findings of section 3.1, indicates that in HCBSO the suppression of phonon-mediated pairing comes from the strong ferromagnetic spin fluctuations (paramagnons), due to the vicinity to a ferromagnetic QCP. The high value of $N_0(x)$ indeed, places this compound in a region of the phase space very sensitive both to the magnetic and to the EP superconducting instability. In both cases fluctuations beyond mean field must be invoked in order to better understand the underlying physics. In the next section I will therefore try to give an estimate of the electron paramagnon coupling in order to address the reduction of such a big EP coupling and to understand the origin of superconductivity in HCBSO.

3.3 Paramagnons and electron-paramagnon coupling constant

The conclusions of sections 3.1 and 3.2 indicate that in Cu_{1-x}BiSO *ab-initio* calculations performed in LSDA and GGA overestimate both the tendency to static magnetism and the electron-phonon superconducting T_c. The simplest hypothesis that gives reasons for these two effects happening at the same time, is that HCBSO is close to a QCP and strong spin fluctuations, on one hand reduce the Stoner parameter, on the other hand reduce the EP coupling constant.

In order to describe in a quantitative way the competition between the magnetic driven superconductivity and the EP one, gaining in this way a better understanding on the origin of superconductivity in Cu_{1-x}BiSO, one has to evaluate the electron-paramagnon coupling constant λ_{SF}. Such an interaction in metals was studied with respect to possible superconductivity in Pd and applied later in Sr_2RuO_4. [62, 99] The first approach appears more qualitative and not very suitable for applications to real materials. The second one makes use of the informations coming from DFT but does not give a general "recipe". Indeed several effects must be taken into account, overall the fact that part of the electron-paramagnon interaction is already included in the actual implementations of DFT. For this reasons, I will construct a theory for λ_{SF} in HCBSO which is an RPA version of the LSDA. In this way I will be able to express the coupling constant λ_{SF} in terms of the Stoner parameter I which is the parameter that governs the magnetic interaction in LSDA. However, in my calculations the Stoner parameter is overestimated with respect to experiment. Therefore I will leave the latter quantity as a free parameter in the following.

Since the electron paramagnon coupling constants for singlet λ^s_{sf} and triplet (λ^t_{sf}) superconductivity are simply proportional to each other ($\lambda^t_{sf} = \frac{1}{3}\lambda^s_{sf}$), in the following I will concentrate myself only on the singlet channel. [316]

The irreducible interaction in the particle-particle singlet channel, evaluated

within RPA, in the paramagnetic case [99] is given by:

$$V^{s}_{sf}(\mathbf{q},\omega) = -I - \frac{3}{2}\left(\frac{I^2\chi_0(\mathbf{q},\omega)}{1-I\chi_0(\mathbf{q},\omega)}\right) - \frac{1}{2}\left(\frac{I^2\chi_0(\mathbf{q},\omega)}{1+I\chi_0(\mathbf{q},\omega)}\right), \tag{3.4}$$

where $\chi_0(\mathbf{q},\omega)$ is the non interacting spin susceptibility at frequency ω and momentum trasferred $\mathbf{q}$. Close to a magnetic instability, the second term dominates so that eq. (3.4) reduces to: [316]

$$V^{s}_{sf}(\mathbf{q},\omega) = -\frac{3}{2}\frac{I^2\chi_0(\mathbf{q},\omega)}{1-I\chi_0(\mathbf{q},\omega)} = -\frac{3}{2}I^2\chi^{RPA}(\mathbf{q},\omega) \tag{3.5}$$

where $\chi^{RPA}(\mathbf{q},\omega)$, defined by:

$$\chi^{RPA}(\mathbf{q},\omega) = \chi_0(\mathbf{q},\omega) + \chi_0(\mathbf{q},\omega)I\chi^{RPA}(\mathbf{q},\omega), \tag{3.6}$$

is the interacting spin susceptibility evaluated within RPA. Here I assume I to be independent both of $\mathbf{q}$ and of the band indices. The ferromagnetic instability happens when $\lim_{(\mathbf{q},\omega)\to(\mathbf{0},0)}\chi_0(\mathbf{q},\omega)I = N_0 I = 1$ *i.e.* the Stoner condition is fulfilled.

The electron paramagnon coupling constant in the singlet channel λ^{s}_{sf}, is defined as an average over the Fermi surface of $V^{s}_{sf}(\mathbf{q},0)$ times the DOS at the Fermi level N_0:

$$\lambda^{s}_{sf} = -N_0\int_0^\infty \frac{\langle \mathrm{Im}\, V^{s}_{sf}(\mathbf{q},\omega)\rangle}{\omega}d\omega = -N_0\,\mathrm{Re}\langle V^{s}_{sf}(\mathbf{q},0)\rangle, \tag{3.7}$$

where the brackets $\langle\ \rangle$ indicate an average of the momentum transfer over the (spherical) Fermi surface. [94, 99, 316] A common approximation is to take $\chi_0(\mathbf{q},0) \equiv \chi_0(\mathbf{q}) = N_0 u_\sigma(\mathbf{q})$ where $u_\sigma(q)$ is the Lindhard function. [94, 99] This implies the underlying assumption of spherical Fermi surface.

In order to calculate λ^{s}_{sf} for HCBSO, I could applying the scheme illustrated above with the approximation of a spherical Fermi surface, and inserting in eq. (3.7) the value of N_0 coming from LDA. In this way however, I would obtain a λ^{s}_{sf} greatly overestimated. Indeed, as it can be seen from Fig. 3.5, the Fermi surface of HCBSO, evaluated in LDA is far from being spherical and the LDA susceptibility doesn't

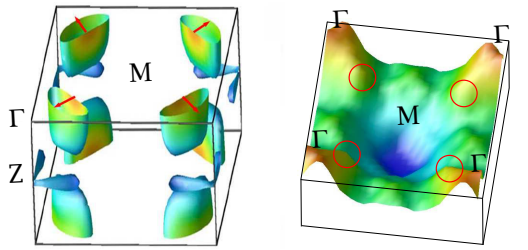

Figure 3.5: *Left*: Fermi surface of $Cu_{0.9}$BiSO adapted form Ref. [200]. The four small red arrows indicated the nesting vectors $\bar{\mathbf{q}} = (\pm\pi/8, \pm\pi/8)$. *Right*: Real part of the LDA spin susceptibility $\chi_0(\mathbf{q}, 0)$ for $Cu_{0.9}$BiSO. The large peak at $\mathbf{q} = \mathbf{0}$ is due to intraband processes. The four smaller peaks at $\bar{\mathbf{q}} \sim (\pi/8, \pi/8)$, emphasized by the red circles, are due to interband transitions.

look as the Lindhard function at all. On the other hand, performing numerically the integral would be computational expensive without giving a sizable gain in accuracy, due to the uncertainty on doping and on the Stoner parameter I. On the other hand, in HCBSO the LDA spin susceptibility has a large peak at $\mathbf{q} = \mathbf{0}$, due to intraband processes, and four smaller peaks at $\bar{\mathbf{q}} \sim (\pi/8, \pi/8)$, due to interband transitions; the relative weight is such that $\chi_0(\mathbf{0}, 0) \approx 2\chi_0(\bar{\mathbf{q}}, 0)$. Near the instability it is reasonable to keep only the contribution at $\mathbf{q} = \mathbf{0}$. Indeed $\chi^{RPA}(\mathbf{q}, 0)$ in eq. (3.6) can be separated into two parts: $\chi^{intra} = \chi^{RPA}(0,0) = N_0/(1 - N_0 I)$ and $\chi^{inter} = 4\chi^{RPA}(\pi/8, 0) = 4N_0/(2 - IN_0)$. Close to the Stoner condition the second term is negligible. Therefore, in the $\omega = 0$ limit I finally obtain:

$$\lambda^s_{\rm sf}(x, I) = \frac{3}{2} \frac{N_0^2(x) I^2}{1 - IN_0(x)}. \tag{3.8}$$

This is what I called **spin density functional version of the RPA**. In the last expres-

sion I have taken into account the doping dependence of N_0 obtained in RBA.

Eq. (3.8) is very similar to the well-known expression for the SF induced interaction in the singlet channel, [316] averaged over the Fermi surface. Moreover it diverges at the LDA Stoner condition *i.e.* I expect the system to be consistently ferromagnetic for the LDA value of I.

Given this expression for the SF coupling it is now possible to study the effect of paramagnons on the EP superconductivity of Cu_{1-x}BiSO and even to establish whether for some parameter range this material could be a SF superconductor as already conjectured in previous calculations. [200] Indeed the expression of the coupling constant in the triplet channel, λ_{sf}^{t}, can be easily obtained from λ_{sf}^{s}. [316]

I will do this in the next section where, using appropriately modified formula for T_c with respect to eq. (3.3), and the expression for the doping dependent EP coupling constant derived in the previous section, I will study the phase diagram of Cu_{1-x}BiSO by studying the behavior of $\lambda_\Delta = \lambda_{ep} - \lambda_{sf}^{s}$ as a function of doping x and Stoner parameter I.

3.4 Phase diagram of Cu_{1-x}BiSO

Sections 3.1 and 3.2 have shown that the calculated ground state of HCBSO is characterized by both weak itinerant magnetism and strong EP coupling. These two characteristics of the ground state compete with each other and SF make the experimental sample to be non magnetic and to have a reduced T_c with respect to the calculated one. In sections 3.2 and 3.3 I also obtained simple expressions for λ_{ep} and λ_{sf}^{s} as a function of doping x and Stoner parameter I. The uncertainty on doping comes from the experiment while the uncertainty on I comes from the fact that, due to their mean-field character, LSDA and GGA overestimate the tendency to static magnetism in systems close to a QCP. [51]

The scope of this section is to collect all these informations and analyze the phase diagram of Cu_{1-x}BiSO as a function of the latter two variables, in order to draw some conclusions about the interplay between superconductivity and magnetism

in this material. The effect of paramagnons is to suppress superconductivity in the singlet channel by depressing the effective coupling constant $\lambda_\Delta(x,I) = \lambda_{ep}(x) - \lambda^s_{sf}(x,I)$ and increasing the effective mass of the carriers by the factor $1+\lambda_Z(x,I) = 1+\lambda_{ep}(x)+\lambda^s_{sf}(x,I)$. This effect has been studied in Ref. [317] where the following expression for T_c was derived (and verified by comparison with numerical solutions of the Eliashberg equations):

$$T_c(x,I) = \frac{\omega_{ln}}{1.2}\exp\left\{-\frac{1+\lambda_Z(x,I)}{\lambda_\Delta(x,I) - \mu^*\left[1+0.5\frac{\lambda_\Delta(x,I)}{1+\lambda_Z(x,I)}\right]}\right\}. \tag{3.9}$$

Here I assume for simplicity that the characteristic frequencies of phonons and paramagnons are the same and equal to ω_{ln}, while μ^* is the usual Coulomb pseudopotential and is fixed at 0.1.

Eq. (3.9) can also be generalized to triplet superconductivity. In this case phonons participate only in the mass enhancement factor, while their contribution to the pairing is canceled out, and superconductivity is completely built up by SF. The generalization of eq. (3.9) to this case is obtained by the substitution:

$$\begin{aligned} \lambda_\Delta(x,I) &\to \lambda^t_{sf}(x,I); \\ \lambda_Z(x,I) &\to \lambda^t_Z(x,I) = \lambda_{ep}(x) + \lambda^t_{sf}(x,I), \end{aligned} \tag{3.10}$$

where $\lambda^t_{sf}(x,I) = \frac{1}{3}\lambda^s_{sf}(x,I)$ is the coupling to spin fluctuations in the triplet channel. [316] In this way it is possible to study the x and I dependence of the effective coupling constant, and the related T_c both in the singlet and in the triplet channel. I will call T^s_c the critical temperature associated with the singlet channel and T^t_c the critical temperature associated with the triplet channel. This allows to obtain a simple estimate of the critical temperature for both symmetries of the superconducting order parameter.

Eq. (3.9) gives an appreciable T_c only if the denominator in the exponential is positive. For small μ^*, this is the case, when $\lambda_\Delta > 0$. I therefore use $\lambda_\Delta(x,I)$ to

define the phase diagram of HCBSO. Moreover, given eq. (3.10), one can obtain information on both the singlet and the triplet channel.

The phase diagram of $Cu_{1-x}BiSO$ is presented in Fig. 3.6 where I plot isocontours

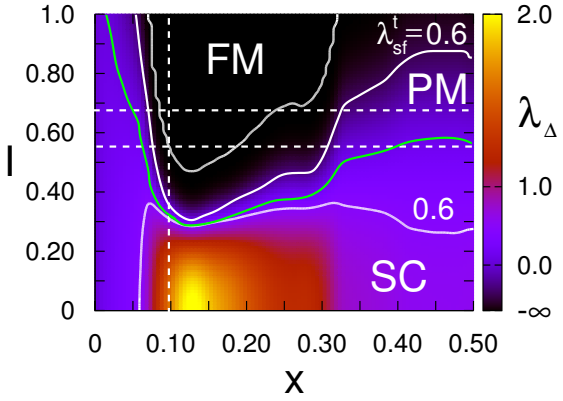

Figure 3.6: Phase diagram of $Cu_{1-x}BiSO$ as a function of doping (x) and Stoner parameter I. The color scale gives the value of λ_Δ. The two horizontal dashed lines correspond to $I_{\rm LDA}$=0.53 eV and $I_{\rm GGA}$=0.67 eV. The vertical dashed line indicates the doping for which superconductivity was observed in Ref. [225]. In the region (FM) the system shows a FM instability, defined by the condition $(N_0(x)I \geq 1)$; elsewhere the system is paramagnetic (PM). Below the green line (which marks the condition $T_c^s = T_c^t$) the ground state is a conventional singlet superconductor. Above the green line a triplet superconducting state is more stable. The isolines $\lambda_\Delta = 0.6$ and $\lambda^t_{sf} = 0.6$ indicate the values of I, x which reproduce the experimental $T_c = 5.8$ K of Ref. [225] in the singlet and triplet channel respectively.

of $\lambda_\Delta(x, I)$ in the I, x plane in which several phases can be outlined.

For small values of x and I, also the value of the DOS at the Fermi level is small and the system is paramagnetic and non superconducting. With increasing doping, the DOS at E_F also encreases and, if $\lambda_\Delta \gg \mu^*$ a conventional EP superconductivity,

albeit suppressed by spin fluctuations, is a stable zero-temperature ground state. This region is the one indicated by SC and delimited by the isoline $\lambda_\Delta = 0.6$. This is indeed the value of λ_Δ needed to reproduce the experimental $T_c = 5.8$ K. At experimental doping $x = 0.1$, if the Stoner parameter is increased, λ_Δ goes down and a competing instability against a triplet state emerges when the critical temperature in the singlet channel T_c^s, becomes equal to the critical tempreature T_c^t in the triplet channel. This condition is graphically indicated by the green line. Finally, as the tendency to magnetism is increased even further, the Stoner criterion $N_0 I > 1$ is fulfilled, and the system becomes ferromagnetic. This region of the phase diagram is indicated in Fig. 3.6 by FM.

The LSDA or GGA value for I are indicated by the two horizontal white dashed lines. For dopings close to $x = 0.1$ these values of I consistently bring Cu_{1-x}BiSO inside the FM region. However, at $x = 0.1$ experiments see no trace of static FM order, a sign of inadequacy of the mean-field character of magnetism in LSDA and GGA. Reducing the LSDA value of I to $I_{\text{eff}} = 0.51$ eV suppresses the magnetic instability at $x = 0.1$; a reduction to $I_{\text{eff}} = 0.39$ eV brings the estimated triplet T_c in agreement with the experimental one, and a reduction to 0.30 eV does the same with the conventional singlet T_c. One way of modeling the effect of fluctuations, and, at the same time, retaining the *ab-initio* information on the dependence of N_0 on x, is to replace the Stoner parameter in eq. (3.8) with a lower, effective value, I_{eff}. This reduction is supposed to account phenomenologically for spin fluctuations. This phenomenological reduction of I, as I showed in chapter 1, has a precise physical justification, and is usually obtained by the comparison with the experimental quantity (spin susceptibility or magnetic moment). Since for Cu_{1-x}BiSO these quantities are not yet available, I_{eff} can estimated to be 0.30 eV $\lesssim I <$ 0.51 eV. Indeed for typical itinerant magnets renormalizing I by $\sim 30 - 40\%$ with respect to LSDA provides reasonable agreement with the experimental magnetic susceptibilities. [51]

Concerning the nature of superconductivity in $Cu_{0.9}$BiSO my calculations, give a quite surprising result. Indeed superconductivity was first supposed to be made by spin fluctuations [200] then, in section 3.2 I showed that actually the EP coupling

is extremely large in this compound and therefore superconductivity could be, most likely, mediated by phonons and eventually suppressed by paramagnons. Finally, in this section, looking at the phase diagram it is clear that both triplet and singlet T_c^s and T_c^t are of the same magnitude and both sizable at experimental doping. Therefore no definite answer can be given on this topic, but a complete new perspective is open. Indeed, given the rich phase diagram of $Cu_{1-x}BiSO$, in principle one could easily switch from one pairing symmetry to another or from ferromagnetism to metallic or insulating state by playing with doping or pressure, making $Cu_{1-x}BiSO$ extremely fascinating material.

3.5 Conclusion and outlook

In order to close this chapter and to point towards to the next ones, it is useful to summarize the results obtained up to now, and collocate this chapter in the wider context of the whole thesis.

In this chapter I presented the results published in Ref. [311] on magnetism and superconductivity in HCBSO.

In section 3.1 I presented DFT calculations concerning the electronic structure of this material. The stoichiometric compound is a band insulator and, for a wide energy range below the VBM, the band structure is characterized by a strong Cu d-S p hybridization. When holes are introduced into the system it becomes metallic and, at experimental doping $x = 0.1$, the Fermi level sits on a flat band which causes a peak in the DOS, making the system slightly instable against ferromagnetism. However the experimental compound is not magnetic therefore SF must be invoked in order to reproduce the experiment. This SF could lead to superconductivity in the triplet channel. This hypothesis was also considered in Ref. [200]. On the other hand the strong Cu d-S p hybridization and the relatively high critical temperature made EP properties worth calculating. Therefore in section 3.2 I calculated the EP coupling and I discovered that also T_c associated with EP superconductivity is overestimated with respect to the experimental one. Therefore SF must be invoked

to reduce the T_c in the singlet channel. For these reasons, in section 3.3 I estimated the electron paramagnon coupling constant both in the singlet and in the triplet channel and I obtained a simple analytical expression for SF-induced interaction as a fuction of doping x and Stoner parameter I. Finally , in the last section I collected all the informations obtained concerning λ_{ep}, $\lambda^{\text{s}}_{\text{sf}}$ and $\lambda^{\text{t}}_{\text{sf}}$ in the resulting phase diagram.

The obtained results sound particularly interesting especially concerning the superconducting state of HCBSO. Indeed this material appears as a unique example where a spin fluctuations-driven superconductivity in the triplet channel and phonon-driven superconductivity in the singlet one are nearly degenerate. The critical temperature is sizable for both symmetries. This fact can be rationalized *a posteriori* in terms of the strong S p-Cu d covalency that characterizes the band structure: the presence of anti-bonding p states at the Fermi level leads to large EP matrix elements, whereas the large susceptibility and the strong magnetic tendency of Cu enhances spin fluctuations. Moreover the flat band in the VBM of the stoichiometric compounds enhances the DOS at the Fermi level and places HCBSO in a region of the phase space particularly sensitive to instability involving both the charge and the spin degrees of freedom. This seems to be confirmed by the experiment in which superconductivity appears to be particularly sensitive with respect to the experimental conditions. [225]

If on one hand this doesn't allow me to give a definitive answer concerning the actual symmetry of the order parameter, on the other hand renders this material particularly interesting and suitable for applications. One could indeed tune, in principle, the pairing symmetry by applying pressure or magnetic field.

However, the uncertainty on the bare interaction parameter I remains an issue. Indeed, concerning the magnetic properties of Cu_{1-x}BiSO I showed that the mean-field nature of LSDA and GGA is inappropriate for describing them and therefore, in order to reproduce the experiment, a phenomenological reduction of the Stoner parameter I is needed. The question that arises at the end of this chapter, and project us towards to the next ones is then the following. **Could it be possible to reduce the Phase diagram of Cu_{1-x}BiSO to only one line?** In other words, could

it be possible to make a completely *ab-initio* prediction of the T_c vs x phase diagram fixing once for all the Stoner parameter I? In chapter 5 I will face exactly this point for a material whose physical properties change under pressure instead of doping. Using a simple method I will be able to tune the Stoner parameter within DFT and, given the peculiar behavior of the DOS under applied pressure, I will be able to derive *ab-initio* the pressure dependence of the magnetic moment.

3.6 Technical Details

For the band structure and density of states (DOS) calculations shown in Fig. 3.2, I employed the Linearly Augmented Plane Wave methods [308], as implemented in the Wien2K code. [309] I used atomic spheres of 2.4, 2.0, 2.0 and 1.8 $a.u.$ for Bi, Cu, S and O respectively; the electronic integration was carried out on as many as 8000 k-points in the full Brillouin zone, using the improved tetrahedron method [318]; similar setups were used for the spin-polarized calculations discussed in the text.

For the EP coupling calculations presented in this chapter, I used the linear response method; all calculations were performed in the generalized gradient approximation [251] using plane waves [307] and ultra-soft pseudopotentials [310], except for the Bi atom for which I employed a Martin-Trouillers norm-conserving pseudopotential. I employed a cut-off of 100 (800) Ryd for the wave functions (charge densities). The electronic integration in the self-consistent cycles was performed over a $4 \times 4 \times 2$ $\mathbf{k}$-mesh. Finer grids ($48 \times 48 \times 24$) were used for evaluating the EP linewidths, and the densities of states (DOS) in the doped regime. Dynamical matrices and EP linewidths were calculated on a $8 \times 8 \times 2$ uniform grid in $\mathbf{q}$-space. Phonon frequencies throughout the Brillouin zone were obtained by Fourier interpolation. The (perturbed) potentials and charge densities, as well as the phonon frequencies, were calculated self-consistently at zero doping ($x = 0$); the effect of doping on the EP coupling was then estimated using the rigid-band approximation. [3]

[3] The rigid band routine was developed with the help of Matteo Calandra.

Chapter 4

Phenomenological approach to the optical properties of LaFePO

In this chapter I present the results of Ref. [319] concerning the optical properties of LaFePO. Both the intraband and the interband contributions to the optical conductivity are calculated. A phenomenological model is applied to the interband optical conductivity in order to account for the overestimation of the overall bandwidth in generalized gradient approximation (GGA). The agreement with the experimental data from Qazilbash et al. [153] *is remarkable. The analysis presented here allows to estimate the spurious effect introduced by low-energy optical interband transitions when the spin fluctuations coupling is extracted from an extended Drude model analysis of the experimental data. I show that the coupling constant for spin fluctuations, which is usually overestimated by optical experiments, is found to be consistent with the one obtained from other experimental probes.*

Introduction

The last example of a phenomenological analysis based on density functional theory (DFT) presented in this thesis, is applied to the interpretation of the optical spectrum of LaFePO, one of the earliest Fe based superconductors discovered. [1] All Fe pnictides have a layered crystal structure and are grouped in different families according to the details of the crystal structure. Most of them share same common features such as the shape of the Fermi surface and the vicinity to a magnetic instability. [53, 54, 72] Given the tendency to magnetism and the low value of the calculated electron-phonon coupling constant, [4, 70, 228] spin fluctuations are thought since the beginning to be the most likely paring interaction. [5, 6]

LaFePO is non magnetic and the critical temperature is relatively low ($T_c = 7$ K), [1] compared to the largest T_c of 56 K found in $Gd_{1x}Th_xFeAsO$ [220] and in $Sr_{0.5}Sm_{0.5}FFeAs$. [221] Fermi surface measurements via de Haas-van Alphen effect, angle-resolved photoemission spectroscopy (ARPES) experiments and thermodynamic specific heat measurements all consistently point to LaFePO as a moderately/weakly correlated compensated metal. [136, 229–231] However optical conductivity measurement analyzed using the extended Drude model (EDM), found a surprisingly large inverse time scattering rate $\tau^{-1}(\omega)$ with a significant frequency dependence. [153] This was interpreted by the authors as an indication for strong many body effects, due to a retarded interaction mediated by spin fluctuations. Within the EDM indeed, under certain conditions and assuming that the interband optical transitions involve energy scales larger than the cut-off frequency ω_c below which the data are analyzed, the ω dependent scattering rate can be linked to the shape of the spectrum of the retarded interaction and consequently to the coupling constant λ. [134] According to Qazilbash *et al.*, for LaFePO the EDM analysis finds $\lambda \approx 0.5$ and an additional renormalization of the bandwidth by a factor of $1 + \lambda_W \sim 2$ is also present. [153] In practice the bare band mass m_b gets renormalized twice:

$$m^* = (1 + \lambda)m_b(1 + \lambda_W) = m_b(1 + \lambda + \lambda_W + \lambda\lambda_W).$$

In this way the total coupling constant $\lambda_{TOT} = \lambda + \lambda_W + \lambda\lambda_W \approx 2$.

After the report of Ref. [153], the same kind of experiments were made also on different Fe pnictides, [154–157] and also in that case the same large ω dependence of $\tau^{-1}(\omega)$ was found and interpreted as due to electron-boson interaction in the strong coupling regime ($\lambda \approx 3-4$). [156, 157]

In LaFePO this leads to a contradiction since a large coupling constant of 2 corresponds also to large effective mass at low-energies in contrast to what measured by de Haas-van Alphen effect, [229] ARPES experiment [136, 229] and specific heat measurement. [230] These measurements all consistently indicate indeed a mass enhancement $m^*/m_b = 1 + \lambda \lesssim 2$, *i. e* total coupling constant lambda ≤ 1.[1]

This inconsistency could be caused by the presence of low-energy interband optical transitions which give a fictitious contribution to the frequency dependence of $\tau^{-1}(\omega)$. The use of the EDM analysis in pnictides indeed, corresponds to implicitly assume that these transitions set in at $\omega_c \sim 2000$ cm^{-1}, [153, 320] even if some authors suggested that this value could be smaller. [155–158]

The analysis of the role of low-energy interband transitions that I carried out in Ref. [319] aimed to clarify how accurate this assumption is.

In this reference, I calculated the effect of low-energy interband transitions on the optical conductivity. For the intraband part, I used a simple low-energy model, introduced in Ref. [195]. Since the model employed for calculating the intraband optical transitions accurately reproduces the low-energy and thermodynamic properties of LaFePO, [185, 195] the comparison with the experiment allows to make a reliable estimate of the location and amplitude of the contribution coming from the interband optical transitions. From this analysis I found that in LaFePO interband transitions give a sizable contribution to the optical conductivity already at low energy. This causes an overestimation of the spin fluctuations coupling constant with respect to other experiments. Therefore the use of the EDM analysis in pnictides is questionable. A consistent estimate of the spin fluctuations coupling constant was

[1] A large mass enhancement factor of 2.63 was found in Ref. [231] but this is probably due to the poor homogeneity of the sample. Indeed the measured critical temperature was $T_c \approx 3$ K, about half of the value measured in other samples. [229]

also obtained.

For the interband part, I used a phenomenological form, made up of two Lorentzian peaks, with variable width, position and weight.

The structure of the chapter is the following. In section 4.1 I present the crystal and electronic structure of LaFePO. In section 4.2, after giving a basic introduction to the EDM analysis, I introduce the low-energy model employed for calculating the Migdal Eliashberg self-energy used for the calculation of the intraband optical conductivity of LaFePO. In section 4.3 I present a preliminary comparison of the calculated intraband optical conductivity with the experiment which permits to define an upper boundary frequency ω_B above which the calculation fails in describing the experiment and an additional contribution must be taken into account. This contribution, which comes from low-energy interband optical transitions, is modeled as a Lorentzian peak characterized by spectral weight S_0, width γ and frequency ω_L. A study of the parameter space of this simple model is also presented and is found that, in order to reproduce the experiment, $\gamma/\omega_L \approx 1$. In section 4.4 the origin of this contribution is addressed calculating the interband optical conductivity of LaFePO within density functional theory. It turns out that the low-energy real part of the interband optical conductivity in GGA is formed by two peaks: one at very low-energy which does not contribute to $\tau(\omega)$ and a broader feature which gives a large contribution. However, while GGA allows to calculate the interband part of the spectrum, due to the underestimation of correlation effects that renormalize the bandwidth in pnictides, [93, 136] the position in frequency of the transitions is overestimated. In an ellipsometry study, Charnukha *et al.* [159] found that in K-doped $BaFe_2As_2$ there is a factor 3 discrepancy between the location of the optical transitions predicted by the LDA calculations and the experiment. Therefore from the DFT calculations I estimated the position of the transitions and their intensity while the final form of the optical conductivity for LaFePO was estimated phenomenologically from the comparison with the experimental data.

This comparison is presented in section 4.5 and the interband optical conductivity is parameterized as a double Lorentzian peak. Finally, given the good agreement with the experiment, some conclusions are drawn in section 4.6. Technical details

are presented in section 4.7.

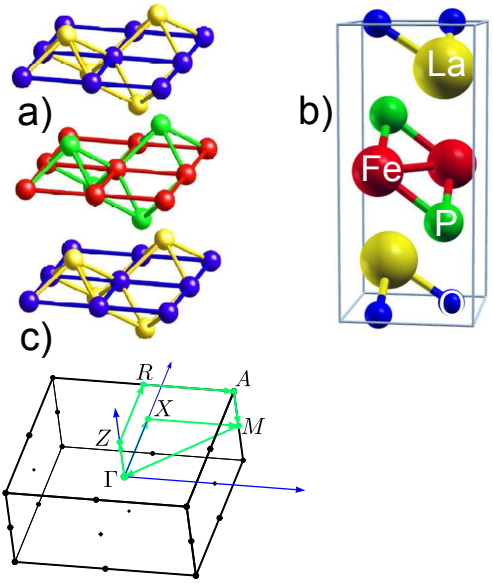

Figure 4.1: ZrCuAsSi-type crystal structure of LaFePO. (a) The Fe(red)-P(green) layers and La(yellow)-O(Blue) ones alternate along the *c* axis. The Fe (O) atoms form a square lattice in which the Fe(O) atoms are tetrahedrally coordinated with the P(La) ones. (b) The unit cell of LaFePO contains two formula units per unit cell. (c) Path (green line) in the Brillouin zone along which the band structure of Figs 4.2 and 4.7 are plotted. The reciprocal lattice vectors (blue arrows) are also shown.

4.1 Crystal and electronic structure

LaFePO belongs to the 1111 family of the Fe pnictides. The compounds belonging to this family have the general formula *Re*Fe*Pn*O where *Re* is a rare earth atom and *Pn* is a pnictogen atom (As, P). [54] Their crystal structure is the ZrCuAsSi-type one (space group $P4/nmm$) and is made by *Re*O layers alternating to Fe*Pn* ones in the same fashion of CuBiSO already described in chapter 3 and shown in Fig. 4.1 (a): in the Fe*Pn* (*Re*O) layer the Fe (O) atoms form a square lattice in which the *Pn* (*Re*) atoms sit in the center of the square alternatively above and below the Fe (O) plane. As a result, the Fe (O) atoms are tetrahedrally coordinated with the *Pn* (*Re*) ones whose distance from the Fe (O) plane is h_{Pn} (h_{Re}). The value of h_{Pn} is related to the internal Wyckoff position of the pnictogen (rare earth) atoms through the relation $z_{Pn} = h_{Pn}/c$ ($z_{Re} = h_{Re}/c$) where c is the length of the lattice vector parallel to the z axis. The Wyckoff positions for the atoms in LaFePO are $2c$ for La and P, $2b$ for Fe and $2a$ for O.

The unit cell shown in Fig. 4.1 (b) is tetragonal and contains two formula units. For LaFePO the formal ionic states are La^{+3} O^{-2} Fe^{+2} P^{-3} and, as for most parent compounds of Fe pnictides, Fe is in the d^6 configuration. In my calculations I used the experimental lattice parameters $a = 3.964$ $\AA$ and $c = 8.512$ $\AA$ and internal coordinates $z_P = 0.3661$ $z_{La} = 0.1487$. [1]

The bandstructure of LaFePO, calculated using the experimental lattice parameters and internal coordinates, is shown on the top of Fig. 4.2 together with the corresponding Fermi surface. The LaO-FeP interaction is strongly ionic, indeed the LaO and FeP partial density of states (DOS) -not shown- remain almost unchanged in LaFePO with respect to LaO and FeP 2D lattices. [321] On the other hand the FeP interaction is pretty covalent and the bandstructure depends crucially on h_P as for pnictides in general. [57, 61, 72, 322]

Two main energy regions, separated by a small gap around ~ 2.5 eV below E_F, can be distinguished in the plot. The states with energy -5 eV $< E < -2.5$ eV have mostly P p character. They strongly hybridize with Fe d states and have bonding character. The antibonding counterpart is located instead at ~ 1.5 eV above the

Fermi level. Above the mentioned small gap, in a region of ~ 5 eV around the Fermi level the bandstructure of LaFePO is constituted by 10 bands with mainly Fe $3d$ character slightly mixed with the P p one. [72, 321, 322] The low-energy bandstructure of LaFePO is plotted along the path highlighted in Fig. 4.1 (c) and is shown in the bottom of Fig. 4.2. The choice of local coordinates is such that the x axis points towards the Fe-Fe bond. In this way the d_{xy} orbital points towards the P atom while the $d_{x^2-y^2}$ one points towards the nearest neighbor Fe.

In a range of 1 eV around E_F (taken as reference for the energy) the electronic structure is characterized by two hole bands with d_{xz}/d_{yz} character crossing the Fermi level around the Γ point and two almost degenerate parabolic electron bands with d_{xz}/d_{xy} and d_{yz}/d_{xy} character located around the M point. An additional band with $d_{3z^2-r^2}$ character is also present and crosses the Fermi level along the $\Gamma-Z$ direction, but experimentally it is not observed. Finally a band with d_{xy} character is also present and is located at ~ 0.2 eV below the Fermi level. The presence of this band at the Fermi level depends crucially on the internal coordinate h_{Pn} and seems to be responsible for the antiferromagnetic instability in Fe pnictides. [194, 322] In LaFePO h_{Pn} is such that this band lies below the Fermi level and this compound is consistently non magnetic.

The Fermi surface is shown at the top left panel of Fig. 4.2 and is made of five sheets. Two concentric and almost cylindrical sheets are centered around the M point and other two are centered around the Γ point. These portions of the Fermi surface are almost bidimensional as can be understood by looking at the flat dispersions along the $\Gamma - Z$ and $M - A$ directions in Fig. 4.2. The fifth sheet centered around the Γ point is instead almost spherical due to the large dispersion along the $\Gamma - Z$ direction of the corresponding $d_{3z^2-r^2}$ band. [321, 322]

In Fig. 4.2 the nesting vector $\mathbf{Q}_{AFM} = (\pi/a, \pi/a, 0)$ -where a is the in plane lattice parameter- is shown with the gray arrow connecting the two electron like cylinders around the M point and the two hole like cylinders around the M point. The Fermi surface topology is an almost universal property of Fe-based superconductors. In some compounds the coupling between the FePn layers is weak, and can be safely neglected. One can then use a smaller, one Fe-atom unit cell, with

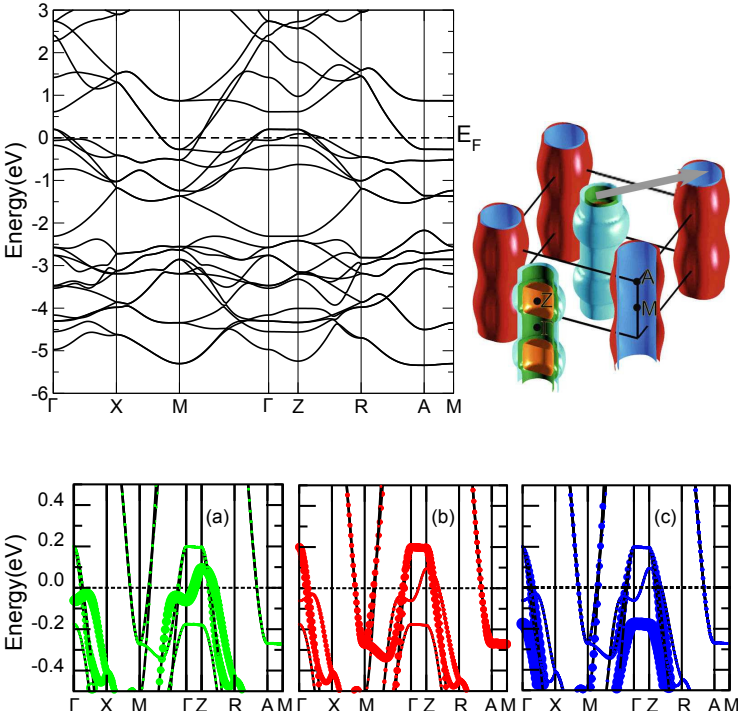

Figure 4.2: *Top*: Band structure of LaFePO calculated with the experimental lattice parameters and internal coordinates (left) and relative Fermi surface (right) adapted from Ref. [323]. *Bottom*:Blow up of the low-energy electronic structure of LaFePO: it is composed by a dispersive hole band with $d_{3z^2-r^2}$ character -green color in (a)- around the Γ point, four almost bidimensional hole and electron bands with d_{xz} and d_{yz} character -red color in (b) and d_{xy} character -blue color in (c)-. Finally a band with d_{xy} character is located at 0.2 eV below the Fermi level.

lattice vector $d = a/\sqrt{2}$. The corresponding Brillouin zone is bidimensional and its area is twice larger than the Γ-X-M plane of the three dimensional one. For those compounds in which the interlayer interaction is weak, the M point unfolds into two inequivalent $\bar{X}$ and $\bar{Y}$ points hosting the d_{xz} and the d_{yz} electron-like Fermi surface sheet respectively, while the three hole like Fermi surface sheets get distributed in the two inequivalent $\bar{\Gamma}$ and $\bar{M}$ points where respectively the $d_{3z^2-r^2}$ and the two $d_{xz/yz}$ and d_{xy} hole pockets sit. As a result the nesting vector is $\bar{\mathbf{Q}} = (0, \pi/d)$ -$d = a/\sqrt{2}$ is the Fe-Fe distance-. [72]

Early ARPES experiment on LaFePO presented in Fig. 4.3 (a), [136] showed that the agreement with LDA calculations is obtained when the experimental bandwidth is renormalized by a factor 2.2 and the band shifted up by ~ 0.11 eV. The renormalization of the bands is due to the effect of local correlations and is a general feature of Fe pnictides. The amount of this factor is instead a peculiarity of the single compound and is found to vary in a large range between 2 and 7. [324–328]

Also the shift of the measured band dispersion with respect to the calculated one is a quite general property of Fe pnictides. [93, 324–335] However these shifts are not rigid as the one presented in Fig. 4.3 (a), rather they have opposite sign for electron and hole bands close to the Fermi level. Concerning this effect in LaFePO, Coldea *et al.*, [229] compared the Fermi surface measured by de Haas-van Alphen experiment with LDA calculations performed using the experimental coordinates and found that the bands close to the Fermi level appear shifted in a selective way, with respect to the LDA ones, according to their particle or hole character. In Fig 4.3 the calculated and the measured de Haas-van Alphen orbits are shown together with the corresponding Fermi surface. In LaFePO the two electron bands giving rise to the electron sheets in Fig. 4.3 (c) are shifted up by -83 and -30 meV respectively and the hole bands are instead shifted down by 53 meV. As a result the Fermi surface volume appears reduced with respect to the LDA one. The calculated yellow orbit in Fig. 4.3 (b) is experimentally not observed.

In the next section I will introduce a model which was used to show that the band shifts observed in Fe pnictides are an indirect evidence of the prevalence of the interband coupling over the intraband one in these materials. [195] I will then

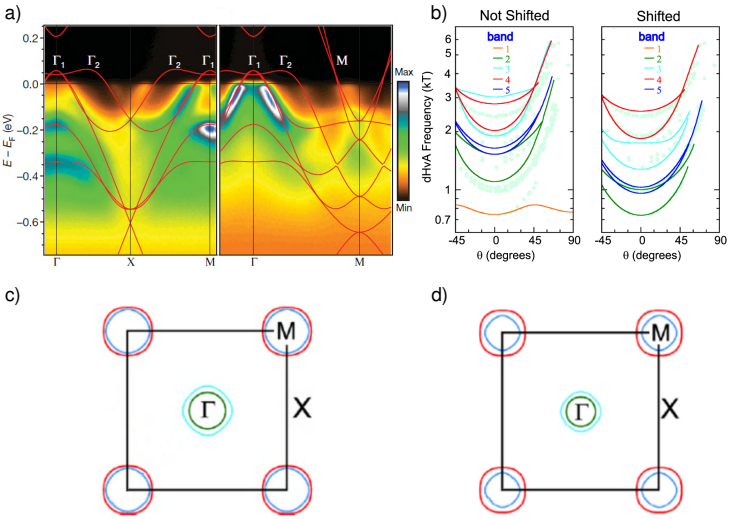

Figure 4.3: Figure from Refs. [136] and [229]. (a) The band dispersion measured by ARPES experiment (color scale) is compared with the LDA band structure obtained using the experimental lattice parameters but relaxed internal coordinates. The bandwidth of the calculated bandstructure was renormalized by a factor of 2.2 and the bands shifted rigidly up by ~ 0.11 eV. (b) The de Haas-van Alphen hole and electron orbits are shifted in a different way. As a results the LDA volume of the Fermi surface (c) results bigger than the one actually measured (d).

use this model to calculate the intraband optical conductivity in LaFePO.

4.2 Intraband transitions

4.2.1 The extended Drude model

The extended Drude model (EDM) analysis is based on the fact that the retarded interaction modifies the Drude formula for the optical conductivity introducing a complex and frequency-dependent relaxation rate $\Gamma \to \tilde{\Gamma}(\omega) = \Gamma_1(\omega) + i\Gamma_2(\omega)$. [133–135] As a consequence, the complex optical conductivity $\tilde{\sigma}(\omega) = \sigma_1(\omega) + i\sigma_2(\omega)$ assumes the following form:[134]

$$\tilde{\sigma}(\omega) = \frac{ne^2}{[\Gamma_1(\omega) + i\Gamma_2(\omega)]m} \frac{1}{1 - \frac{i\omega}{[\Gamma_1(\omega)+i\Gamma_2(\omega)]}} = \frac{ne^2}{m[1+\lambda(\omega)]} \frac{1}{\frac{\Gamma_1(\omega)}{1+\lambda(\omega)} - i\omega} \tag{4.1}$$

where n is the carrier density, m is the band mass and I have introduced the quantity $\lambda(\omega) = -\Gamma_2(\omega)/\omega$.

For $\lambda(\omega) \to 0$, eq. (4.1) reduces to the well known Drude formula for the optical conductivity, otherwise it gives origin to a frequency-dependent scattering rate and a frequency-dependent mass enhancement factor:

$$\frac{m^*(\omega)}{m} = \frac{\omega_P^2}{4\pi\omega} \frac{\sigma_2(\omega)}{\sigma_1^2(\omega) + \sigma_2^2(\omega)} \tag{4.2}$$

$$\tau^{-1}(\omega) = \frac{\omega_P^2}{4\pi} \frac{\sigma_1(\omega)}{\sigma_1^2(\omega) + \sigma_2^2(\omega)}, \tag{4.3}$$

where both the electron mass m and the inverse time scattering rate τ^{-1} are renormalized by the factor $1 + \lambda(\omega)$. Eqs.(4.1)-(4.3) define the **extended Drude model** for the complex optical conductivity. The renormalization effect characterizes the low-energy part of the spectrum and, with increasing frequency, $\lambda(\omega) \to 0$, m^* approaches the band mass and $\Gamma_1(\omega)$ approaches the inverse impurity scattering time present in the Drude formula. [134]

Both $\tau^{-1}(\omega) = \Gamma_1(\omega)$ and $1+\lambda(\omega) = m^*(\omega)/m$ can be computed by calculating or measuring the complex optical conductivity $\tilde{\sigma}(\omega)$ and the plasma frequency $\omega_P^2 = 4\pi ne^2/m$.

Since both $\tilde{\Gamma}(\omega)$ and $\tilde{\sigma}(\omega)$ obey the causality principle it is sufficient to calculate or to measure $\sigma_1(\omega)$: the other quantities follow then from the Kramers-Kronig relations. Notice that the EDM analysis implicitly assumes two hypothesis:

- Interband transitions are negligible at low energies. For Fe pnictides a lower cut-off $\omega_c \sim 2000 - 3000$ cm^{-1} was estimated. [153–157]
- Validity of the Luttinger theorem (*i.e.* the interacting system has the same Fermi surface volume as the non interacting one).

In compensated metals the decrease in the number of holes can be compensated by a decrease in the number of electrons. As a result, the decrease in $\sigma_1(\omega)$ does not come from the factor $1 + \lambda(\omega)$ in eq. (4.1) only, but also from the reduction of the charge density n under the effect of the interaction. [336]

4.2.2 The microscopic model

In order to calculate the intraband contribution to the optical conductivity due to the interaction of holes and electrons at the Fermi level, I use the model presented in Ref. [195]. The model was already used for describing the low-energy properties of LaFePO and reproduced the experimentally observed Fermi surface reduction with respect to LDA calculations. [195] The low-energy non-interacting bandstructure is approximated by two parabolic hole bands placed at the Γ point and two parabolic degenerate electron bands located at the M point. The fifth $d_{3z^2-r^2}$ band lies experimentally below the Fermi level and is therefore not considered. The band dispersions can be expressed in the following way:

$$\varepsilon_{\mathbf{k},\alpha} = E_{max,\alpha} - \frac{\hbar^2 \mid \mathbf{k} \mid^2}{2m_\alpha}, \qquad \alpha = 1,2 \qquad \text{(hole bands)} \tag{4.4}$$

$$\varepsilon_{\mathbf{k},\alpha} = E_{min,\alpha} + \frac{\hbar^2 \mid \mathbf{k} \mid^2}{2m_\alpha}, \qquad \alpha = 3,4 \qquad \text{(electron bands).} \tag{4.5}$$

The band parameters $E_{max,\alpha}$, $E_{min,\alpha}$ and band masses m_α are taken from the DFT calculations made by Lebégue. [321] More explicitly, since the hole (electron) bands

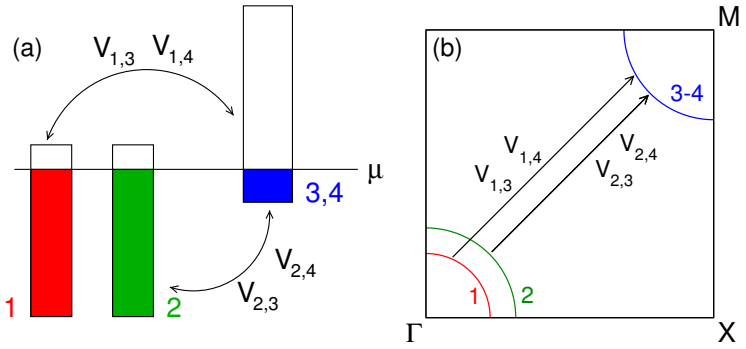

Figure 4.4: Figure from Ref. [195] Sketch of the band structure for LaFePO (a) and Fermi surface (b) as represented by eqs. (4.5). The non zero element of the interaction matrix $V_{\alpha\beta}$ are also shown.

do not disperse along the $\Gamma - Z$ ($M - A$) direction, I focus on the $k_z = 0$ plane. From the $\Gamma - X$ ($M - X$) cut of the Fermi surface I extract the Fermi vector $k_{F,\alpha}$ for the hole (electron) bands. Setting the chemical potential $\mu = 0$, I also extract from DFT calculations the hole (electron) band edges $E_{max,\alpha}$ ($E_{min,\alpha}$). The non interacting band mass m_α is estimated from $E_{max,\alpha}$ ($E_{min,\alpha}$), namely $m_\alpha = \hbar^2 k_{F,\alpha}^2 / 2E_{max(min),\alpha}$. Within the parabolic approximation the density of states (DOS) is flat and can be obtained from the band mass and the lattice parameter a as $N_{0,\alpha} = m_\alpha a^2 / 2\pi\hbar^2$. The effective band edges far from the Fermi level are obtained from the relation $N_{0,\alpha} = 1/(E_{max,\alpha} - E_{min,\alpha})$. [2] Finally the band dispersions are renormalized by a factor of two in order to account for local correlation effects not included in the model. [136] The values of the band parameters are reported in table 4.1.

The interaction is considered to be purely interband and mediated by spin fluctuations treated within the Migdal-Eliashberg approximation. The retarded local

[2] This value does not represent the true band edge as given in DFT calculations, rather an effective one needed to guarantee the total number of states.

Band parameters for LaFePO

α	m_α/m_e	$E_{\max,\alpha}$ (eV)	$E_{\min,\alpha}$ (eV)	$N_{0,\alpha}$ (st. /eV)
1	1.16	0.102	-2.516	0.382
2	2.28	0.102	-1.231	0.750
3,4	1.58	1.776	-0.147	0.520

Table 4.1: Microscopic band parameters entering the four-band model used for calculating the intraband optical conductivity of LaFePO. [195, 319] The parameters are obtained by renormalizing by a factor of two the band parameters obtained in DFT from Ref. [321].

self-energy in the Matsubara space can be expressed in the following way:

$$\Sigma_\alpha(i\omega_n) = -T\sum_{m,\beta} V_{\alpha\beta} D(\omega_n - \omega_m) G_\beta(i\omega_m) \tag{4.6}$$

where $V_{\alpha\beta}$ is the interaction matrix and $G_\beta(i\omega_m)$ is the local one particle Green's function defined as $\int \frac{d\mathbf{k}^2}{4\pi^2} G_\beta(\mathbf{k}, i\omega_m)$ and

$$G_\beta(\mathbf{k}, i\omega_m) = \frac{1}{i\omega_m - \varepsilon_{\mathbf{k},\beta} - \Sigma_\beta(i\omega_m) + \mu}. \tag{4.7}$$

The integral over $\mathbf{k}$ in the definition of $G_\beta(i\omega_m)$ can be replaced by an energy integral over ε:

$$G_\beta(i\omega_m) = N_{0,\beta}\int_{E_{\beta,min}}^{E_{\beta max}} d\varepsilon \frac{1}{i\omega_m - \varepsilon - \Sigma_\beta(i\omega_m) + \mu}$$

where I used the fact that a two dimensional parabolic band has a flat density of states $N_{0,\beta}$. In this way the adimensional matrix elements $\lambda_{\alpha\beta} = V_{\alpha\beta}N_{0\beta}$ can be defined. In eq. (4.6) $D(\omega_n - \omega_m)$ is the bosonic propagator which mimics the effect of antiferromagnetic spin fluctuations in LaFePO and requires further discussion.

For a nearly antiferromagnetic Fermi liquid the spin susceptibility can be written as: [17, 169]

$$\chi(\mathbf{q},\omega) \propto \frac{\omega_0}{\Gamma_{\mathbf{q}} - i\omega} \tag{4.8}$$

where $\Gamma_{\mathbf{q}} = \omega_0[1+(\mathbf{q}-\mathbf{Q})^2]\xi^2/(\xi/a)^2$, ξ is the spin fluctuations correlation length, ω_0 is their characteristic energy scale, $\mathbf{Q}$ is their characteristic $\mathbf{q}$ vector and a is the lattice parameter.

The imaginary part of the susceptibility defined by (4.8) is given by:

$$\chi''(\mathbf{q},\omega) \propto \frac{\omega_0\omega}{\Gamma_{\mathbf{q}}^2 + \omega^2} \tag{4.9}$$

and does not obey the sum rule giving the total number of spins at $T = 0$:

$$\sum_{\mathbf{q},\omega} \chi''(\mathbf{q},\omega) < S(S+1) = 3/4. \tag{4.10}$$

Indeed $\chi''(\mathbf{q},\omega)$ vanishes as $1/\omega$ at high ω, therefore the left side of eq. (4.10) diverges logarithmically.

For this reason Millis introduced a cut-off ω_D which makes the spin susceptibility in eq. (4.8) fulfill the condition (4.10) and applied the Eliashberg scheme for obtaining the retarded self-energy for a system of electrons with dispersion $\varepsilon_{\mathbf{k}}$ interacting with spin fluctuations. [171]

The modified expression for $\chi(\mathbf{q},\omega)$ in the Matsubara space is the following:

$$\chi(\mathbf{q},\Omega_n,\omega_D) \propto$$

$$-\omega_0 \frac{|\,\Omega_n\,| - (2\Omega_n/\pi)\tan^{-1}(\Omega_n/\omega_D) - \Gamma_{\mathbf{q}} + (2\Gamma_{\mathbf{q}}/\pi)\tan^{-1}(\Gamma_{\mathbf{q}}/\omega_D)}{\Gamma_{\mathbf{q}}^2 - |\,\Omega_n\,|^2}. \tag{4.11}$$

Eq. (4.8) is recovered in the limit of large ω_D and with the substitution $\Omega_n \to -i\omega$.

In the following calculations, the bosonic propagator $D(\omega_n - \omega_m)$ is the propagator of spin fluctuations. Therefore it is chosen as the dynamical spin susceptibility in eq. (4.11) in the limit of large cut-off ω_D:

$$D(\Omega_n) = \lim_{\omega_D \to \infty} \chi(\mathbf{q}, \Omega_n, \omega_D).$$

Indeed I'm not interested in calculating the $T = 0$ properties and moreover the total number of spins does not enter the calculations. Moreover the propagator in eq. (4.11) is found to converge quite fast increasing the cut-off ω_D.

The $\mathbf{q}$-dependent energy scale $\Gamma_{\mathbf{q}}$ is assumed to be constant and equal to the characteristic energy scale ω_0 of spin fluctuations in LaFePO measured by neutron scattering. This is equivalent to setting $\mathbf{q} = \mathbf{Q}$ and $\xi \sim a$ in the expression for $\Gamma_{\mathbf{q}}$.

Indeed the $\mathbf{q}$ dependence of the interaction is modeled by choosing only the interband terms in the coupling constant $\lambda_{\alpha\beta}$.[3] With all these assumptions the final expression for the bosonic propagator times the scattering matrix $V_{\alpha\beta}$ used in the calculations has the following form:

$$V_{\alpha\beta} D(\omega_n - \omega_m) = V_{\alpha\beta} \frac{\omega_0}{\omega_0 + \mid \omega_n - \omega_m \mid}. \tag{4.12}$$

For reproducing the low temperature properties of LaFePO close to T_c, the value of ω_0 was fixed at 20 meV in order to resemble the spin fluctuations spectrum revealed by neutron scattering experiment on pnictides. [149–151]

In Fig. 4.4 a sketch of the non interacting low-energy band structure of LaFePO is shown, and the arrows indicate the non zero elements of $V_{\alpha\beta}$ which represent the interaction between the two hole pockets at the Γ point and the two electron pockets at the M point, namely $V_{1,3}$,$V_{1,4}$,$V_{2,3}$,$V_{2,4}$ and their symmetric elements ($V_{\alpha\beta}$ is indeed symmetric). The non zero element of $V_{\alpha\beta}$ are all fixed at the same

[3] Spin fluctuations in pnictides are strongly enhanced at $\mathbf{Q}_{AFM} = (\pi/a, \pi/a, 0)$ due to the nesting condition between the hole pockets at Γ and the electron pockets at M. Therefore, by assuming a separable form of the bosonic propagator $\tilde{D}(\Omega_n, \mathbf{q}) = V(\mathbf{q})D(\Omega_n)$, the $\mathbf{q}$ dependence of the propagator $D(\Omega_n, \mathbf{q})$ is transferred to the coupling matrix $V_{\alpha,\beta}$ and consequently to the coupling constant $\lambda_{\alpha,\beta}$.

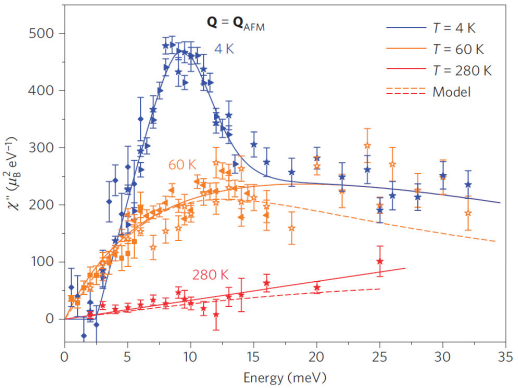

Figure 4.5: Figure from Ref. [152]. Temperature dependence of $\chi''(\mathbf{Q}_{AFM}, \omega)$ measured by neutron scattering. The solid lines are guides to the eye. The dashed lines represent global fits with the eq. (4.9). The error bars represent the statistical error.

value $V = 0.46$ meV. This choice of V gives indeed the best agreement with the experiments. [1, 185, 195, 229–231, 336]

At this point, instead of V is convenient to introduce the adimensional quantity $\lambda_{\text{av}} = \sum_{\alpha\beta} \lambda_{\alpha\beta}/4$ which is an average of the dimensionless coupling constant in each of the four bands included in the microscopic model. I found that the value of $\lambda_{\text{av}} \sim 0.5$ needed to reproduce the experimental Fermi surface volume measured at low temperature, [229] was found to reproduce also the superconducting $T_c = 7$ K [1] and the specific heat measurements. [230, 231] At higher temperature, both the coupling constant λ_{av} and the characteristic energy scale of the spin fluctuations mode ω_0 change. In particular ω_0 shifts towards higher energy ($\omega_0 \sim 60$ meV), as measured by Inosov *et al.* [152] in BaFeCo. They measured the imaginary part of the spin susceptibility of $BaFe_{1.85}Co_{0.15}$ and fit the experimental results with formula 4.9 as shown in Fig. 4.5. The temperature dependence of ω_0 was estimated

to be: [152]

$$\omega_0(T) = \omega_{00}(T + \theta), \tag{4.13}$$

with $\omega_{00} = 0.14 \pm 0.004$ meV/K and $\theta = 30 \pm 10$ K. This means that $\omega_0(T \sim 300\text{ K}) \approx 3\omega_0(T \sim 7\text{ K})$. This increasing of ω_0 is accompanied by the weakening of the antiferromagnetic correlations which can be parameterized as a reduction by a factor of 3 in λ_{av}, whose value at $T = 300$ K can be estimated as $\lambda_{\text{av}}(T \sim 300\text{ K}) \sim 0.17$.

4.2.3 Intraband optical conductivity

Since the self-energy in eq. (4.6) is **q** independent, the vertex corrections vanish and the intraband optical conductivity $\sigma^{\text{intra}}(\omega)$ can be computed in the simple-bubble approximation. [337–339] Its real part can be thus written as $\sigma_1^{\text{intra}}(\omega) = \sum_\alpha \sigma_{1\alpha}(\omega)$, where

$$\sigma_{1\alpha}(\omega) = \frac{-2\pi e^2}{\hbar} \int_\infty^\infty dz \frac{f(z-\mu+\omega) - f(z-\mu)}{\omega} \times$$

$$\times \int \frac{d\mathbf{k}^2}{4\pi^2} v_{\mathbf{k},\alpha}^2 A_\alpha(\varepsilon_{\mathbf{k},\alpha}, z+\omega) A_\alpha(\varepsilon_{\mathbf{k},\alpha}, z). \tag{4.14}$$

In eq. (4.14) $f(z) = 1/(\exp^{-z/T} + 1)$ is the Fermi function, $v_{\mathbf{k},\alpha} = \partial\varepsilon_{\mathbf{k},\alpha}/\partial k_x$ is the quasi particle velocity and the spectral function, defined as $A_\alpha(\varepsilon_{\mathbf{k},\alpha}, z) = -\frac{1}{\pi} Im G_\alpha(\mathbf{k}, \omega + i0^+)$, [340] can be written in the following way: [336]

$$A_\alpha(\varepsilon_{\mathbf{k},\alpha}, z) = \frac{1}{\pi} \frac{\Gamma_\alpha^{qp}(\omega)}{\left[\omega - \varepsilon_{\mathbf{k},\alpha} - \chi_\alpha(\omega)\right]^2 + \left[\Gamma_\alpha^{qp}(\omega)\right]^2}. \tag{4.15}$$

In eq. (4.15) $\chi_\alpha(\omega)$ is the real part of the self-energy and $\Gamma_\alpha^{qp}(\omega) = \Gamma_\alpha(\omega) + \Gamma_0$, where $\Gamma_\alpha(\omega) = -Im\Sigma_\alpha(\omega)$ and $\Gamma_0 = 10$ meV is an impurity finite quasiparticle scattering rate obtained by estimating the approximate width of the low-energy optical spectra from the experiment in Ref. [153].

The analytic continuation for $G_\alpha(\mathbf{k}, i\omega_n) \rightarrow G_\alpha(\mathbf{k}, \omega + i0^+)$ and $\Sigma_\alpha(\mathbf{k}, i\omega_n) \rightarrow \Sigma_\alpha(\mathbf{k}, \omega + i0^+)$ was obtained with the Marsiglio-Schossmann-Carbotte procedure. [341]

The imaginary part of the of the optical conductivity can be obtained from the Kramers-Kronig relations. Finally $\tau^{-1}(\omega)$ is calculated from eq. (4.3).

In this section I introduced the model and the basic assumptions for the intraband optical properties of LaFePO. First I presented the extended Drude model which assumes a frequency-dependent inverse time scattering $\tau^{-1}(\omega)$ due to retarded interaction. This quantity can be obtained by calculating the real part of the complex optical conductivity $\sigma_1(\omega)$, once the low-energy band structure is modeled. The low-energy bandstructure was modeled with two hole bands sitting at the Γ point and two degenerate electron bands sitting at the M point. The interaction was assumed to be purely interband and mediated by spin fluctuations. The propagator of the retarded interaction was supposed to be proportional to the spin susceptibility modeled by Millis. [171] The self-energy was obtained in the Migdal Eliashberg approximation with a local approximation on the dressed Green's function. Since the obtained self-energy is $\mathbf{q}$ independent the optical conductivity was calculated by neglecting vertex corrections.

4.3 Role of interband transitions

In this section I compare the intraband optical conductivity calculated from the many-body model introduced in the previous section with the experimental data of Ref. [153]. The large difference between the optical conductivities can be explained by assuming low-energy interband transitions ($\omega \lesssim 1000$ cm^{-1}).

The real part of the intraband optical conductivity, and the corresponding ω dependent inverse time scattering are shown in Fig. 4.6 and compared with the experimental data from Ref. [153]. From the experimental data two regimes can be clearly distinguished. At low frequencies ($\omega \lesssim 500$ cm^{-1}), $\sigma_1(\omega)$ shows a narrow Drude-like behavior and $\tau^{-1}(\omega)$ is constant ~ 400 cm^{-1}. Above this frequency,

$\sigma_1(\omega)$ appears to be flat while $\tau^{-1}(\omega)$ increases linearly.

I remark that impurity scattering gives rise to a constant $\tau^{-1}(\omega)$ while collective modes like phonons make this quantity grow up to a saturation point above the characteristic energy scale of the excitations involved. [342] For these reasons at first glance the experimental data seem to indicate the presence of collective modes with typical energy scales well beyond 500 cm^{-1}. Therefore phonons were ruled out since their energy scale in pnictides does not exceed 500 cm^{-1}. [4, 153] The collective modes responsible for the observed behavior of the optical properties in LaFePO could be due to spin fluctuations. [153] Indeed, since χ'' in eq. (4.9) decays slowly with ω, [171] the spectrum of spin fluctuations extends well beyond 500 cm^{-1}.

In the previous section I presented an effective low-energy model for LaFePO, which describes the low-energy properties of this material in a consistent framework. The basic ingredient is the exchange of antiferromagnetic spin fluctuations among holes and electrons located in different parts of the Brillouin zone, connected by the $\mathbf{Q}_{AFM} = (\pi/a, \pi/a, 0)$ nesting vector. In Fig. 4.6 I show as blue dots the experimental data from Ref. [153] and the lines represent the calculations using two different values of λ_{av}. With red dashed line the theoretical curves obtained by using $\lambda_{\text{av}} = \lambda_1 \equiv 0.55$ are indicated.

This value is chosen in order to reproduce the linear behavior of the experimental inverse lifetime scattering $\tau^{-1}(\omega)$ and it is slightly larger than $\lambda_{\text{av}} = 0.5$ used to reproduce the low-energy properties. [1, 229–231]

The black continuous lines are obtained by using a value of the average coupling constant λ_{av} reduced by a factor of 3 with respect to the one used at $T \sim T_c$, which takes into account the temperature-dependence of the spectrum: $\lambda_{\text{av}} = \lambda_2 \equiv 0.5/3 = 0.17$.

The optical conductivity was calculated according to section 4.2.3 and the inverse scattering time $\tau^{-1}(\omega)$ was calculated with formula (4.3) of section 4.2.1 using the experimental value of $\omega_P = 14900$ cm^{-1}. [153] The comparison between the theoretical results and the experimental data shown in Fig. 4.6 is unsatisfactory and inconsistent in terms of the used parameters. Indeed the value of the average

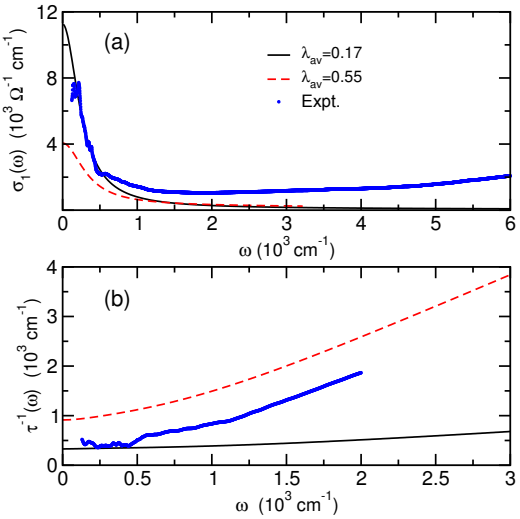

Figure 4.6: Figure from Ref. [319]. Comparison between the experimental data (filled blue circles) at $T = 300$ K from Ref. [153] and theoretical calculations of the intraband contribution (black continuous and red dashed lines) for (a) the optical conductivity and (b) the corresponding $\tau^{-1}(\omega)$ as extracted from the extended Drude model analysis of LaFePO. Different values of the average coupling $\lambda_{\rm av}$ are considered here (see text).

coupling constant $\lambda_{\rm av} = \lambda_1$ required to reproduce the linear behavior of $\tau^{-1}(\omega)$, is too large compared to the one used for reproducing the de Haas-van Alphen Fermi surface volume and the thermodynamic properties at low temperature and is completely out of the experimental curve for the optical conductivity. Moreover, $\lim_{\omega\to 0}\tau(\omega,\lambda_1)$ is more than twice as large as the experimental one. The experimental spectrum is taken at $T = 300$ K. [319] Taking into account the effect of temperature on $\lambda_{\rm av}$, *i. e.* using the reduced value λ_2 (black lines in Fig. 4.6),

improves definitely the agreement between the theoretical and the experimental curve for the low frequency optical conductivity. However, above 500 cm^{-1} the two curves completely depart from each other and the theoretical results for $\tau^{-1}(\omega)$ above 500 cm^{-1} are definitely in disagreement with the experiment. On the other hand, below 500 cm^{-1}, the agreement with the experiment is satisfactory. The question why the low-energy model fails above this limit remains, even assuming for spin fluctuations the long tailed energy spectrum of eq. (4.9). [171]

The answer could reside in the definition of "low-energy" range and in the assumption of absence of interband transitions below 2000 cm^{-1} implicit in the use of the extended Drude model analysis -see end of subsection 4.2.1. [134] Low-energy interband transitions, within the range where the EDM is applied, could indeed give a contribution that makes the real part of the optical conductivity flat in the mid-infrared region (500 cm^{-1} $\lesssim \omega \lesssim$ 2500 cm^{-1}) and causes the linear behavior of the inverse time scattering. The experimentally observed flat behavior of the optical conductivity in the mid-infrared region, [153, 320] could be then misinterpreted as coming from spin fluctuations. Some authors indeed suggested that interband transitions in pnictides could be present already in the low-energy range ($\omega <$ 2000 cm^{-1}). [154–158]

In order to investigate quantitatively their role on the optical conductivity of LaFePO, I introduce a phenomenological model in which these transitions are approximated as a Lorentzian peak with characteristic frequency ω_L, spectral weight S_0 and width γ. The resulting optical conductivity $\sigma^{\text{try}}(\omega)$ is given by:

$$\sigma^{\text{try}}(\omega) = \sum_{\alpha} \sigma_{1\alpha}(\omega) + \frac{S_0^2}{4\pi} \frac{\omega}{\omega\gamma + i(\omega_L^2 - \omega^2)}. \tag{4.16}$$

In eq. (4.16) $\sigma_{1\alpha}(\omega)$ are the intraband contributions given from eqs. (4.14) and (4.15). Fig. 4.7 shows the results for $\sigma_1(\omega) = Re[\sigma^{\text{try}}(\omega)]$ and for the corresponding $\tau^{-1}(\omega)$ using different values of ω_L, S_0 and γ. For $\gamma/\omega_L \ll 1$ (red and green curves) interband transitions appear as a sharp peak centered at the respective ω_L both in $\sigma_1(\omega)$ and in $\tau^{-1}(\omega)$. On the other hand, when $\gamma/\omega_L \approx 1$, the Lorentzian contribution adds smoothly to $\sigma_1^{\text{intra}}(\omega) = \sum_\alpha \sigma_{1\alpha}(\omega)$, and this causes a smooth

increase of $\tau^{-1}(\omega)$ which is more pronounced as soon as S_0 approaches ω_p^2 (light and dark blue curves). An interesting thing is that, for a given value of S_0, the height of the peak in $\tau^{-1}(\omega)$ grows with increasing ω_L, therefore very low frequency contributions in $\sigma_1^{try}(\omega)$ do not affect $\tau^{-1}(\omega)$ at all.

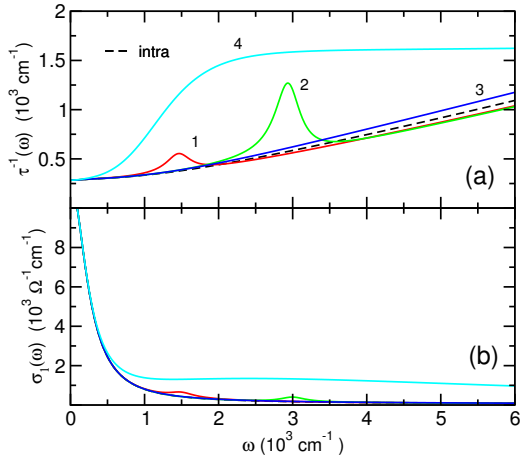

Figure 4.7: Figure from Ref. [319]. Scattering rate (a) resulting from the EDM analysis of the optical conductivity $\sigma(\omega)$ from Eq. (4.16), and its real part $\sigma_1(\omega)$ (b). The intraband term is computed here with $\lambda_{av} = 0.17$ and the microscopic parameters reported in section 4.2.2. The Lorentzian parameters are: (1) $\omega_L = 1500$ cm^{-1}, $\gamma = 400$ cm^{-1}, $S_0 = 2400$ cm^{-1}; (2) $\omega_L = 3000$ cm^{-1}, $\gamma = 400$ cm^{-1}, $S_0 = 2400$ cm^{-1}; (3) $\omega_L = 3000$ cm^{-1}, $\gamma = 8000$ cm^{-1}, $S_0 = 2400$ cm^{-1}; (4) $\omega_L = 3000$ cm^{-1}, $\gamma = 8000$ cm^{-1}, $S_0 = 24000$ cm^{-1}.

From this analysis it emerges that the experimental data in Fig. 4.6 could be fitted with a Lorentzian contribution like the one shown in light blue in Fig. 4.7 added to the calculated intraband optical conductivity shown by the black dashed line. The origin of such a contribution and its estimate by means of density functional theory

(DFT) calculations will be the topic of the next section.

In this section I made a preliminary comparison between the intraband optical conductivity calculated in the previous section and the experimental results of Ref. [153]. A boundary frequency $\omega_B \approx 500$ cm^{-1} emerges below which the optical spectrum is in agreement with the calculated optical conductivity. Above ω_B instead the agreement disappears. Since the calculated intraband contribution alone is not sufficient for reproducing the experiment, I explored the possibility of having low-energy optical interband transitions in the spectrum of LaFePO. I modeled their contribution as an additional Lorentzian peak. The result of this investigation shows that the flat feature of $\sigma_1(\omega)$ and linear behavior of $\tau^{-1}(\omega)$ observed in Refs. [153, 320] could be captured by a Lorentzian contribution located at $\omega_L \sim 3000$ cm^{-1} and having width $\gamma = 8000$ cm^{-1}.

4.4 Origin of interband transitions

In order to understand where the mid-infrared contribution to the optical spectrum of LaFePO comes from, I calculate the complex dielectric function $\tilde{\varepsilon}(\omega) = \varepsilon_1(\omega) + i\varepsilon_2(\omega)$ for this material within density functional theory (DFT). The diagonal terms of the imaginary part of the dielectric tensor can be indeed calculated from the eigenvalues and the wave functions of a band calculation according to the following formula: [343]

$$\varepsilon_2^{\alpha\alpha}(\omega) = \frac{4\pi e^2}{m^2\omega^2} \sum_{i,f} \frac{\int 2d\mathbf{k}^3}{(2\pi)^3} \mid \langle i\mathbf{k} \mid P_\alpha \mid f\mathbf{k} \rangle \mid^2 f_i^{\mathbf{k}}(1 - f_f^{\mathbf{k}})\delta(E_f^{\mathbf{k}} - E_i^{\mathbf{k}} - \hbar\omega) \quad (4.17)$$

where i and f indicate the initial and the final state (sitting below and above the Fermi level E_F) respectively, $\mid i\mathbf{k}\rangle$ indicates the ket associated with the eigenstate with wave vector $\mathbf{k}$ and band index i, and $E_i^{\mathbf{k}}$ is the corresponding eigenvalue. Finally $f_i^{\mathbf{k}} = 1/(\exp^{(E_i^{\mathbf{k}} - E_F)/k_B T} + 1)$ is the Fermi function, k_B the Boltzmann's constant and P_α the α component of the momentum operator. From now on I will abandon the

index α since I consider only $\alpha = x$. The real part of the dielectric function $\varepsilon_1(\omega)$ was obtained by Kramers Kronig transformation. The interband contribution to the real part of the optical conductivity is given by $\sigma_1^{\text{inter}}(\omega) = \omega\varepsilon_2(\omega)/4\pi$. Technical details of the calculations are given in section 4.7. The calculated $\sigma_1^{\text{inter}}(\omega)$ is shown in the upper part of Fig. 4.8 and it is found in very good agreement with previous calculations. [153] The spectrum shows a peak at very low-energy indicated with "A" and a broader feature at higher energies labeled with "B". The origin of such contributions can be qualitatively understood by looking at the low-energy band structure of LaFePO plotted at the bottom of Fig. 4.8. Here, in order to allow a direct comparison with the upper part of the figure, the energy is measured in cm^{-1} which is the natural unit for optical experiments. [134]

The relatively sharp peak at low-energy comes from interband transitions involving the hole pockets around the Γ point and the electron pockets around the M point as indicated by the blue arrows. Since the electron pockets are degenerate along the $X - M$ direction and split along the $\Gamma - M$ one, their contribution goes down to zero energy. Note that if the band character are purely d these transitions are not allowed. Moreover, as explained in section 4.1, if one considers the unit cell with only one Fe per unit cell (neglecting the interlayer coupling), the Brillouin zone volume is doubled and the electron pockets which in Fig. 4.8 sit at the M point are located around two different point of the extended Brillouin zone. Therefore the transition is not optical anymore. [72] For this reason the intensity of the very low-energy interband transition can be somehow related to the intensity of the interlayer coupling in Fe pnictides. Furthermore, since almost all the Fe pnictides show very similar band structures compared to LaFePO, the general shape of the feature in the optical spectrum is expected to be also quite general.

From the analysis made in section 4.3, the presence of this low-energy feature is expected to modify only slightly the shape of the real part of the total optical conductivity while it does not affect the scattering rate $\tau^{-1}(\omega)$ at all. What instead influences crucially the shape of $\tau^{-1}(\omega)$ is the broader feature which starts at $\sim 2500\ \text{cm}^{-1}$ indicated with "B" in Fig. 4.8 (a). This contribution comes from the transitions involving Fe $3d$ bands and indicated by the golden arrow in Fig. 4.8.

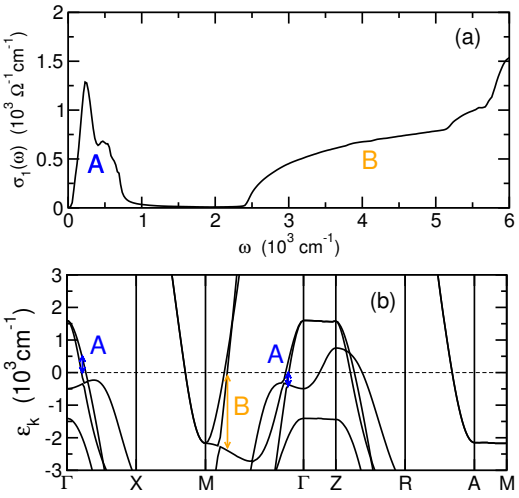

Figure 4.8: Figure from Ref. [319]. Real part of the interband optical conductivity of LaFePO evaluated in DFT calculations (a), and the corresponding bandstructure (b). The arrows in panel (b) indicate a few representative optical transitions contributing to the structures in the real part of the optical conductivity labeled as A and B in panel (a).

Due to correlation effects described in section 4.1 it is expected to affect the optical conductivity even at lower energies. However in Ref. [153] these transitions are located at 7000 cm^{-1} and completely neglected while performing the EDM analysis.

A systematic assignment of the optical interband transitions in Fe pnictides was made, after my work [319] appeared, by Charnukha *et al.* [159] and they are shown in Fig. 4.9. By comparing the ellipsometry measurement on $Ba_{0.68}K_{0.32}Fe_2As_2$ (belonging to another family of Fe pnictides with respect to LaFePO) with LDA calculations, they showed that the interband transitions among the Fe 3d bands,

which in LDA start around 2500 cm^{-1} and have their maximal intensity at $\sim$ 12000 cm^{-1}, in the experiment are found at much lower energies. Due to correlation effects indeed the Fe d bands get renormalized and the maximal intensity for these transitions is found at energy $E \sim 4000$ cm^{-1} *i.e.* a factor of ~ 3 smaller than LDA. [159] Note that this number is sensibly larger that the renormalization factor of 2 found in LaFePO by ARPES measurement [136] and discussed in section 4.1. Indeed correlation effects are found to be smaller in LaFePO than in other families of pnictides. [68]

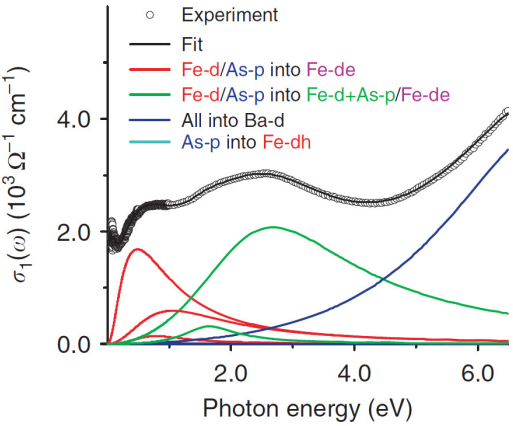

Figure 4.9: Figure from Ref. [159]. Real part of interband optical conductivity from ellipsometry experiment on K-doped $Ba_{0.68}K_{0.32}Fe_2As_2$.The different contribution to the total optical conductivity where assigned by the comparison with LDA calculations. Fe-de indicates the Fe d electron bands, Fe dh indicates the Fe d hole bands.

The results shown in Fig. 4.9 bring to the conclusion that the low-energy interband optical transitions actually affect the optical properties of pnictides but they cannot be estimated simply by the bare LDA calculations. Indeed LDA calculations

can give an indication about the position and the intensity of these transitions but a renormalization factor must be introduced and, at the end, only the comparison with the experiment can give a conclusive answer concerning this effect.

In this section I calculated the optical spectrum of LaFePO within DFT in order to investigate the origin of the flat behavior of the experimental $\sigma_1(\omega)$. Optical interband transitions are actually present at very low-energy and involve the hole bands and the electron bands around the Fermi level. The optical conductivity shows a peak around ≈ 500 cm^{-1} and a broader feature starting from ≈ 2500 cm^{-1} but, due to the overestimation of the bandwidth in GGA, these transitions should be observed at lower energies.

4.5 Phenomenological model and comparison with the experiment

The analysis of the experimental data [153] made up to now, shows clearly two regimes in the optical spectrum of LaFePO. The boundary between these two regions can be fixed at $\omega_B \sim 500$ cm^{-1} where the real part of the optical conductivity shows an upturn and becomes flat and $\tau^{-1}(\omega)$ starts to increase roughly linearly with ω. The two regimes are characterized by two different contributions to the optical spectrum. At low frequency the interaction effects are predominant and the main consequence is a reduction of the optical spectral weight transferred to higher energies. [336] However this kind of physics has basically no consequences on the scattering rate and $\tau^{-1}(\omega)$ approaches its constant Drude limit. Above ω_B the intraband contribution to $\sigma_1(\omega)$ drops rapidly but the interband transitions start to set in. In order to get a complete description of the optical properties of LaFePO in the far/mid-infrared ($100 \lesssim \omega \lesssim 2500$ cm^{-1}) regime it is then sufficient to merge the theoretical results obtained up to now by adding the interband optical conductivity to the intraband one. However the comparison between the experimental and theoretical results made in Ref. [159] for the K doped $BaFe_2As_2$

S_1	ω_1	γ_1	S_2	ω_2	γ_2	ϵ_{high}
2300	750	40	33500	4500	20200	15

Table 4.2: Interband parameters of the model (4.18) expressed in units of cm^{-1} (S_i, ω_i, γ_i) and in dimensionless units (ϵ_{high}).

system, showed that DFT locates the d-d transitions at higher energy with respect to the experiment and this is consistent with the bandwidth overestimation by roughly a factor of 2 found by the comparison of DFT calculations with ARPES experiment. [136] For this reason the DFT interband optical conductivity calculated in section 4.4 cannot be directly used to construct the theoretical curve. In order to use all the informations encoded in the DFT optical conductivity, overcoming at the same time the problem associated with the underestimation of correlation effects, I model the interband optical conductivity in the following way. I add two Lorentzian peaks to the intraband optical conductivity calculated by means of the microscopic model presented in section 4.2.2:

$$\sigma(\omega) = \sigma^{\text{intra}}(\omega) + \sum_{i=1,2} \frac{S_i^2}{4\pi} \frac{\omega}{\omega\gamma_i + i(\omega_i^2 - \omega^2)}, \tag{4.18}$$

plus a high energy dielectric constant ϵ_{high} to account for processes at higher energies. The parameters of the model are the same as the one used to calculate the intraband conductivity in section 4.2.2 and shown in Figs. 4.6 and 4.7: $\lambda_{\text{av}} = 0.17$ and $\omega_0 = 60$ meV. The Lorentzian parameters S_i,γ_i and ω_i, were instead chosen in order to reproduce the two feature characterizing the DFT interband optical conductivity of Fig. 4.8 and the frequencies were adjusted for reaching the best agreement with the experimental curve. The values of S_i,γ_i and ω_i are listed in table 4.2 and the comparison with the experiment is shown in Fig. 4.10.

The first thing to notice is the very good agreement with the experimental data from Ref. [153]. The effect of interband transitions is to enhance the optical conductivity shown in panel (a) above 500 cm^{-1} and, as a consequence, to reinforce the magnitude and the frequency dependence of $\tau^{-1}(\omega)$. The comparison made in

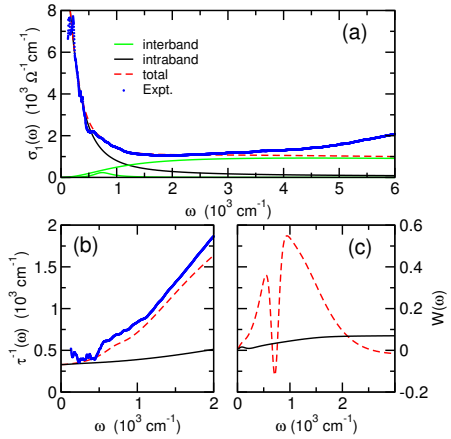

Figure 4.10: Figure from Ref. [319]. (a) Real part of the optical conductivity $\sigma_1(\omega)$ computed using Eq. (4.18) (red dashed line, labeled as "total" in the caption), along with the intraband part (solid black line) and the interband part (solid green line). The symbols represent the experimental data of Ref. [153]. (b) $\tau^{-1}(\omega)$ extracted from the extended-Drude-model using the total conductivity (dashed red line) or the intraband part only (solid black line), along with the experimental data (symbols) (c) Approximate electron-boson Eliashberg function $W(\omega)$ extracted from $\tau^{-1}(\omega)$ with the second-derivative method (see text) using either the total conductivity (dashed red line) or the intraband part only (solid black line).

panel (b) shows indeed that, due to the contribution of low-energy interband optical transitions the slope increases about 4 times. The comparison with the experiment is limited to frequencies up to 2000 cm^{-1}; in order to get a perfect fit to experiment also interband transitions at higher energies could have been included. However this was not done for two main reasons. First because interband transition are expected above 2000 cm^{-1}. The second reason is because the main scope of this work was to explain the linear behavior of $\tau^{-1}(\omega)$ at low frequency.

If interband transitions are neglected, there is a severe misinterpretation of the experimental data. Indeed, the ω dependence of $\tau^{-1}(\omega)$ can be connected with the spectrum of the retarded interaction $\alpha^2F(\omega)$ from which it is generated. This connection is made, under certain conditions, by assuming that: [134]

$$\frac{1}{\tau(\omega)} \approx \frac{2\pi}{\omega}\int_0^{\omega}(\omega-\Omega)\alpha^2F(\Omega)d\Omega$$

and then identifying the quantity $W(\omega)=\frac{1}{2\pi}d^2[\omega\tau^{-1}(\omega)]/d\omega^2$ with the electron-boson Eliashberg function $\alpha^2F(\omega)$. For spin fluctuations-mediated superconductors $\alpha^2F(\omega)$ is given by $\chi''(\omega)$ in eq. (4.9). The coupling constant λ is then obtained as the integral $\lambda_{eff}=2\int_0^{\omega_c}d\omega W(\omega)/\omega$ where ω_c is a cut-off beyond which interband transitions are supposed to be important.

In the following, I use the full (inter and intra-band) theoretical model derived in the previous section to demonstrate that neglecting low-energy interband transitions can lead to a severe misinterpretation of the experimental data in LaFePO and in Fe pnictides in general. In fig. 4.10 I compare several quantities, calculated for the full model (red lines), and for the intraband contribution alone (black lines).

In panel c, the two sets of data are used to estimate $W(\omega)$, and hence the Eliashberg spectrum $\alpha^2F(\omega)$. The figure clearly shows that the spectra estimated in the two cases are very different, and also give rise to very different values of the effective coupling constant λ_{eff}. In particular, when the analysis is made on the black curve (considering only σ^{intra}), one obtains $\lambda_{eff}=0.27$ larger than the input value for our model $\lambda_{\text{av}}=0.17$, but the order of magnitude is the same. On the other hand considering only this contribution does not reproduce the experimental data in panel (a) and (b) of Fig. 4.10. In order to reach the agreement with the experiment the contribution to $\sigma(\omega)$ coming from the interband transitions must be added. However, if these are not properly subtracted from the spectrum, they give a large spurious contribution to $W(\omega)$,leading to an effecting coupling constant $\lambda_{eff}=1.31$, much larger than the input λ_{av}.

This analysis demonstrates that it is not possible to reproduce the experiment without including the contribution coming from low-energy optical interband transi-

tions to the optical conductivity of LaFePO. At the same time I showed that, due to this contribution, the coupling obtained from the EDM analysis of the experimental data gives a value of the coupling constant, associated with the electron-boson interaction, which is one order of magnitude larger than the one actually generated by the fluctuating modes. This analysis explains why the coupling constants extracted from optical measurements in Fe pnictides [156, 157] are usually much larger than the one extracted from other experimental probes. [136, 229–231]

4.6 Conclusion

In this chapter I studied the effect of low-energy interband optical transitions on the optical properties of LaFePO. This material belongs to the wide class of the Fe-based superconductors. As shown in section 4.1, these are layered materials characterized by the presence of many bands at the Fermi level. Moreover the hole and the electron bands, connected by the nesting vector $\mathbf{Q}_{AFM} = (\pi/a, \pi/a, 0)$, interact via the exchange of antiferromagnetic spin fluctuations. These features have two main consequences on the optical properties. The intraband optical conductivity is affected by the retarded interaction with spin fluctuations and, at the same time, interband optical transitions set in at lower energy with respect to single band metals. The latter effect gets even reinforced whenever the overall bandwidth is renormalized under the effect of correlation. In order to extract informations about the spectrum of the bosonic mode involved in the interaction and about the relative coupling constant, the EDM is often used for analyzing the experimental data. This model introduces both a frequency-dependent scattering rate $\tau^{-1}(\omega)$ and a mass enhancement factor $m^*(\omega)/m = 1 + \lambda(\omega)$ into the Drude formula for the low frequency optical conductivity. The same two quantities can also be calculated by computing the complex optical conductivity $\tilde{\sigma}(\omega)$ within an appropriate model. In section 4.2 I illustrated the EDM and I presented the low-energy model used for calculating $\tilde{\sigma}(\omega)$. In section 4.3 I showed, through a preliminary comparison

with the experimental results of Ref. [319], that the calculated intraband optical conductivity, cannot reproduce alone the low-energy optical properties of LaFePO. For this reason I explored the possibility of adding low-energy interband transitions modeled by a Lorentzian peak to the calculated intraband optical conductivity and studying the behavior of $\tau^{-1}(\omega)$ for different values of frequency ω_L of the peak, width γ and its spectral weight S_0. The result of such a study is that the features in the experimental optical properties of LaFePO could be originated by the presence of low-energy interband transition with $\omega_L/\gamma \sim 1$ and $\omega_L \sim 3000$ cm^{-1}. In order to verify the actual presence of these transitions and to have a better understanding about their origin I calculated, in section 4.4, the interband optical conductivity of LaFePO in GGA, and it turned out that these transitions are actually present and come from the hole bands placed around the Γ point and the electron bands around the M point. The real part of the optical conductivity shows one peak at very low-energy which does not contribute to $\tau^{-1}(\omega)$ at all, and a broader feature at higher energy which strongly affects this quantity.

Since in GGA the bandwidth is overestimated with respect to the experiment, the total optical conductivity cannot be calculated simply by summing together the interband contribution calculated in GGA and the intraband one calculated in section 4.2. For this reason in section 4.5 I modeled the contribution to $Re[\tilde{\sigma}(\omega)]$ coming from the interband optical transitions as two Lorentzian peaks: a narrow peak at low-energy and wider one at higher energy. The result is in perfect agreement with the experiment both for $Re[\tilde{\sigma}(\omega)]$ and $\tau^{-1}(\omega)$. This has important consequences on the physical understanding of LaFePO and of pnictides in general. In fact, in the previous section I have shown that the presence of low energy interband transitions introduces spurious effects in the EDM analysis resulting in a ficticious contribution to the amplitude of the coupling constant. Since all the pnictides have similar low-energy bandstructure, the presence of low-energy interband optical transitions is expected to be a quite general feature in this class of materials. As a consequence the spin fluctuations coupling constant estimated via optical experiment are generally overestimated. The phenomenological model for the interband optical conductivity shown in section 4.5 allows instead to describe the low-energy optical spectrum

of LaFePO with an average coupling constant λ_{av} perfectly consistent with the one extracted from other experimental probes.

4.7 Technical details

The interband optical conductivity $\tilde{\sigma}^{inter}(\omega)$ of LaFePO was calculated using the full-potential linearized plane wave (LAPW) method as implemented in the WIEN2K package. [251, 308, 309, 344] The Brillouin zone sampling for the optical calculations was done using a very dense gride of more than 5000 **k** points in the symmetry irreducible wedge. $\tilde{\sigma}^{inter}(\omega)$ was evaluated usng a broadening factor $\eta = 1$ meV.

Chapter 5

Toward an *ab-initio* estimate of the Stoner I

In this chapter I present a new and simple method for correcting the magnetic properties of itinerant magnets within DFT. The method, developed in Ref. [345] and called reduced Stoner theory (RST), is computationally inexpensive and easy to implement. In the following, using the extended Stoner theory by Andersen et al., [253] *I show that this new method is in direct connection with the selfconsistent renormalization theory by* Moriya. [17] *Finally, I apply it to the ferromagnetic-paramagnetic transition of Ni_3Al under pressure, as a prototypical example of itinerant ferromagnet. I find that in this material the near-critical spin fluctuations renormalize the Stoner parameter by an almost pressure independent quantity. The transition from ferromagnetic to paramagnetic state is thus entirely driven by a bandstructure effect. Exploiting the perfect scaling of the band structure with pressure, I describe the magnetic moment vs pressure curve completely* ab initio. *Moreover I compare my results with the experimental data concerning the Curie temperature as a function of pressure reported*

in Ref. [201]. The agreement is remarkable and I also give a microscopic justification to the phenomenological model used therein for interpreting the experimental data.

Introduction

As shown for the systems studied in chapters 2 and 4, DFT is a very accurate theoretical tool for obtaining the ground state of real materials. The secret resides in the variational nature of the method. [46] However the mean field approximations needed to implement DFT reduce a lot its power.

A well known problem in LSDA (and GGA) is for example the overestimation of the tendency to magnetism in systems close to a quantum critical point (QCP). [263] Indeed the mean field nature of LSDA (and GGA) does not allow to take into account the detrimental effect of near critical fluctuations on the long-range magnetism, so that the calculated magnetic moment is sensibly larger than the experimental one. Typical examples of materials where this happens are, together with CuBiSO analyzed in chapter 3, FeAl [50], Pd [51] and the more recent, Fe pnictides. [54, 57, 72] In the latter case it was shown that a reduction of the magnetic moment can be achieved within the $LDA+U$ method, [50] by means of a negative Hubbard interaction U. [65] The underlying idea is that in itinerant systems the local interaction U is overestimated at the LDA level and the local moment as well. Therefore a negative U should correct the overestimated Coulomb interaction in LDA and bring the theoretical results in agreement with the experiments, by mimicking the effect of long wavelength fluctuations. However the physical meaning of a negative Coulomb interaction among the electrons is rather questionable. Other approaches which go in the direction of adding fluctuations -beyond L(S)DA- into the system by considering Hubbard type of local interaction are DMFT [66–68] and the Gutzwiller approach. [69] However the Hubbard type of interaction U, is a local interaction and is highly unlikely that a phenomenon due to non local fluctuations can be captured by a local type of interaction. [73] Moreover, in all these cases, the computational

load is well beyond the typical one of an L(S)DA calculation.

An alternative way of treating the effect of non local fluctuations in itinerant magnets is given by the selfconsistent renormalization (SCR) theory by Moriya. [17] However this theory involves quantities, like the spin susceptibility, which are difficult to evaluate numerically within the standard band structure calculations, even when an approximated form is used. [51] Therefore it would be important to include the corrections due to the effect of non local spin fluctuations directly in a more accurate DFT functional than LSDA or GGA.

For these reasons in this chapter I present a new method which corrects the LSDA within DFT. It takes into account the effect of non local fluctuations in suppressing the tendency to magnetism in itinerant systems. The method is easy to implement, computationally as expensive as a normal spin polarized LDA calculation, and has its justification in the connection with the SCR theory by Moriya. The basic concept is that non local fluctuations tend to reduce the gain in energy due to the spin polarization. In the LSDA formalism this is the Stoner interaction. Therefore it is possible to start from the LSDA and build up a more accurate functional simply by scaling the Stoner parameter as much as suggested by the Moriya's theory. For this reason the method is called reduced Stoner theory (RST). As an example I apply this method to the ferromagnetic-paramagnetic transition of Ni_3Al under pressure, which is a typical example of itinerant ferromagnet. For the first time in this material, the magnetic moment as a function of pressure calculated *ab initio*, is in agreement with the experiment.

Ni_3Al is a classic example of itinerant ferromagnet and the importance of non local spin fluctuations in suppressing the tendency to magnetism in this material was demonstrated both theoretically and experimentally. [52, 201, 346, 347] At ambient pressure Ni_3Al is a ferromagnet with a low magnetic moment. Under pressure it undergoes a transition to a paramagnetic state. The behavior of the Curie temperature with pressure is in agreement with the scaling law $T_c \propto (P - P_c)^{3/4}$ proposed by Moriya, if the static inverse susceptibility is supposed to be linear in $(P - P_c)$, where P_c is the critical pressure. [201]

I show that this scaling law is a consequence of a peculiar property of the

bandstructure and I use it as an information on the pressure dependence of the LSDA Stoner parameter.

The present chapter is structured in the following way.

In section 5.1 I present standard DFT results on Ni_3Al under pressure. The magnetic moment at zero pressure is 3 times larger than the experimental one. Under pressure it decreases linearly up to a critical pressure P_c, which is also overestimated with respect to experiment. The band structure in an energy interval of ~ 4 eV around the Fermi level scales almost exactly with pressure, with a linear increase of the bandwidth. Since the Stoner parameter is found to be pressure independent and given the scaling of the density of states with pressure, the LSDA ferromagnetic-paramagnetic transition can be explained simply within the Stoner theory. However, in order to bring the DFT results in agreement with the experiment, the LSDA Stoner parameter must be reduced.

In section 5.2, I describe the origin of this overestimation by means of a phenomenological application of Moriya's theory, *i.e* taking the average amplitude of spin fluctuations as a parameter instead of calculating it via the fluctuation dissipation theorem. Using the extended Stoner theory (EST), [45, 253] I show that the renormalization of the coefficients of the energy expansion in terms of the magnetization m obtained with LSDA is equivalent to a reduction the Stoner parameter in LSDA by a quantity proportional to the square of the average amplitude of spin fluctuations (ξ^2). I define s as the ratio between the "reduced" Stoner parameter and the bare one.

In section 5.3 I apply the RST to Ni_3Al at zero pressure. The method consists in scaling the spin polarized part of the exchange and correlation potential by a quantity s. By comparing the magnetic moment as a function of the Stoner parameter obtained both in RST and in EST I give an *a posteriori* proof of the equivalence of these two methods. However, RST is more accurate because the magnetic moment is obtained self-consistently, and not through a rigid-band shift of the paramagnetic DOS.

In section 5.4 I apply the RST to the ferromagnetic-paramagnetic transition of Ni_3Al under pressure. Here, exploiting the scaling property of the bandstructure,

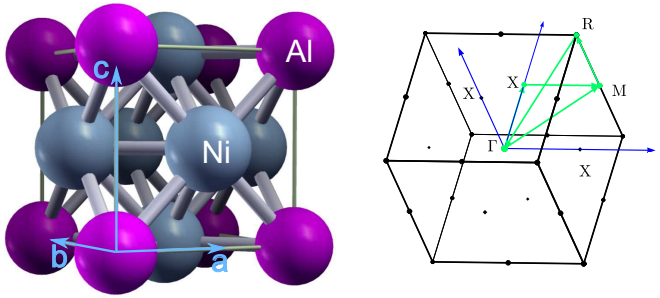

Figure 5.1: Cu_3Au $cP4$ crystal structure of Ni_3Al. (*Left*) Unit cell is simple cubic and contains one formula unit. (*Right*) Brillouin zone used to plot the band structure in Fig. 5.2. The reciprocal lattice vectors are also shown (blue arrows).

I give a completely *ab initio* description of the magnetic moment as a function of pressure. I then compare my data with the Curie temperature as a function of pressure measured by Niklowitz *et al.* [201] which fit the data with a power law behavior whose exponent is $\beta = 3/4$. I find the agreement with the experiment very good and explain that this scaling behavior is a direct consequence of the scaling law of the bandstructure.

Section 5.5 contains the Conclusions of the present chapter. Technical details of the DFT calculations are given in section 5.6.

5.1 Magnetic and paramagnetic DFT results

Ni_3Al crystallizes in the ideal cubic Cu_3Au $cP4$ structure with the unit cell shown in the left panel of Fig. 5.1. [348] The experimental lattice parameter is $a_0 = 3.5680$ *Å*. In this structure four Al atoms are at the corners of a cube and 6 Ni atoms

share the faces of the cube. Therefore the unit cell contains one formula unit. The electronic configuration of atomic Ni is $3d^8 4s^2$ and the one of Al is $3s^2\ 3p^1$. Due to their similar electronegativity (1.8 for Ni and 1.5 for Al) the bond is expected to be metallic. Moreover, as soon as Ni takes more and more electrons from Al, also the Ni $4p$ states get more and more involved in the bond as for other intermetallic compounds. [349, 350] Due to the metallic nature of the bond, the Ni s and p states are expected to hybridize together with the s and p states of Al and form a wide free electron band. Al shares also its three electrons in such a way that the electron count of Ni reaches the d^9 configuration.

The chemical view point is confirmed by the paramagnetic bandstructure obtained by using the experimental lattice parameter. The paramagnetic bands are calculated along the path shown in Fig. 5.1 and plotted in Fig. 5.2 together with the DOS. The 15 d bands with prevalent Ni character extend from 3.5 eV below E_F up to ~ 0.5 eV above it; the hybridized $s-p$ states coming from Ni and Al have much wider energy range: they start from -10 eV below E_F end extend up to 10 eV at least. [1]

For this reason in the DOS only the d states of Ni are highlighted. The electron count of Ni is confirmed to be d^9, different from its atomic configuration. The value of the DOS at the Fermi level is $N_0 = 3.15$ states/eV/spin/f.u. This considerable high value of the DOS at the Fermi level is given by the presence of several flat bands close to the Fermi level.

Considering the Stoner parameter of atomic Ni ($I_{Ni} = 0.97$ eV) and the value of N_0 given above, the Stoner criterion can be calculated and one obtains a value of $N_0 I > 3$ which is well above the Stoner criterion for ferromagnetism. Of course, as for CuBiSO, also in this case the effect of hybridization must be taken into account. This was done by A. Aguayo *et al.* in Ref. [52] and a much smaller Stoner parameter was found, which leads to a Stoner criterion $N_0 I = 1.21$.

At ambient pressure Ni_3Al is indeed ferromagnetic both experimentally and in LSDA, [348] but the theoretical value of the magnetic moment is greatly overesti-

[1] 10 eV above E_F is the largest value of energy for which I calculated the DOS.

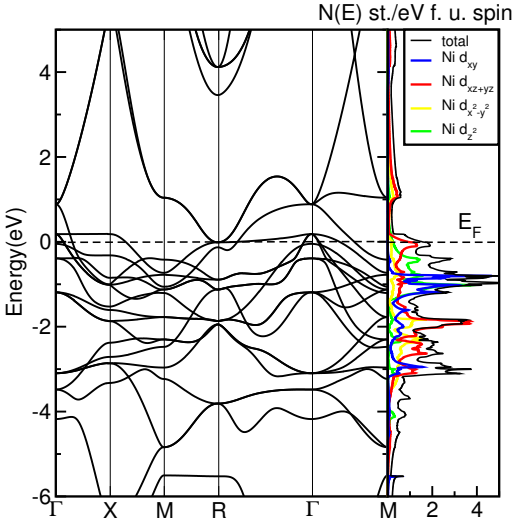

Figure 5.2: LDA band structure and DOS of Ni_3Al obtained using the experimental lattice parameter. The bands are plotted along the path shown in Fig. 5.1 and the DOS is shaded according to the partial Ni d character. The total DOS, marked as total is divided by a factor of 4 for graphical convenience. The black dashed line marks the Fermi level E_F.

mated. The critical pressure P_c is also overestimate by about 5 times with respect to experiment.

In Fig. 5.3 I show the results for Ni_3Al with and without spin polarization. For the spin-polarized calculations, I considered only the ferromagnetic order, which is the ordering actually found in this material. [351] AFM calculations with the spins aligned along the 111 direction converged to a non-magnetic solution.

The equilibrium lattice parameter, both in the magnetic and in the non magnetic case, is found to be $a_0 = 3.4825$ *Å* *i.e.* 2% smaller than experiment. The value of

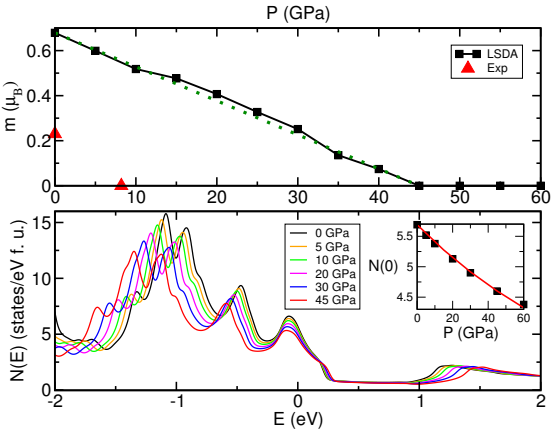

Figure 5.3: Figure adapted from Ref [345]. *Top*: Magnetic moment of Ni_3Al per unit cell, as a function of pressure, calculated in LSDA (black dotted line). Both the magnetic moment at zero pressure $m(0)$ and the critical pressure P_c are overestimated with respect to the experimental data from Ref. [348] (red triangles). The green dots are a linear interpolation of the data. *Bottom*: Paramagnetic density of states as a function of energy calculated for different pressures in LDA. *Inset*: Density of states at the Fermi level calculated as a function of pressure (black squares). The data are fitted with eq. (5.1) (red continuous line).

the DOS at the Fermi level (N_0) at zero pressure is $N_0(0) = 2.85$ st./eV/ spin f.u and the magnetic moment was found to be $m(0) = 0.68\ \mu_B$ per unit cell in LSDA and $m(0) = 0.73\ \mu_B$ per unit cell in GGA. In both cases they are a bit smaller but in agreement with value found in Ref. [52], where the authors use the experimental value of a_0.

The calculated magnetic moment, decreases approximately linearly up to a critical pressure $P_c = 45$ GPa whose experimental value is $P_c^{Expt.} = 8.2$ GPA. Therefore LSDA (and GGA) overestimates both the magnetic moment at zero pressure and the critical pressure.

Before introducing the new method for spin fluctuations, I briefly describe the LSDA calculations. For this reason I plot, at the bottom of Fig. 5.3, the calculated paramagnetic DOS $N(E)$ for several pressures.

I find that, within ~ 4 eV around the Fermi level, $N(E,P)$ scales almost perfectly with P according to the following law:

$$N(E,P) = \frac{N\left[\alpha(P)E, 0\right]}{\alpha(P)}, \tag{5.1}$$

with $\alpha(P) = 1 + 0.005P$, and the scaling is obeyed up to 45 GPa. This is due to the fact that the $d-d$ hopping parameter scales with a negative power law -5 with the lattice constant a. [352] The contraction of the lattice parameter under pressure can be expressed, in the lowest order, as a linear expansion around its equilibrium value a_0 such that $a(P) = [1 - \delta P]a_0$, with δ small and positive. As a consequence, the bandwidth W is expected to scale linearly with pressure as $W(P) \sim W(0)\alpha(P)$. The surprising thing is that this linear scaling is almost exactly obeyed in such wide range of energy and pressure. [2]

I expect that the Stoner parameter changes little with pressure and thus the transition be driven by a reduction of $N_0(P)$. For this reason I performed fixed spin moment calculations in order to extract the Stoner I with a procedure which I will explain in the next section. I found the Stoner parameter is actually pressure independent and ~ 0.41 eV in LSDA, while in GGA is simply 17% larger $I^{GGA} = 1.17 I^{LSDA}$. At $P = 45$ GPa the Stoner criterion $N_0(45GP)I = 0.95 < 1$ is consistently released and the system is out of the ferromagnetic instability. Similar results can be found also in Ref. [52]. Since the Stoner parameter in LSDA and GGA are simply proportional, from now on I will consider exclusively the L(S)DA results.

This analysis shows that, while the LSDA results can be quite well understood in terms of the Stoner model, the agreement with the experiment is instead completely missing. This is due to the overestimation of the Stoner I in LSDA. Indeed given

[2] Not only the scaling of the DOS (which is an integrated quantity) is perfect but also the one of the bandstructure.

eq. (5.1) $N_0(P)$ decreases monotonically. In the simplified Stoner model, the condition for P_c is given by $N_0(P_c) = 1/I$, therefore the overestimation of P_c is directly connected with the overestimation of I. Thus, in order to bring the LSDA results in agreement with the experiment, one has to take into account a renormalization of I. The physical origin of this renormalization is the central topic of the next section.

In this section I presented the LDA and LSDA results for Ni_3Al itinerant ferromagnet under pressure. Concerning the paramagnetic calculations I showed that in this compound the bandstructure and the DOS scale almost perfectly with pressure in a wide range of energy and pressure. Both the d^9 Ni electron count and the high value of the DOS at the Fermi level point towards the tendency to magnetism. Indeed the compound is magnetic in LSDA but due to the mean field nature of this approximation, both the magnetic moment at zero pressure and the critical pressure are overestimated. The analysis of the LSDA data in terms of a simplified Stoner model, indicates that these overestimations could be due to an overestimation of the Stoner parameter in LSDA for this compound.

5.2 The renormalization of the Stoner parameter $I \rightarrow \tilde{I}$

A refined version of the Stoner model which makes use of the Andersen force theorem is the extended Stoner theory (EST) which I derived in chapter 1. [253, 254, 353] This theory gives an approximated expression for the LSDA total energy E as a function of the magnetic moment m in terms of the LDA paramagnetic DOS:

$$E(m,I) = \frac{1}{2}\int_0^m \frac{m'dm'}{\tilde{N}(m')} - \frac{1}{4}Im^2. \tag{5.2}$$

In formula (5.2) $\tilde{N}(m)$ is the average DOS over the Fermi level and I is the Stoner parameter which governs the magnetic interaction. [253] The condition of minimum for $E(m,I)$ is given by $\partial E(m,I)/\partial m = 0$ and $\partial^2 E(m,I)/\partial m^2 > 0$ which imply

respectively

$$\tilde{N}(m) = 1/I \quad \text{and} \quad \frac{d\tilde{N}(m)}{dm} < 0. \tag{5.3}$$

Therefore, around the minimum of $E(m, I)$, $\tilde{N}(m)$ is concave and decreasing I makes m to decreases as well. If $1/I > \tilde{N}(m)\ \forall\ m$, then no magnetic solution exists. [253]

The fixed spin moment calculations (FSMC) allow to obtain a similar $E(m)$ curve by minimizing selfconsistently the energy E once a given magnetic moment m is imposed. Comparing eq. (5.2) with the fixed spin moment calculations it is possible to extract the value of the Stoner parameter I in LSDA. [52, 63] This is shown in Fig. 5.4 where I compare the fixed spin moment calculations represented by red dots and the EST represented by the green line. Note the different depth of the energy minima. This gives an estimate of the difference in the total energy caused by the rearrangement of the bands due to spin polarization (beyond the rigid band splitting). [45]

As I showed in the previous section, LSDA overestimates the magnetic moment, with respect to experiment, in the entire range of pressure. The correct value of the magnetic moment can only be obtained using a reduced value of I. In order to clarify the origin of the renormalization of the Stoner parameter under non local fluctuations I briefly recall here the results of chapter 1 concerning the self-consistent renormalization theory. For small magnetic moments, the total energy can be expanded in terms of a Landau functional as function of the square of the uniform magnetization M^2, in the following way:

$$E(M) = a_0 + a_2 M^2/2 + a_4 M^4/4 + a_6 M^6/6 + \cdots, \tag{5.4}$$

Taking into account fluctuations of the magnetization with respect to its average $\delta M = M(\mathbf{r}) - M$ leads, in the gaussian approximation, to a renormalization of the bare coefficients $\{a_i\}$ and therefore to the following expression for the energy:

$$\tilde{E}(M) = \tilde{a}_0 + \tilde{a}_2 M^2/2 + \tilde{a}_4 M^4/4 + \tilde{a}_6 M^6/6 + \cdots, \tag{5.5}$$

where the renormalized coefficients $\{\tilde{a}_i\}$ can be expressed recursively in terms of the bare ones $\{a_i\}$ and $\xi^2 = \langle \delta M^2 \rangle$, where the $\langle\rangle$ brackets represent the gaussian average. In chapter 1 I reported the recursive relations. [235]

The value of ξ can be obtained by the fluctuation dissipation theorem (FDT):

$$\xi^2 = \frac{3\hbar}{\Omega} \int d\mathbf{q} \int \frac{d\omega}{2\pi} \frac{1}{2} Im\chi(\mathbf{q}, \omega), \tag{5.6}$$

where Ω is the volume of the unit cell and $\chi(\mathbf{q}, \omega)$ is the interacting spin susceptibility of the system. In this sense the renormalization of the LSDA Stoner parameter can be obtained, in principle, selfconsistently. In Ref. [52] an approximation on $\chi(\mathbf{q}, \omega)$ is made and the integral performed analytically in terms of N_0, the Fermi velocity v_F, the band velocity v and a cut off q_c - in principle unknown and fixed phenomenologically-.

I now assume ξ to be a parameter and I describe a phenomenological approach to bring the LSDA and the EST results in agreement with the experiment. In this way I obtain an estimate of the average spin fluctuations amplitude ξ^2 in Ni_3Al at zero pressure, and I show that the renormalization of the Stoner parameter $I \rightarrow \tilde{I}$ comes mainly from the renormalization of a_2. In this sense $E(m, \tilde{I})$ and $\tilde{E}(m)$ are equivalent.

The actual value of the bare coefficients $a_1, \cdots, a_n$ can be obtained by fitting the fixed spin moment calculations with a polynomial expansion up to order n. Thus, imposing that the minimum of eq. (5.5) coincides with the experimental value of the magnetic moment $\tilde{m}_0 = 0.23\ \mu_B$ per unit cell, the parameter ξ can be then expressed in terms of the bare coefficients $a_1, \cdots, a_n$ and $\tilde{m}_0$. In Fig. 5.4 I compare eq. (5.4) with eq. (5.5) by fitting the fixed spin moment calculations up to the 6th order. Under the effect of non local fluctuations parameterized by ξ, the minimum of $\tilde{E}(m)$ moves towards the experimental one. Assuming the minimum of eq. (5.2) to be the experimental one $\tilde{m}_0$, as done before for extracting the LSDA Stoner parameter, I obtain a value of $\tilde{I} = 0.358$ eV.

As can be seen from the figure, and will be clear in a moment, renormalizing the coefficients of the $E(m)$ expansion is equivalent, in the lowest order, to renormalize

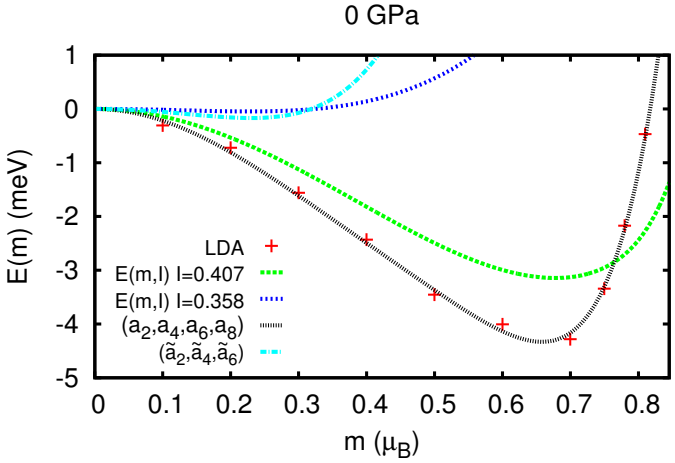

Figure 5.4: Comparison between the fixed spin moment calculations and the EST at $P = 0$ GPa. The fixed spin moment calculations in LSDA (red dots) are fitted with a Landau expansion up to the sixth order (black line). In order to bring the minimum of the EST curve (green line) in correspondence of the minimum of LSDA the Stoner parameter $I = 0.407$ must be used in eq. (5.2). The dark blue and light blue curve represent respectively eq. (5.2) with I=0.358 and eq. (5.5) with ξ phenomenologically tuned.

the Stoner parameter. Indeed, the renormalized second order coefficient of eq. (5.5) (the renormalized static susceptibility) can be expressed in terms of ξ and $\{a_i\}$ in the following way:

$\tilde{\chi}^{-1} = \partial^2 \tilde{E}(M)/\partial M^2 \mid_{M=0} = \tilde{a}_2 = a_2 + (5/3)a_4\xi^2 + (35/9)a_6\xi^4 + \cdots$

On the other hand, the LSDA static susceptibility is easily obtained from eq.

(5.2):
$\chi^{-1} = \partial E(m,I)/\partial m\,|_{m=0} = a_2 = \frac{1}{2}[1/N_0 - I]$,
where N_0 is measured in states/eV/spin /f.u. By comparing this expression with the one for $\tilde{a}_2$ it appears clear that under non local critical fluctuations, the Stoner parameter is renormalized according to:

$$\tilde{I} = I - (10/3)a_4\xi^2, \tag{5.7}$$

which can be written as a function of $s = \tilde{I}/I \leq 1$. In my calculations I obtained $\xi = 0.38\ \mu_B$ and $\tilde{I} = 0.358$ eV.

Fig. 5.5 shows that the renormalization of the second order coefficient of the expansion, *i.e.* the static inverse spin susceptibility, shifts the minimum of $E(m)$ while the renormalization of the higher order coefficients modifies the curve at higher values of energy and magnetic moment. Also in this case the dashed lines are different compared to the red dots because within EST the magnetic energy is basically obtained by a rigid shift of the paramagnetic DOS while the expansion in eq. (5.4) and (5.5) are obtained by fitting the fully selfconsistent calculations. The resulting effect of non local fluctuations in itinerant system is then to reduce the Stoner parameter by a factor $s \leq 1$.

In this section I showed a phenomenological method, based on the SCR theory, which allows to bring the LSDA results in agreement with the experiment in Ni_3Al itinerant ferromagnet at zero pressure. This is done by taking into account non local fluctuations of the magnetization at the gaussian level. This simple method shows in a transparent way that the effect of non local fluctuations is to suppress the Stoner parameter I. Therefore it puts in evidence the underlying connection between the SCR theory and whatever method, whose main aim is to suppress magnetism in LSDA by suppressing the Stoner parameter.

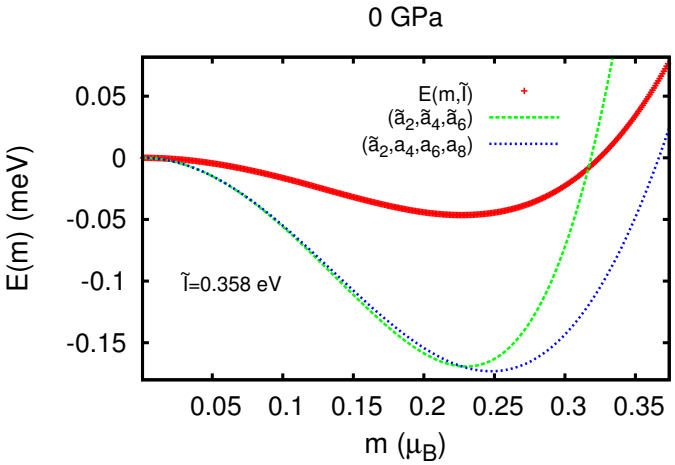

Figure 5.5: Figure adapted from Ref. [345]. Energy E as a function of the magnetic moment m for $P = 0$ GPa. The red dots show the curve obtained by means of EST with a renormalized Stoner parameter $\tilde{I} = 0.358$. The green and the blue lines mark respectively the Landau functional where all the coefficients are renormalized and the one where only the first coefficient of the expansion is renormalized.

5.3 *Ab-initio* renormalization of I: the reduced Stoner theory

Having clarified the phenomenology associated with the renormalization of the Stoner parameter under the effect of non local spin fluctuations in itinerant systems, in this section I want to go beyond this description, and correct the LSDA Stoner parameter within the DFT formalism. Indeed, given the connection between the

LSDA and the SCR theory via the EST, one can think that the renormalized value of the Stoner parameter $\tilde{I}$ can be achieved, within DFT, by a suitable more accurate functional than the LSDA and GGA ones. Therefore the method that I'm going to present includes the phenomenological reduction of the Stoner parameter directly inside the LSDA functional.

For this purpose I use the von Bart-Hedin scaling (1.58) of the exchange and correlation energy: [43]

$$E_{xc} = \int \varepsilon_{xc}(n,m)n(\mathbf{r})d\mathbf{r} \tag{5.8}$$

$$\varepsilon_{xc}(n,\zeta) = \varepsilon^{P}_{xc}(n) + f(\zeta)\Delta\varepsilon_{xc}(n), \tag{5.9}$$

where $n = (n_\uparrow + n_\downarrow)$, and $m = (n_\uparrow - n_\downarrow)$. In eq. (5.9) $\varepsilon^{P}_{xc}(n)$ and $\Delta\varepsilon_{xc}(n)$ do not depend on m, while $f(\zeta)$ is a known function of $\zeta(\mathbf{r}) = m(\mathbf{r})/n(\mathbf{r})$. Therefore the response to magnetism is entirely defined by the $\Delta\varepsilon_{xc}(n)$ functional, as the energy difference between the fully polarized and unpolarized electron gas:

$$\frac{\partial\varepsilon_{xc}}{\partial n} = \frac{\partial\varepsilon^{P}_{xc}}{\partial n} + f(\zeta)\frac{\partial\Delta\varepsilon_{xc}(n)}{\partial n} - f'(\zeta)\Delta\varepsilon_{xc}(n)\frac{\zeta}{n} \tag{5.10}$$

$$\frac{\partial\varepsilon_{xc}}{\partial m} = f'(\zeta)\Delta\varepsilon_{xc}(n)\frac{1}{n}. \tag{5.11}$$

If $\Delta\varepsilon_{xc}(n) = 0$ the system is non magnetic, while for $\Delta\varepsilon_{xc}(n) \neq 0$ a ferromagnetic state with magnetic moment m is realized. The charge potential is influenced by $\Delta\varepsilon_{xc}(n)$ as well. Therefore, scaling this term by a factor s not only scales $\frac{\partial\varepsilon_{xc}}{\partial m}$, but modifies at the same time the charge potential. In this sense is not possible to find an analytical expression for f and $\Delta\varepsilon_{xc}$ in such a way that $\partial\varepsilon_{xc}/\partial m$ is modified (reduced) without changing $\partial\varepsilon_{xc}/\partial n$ at the same time. In this sense the charge and spin contributions to the total energy are not separable. On the other hand, for the reason given above, scaling $\Delta\varepsilon_{xc}(n)$ by a factor s appears to be the most natural choice to suppress magnetism within DFT.

This leads to the following set of scaled equations:

$$\varepsilon_{xc}(n,\zeta) = \varepsilon^{P}_{xc}(n) + sf(\zeta)\Delta\varepsilon_{xc}(n) \quad (5.12)$$

$$\frac{\partial \varepsilon_{xc}}{\partial n} = v^{P}_{xc} + s[f(\zeta)\Delta v_{xc}(n) - f'(\zeta)\Delta\varepsilon_{xc}(n)\frac{\zeta}{n}] \quad (5.13)$$

$$\frac{\partial \varepsilon_{xc}}{\partial m} = sf'(\zeta)\Delta\varepsilon_{xc}(n)\frac{1}{n} \quad (5.14)$$

where the part in the square brackets is simply the additional charge potential that appears because of spin polarization. It is easy to verify that this functional produces an exchange-correlation potential scaled by s, and the charge potential remains unchanged:

$$\tilde{V}_{\uparrow}(\mathbf{r}) - \tilde{V}_{\downarrow}(\mathbf{r}) = s[V_{\uparrow}(\mathbf{r}) - V_{\downarrow}(\mathbf{r})] \quad (5.15)$$
$$\tilde{V}_{\uparrow}(\mathbf{r}) + \tilde{V}_{\downarrow}(\mathbf{r}) = [V_{\uparrow}(\mathbf{r}) + V_{\downarrow}(\mathbf{r})]$$

In this way the Stoner kernel $\delta^2 E_{xc}/\delta m^2(\mathbf{r})$ is also scaled by s, and the Stoner parameter is reduced as I wanted. For this reason I call this approach **reduced Stoner theory (RST)**.

In general eq. (5.15) can be used to obtain correct magnetic moments and the corresponding electronic structure in materials near ferro *or antiferro*magnetic QCP. Moreover the implementation is quite easy and the calculations are as computationally expensive as a normal spin polarized calculation.[3] Furthermore, given eqs. (5.6) and (5.7), s gives also an indication of the strength of spin fluctuations acting in the system. In the next section I will use the modified exchange and correlation functional in eq. (5.15) to obtain the correct magnetic moment of Ni_3Al under pressure. Before this, it is however instructive to compare the RST results with the one obtained with the EST at zero pressure.

In Fig. 5.6 I compare the magnetic moment as a function of the renormalized Stoner parameter $\tilde{I} = sI$ obtained in EST and in RST using the scaling exchange factor s. In RST this is obtained by making selfconsistent spin polarized calculations

[3] A patch for the popular WIEN2K program is available by request from Peter Blaha. The value of s enters as a variable in one of the input files.

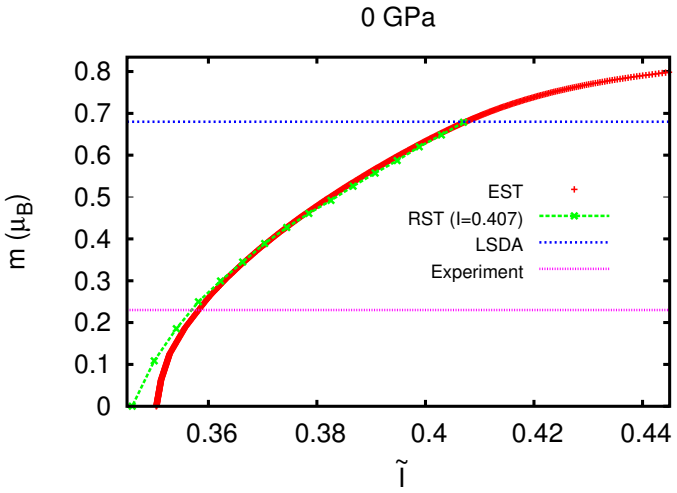

Figure 5.6: Figure adapted from Ref. [345]. Magnetic moment m as a function of the reduced Stoner parameter $\tilde{I} = s * I$ for Ni_3Al at 0 GPa in EST (red dots) and RST (green dotted line). The bare value of the Stoner parameter $I = 0.407$ eV was chosen in order to have the same value of m for $s = 1$.

for several values of $0 \leq s \leq 1$. The EST curve is obtained instead by extracting the magnetic moment m from the inversion of the relation $\tilde{N}(m) = 1/\tilde{I}$. The value of $I = 0.407$ eV was chosen in such a way that the LSDA and the EST magnetic moment have the same value for $s = 1$. The agreement between the two curves is remarkable and this value of I estimated in this way is in perfect agreement with the one found by fixed spin moment calculations. The value of $\tilde{I}$ necessary to reach the experimental magnetic moment is ~ 0.360 eV and is in very good agreement with

the one extracted, in the previous section, by comparing the renormalized Landau expansion with the experiment. The value of s needed to reproduce the experiment is $s \approx 0.88$.

In this section I presented the reduced Stoner theory (RST) which is a simple and computationally non demanding method to correct the magnetic properties of itinerant systems close to a QCP where DFT, in its mean field implementations, usually overestimates the tendency to magnetism. The method consists in scaling the spin polarized part of the exchange and correlation potential within the von Bart-Hedin scaling. This method gives also an estimate of the amount of fluctuations acting in the system as the ratio between the renormalized value of the Stoner parameter and the bare one. I also compared this new method with the results coming from the RST for Ni_3Al at zero pressure and the agreement is remarkable. This comparison allows to extract the bare value of the Stoner parameter which was found in perfect agreement with the one extracted from fixed spin moment calculations.

5.4 Ferromagnetic-paramagnetic transition in Ni_3Al under pressure

In this section I finally apply the new and simple method of the RST to the ferromagnetic-paramagnetic transition of Ni_3Al under pressure. As shown before, this material at ambient pressure is experimentally a weak ferromagnet. At a pressure of ~ 8.2 GPA the magnetic moment is completely suppressed and the system undergoes a ferromagnetic-paramagnetic transition. Since the paramagnetic bandwidth W increases linearly with pressure, the LDA bandstructure and DOS scale almost perfectly with pressure according to eq. (5.1). Using fixed spin-moment calculations, I estimated the Stoner parameter I, and found it to be $I = 0.41$ eV, and pressure-independent. Indeed LSDA overestimates the magnetic moment at zero pressure and the critical pressure P_c by about 3 and 5 times respectively. With the

RST I aim to achieve the agreement with experiment by suppressing I within DFT. As I will show below, the scaling property of the bandstructure, will also allow me to overcome the integral in eq. (5.6) and make an *ab initio* description of the m vs P curve for Ni_3Al using the connection between the RST and the SCR theory by Moriya.

I apply the RST by making calculations for several values of s for $P = 0$ GPa and $P = 6$ GPa. I found that, for both values of pressure the value of s needed in order to bring the magnetic moment in agreement with the experiment is $s \approx 0.88$. This implies that ξ is almost pressure independent. Indeed I recall here that $s = 1-(10/3)a_4\xi^2/I$ and a_4 was found to vary only by 4% in this range of pressure. The reason why ξ is almost pressure independent needs more investigation. Indeed one would expect that close to the QCP, where the magnetic order is suppressed, the amplitude of the fluctuations should grow. On the other hand the fluctuations are parameterized by $\chi(\mathbf{q},\omega)$ -the two point correlation function- while ξ is defined by eq. (5.6) as an integral in ω over the entire Brillouin zone. Therefore, if the susceptibility diverges at a particular $\mathbf{q} = \mathbf{0}$ point, this may or may be not affect ξ.

In order to better understand this, in the following I will adopt the approximation made in Ref. [52] and perform the integral of eq. (5.6) analytically. In this way ξ can be expressed in terms of the band parameters like the band velocity and DOS and, from their scaling with pressure, I can obtain the pressure dependence of ξ. In this way, I explicitly use of the connection between the RST and the SCR theory by Moriya.

Using the lowest order expansion in $q = \mid \mathbf{q} \mid$ and ω for $\chi(\mathbf{q},\omega)$,

$$\chi_0(\mathbf{q},\omega) \quad = \quad N_0 - aq^2 + ib\omega/q \tag{5.16}$$

$$\chi^{-1}(\mathbf{q},\omega) \quad = \quad \chi_0^{-1}(\mathbf{q},\omega) - I, \tag{5.17}$$

where $\chi_0(\mathbf{q},\omega)$ is the non interacting susceptibility, one can derive a formula for ξ^2 whose coefficients can be related to the band parameters. [51, 235, 263, 354] The parameters a and b in eq. (5.16) are linked to the band velocity $v = \sqrt{v_x^2 + v_y^2 + v_z^2}$,

the Fermi velocity $v_F = \sqrt{3\frac{\langle N_0 v_x^2\rangle}{N_0}}$ and the density of states at the Fermi level. Their expression as a function of pressure is the following:

$$\begin{aligned} a(P) &= \frac{1}{12}\frac{d^2\langle N_0(P)v_x^2(P)\rangle}{dE_F^2}, \\ b(P) &= \frac{1}{2}\langle N_0(P)v^{-1}(P)\rangle. \end{aligned}$$

The brackets indicate the average over the Fermi surface. Since the Fermi velocity scales inversely with the DOS, $v(P) = v(0)\alpha(P)$, these parameters scale as: $a(P) = a(0)\alpha(P)$, and $b(P) = b(0)/\alpha^2(P)$.

The final expression for $\xi(P)$ is: [51, 52, 263]

$$\xi^2(P) = \frac{b(P)v_F^2(P)N_0^2(P)}{8a^2(P)\Omega(P)}[Q^4\log(1+Q^{-4}) + \log(1+Q^4)].$$

The parameter Q in eq. (5.18) depends on the cutoff vector, $Q = q_c\sqrt{a(P)/b(P)v_F(P)}$. A possible choice for q_c is $q_c = \sqrt{N_0/a}$, because at that point the expansion of χ loses its physical meaning (χ_0 changes sign). Then $Q = \sqrt{N_0(P)/b(P)v_F(P)}$ does not depend on pressure. This implies that ξ does actually scale with pressure as:

$$\xi(P) \propto \sqrt{\frac{1}{\Omega(P)}}, \tag{5.18}$$

where $\Omega(P)$ is the unit cell volume as a function of pressure (equation of state). Eq. (5.18) indicates that close to the transition the role of spin fluctuations is just to renormalize the Stoner parameter by a (almost) constant factor. The transition itself is not driven by a change in the interaction parameter, but is completely driven by the band structure. Moreover, ξ can be viewed as the length scale associated with the destruction of the magnetic order parameter. Thus, the fact that it doesn't diverge and does not even grow substantially near P_c -even if eq. (5.17) shows that $\chi(\mathbf{q},\omega)$ does diverge-, it makes very unlikely that other instabilities show up

at the critical point. In fact, if the opposite case was true, a competing instability could profit of this emerging length scale in order to build up an alternative order parameter. Using the equation of state $\Omega(P)$ that I calculated, I obtain that $\sqrt{\Omega(6\text{ GPA})/\Omega(0\text{ GPA})} = 0.98$ implying that ξ varies only about 2%. Using the phenomenological approach described in section 5.2, where ξ is a parameter, I found instead that $\xi(0\text{ GPA})/\xi(6\text{ GPA}) \sim 0.95$. However simply using a pressure independent ξ, *i.e.* fixing $s = 0.88$, provides a good agreement with the experiment (a part a small underestimation of P_c) and allow to predict the entire curve $m(P)$ which up to now was impossible!

In Fig. 5.7 I show the magnetic moment m as a function of pressure P calculated within the RST for Ni_3Al with $s = 0.88$. Unfortunately, there are no magnetization measurements on this material for pressure $0 \leq P \leq P_c$. However resistivity measurement by Niklowitz *et al.* allowed to trace the experimental behavior of the Curie temperature T_c under pressure. [201] I will therefore compare my results with $T_c(P)$, assuming the proportionality relation $T_c \propto m^{3/2}$ coming from Moriya's theory, where $m = \mid \mathbf{m} \mid$. [17]

This relation is also used in Ref. [201] to fit the experimental data together with the following equation of state for the magnetic field **H**:

$$\mathbf{H} = a_2\mathbf{m} + a_4\mathbf{m}^3 - c\nabla^2\mathbf{m}, \tag{5.19}$$

where the coefficient $a_2 \propto P - P_c$ in the same spirit of the Landau second order phase transitions, where the pressure P plays the role of the temperature T. This approach is, in principle, questionable. Indeed the temperature is not supposed to change the bandstructure but only to change the entropy in the system making the spin order favored below T_c and unfavored above T_c (see chapter 1). Instead, as I showed in section 5.1, the bandstructure of Ni_3Al, even if in a trivial way, depends crucially on pressure, and the appearance of the ferromagnetic state is governed by the Stoner condition. By assuming $a_2 \propto P - P_c$ and neglecting spatial fluctuations in eq. (5.19), one obtains $m \propto (P_c - P)^\beta$ with $\beta = 1/2$. Consequently the Curie temperature is expected to follow the $T_c \propto (P_c - P)^{3/4}$ behavior. Indeed Fig. 5.7 shows that, apart from a small underestimation of P_c due to the underestimation

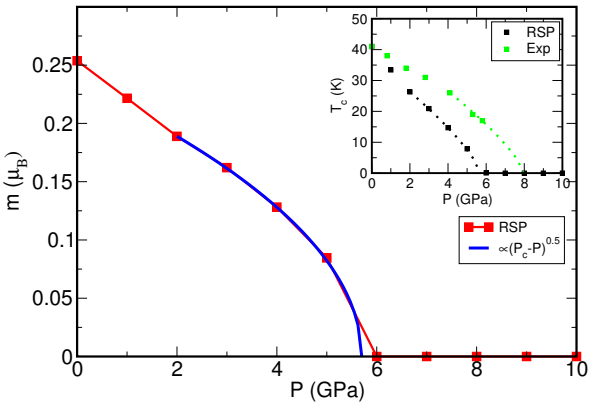

Figure 5.7: Figure adapted from Ref. [345]. Predicted magnetic moment as a function of pressure calculated within the RST (red dotted line). The critical behavior $m \propto (P_c - P)^{1/2}$ (blue line) is followed between 2 and 6 GPa. The Curie temperature $T_c \propto m^{3/2}$ is shown in the inset by black dots. Apart from the underestimation of the critical pressure, the agreement with the experimental data taken from Ref. [201] (green dots) is very good. In fact, both theoretically and experimentally, the extrapolation of the data at 5.7 GPa (black dashed line) and 8 GPa (green dashed line) respectively, give both the same critical behavior $T_c \propto (P_c - P)^{3/4}$, as observed by Nicklovic *et al.* [201]

of a_0, both the experimental data and the RST ones follow this behavior. However, while for the RST data this behavior comes from the fact that, for small magnetic moment, the relation $m \propto (P_c - P)^{1/2}$ is actually obeyed, for the experimental data the question why this relation holds, remains open.

In the following I give an answer to this question, offering also a microscopic justification for using the model (5.19).

For small value of the magnetic moment in the fluctuations-corrected LSDA, $a_2 = \frac{1}{2}\left[1/N_0 - I\right]$, $c = 0$, and $\tilde{I}$ is adjusted in order to get $N_0\tilde{I} = 1$ at $P = P_c$. Because of eq. (5.1),

$$a_2(P) = \frac{1}{2}\left[\frac{\alpha(P)}{N_0(0)} - \tilde{I}\right] = \frac{\tilde{I}}{2\alpha(P_c)}\left[\alpha(P) - \alpha(P_c)\right] \propto (P - P_c). \tag{5.20}$$

The linear behavior of the inverse susceptibility a_2 is not anymore an assumption but comes directly from the scaling property of the DOS with pressure. This gives then a microscopically justification of the observed behavior of the Curie temperature with pressure.

In this section I applied the RST to the ferromagnetic-paramagnetic transition of Ni_3Al under pressure. The value of s needed in order to bring the calculated moment in agreement with the experiment was found to be the same at the edges of the phase diagram ($P = 0$ and $P = P_c$). By using an approximated form for the spin susceptibility I expressed the average amplitude of the spin fluctuations ξ, in terms of the band parameters of the compound. Due to the particular scaling of the DOS with pressure I was able to show that assuming $s = 0.88$ independent on pressure is a good approximation. Since s was not a parameter anymore, I was able to calculate *ab initio* the magnetic moment as a function of pressure. Since there are not yet magnetization measurements available, I compared the RST result with the measured Curie temperature as a function of pressure assuming by the Moriya's scaling $T_c \propto m^{3/2}$ to be valid. I found a good agreement with the experiment which confirms the connection between the RST and the SCR theory. Finally I showed that the model used to interpret the data lives on the assumption that the DOS scales with pressure like $N_0(P) \propto N_0(0)/(1 + AP)$ where A is a constant. Since this is exactly the scaling that I found in Ni_3Al, this gives also a microscopic justification to that model.

5.5 Conclusion

In order to give some conclusions about the new method presented and about the physics of Ni_3Al, to which the method was applied, it is useful to summarize the

results of Ref. [345] presented in this chapter.

In section 5.1, the DFT results for Ni_3Al under pressure were presented. These show that the paramagnetic bandwidth in an energy interval of ~ 4 eV around E_F scales linearly with pressure according to eq. (5.1). Spin polarized calculations correctly converge to a ferromagnetic solution, with values of the magnetic moment and critical pressure that are strongly overestimated compared to experiment. This calls for a reduction of the LSDA Stoner parameter as for other itinerant magnets.

In section 5.2 I performed spin polarized calculations with a fixed value of the magnetic moment, to construct a E vs m Landau functional.

Fitting the curve with a 6th order polynomial, I extracted the value of the average amplitude of spin fluctuations ξ for Ni_3Al at zero pressure. Moreover I showed that under the effect of ξ the Stoner parameter gets reduced by a quantity $s < 1$. This connects the SCR theory by Moriya, in which ξ is obtained selfconsistently by assuming the validity of the fluctuation dissipation theorem, with whatever method aims to reduce the Stoner parameter within DFT.

In section 5.3 I presented the RST applied to Ni_3Al at zero pressure. The method consists of scaling the spin polarized part of the exchange and correlation potential by the quantity s. In this way the Stoner kernel is reduced as well. Indeed comparing the EST and RST concerning the scaling of the magnetic moment m with the reduced Stoner parameter $\tilde{I}$, I showed that the two methods are actually equivalent and the value of the bare Stoner parameter obtained by this comparison is in perfect agreement with the one obtained with fixed spin moment calculations. The RST is also more accurate, indeed in EST the magnetic moment is obtained by shifting rigidly the paramagnetic DOS, while in RST the effect of "band rearranging" under magnetic perturbation is also taken into account.

In that section I used s as a parameter but given its link with ξ it could be, in principle, calculated. This is the explicit connection between RST and the SCR theory by Moriya.

In section 5.4 I made an explicit use of this connection by calculating ξ, and its scaling with pressure, in an approximate way. I showed that in Ni_3Al both s and ξ are pressure independent. As a consequence the transition is entirely driven by the

peculiar scaling property of the band structure. Moreover I was also able to give an estimate of the average amount of spin fluctuations in this material.

The RST is a new method which accounts for the detrimental effect of near critical spin fluctuations on the LSDA magnetic properties without any additional computational load. This method can be used at the phenomenological level but is in principle *ab initio*. It can be used in all itinerant systems where LSDA usually overestimates the tendency to magnetism, moreover it can be easily applied also to the antiferromagnetic order and used for studying the stability of different magnetic orders by studying the $m(I)$ curve.

5.6 Technical details

The LDA and LSDA and GGA calculations were done using the general potential linearized augmented-plane-wave (LAPW) method as implemented in the WIEN2K package. [44, 251, 309] Up to 1330 **k** points were used in the self-consistent calculations with an LAPW basis defined by the cutoff $R_S K_{\max} = 9$ both in the magnetic and in the non magnetic calculations. A large number of 4960 **k** points in the irreducible wedge, corresponding to a $58 \times 58 \times 58$ grid, were used for calculating the non magnetic DOS. Pressure was simulated performing calculations for different values of the lattice parameter a_0, and fitting them to a Murnagham equation of state: [355] $E = E0 + [B\frac{V}{B'}(\frac{(V0/V)^{B'}}{(B'-1)} + 1) - \frac{B*V0}{(B'-1)}]/14703.6$ where V/V_0 is the volume compression. $P = B/B'^{B'} - 1$ with $V_0 = 284.6\ Bohr^3$, $B = 237.0$ GPa, $B' = 3.841$. B and B' are the Bulk modulus and derivative. The lattice parameters both in the magnetic and in the non magnetic case were found to be the same.

Conclusion

During my PhD activity I investigated superconductivity and itinerant electron magnetism in order to clarify their interplay in novel compounds. In the present thesis, I described a general phenomenological approach which aims to account for the effect of spin fluctuations on itinerant magnetism and superconductivity. This approach uses the discrepancies (whenever present) between density functional theory (DFT) calculations and the experiments in order to explain the physical properties of real materials, through an appropriate parameterization of the spin susceptibility. This is indeed the basic quantity which describes the effect of spin fluctuations.

DFT is in principle the only way to access the ground state of real materials. This allows a direct comparison with the experiment and sometimes also to make predictions. However, the most common implementations of DFT reduce dramatically its predictive power. This is basically due to the mean field nature of the approximations adopted in the DFT implementations like local (spin) density approximation -L(S)DA- and generalized gradient approximation (GGA). In particular DFT fails in those systems where several ground states compete against each other making the system "undecided" and characterized by strong fluctuations. Fluctuations beyond mean field, usually tend to destroy the order and favor the competing ground state, as soon as the so called quantum critical point (QCP) is reached. As a consequence,

the value of an observable, like the spin susceptibility, evaluated in a mean field approximation is usually overestimated with respect to the experimental one. [51, 61–63] This fact traces the route for going beyond the DFT implementations starting from them. Indeed, in systems where fluctuations can be neglected, the DFT scheme can be applied straightforwardly in order to reach the ground state of the system and reproduce the experiments with great accuracy. In systems where fluctuations cannot be neglected, one can use the L(S)DA or GGA values of the observable as starting point and then from the comparison with experiment, understand how strong are the fluctuations and understand their origin by probing which are the competing ground states.

The reason why fluctuations are so important is because they involve large wave length and large energy scale that can be used by the system to build up macroscopically coherent states like superconductivity. On the other hand the large energy scale involved in this phenomenon makes also difficult to give an accurate description of the real system where this phenomenon is realized.

In the present thesis I used LSDA and GGA as mean field starting point and I used the discrepancies with respect to experiments as "markers" of the average amplitude of spin fluctuations acting in the system. In this way I constructed a phenomenological method based on *ab initio* calculations of the observables taken as mean field values *i. e.* the values of the quantities that would be measured if fluctuations were not there.

The original motivation of this work was given by the discovery of the Fe pnictides for which, during my master thesis, I constructed a low-energy model which successfully accounted for the discrepancies between DFT calculations and the experiments regarding the low-energy properties of LaFePO. [195] From the discrepancies between the experiment and DFT calculations I was able to establish that in this material the interband interaction channel is prevalent with respect to the intraband one. Moreover I extracted a value of the coupling constant which gave a critical temperature in agreement with the experiment. The input parameters describing the non interacting bandstructure in the model for LaFePO, were taken from the GGA calculations by Lebégue. [321]

I started my PhD activity with the intention of learning how to calculate such parameters by using DFT. It was then natural to calculate the optical properties of LaFePO using both the model applied for describing its low-energy properties [195] and DFT calculations, in order to interpret the large ω dependence of the inverse scattering time claimed in the experiment. [153] While I was learning DFT, the $A\mathrm{Pt_3P}$ compounds were discovered by Takayama *et al.* [197] and for these materials DFT alone revealed all its power in describing the material properties with no need for additional corrections. Superconductivity in hole-doped CuBiSO was reported at the beginning of my PhD activity and its origin was controversial. [225, 227] Early DFT calculations attributed indeed superconductivity to spin fluctuations, without evaluating explicitly their contribution to the pairing and without calculating the electron-phonon coupling. [200] In this case, I started by calculating the electron-phonon coupling contribution to the superconducting pairing. I realized that the critical temperature was too high. At the same time, the ground state was found to be weakly ferromagnetic. I realized that this could be the case of a material, where electron-phonon interaction and spin fluctuations compete against each other. Not being able to construct a first-principles model for spin fluctuations, I devised an ad-hoc procedure based on the phenomenological reduction of the Stoner parameter. Form there it came the idea to combine the Stoner formalism with Moriya's theory [17] and include everything in the LSDA functional. In this way the reduced Stoner theory (RST) came out and, I applied it to the $\mathrm{Ni_3Al}$ under pressure as prototypical system.

My thesis can be thought of as an excursion in different materials, which each illustrate a different aspect of magnetism and superconductivity, and the respective problems connected with their description.

From the point of view of a phenomenological approach based on the DFT ground state, the $A\mathrm{Pt_3P}$ superconductors represent the "zero fluctuations" starting point. In these systems indeed the GGA calculations are in perfect agreement with the experiment and one can reach a complete understanding of the physics with no need of phenomenological parameters apart from the Coulomb pseudopotential μ^* which, on the other hand, is fixed once for all when calculating T_c. The results

obtained for these systems show also how accurate DFT can be in reproducing the properties of real materials. The Fe-pnictides represent the opposite limit. Here the LSDA magnetic moment is overestimated and the electron-phonon coupling cannot account for the high T_c. In this thesis I considered the case of LaFePO which is magnetic in LSDA and non magnetic in the experiment. There I described antiferromagnetic spin fluctuations, which characterize the system both in the normal and in the superconducting state, as a bosonic mode whose spectrum can be modeled phenomenologically [171] or obtained from a measure of the imaginary part of the spin susceptibility. [150]

An intermediate example is represented by the hole-doped CuBiSO where the singlet electron-phonon-driven s-wave superconductivity and the triplet spin fluctuations-driven p-wave superconductivity compete each other and both T_c's are sizable. There, the important fluctuations are the ferromagnetic ones which, due to the connection between LSDA and the Stoner model, can be easily modeled by assuming a phenomenological reduction of the Stoner parameter. Also in this case both the effect on magnetism and on superconductivity was evaluated through a suitable model for the spin susceptibility.

The connection between LSDA and the Stoner model marks the route toward an *ab-initio* description of spin fluctuations beyond LSDA. Indeed the overestimation of the magnetic moment corresponds to an overestimation of the Stoner parameter. Therefore a correction of the LSDA Stoner parameter should correctly account for magnetism in itinerant systems. This is proved by the results obtained in Ni_3Al under pressure for which, apart from an underestimation of the critical pressure, the agreement with the experiment is remarkable.

The reduced Stoner theory described in chapter 5 and applied to Ni_3Al can be widely used in all the systems where LSDA overestimates the tendency to magnetism or whenever one needs to monitor the evolution of the electronic structure from non magnetic to magnetic. In this sense the magnetic moment as a function of the scaling parameter s, can be used as a response function of the system to a magnetic perturbation. Moreover the method can be easily applied to the antiferromagnetic case and help in this way in analyzing the stability of the different orders. In

systems where the magnetic moment is overestimated the value of s needed to bring the magnetic moment in agreement with the experiment gives an estimate of the average amplitude of fluctuations that can give an important information about the degree of non local correlations in these systems. The RST aims to give the correct value of the Stoner parameter. In this sense, if applied CuBiSO the Stoner parameter would not be a free parameter anymore (as I assumed in chapter 3). As a result, the phase diagram of CuBiSO as a function of doping x and Stoner parameter I would be reduced to one line only. When applied to pnictides, this method could distinguish between nesting effect and Stoner-like origin of the several magnetic orders studied in literature.

Zusammenfassung

Die Entdeckung der Supraleitung in Eisen-Pniktidverbindungen durch Kamihara *et al.* [1] und die darauffolgende Erhöhung der kritischen Temperatur T_c auf bis zu 26 K durch das partielle Ersetzen von O mit F in dem antiferromagnetischen Metall LaOFeAs, [2, 3] weckte das Interesse am Wechselspiel von Supraleitung mit itinerantem Magnetismus. Tatsächlich zeigten bereits erste Berechnungen [4] dieser Verbindung, dass die Elektron-Phonon Wechselwirkung nicht ausreichend ist um T_c zu beschreiben. Aus diesem Grund wurde eine Beschreibung der Supraleitung basierend auf dem Austausch von antiferromagnetischen Spin-Fluktuationen vorgeschlagen. [5]

Im Gegensatz zu auf Elektron-Phonon Wechselwirkung basierenden Supraleitern, für welche schon eine anerkannte Methode existiert um die kritische Temperatur ausgehend von *ab-initio* Rechnungen zu berechnen, [7–16], existiert noch keine einheitliche Beschreibung für auf Spin-Fluktuationen basierende Supraleitung. Der Grund hierür liegt bei den Spin-Fluktuationen, welche einzig durch die elektronischen Freiheitsgrade bestimmt sind. Dadurch benötigt man für eine akkurate Beschreibung eine gute Näherung für die Elektron-Elektron Wechselwirkung in einem relativ großen Energiebereich. Die Spin-Suszeptibilität gibt in solchen Verbindungen die magnetische Antwort im Teilchen-Loch Bereich vor, und bestimmt darüber hinaus die supraleitende Antwort im Teilchen-Teilchen Bereich. Deshalb ist

für eine exakte Beschreibung der Supraleitung in solchen Systemen eine genaue Beschreibung der magnetischen Eigenschaften zwingend notwendig.

In itineranten Elektron-Systemen beeinflussen die Spin-Fluktuationen wesentlich die magnetischen Eigenschaften, da die Spin-Suszeptibilität selbst-konsistent renormalisiert wird. [17] Weil in solchen itineranten Systemen normalerweise lokale Korrelationen vernachlässigbar sind, können Grundzustandseigenschaften, z.B. die Gesamtenergie oder die elektronische Struktur, im paramagnetischen Zustand gut durch Molekularfeldnäherungen wie die lokale Spin-Dichtenäherung (LSDN) in der Dichtefunktionaltheorie (DFT) beschrieben werden.

Folglich ist eine *ab-initio* Beschreibung von realen Materialien wie Elektron-Phonon basierenden Supraleiter und schwach korrelierten Metallen möglich. Für itinerante Magneten und auf Spin-Fluktuationen basierende Supraleiter allerdings müssen *ad hoc* Näherungen angenommen, und phänomenologische Modelle zur Beschreibung gewählt werden.

Den Ansatz, den ich in dieser Arbeit vorstelle, benutzt die Unterschiede zwischen DFT Rechnungen und Experimenten um phänomenologische Modelle zu konstruieren, die die magnetischen, supraleitenden und optischen Eigenschaften der vier repräsentativen Supraleitern und itineranten Magneten erklären. Das Hauptaugenmerk richtet sich dabei auf die Eigenschaften im supraleitenden und im normalleitenden Zustand der vor kurzem entdeckten supraleitenden Klasse $A\mathrm{Pt}_3\mathrm{P}$, das Wechselspiel zwischen Magnetismus und Supraleitung in Loch-dotiertem CuBiSo, die optischen Eigenschaften von LaFePO und schließlich auf den Phasenübergang von ferromagnetisch zu paramagnetisch von $\mathrm{Ni}_3\mathrm{Al}$ unter äußerem Druck.

Diese Arbeit kann als ein Exkurs über verschiedene Materialien angesehen werden, welche jeweils einen anderen Aspekt des Magnetismus und der Supraleitung erläutern. Dabei wird auf die Probleme, die bei der Beschreibung dieser Materialien auftreten, ausdrücklich eingegangen.

Die Klasse der $A\mathrm{Pt}_3$ Verbindungen und die Loch-dotierten CuBiSo wurden erst vor kurzem entdeckt. In beiden Fällen wird über den Ursprung der Supraleitung noch kontrovers diskutiert. [197–200] Die optischen Eigenschaften von LaFePO scheinen experimentell durch die Dynamik der Spin-Fluktuationen bestimmt zu sein,

wobei allerdings die Rolle der Band-Band Übergänge ungeklärt ist. [154–157] Zum Schluss gehe ich auf Ni_3Al ein, welches unter äußeren Druck einen Phasenübergang von ferromagnetisch zu paramagnetisch aufweist [201]. Dieser wird qualitativ durch die LSDN beschrieben, jedoch werden dabei das magnetische Moment bei Umgebungsdruck und der kritische Druck bei weitem überschätzt. [52]

Als Grundlage für all diese Verbindungen benutze ich DFT Rechnungen um die elektronischen Eigenschaften, die Zustandsdichte der Phononen und die Elektron-Phonon Wechselwirkung zu untersuchen. In der Tat ist DFT ein guter Ausgangspunkt für das Verständnis der Eigenschaften von itineranten Elektronsystemen bei niedrigen Anregungsenergien. [46] Außerdem, auf Grund der hohen Genauigkeit aktueller Elektron-Phonon Berechnungen [12, 202], kann man dieses Verfahren auch nutzen um die Elektron-Phonon Wechselwirkung "zu untersuchen", und gemeinsam mit dem Experiment die Physik realer Materialien zu ergründen. Anfangs werden die Spin-Fluktuationen nur phänomenologisch berücksichtigt. Im weiteren Verlauf wird dann eine neue Methode vorgestellt – basierend auf einem modifizierten LSDN Funktional – welche die magnetischen Momente itineranter Systeme unterdrückt.

Im Folgenden gebe ich eine kurze Übersicht über die Schwerpunkte und Ergebnisse meiner Forschungsarbeit.

In Kapitel 1 präsentierte ich eine Übersicht der zu Grunde liegenden theoretischen Konzepte dieser Arbeit und beschreibe kurz die verwendeten Methoden. Das Problem des Magnetismus wird durch zwei Grenzmodelle – lokalisierter und itineranter Magnetismus – erläutert. Dabei werden die beiden Ansätze, ihre Näherungen, und ihre Gültigkeitsbereiche diskutiert. Danach folgt eine kurze Einführung in Dichtefunktionaltheorie (DFT) und die in dieser Arbeit genutzten Näherungen. Insbesondere gehe ich auf den Zusammenhang zwischen der lokalen Spindichtenäherung und der Theorie des Magnetismus von Stoner ein. An diesem Punkt wird die Rolle der Spin-Fluktuationen – nämlich die Unterdrückung von Magnetismus in itineranten Systemen – mit Hilfe der Theorie von Shimizu-Moriya erklärt. Anschließend werden noch ein paar neuere Entwicklungen in der Theorie der Paramagnonen kurz vorgestellt. Am Ende dieses Kapitels gebe ich einen knappen Überblick der BCS Theorie für den Fall der auf Spin-Fluktuation basierenden Supraleitung.

In Kapitel 2 diskutierte ich die Supraleitung in der vor kurzen entdeckten Klasse der APt$_3$P Supraleiter. [197] Diese neue Klasse von Supraleitern hat sofort viel Aufmerksamkeit der wissenschaftlichen Gemeinde auf sich gezogen auf Grund ihrer relativ hohen kritischen Temperaturen ($T_c = 8.4$ K in SrPt$_3$P, $T_c = 6.6$ K in CaPt$_3$P und $T_c = 1.5$ K in LaPt$_3$P) und ihrer speziellen Kristallstruktur, welche das inversionssymmetrische Pendant zu CePt$_3$Si ist. [198, 199, 218] In der Tat behaupten die Autoren, welche erstmalig über die Supraleitung der APt$_3$P [197] berichteten, dass die Synthese von solchen Verbindungen Erkenntnisse über die Supraleitung in Kristallen ohne Inversionssymmetrie liefern kann, in dem man isoelektrische Verbindungen von Strukturen mit und ohne Inversionssymmetrie vergleicht.

Zudem wurde experimentell für SrPt$_3$P ein sehr großer α-Quotient ermittelt, was ein starker Anhaltspunkt für Mehrband-Supraleitung ist. [197] Diese Erklärung wurde unterstützt durch mehrere Taschen in der Fermifläche abgeleitet aus Hall-Widerstandsmessungen. Sie wurden danach auch in DFT Rechnungen gefunden. [197, 198] Außerdem, auf Grund der starken Spin-Bahn Wechselwirkung von Pt, konnte man *a priori* die Möglichkeit von unkonventioneller Supraleitung nicht ausschließen, welche z.B. für LaPt$_3$P vorgeschlagen wurde. [199] Letztendlich kann nicht einmal Elektron-Phonon Kopplung als Paarungsmechanismus den doppelt so hohen Sprung in der spezifischen Wärme ΔC bei T_c in SrPt$_3$P im Vergleich zu CaPt$_3$P erklären. Letzteres ist eine isoelektronische Verbindung, die zur selben Klasse gehört wie SrPt$_3$P und auch eine vergleichbare Sprungtemperatur besitzt ($T_c = 8.4$ K in SrPt$_3$P and $T_c = 6.6$ K in CaPt$_3$P).

In diesem Kapitel beschreibe ich ausführlich die Kristallstruktur der APt$_3$P Verbindungen, welche in der tetragonalen Anti-Perowskit Struktur (Raumgruppe $P4/nmm$) kristallisieren. Die Struktur besteht aus Pt$_6$P Oktaedern, welche ihre Ecken miteinander teilen. Dabei ist jeder Oktaeder von einem Parallelepiped umgeben. In der Tat sind die Oktaeder deformiert, und somit die Pt(1) Atome in der Basisebene und die apikalen Pt(2) Atome nicht mehr equivalent. Zudem wird das P Atom aus der Basisebene geschoben und nähert sich somit einem der Pt(2) Atome, währenddessen das andere Pt(2) Atom sich in Richtung Basisebene bewegt um eine dichteste Kugel-

packung zu gewährleisten. Dadurch verliert der Oktaeder die Inversionssymmetrie. Dieser Verlust überträgt sich auf die Kristallstruktur, falls die Einheitszelle nur einen deformierten Oktaeder enthält. Die Inversionssymmetrie kann man zurückbekommen, wenn die Einheitszelle eine gerade Anzahl von deformierten Oktaedern besitzt, die sich in der sogenannten anti-polaren Anordnung befinden. Die Einheitszelle von $A\mathrm{Pt_3P}$ enthält zwei Formeleinheiten und hat somit das doppelte Volumen im Vergleich zu ihrem Pendant ohne Inversionssymmetrie: $A_1\mathrm{Pt_3Si}$ (A_1=Ce, La) mit Raumgruppe $P4mm$. Durch Berechnung der Gesamtenergie der Systeme zeige ich, dass die energetische Schwelle zwischen den beiden Strukturtypen der $A\mathrm{Pt_3P}$ Klasse klein ist ($\sim$ 20 meV). Die gleiche Barriere in den $A\mathrm{Pt_3Si}$ Siliziden ist stattdessen eine Größenordnung darüber.

Nach der Analyse der strukturellen Eigenschaften zeige ich die Ergebnisse für die elektronische Struktur der $A\mathrm{Pt_3P}$ Verbindungen. Der Effekt der Spin-Bahn Wechselwirkung (SBW) von Pt ist vernachlässigbar und die Bandstruktur ist hauptsächlich durch Pt d Zustände und P p Zustände, welche am Fermi-Niveau hybridisieren und anti-bindende Zustände ausbilden, gegeben. In den $A^{+2}\mathrm{Pt_3P}$ (A^{+2}=Ca, Sr) Verbindungen werden diese Zustände durch die Pt(1) $d_{x^2-y^2}$ und die Pt(2) d_{xz-yz} Orbitale, welche mit den P $p_{x,y}$ hybridisieren, gebildet. In $\mathrm{LaPt_3P}$ – die Anzahl der Elektronen in $A^{+2}\mathrm{Pt_3P}$ und in $\mathrm{LaPt_3P}$ ist verschieden – gibt es auch die Pt(1) d_{yz} Orbitale, die mit den P $p_{x,y}$ hybridisieren. Die Fermifläche von $A^{+2}\mathrm{Pt_3P}$ wird durch zwei große, nur schwach dispergierende Flächen, die hauptsächlich durch Pt(1) $d_{x^2-y^2}$ Orbitale bestimmt sind, und zwei dispergierenden Taschen mit Anteilen von Pt(2), P und Zwischengitterplätzen gebildet. Dahingegen besteht die Fermifläche von $\mathrm{LaPt_3P}$ aus stark dispergierenden Flächen mit gemischten orbitalen Beiträgen von Pt(2), Pt und Pt(1). Der Unterschied zwischen den Fermiflächen der $A^{+2}\mathrm{Pt_3P}$ Verbindungen und der Fermifläche von $\mathrm{LaPt_3P}$ ist der Hauptbeitrag für die unterschiedlichen supraleitenden Eigenschaften dieser Materialien.

Die Dispersion der Phononen ist stabil, and sehr ähnlich in den drei Verbindungen. Die Kopplung zwischen den Elektronen und Phononen ist gleichförmig in $\mathrm{LaPt_3P}$ wohingegen sie in $\mathrm{CaPt_3P}$ und $\mathrm{SrPt_3P}$ auf niedrige Frequenzen konzentriert und eher anisotrop ist. Diese Region der Phononenzustandsdichte wird durch

Atmungsmoden der Pt(1) Atome dominiert, welche stark mit elektronischen Zuständen in der selben Ebene koppeln. Deshalb ist die Elektron-Phonon Kopplung groß im Falle von $SrPt_3P$, moderat für $CaPt_3P$ und recht schwach in $LaPt_3P$. Dieses Verhalten wird durch die Form von $\alpha^2F(\omega)$ wiedergegeben, welche für die Sr Verbindungen einen scharfen Peak bei ~ 50 cm^{-1} aufweist im Kontrast zu der La Verbindung, in der $\alpha^2F(\omega)$ eher proportional zur Zustandsdichte der Phononen ist. Trotz ähnlicher kritischer Temperaturen T_c, variiert die Kopplungskonstante λ^{br} zwischen den A^{+2}-Verbindungen um den Faktor drei. Es wird gezeigt, dass dies ein struktureller Effekt ist, denn durch die Erhöhung des in der Ebene liegenden Gitterparameters kommt es zu einer Verschiebung der Atmungsmode hin zu niedrigeren Energien. Diese Verschiebung in den $A^{+2}Pt_3P$ erhöht die Quotienten α und α_1, beeinflusst aber nicht die kritische Temperatur T_c selbst.

Zum Schluss benutze ich die *ab-initio* Phononenzustandsdichte und die Eliashberg Funktion um die thermodynamischen Eigenschaften der APt_3P Verbindungen im Normalzustand und im supraleitenden Zustand zu berechnen. Diese ermöglichen einen direkten Vergleich mit dem Experiment von Takayama *et al.* [197] und eine Klassifizierung der neuen Supraleiter nach Marsiglio und Carbotte. [236]

Auf Grund der guten Übereinstimmung mit den Experimenten, kann man folgende Schlussfolgerungen ziehen. Im Kontrast zu Ref. [199], ist der Einfluss der Spin-Bahn Wechselwirkung vernachlässigbar für die elektronischen Zustände in der Region des Fermi-Niveaus und, angesichts der bemerkenswerten Übereinstimmung der berechneten und gemessenen spezifischen Wärme im normalleitenden Zustand, kann die in Ref. [199] gefundene dynamische Instabilität ausgeschlossen werden. Die Übereinstimmung der Einband-Migdal-Eliashberg Rechnungen und den supraleitenden Eigenschaften gemessen von Takayama *et al.* ist so gut, dass es keinen Spielraum für exotische Paarungsmechanismen – wie z.B. die in Ref. [198] vorgeschlagene, unkonventionelle [199] oder Mehrband-Supraleitung [197] gibt. Meine Rechnungen zeigen, dass die Klasse der APt_3P Supraleiter ein Lehrbuchbeispiel für Elektron-Phonon Supraleiter sind. Die unterschiedliche Anzahl an Elektronen in $LaPt_3P$ im Vergleich zu $A^{+2}Pt_3P$ (A^{+2} = Sr, Ca) Verbindungen macht den größten Unterschied in der Kopplung der Elektronen und Phononen aus. Diese ist schwach

in $LaPt_3P$, moderat in $CaPt_3P$ und groß in $SrPt_3P$. Der kleine Unterschied zwischen $CaPt_3P$ und $SrPt_3P$ kommt durch die Verschiebung der Phononenzweige (die einen Beitrag zur Supraleitung liefern) zu niedrigeren Frequenzen durch unterschiedliche Gitterkonstanten. In den A^{+2} Verbindungen, entsteht die Supraleitung hauptsächlich durch die Kopplung der Pt(1) Atmungsmoden in der Ebene mit elektronischen Zuständen in derselben Ebene. Ändert man die Gitterkonstante, die diese Ebene aufspannt, ändert man ebenfalls die Frequenz der Atmungsmoden. Durch diesen Zusammenhang könnte man diese Klasse von Supraleitern optimieren – entweder mittels Druck oder Dotierung. Auf Grund der Berechnungen der Gesamtenergie, befürworte ich den Vorschlag von Takayama *et al.* [197], den Effekt der fehlenden Inversionssymmetrie auf die Supraleitung zu erforschen in dem man isoelektronische Verbindungen mit und ohne Inversionssymmetrie untersucht. Dies kann in den APt_3P Verbindungen erreicht werden durch Variation der Synthesebedingungen, da die energetische Schwelle zwischen beiden Strukturtypen sehr klein ist (~ 20 meV).

In Kapitel 3 präsentiere ich meine Ergebnisse für den neuen Loch-dotierte Supraleiter CuBiSO. Die stöchiometrische Verbindung erhält man durch die Substitution von Fe and Pn mit Cu and S in der Struktur $ReOFePn$ (Re = rare earth) der 1111 Eisen-Pniktide. [225] Die Existenz der supraleitenden Phase ist nicht gesichert [226, 227] – im Gegenteil – Messungen der optischen Leitfähigkeit fanden einen Isolator mit einer Bandlücke von ca. 1.1 eV. [226] Die Supraleitung wurde bislang nur in Loch-dotierten CuBiSO gefunden, wobei die entsprechende Probe stark verunreinigt war. [225] Die nominale Dotierkonzentration war etwa 10%. [225] Loch-dotiertes CuBiSo (HCBSO) hat eine relativ hohe kritische Temperatur $T_c = 5.8$ K (in LaFePO, dem ersten entdeckten Fe-basierenden Supraleiter, beträgt $T_c = 7$ K [1]). Für dieses Material zeigten erste Rechnungen von Mazin [200] eine schwache ferromagnetische Instabilität und aus diesem Grund wurden Spin-Fluktuationen vorgeschlagen als wahrscheinlichste Paarwechselwirkung. Allerdings wurden keine Berechnungen basierend auf der Elektron-Phonon Kopplung durchgeführt und experimentell wurden keine Spur von Magnetismus gefunden. Außerdem wird Triplett-Supraleitung meistens durch eine wesentlich geringere Sprungtemperatur als 5.8 K [105, 112] charakterisiert.

Meine Berechnungen für die stöchiometrische Verbindung fanden einen Bandisolator mit einer durch starke Cu d-S p Hybridisierung charakterisierten Bandstruktur. Im Allgemeinen ist die Bandstruktur sehr ähnlich zu der anderer Eisen-Pniktide wie LaOFeAs, aber das Fermi-Niveau ist um ~ 1.5 eV nach oben verschoben auf Grund der unterschiedlichen Anzahl an Elektronen von Cu d^{10} im Vergleich zu Fe d^6. Demzufolge, sobald man Löcher in das System einfügt, bewegt sich das Fermi-Niveau in die anti-bindende Region der Bandstruktur, welche durch ein zweifach entartetes flaches Band mit gemischten Anteilen von Cu d_{xz+yz} und S p_{x+y} charakterisiert wird. Bei experimenteller Dotierung von $x = 0.1$ findet man das Fermi-Niveau E_{F} auf einem lokalen Maximum der Zustandsdichte (ZD). Diese Eigenschaft macht das System leicht instabil bezüglich Ferromagnetismus, auch wenn der effektive Stoner Parameter von Cu $I_{Cu} = 0.9$ eV durch die Hybridisierung zwischen Cu d-S p reduziert wird. In der Tat findet man den effektiven Stoner Parameter durch die Aufspaltung der Spinzustandsdichte in Minoritäts- und Majoritätsanteil. In der LSDN beträgt er $I^{LSDN} = 0.53$ eV und in der spin-polarisierten Gradientennäherung [englisch: Generalized Gradient Approximation (GGA)] $I^{GGA} = 0.67$ eV. Das steht im Kontrast zu den Eisen-Pniktiden, bei denen sich das Fermi-Niveau in der nicht bindenden Region der Bandstruktur befindet. Diese wird dominiert durch Fe d Orbitale und ist charakterisiert durch schwache Elektron-Phonon Kopplung. [4, 72] In diesem Fall begünstigt der kleine Wert der Zustandsdichte am Fermi-Niveau zusammen mit der Nesting-Bedingung eine antiferromagnetische Instabilität. [72]

Um die Supraleitung zu begründen, berechne ich die Elektron-Phonon Kopplung von HCBSO. Diese wird dominiert durch Cu-S Phononen, die nur Beiträge senkrecht zur Ebene haben. Diese Moden sind merklich an die Elektronen gebunden und kaum von der Dotierung abhängig. Die Eliashberg Funktion wird folglich durch zwei Maxima charakterisiert in Übereinstimmung mit den senkrecht zur Ebene verlaufenden Phononmoden der Cu-S Schichten. Außerdem ist sie unabhängig von der Dotierung. Das erlaubt es die Dotierabhängigkeit der Elektron-Phonon Kopplungskonstante entsprechend zu vereinfachen. Die kritische Temperatur, berechnet aus den *ab initio* Parametern, ist etwa 6 Mal größer als die, die experimentell ermitteltet wurde. Der größte Beitrag zu λ_{ep} kommt von dem hohen Wert der Zustandsdichte am Fermi Ni-

veau. Weil beide, das magnetische Moment sowie die kritische Temperatur basierend auf der Elektron-Phonon Kopplung, überschätzt werden, müssen ferromagnetische Fluktuationen berücksichtigt werden. Ich erreiche das durch eine Näherung der Spin-Suszeptibilität unter der Verwendung Random Phase Approximation (RPA) in ihrer Formulierung als Spindichtefunktional. Diese Näherung entspricht der Anwendung des Berk/Schrieffer Verfahrens [94], wobei ich für die nicht-wechselwirkende Suszeptibilität die der LDN und als Wechselwirkungsparameter den LSDN Stoner Parameter wähle. Der Effekt von nicht-lokalen Spin-Fluktuationen (Reduzierung der Tendenz zu Magnetismus) wird dadurch simuliert, dass man den Stoner Parameter als frei wählbaren Parameter ansieht. Da sich die von der Dotierung abhängige Elektron-Phonon Kopplung (in der Rigid Band Approximation) als einfach proportional zur Zustandsdichte als Funktion der Dotierung herausstellt, ist es nicht schwierig den gesamten Phasenraum zu untersuchen. Dieser wird aufgespannt durch die Gesamtkopplung (Differenz zwischen der Elektron-Phonon Kopplung und der auf Spin-Fluktuation basierenden Kopplung) als Funktion der Dotierung und des Stoner Parameters. Mit Hilfe einer modifizierten Formel für die kritische Temperatur T_c [317], konnte ich zeigen, dass Singulett- und Triplett-Supraleitung für die im Experiment verwendeten Dotierungen entartet sind.

Die erreichten Ergebnisse scheinen vor allen Dingen im Hinblick auf den supraleitenden Zustand von HCBSO interessant zu sein. Diese Verbindung ist ein einzigartiges Beispiel dafür, dass Supraleitung basierend auf Spin-Fluktuationen im Triplett-Kanal und Supraleitung basierend auf der Elektron-Phonon Wechselwirkung im Singulett-Kanal entartet sein können. Die kritische Temperatur ist beträchtlich für beide Symmetrien. Dieser Fakt kann *a posteriori* mit Hilfe der starken Kovalenz zwischen S p und den Cu d erklärt werden, welche die Bandstruktur charakterisiert: die Existenz von anti-bindenden p Zuständen am Fermi-Niveau führt zu großen Elektron-Phonon Matrixelementen, wohingegen die große Suszeptibilität und die starke magnetische Tendenz von Kupfer die Spin-Fluktuationen erhöhen. Außerdem verstärkt das flache Band im Valenzbandmaximum der stöchiometrischen Verbindung die Zustandsdichte in der Nähe des Fermi-Niveaus und platziert damit HCBSO in einer instabilen Region des Phasenraumes mit Ladungs- als auch Spinfreiheitsgra-

den. Dies scheint sich im Experiment zu bestätigen, da die Supraleitung stark von den experimentellen Bedingungen abhängig ist. [225]

Auch wenn es mir nicht möglich ist eine endgültige Antwort auf die Frage nach der Symmetry des Ordnungsparameters zu geben, könnte das Material auf Grund der Entartung der supraleitenden Ordnungsparametern sehr nützlich in der angewandten Forschung sein. Tatsächlich könnte man im Prinzip die Paarungssymmetrie durch die Anwendung äußeren Druckes oder aber eines magnetisches Feld durchstimmen und somit wesentlich die Eigenschaften eines Zweischichtsystems ändern (z.B. bestehend aus einem Supraleiter und einem Metall).

In Kapitel 4 berechne ich die optischen Eigenschaften von LaFePO. Als erstes gebe ich eine Einführung in das Modell und seine wesentlichen Näherung für die optische Leitfähigkeit unter Berücksichtigung von Übergängen innerhalb eines Bandes. Dazu verwende ich das erweiterte Drude Modell welches auf einer Frequenz abhängigen mittleren Streuzeit $\tau(\omega)$ basiert. Diese kann aus dem Realteil der optischen Leitfähigkeit $\sigma_1(\omega)$ berechnet werden, sobald man eine Modell für niedrig-energetische Anregungen der Bandstruktur aufgestellt hat. In diesem Fall habe ich zwei Loch-artige Bänder am Γ-Punkt und zwei entartete Elektron-artige Bänder am M-Punkt verwendet. Die Wechselwirkung wurde auf Übergänge zwischen den Bändern beschränkt und nur Spin-Fluktuationen wurden zugelassen. Der Propagator der retardierten Wechselwirkung wurde als proportional zur Spinsuszeptibilität von Millis angenommen. [171] Die Selbstenergie wurde in der Migdal Eliashberg Näherung berechnet mit einer lokalen Näherung angewandt auf die wechselwirkende Greens Funktion. Da die Selbstenergie $\mathbf{q}$-unabhängig ist, kann man zur Berechnung der optische Leitfähigkeit Vertex-Korrekturen vernachlässigen.

Der vorläufige Vergleich zwischen der berechneten optischen Leitfähigkeit für Übergänge innerhalb eines Bandes und den experimentellen Ergebnissen aus Ref. [153] zeigt, dass unterhalb der Grenze $\omega_B \approx 500$ cm^{-1} das berechnete Spektrum gut mit dem Experiment übereinstimmt. Da oberhalb von ω_B die berechneten Beiträge für Übergänge innerhalb eines Bandes allein nicht mehr ausreichend sind, untersuche ich im Folgenden den Beitrag von Übergängen zwischen den Bändern im Spektrum von LaFePO. Diesen Beitrag beschreibe ich durch eine zusätzlichen

Lorentz-artige Verteilung in der optischen Leitfähigkeit. Das Ergebnis zeigt, dass der flache Beitrag bei $\sigma_1(\omega)$ und das lineare Verhalten von $\tau^{-1}(\omega)$ [153, 320] durch eine Lorentz-Verteilung mit dem Schwerpunkt bei $\omega_L \sim 3000$ cm^{-1} und einer Breite von $\gamma = 8000$ cm^{-1} beschrieben werden kann.

Um den Ursprung des experimentellen Verlaufes von $\sigma_1(\omega)$ zu untersuchen, berechne ich das optische Spektrum von LaFePO mittels DFT. Die optischen Übergänge zwischen den Bändern sind bereits bei sehr kleinen Anregungsenergien vorhanden und umfassen dabei die Elektron- und Loch-artigen Bänder am Fermi-Niveau. Die optischen Leitfähigkeit zeigt dabei ein Maximum bei $\omega =\approx 500$ cm^{-1} und ein etwas breiteres bei $\omega \approx 2500$ cm^{-1}. Aber, da die Bandbreite durch GGA überschätzt wird, sollten die Übergänge im Experiment bei niedrigeren Anregungsenergien liegen.

Auf Grund der Unterschätzung von Korrelationseffekten bei Berechnungen auf LSDN Niveau der Übergänge innerhalb eines Bandes, kann man diese nicht direkt mit dem Experiment vergleichen. Allerdings sind sie hilfreich um den Ursprung der Zwischenbandübergänge und ihre relativen Intensitäten zu verstehen. Tatsächlich werden in Eisen-Pniktiden die Übergangsfrequenzen überschätzt. [159]

Aus diesem Grund beschreibe ich die Zwischenbandübergänge als zwei Lorentz-Verteilungen und füge sie der berechneten optischen Leitfähigenkeit hinzu, welche nur Übergänge innerhalb eines Bandes enthält. Analog zu den GGA Ergebnissen verwende ich für den Realteil der optischen Leitfähigkeit der Zwischenbandübergänge eine schmale Lorentz-Funktion bei $\omega_1 = 750$ cm^{-1} – diese beeinflusst $\tau^{-1}(\omega)$ nicht – und eine etwas breitere bei $\omega_2 = 4500$ cm^{-1}. Diese Werte wurden so gewählt, dass eine sehr gute Übereinstimmung mit dem Experiment erreicht werden konnte. Am Ende zeige ich, dass die Kopplungskonstante, die man aus der Analyse von $\tau^{-1}(\omega)$ der theoretischen Kurve entnehmen kann, nicht mit der übereinstimmt, die im Modell verwendet wurde.

Abschließend kann man feststellen, dass die experimentellen Ergebnisse unterhalb von $\omega = 500$ cm^{-1} gut durch die optische Leitfähigkeit unter ausschließlicher Verwendung von Übergängen innerhalb der einzelnen Bänder beschrieben wird. [195] Dieser Beiträg entspricht einer fast konstanten Streuzeit $\tau(\omega)$. Jedoch um die starke ω-Abhängigkeit der Streuzeit zu berücksichtigen, müssen auch

Übergänge zwischen den Bänder betrachtet werden. Dies zeigt, dass die starke ω-Abhängigkeit von $\tau(\omega)$, welche experimentell als Anzeichen für starke Korrelation interpretiert wurde, die zu einer Umordnung der Zustände in der Nähe des Fermi-Niveaus von LaFePO führen, nur ein störender Beitrag auf Grund der Zwischenbandübergänge im Niedrigenergiespektrum ($500 < \omega < 3000$ cm^{-1}) dieses Materiales ist. Diese Übergänge wurden in anderen Pniktiden wie z.B. in K-dotiertes $BaFe_2As_2$ mittels Ellipsometriemessungen bestätigt. [159] Die obige Betrachtung zeigt eindeutig, dass die Auswertung von optischen Spektren der Pniktide mit Hilfe eines erweiterten Drude Modells fragwürdig ist, da es zu einer schweren Überschätzung der Korrelationseffekte führt.

In Kapitel 5 präsentiere ich eine einfache Methode um langreichweitige Fluktuationen, welche nicht in der LSDN enthalten sind, zu berücksichtigen und wende sie danach auf Ni_3Al an – einem Ferromagneten unter Druck. Dabei zeige ich, dass die Bandstruktur und die Zustandsdichte im Falle der LDN paramagnetischen Rechnung fast perfekt mit dem Druck in einem großen Energie- und Druckbereich skaliert. Sowohl die Ni d^9 Konfiguration als auch die hohe Zustandsdichte am Fermi-Niveau sind Indizien für die Tendenz zu Magnetismus. Tatsächlich ist das Material in der LSDN magnetisch, aber auf Grund der Molekularfeldnäherung werden das magnetische Moment bei Umgebungsdruck sowie die kritische Temperatur überschätzt. Die Auswertung der LSDN Rechnungen im Sinne eines einfachen Stoner Modells zeigen, dass die Abweichung direkt proportional zu einer Überschätzung des Stoner Parameters in der LSDN ist.

Danach stelle ich einen phänomenologischen Ansatz vor, der auf der Theorie selbst-konsistenter Renormalisierung (SKR) basiert und häufig in der Literatur zur Korrektur der magnetischen Eigenschaften von itineranten Systemen im Bereich von quantenkritischen Punkten (QKP) verwendet wird. [51, 52, 61–64, 234, 263, 268] Jene Methode erlaubt es die Ergebnisse der LSDN in Übereinstimmung mit dem Experiment bei Umgebungsdruck zu bringen. Dies wird erreicht durch Berücksichtigung von nicht-lokalen Fluktuationen unter Annahme einer Gauß-artigen Verteilung der Magnetisierung. Dieser einfache Ansatz zeigt auf eine transparente Art und Weise, dass der Einfluss von nicht-lokalen Fluktuationen zu einer Unterdrückung des

Stoner Parameters I führt. Das ist ein Hinweis für die Verbindung der SKR Theorie und anderen Methoden, deren Hauptziel es ist den Magnetismus in der LSDN durch eine Reduzierung des Stoner Parameters zu unterdrücken.

Ich berücksichtige die Abschwächung des Stoner Parameters durch eine Modifikation des Austausch-Korrelations-Potentials. Diesen Ansatz nenne ich reduzierte Stoner Theorie (RST), eine einfache und numerisch nicht aufwendige Methode um die magnetischen Eigenschaften von itineranten Systemen in der Nähe des QKP zu korrigieren. DFT im Allgemeinen – in ihrer Implementierung als Molekularfeldtheorie – überschätzt gewöhnlich die Tendenz zu Magnetismus. Der Ansatz besteht aus einer Skalierung des Spin-polarisierenden Anteiles des Austausch- und Korrelationspotentials im Sinne der von Bart-Hedin Skalierung. [43] Er liefert außerdem eine Abschätzung für die stärke der Fluktuationen des Systems – der Quotient aus dem renormalisiertem Stoner Parameter und seinem ursprünglichen Wert. Vergleiche dieses neuen Ansatzes mit Ergebnissen der RST für Ni_3Al bei Umgebungsdruck zeigen eine erstaunliche Übereinstimmung beider. Aus diesem Vergleich kann man den ursprünglichen Stoner Parameter bestimmen, der gut mit dem übereinstimmt, den man von Rechnungen mit festen Spinmomenten erhält.

Ich habe die neue Methode auf den Phasenübergang von Ni_3Al unter Druck von ferromagnetisch zu paramagnetisch angewandt. Der notwendige Skalierungswert s um die berechneten magnetischen Momente in Übereinstimmung mit dem Experiment zu bringen, ist bei $P = 0$ und $P = P_c$ identisch. Unter Verwendung eines genäherten Ausdrucks für die Spinsuszeptibilität, kann ich die gemittelte Amplitude der Spinfluktuationen ξ in Abhängigkeit der Bandparameter dieser Verbindung angeben. Auf Grund der speziellen Skalierung der Zustandsdichte mit dem Druck, zeige ich, dass die Annahme eines Druck unabhängigen Parameters $s = 0.88$ gerechtfertigt ist. Da nun s kein Parameter mehr ist, kann man die magnetischen Momente *ab initio* als Funktion des Druckes berechnen. Weil im Moment noch keine Magnetisierungsmessungen vorhanden sind, vergleiche ich die Ergebnisse der RST mit der Curie-Temperatur T_c als Funktion des Druckes gemessen von Niklowitz *et al.* [201], unter der Annahme, dass Moriya's Skalierung $T_c \propto m^{3/2}$ anwendbar ist. Eine gute Übersteinstimmung mit dem Experiment wurde gefunden, was die

Verbindung zwischen RST und SCR Theorie bestätigt. Am Schluss zeige ich, dass das Modell, welches Niklowitz *et al.* [201] verwenden um Ihre Daten zu interpretieren auf der Annahme basiert, dass die Zustandsdichte mit dem Druck skaliert wie $N_0(P) \propto N_0(0)/(1+AP)$, wobei A eine Konstante ist. Da das genau die Skalierung ist, die ich für Ni_3Al gefunden haben, ist meine Rechnung eine mikroskopische Begründung für ihr Modell.

In der vorliegenden Arbeit habe ich LSDN und GGA als Ausgangspunkt auf Basis der Molekularfeldnäherung benutzt und Abweichungen zum Experiment als "Hinweis" für Freiheitsgrade der Spinfluktuationen in diesen Systemen angesehen. Auf diese Weise konnte ich ein phänomenologisches Modell basierend auf *ab initio* Berechnungen der Observablen in Molekularfeldnäherung konstruieren, wobei die Observablen die Werte annehmen, die man messen würde, wenn keine Fluktuationen vorhanden wären.

Die ursprüngliche Motivation dieser Arbeit war die Entdeckung der Eisen-Pniktide. Für sie habe ich in meiner Masterarbeit ein Niedrigenergie-Modell konstruiert, welches erfolgreich die Abweichungen zwischen LDN Rechnungen und den Experimenten in LaFePO beschreibt. [195] Die Unterschiede zwischen dem Experiment und den DFT Rechnungen ergaben, dass in diesen Material hauptächlich Wechselwirkungen zwischen den einzelnen Bänder eine Rolle spielen als Wechselwirkungen innerhalb eines Bandes. Außerdem konnte ich eine Kopplungskonstante bestimmen, welche eine kritische Temperatur vergleichbar mit dem Experiment ergibt. Folglich berechnete ich basierend auf den Modellparametern die optischen Eigenschaften um die experimentall auftretende starke ω-Abhängigkeit der Streuzeit zu untersuchen. [153] Die Startwerte für das Modell von LaFePO, und die Parameter für die nicht-wechselwirkende Bandstruktur wurden von Lebégues GGA Rechnungen [321] abgeleitet. Ich begann meine Doktorstudium mit der Absicht, mehr über die Berechnung solcher effektiven Parameter auf Grundlage von DFT Rechnungen zu lernen. Während ich mich in die Grundlagen der DFT einarbeitete, wurden die APt_3P Verbindungen durch Takayama *et al.* [197] entdeckt. Für diese Klasse ist die DFT vollkommen ausreichend um alle Materialeigenschaften zu beschreiben. Über Supraleitung in Loch-dotierem CuBiSO wurde erstmals zu Beginn meines Doktorstudiums

berichtet, wobei ihr Ursprung kontrovers diskutiert wurde. [225, 227] Erste DFT Rechnungen führten die Supraleitung auf Spin-Fluktuationen zurück, ohne explizit ihren Beitrag zur Paarbildung und die Kopplung der Elektronen mit den Phononen zu berechnen. [200] In diesem Fall begann ich mit der Berechnung des Beitrages der Elektron-Phonon Kopplung zur Paarbildung in der Supraleitung. Allerdings ist die resultierende kritische Temperatur zu hoch. Zum selben Zeitpunkt wurde berichtet, dass der Grundzustand schwach ferromagnetisch ist. Ich erkannte, dass dies eine Verbindung sein könnte, in der die Elektron-Phonon Wechselwirkung und die Spin-Fluktuationen im Wechselspiel miteinander stehen. Da es nicht möglich war eine *ab initio* Beschreibung der Spin-Fluktuationen zu konstruieren, entwickelte ich ein Modell basierend auf der phänomenologischen Reduktion des Stoner Parameters. Daraus entstand die Idee, den Stoner Formalismus mit der Theorie von Moriya [17] zu verbinden und alles in einem LSDN Funktional zu berücksichtigen. Auf diese Weise wurde die reduzierte Stoner Theorie (RST) geboren, welche sofort auf die prototypische Verbindung Ni_3Al unter Druck angewandt wurde.

Aus der Sicht phänomenologischer Ansätze, welche auf DFT Grundzuständen basieren, stellen die APt_3P Supraleiter den Ausgangspunkt "ohne Fluktuationen" dar. Tatächlich sind in diesen Verbindungen die GGA-Rechnungen in perfekter Übereinstimmung mit den Experimenten und man kann die gesamte Physik ohne phänomenologische Parameter verstehen – abgesehen vom Coulomb-Pseudopotential μ^*, welches einmalig fest gewählt werden muss um T_c zu berechnen. Die Eisenpniktide hingegen symbolisieren den entgegengesetzten Grenzwert. In ihnen werden in der LSDN die magnetischen Momente überschätzt. Auch kann die Elektron-Phonon Kopplung nicht allein ursächlich für die Supraleitung sein. In der vorliegenden Arbeit habe ich den Fall von LaFePO untersucht. Diese Verbindung ist magnetisch in der LSDN Rechnung, aber unmagnetisch im Experiment. Diesen Unterschied beschreibe ich durch antiferromagnetische Spin-Fluktuationen – welche das System im normalleitenden als auch im supraleitenden Zustand bestimmen – als bosonische Moden deren Spektrum entweder phänomenologisch beschrieben [171] oder aber durch den Imagninärteil der Spin-Suszeptibilität erhalten werden kann. [150]

Ein Beispiel, das zwischen den beiden vorher genannten Grenzen liegt, ist das

Loch-dotierte CuBiSO, in dem Elektron-Phonon basierende *s*-Wellen Supraleitung in Konkurrenz mit Spin-Fluktuation basierender *p*-Wellen Supraleitung steht. Die wichtigsten Fluktuationen sind von ferromagnetischer Natur, welche durch die Verbindung von LSDN und dem Stoner Modell, leicht beschrieben werden können, wenn man eine phänomenologische Reduzierung des Stoner Parameters annimmt. Auch in diesem Fall wurden beide Effekte – der Magnetismus als auch die Supraleitung – durch eine passendes Modell der Spin-Suszeptibilität berechnet.

Der Zusammenung zwischen LSDN und Stoner Modell markiert den Weg hin zu einer *ab-initio* Beschreibung von Spin-Fluktuationen über die LSDN hinaus. Tatsächlich entspricht die Überschätzung des magnetischen Moments der Überschätzung des Stoner Parameters. Deshalb sollte die Korrektur des LSDN Stoner Parameters eine korrekte Beschreibung des Magnetismus in itineranten Systemen ermöglichen. Dieser Ansatz wurde an Ni_3Al unter äußerem Druck erprobt. Die Übereinstimmung mit dem Experiment ist außergewöhnlich gut abgesehen von einer Unterschätzung der kritischen Temperatur.

Die in Kapitel 5 beschriebene reduzierte Stoner Theorie kann auf alle Verbindungen angewandt werden, in denen die LSDN die Tendenz zum Magnetismus überschätzt. Außerdem kann man mit ihr die Veränderungen der elektronischen Struktur von nicht-magnetisch zu magnetisch untersuchen. In diesem Sinne ist das magnetische Moment als Funktion des Skalierungsparameters *s* eine Antwortfunktion des Systems auf eine magnetische Störung. Des Weiteren kann diese Methode einfach auf den antiferromagnetischen Fall erweitert werden und hilft auf diese Weise die Stabilität verschiedener magnetischer Ordnungen zu untersuchen. In Systemen, in denen das magnetische Moment überschätzt wird, ist der Wert *s*, der das magnetische Moment in Übereinstimmung mit dem Experiment bringt, eine Abschätzung für die durchschnittliche Amplitude der (Spin-)Fluktuationen. Diese ist ein wichtiger Indikator für das Maß nicht-lokalen Korrelationen in solchen Verbindungen. Da die RST den korrekten Stoner Parameter liefert, kann das Phasendiagramm von CuBiSO – mit den Näherungen aus Kaptiel 3 – auf eine Linie reduziert werden. Angewandt auf Pniktide, kann diese Methode den Unterschied zwischen Nesting-Effekten und Stoner-artigem Ursprung der diversen magnetischen

Anordnungen, die in der Literatur besprochen werden, liefern.

List of publications

Publications on international refereed journals:

1. L. Ortenzi, S. Biermann, O. K. Andersen, I.I. Mazin, L. Boeri
   "Competition between electron-phonon coupling and spin fluctuations in superconducting hole-doped CuBiSO"
   Phys. Rev. B **83**, 100505(R) (2011).

2. L. Benfatto, E. Cappelluti, L. Ortenzi and L. Boeri
   "Extended Drude model and role of interband transitions in the midinfrared spectra of pnictides"
   Phys. Rev. B **83**, 224514 (2011).

3. L. Ortenzi, I.I. Mazin, P. Blaha and L. Boeri
   "Accounting for spin fluctuations beyond LSDA in the density functional theory"
   Phys. Rev. B **86**, 064437 (2012).

4. Alaska Subedi, Luciano Ortenzi, Lilia Boeri
   "Electron-phonon superconductivity in APt3P (A=Sr, Ca, La) compounds: From weak to strong coupling"
   Phys. Rev. B **87**, 144504 (2013).

Acknowledgements

I would like to end this thesis by thanking all the people that helped me in these four years of work and made the experience of the PhD into a deep scientific and human experience.

First of all I would like to thank prof. Ole Krogh Andersen for having accepted to be my "Doktorvater" and for his capability of shaking the foundations of my physical knowledge. I also thank for suggesting corrections and references included in the final version of this thesis. Together with him I also would like to thank my "day by day" supervisor Lilia Boeri for all the work, time and efforts she spent together with me along these almost four years. I would like also to thank her because she managed to build up a small group which was at the same time efficient and very friendly. Lilia thanks a lot! I also would like to thank prof. Walter Metzner for his kind support and positive mentorship, and prof. Aleandro Muramatsu and prof. Martin Dressel for taking care of my PhD defense. I hope they liked the examination. I definitely enjoyed it! Thanks a lot also to prof. Dirk Manske for being part of my internal PhD committee at MPI. At this point my thought goes also to George Libuda and Mrs Stein who helped me in dealing with all the administrative paperwork. Mrs Stein in particular did really a great job!

Among my collaborators I thank Silke Biermann, Lara Benfatto, Peter Blaha, Alaska Subedi Igor I. Mazin, Emmanuele Cappelluti. In particular I thank Igor for his

scientific enthusiasm and for his kind courtesy. He always offered me the occasion for learning a lot and to restart every time I thought my ignorance was too deep for going on. He always exploited all the good that came from me by purging what was unimportant and correcting what was wrong. I really hope that in the future there will be other occasions for continue our collaboration. Emmanuele is my master and I'm extremely happy that, thanks to prof. Luciano Pietronero, I will have the occasion to work with him again in Rome.

Among the people in Lilia's group (former and present) I would like to thank Marc Höppner for all the precious help he gave me with this thesis. From him I learned how to use tools for making figures and he also took care of the translation of the Zusammenfassung of the present thesis and also of myself when I was tired and demotivated. He demonstrated me devoted and sincere friendship being always present and available when I needed help, and I really bothered him a lot! Danke für deine freundschaft!

A dear friend I want to thank is of course Alaska Subedi (former member of Lilia's group). The reasons why I'm grateful to him are too many. One of the most "famous" and peculiar is for having offered me a place to sleep when it was "too late" for me for getting home on my own... Moreover I thank him for advertising my olive oil around the world. He introduced me at the same time to the oriental and to the american world and he gave me the occasion for very interesting discussions about basically everything, often accompanied with good food and wine (of course!).

Among the people in Andersen's department I'm grateful to many people and friends. First of all I have to thank Maurits Haverkort and his wife Larissa, for their kind friendship. In particular I would like to thank Maurits for spending time with me teaching how to calculate electronic properties *ab-initio*. I thank O. Dolgov for the suggestions of nice and instructive references on electron-boson coupling in spin fluctuations superconductors. Moreover I'm indebted to Olle Gunnarssonn and Alexander (->Alexsasha-> Sasha) Yaresko for guiding me trough the wonderful world of band magnetism. I know, I still have to learn a lot and I hope they will still be available in the future as they did during these (almost) four years. I would like to thank them once more for the illuminating discussions, suggestion of precious

references and cordial friendship. Sasha thanks a lot also for your nice jokes and wonderful picture! Olle thanks also for the nice discussions on economics and for your loquacious silences! Furthermore I would like to thank Yoshiro Nohara (keniu) for the affection he showed in my regards and towards my family. Sorry if I made your life sometimes too "colorful"... Among the first people I met at MPI there is Claudia Hangermann. What to say?! She is simply fantastic! Thanks a lot for helping me at the beginning and moreover thank you once more for coming to the defense. I know this was not easy for you. Thanks again! Of course I would like to thank also Claudia's "nachfolgerin" with whom I got in closer contact during Ole's last conference. I want to thank her for being such a lovely person and efficient worker. Now I have to find my best words for thanking the most beautiful couple in the institute: Virginia and Ove Jepsen (ladies first...). Well, they have welcomed me in a way I would never imagine! Moreover is due to them if I can communicate now in English. In particular Ove had lunch and coffee with me every day and I really could ask everything to him: from the bandstructure of La_2CuO_4 up to how to write an application letter (included the translation of the title and abstract of my thesis to German...), and our discussions went through the all human knowledge. Virginia is a person with open heart and bright spirit, Ove is a nordic man with a southern heart, sharp mind and biting irony. I'm really glad of having met such nice people here!

Among the MPI scientist I got many friends. I'm particularly grateful for the fantastic friendship with Reinhard Kremer who gained the title of honorary grandfather of my son Paolo. He really treats me like his youngest child and this helps me to fill myself somehow at home! From the scientific point of view he is a wise and rigorous scientist. Among the (many) things I learned from him there is the Slater-Pauling curve and the german interpretation of "Il barbiere di Siviglia" by Hans Hotter: both things I will never forget in my life! Thanks to Reinhard I met Fereidoon S. Razavi who also helped me in formulating some sentences in Chap. 3 in a understandable way. I also want to thank Jürgen Köhler for a nice discussion concerning the metallic bond in Ni compounds. MPI is of course a prestigious institute where a PhD student has the occasion of meeting international scientists

of outstanding level and very kind persons. Among these I would like to thank Sergej Savrasov for the nice experience I made when he was here at MPI. I hope we can go skying somewhere, sometimes together (of course you have to teach me....) I also would like to than Prof. Renato Gonnelli which I never manage to call Renato (and I do not think I will do in the future...) prof. Gonnelli thank you for your kind friendship, loyalty and sincerity. Among the people that helped me in my work and in particular with the present thesis I have to thank Alaska Subedi and Marc Hoeppner ONCE MORE. And then of course Ove, Olle, and Sasha AGAIN for having guided me through the examination training me as a boxer and curing me as a kid. Many thanks also to Jitae Park, Aliaksei Charnukha, Andreas Eberlein, Philipp Hansmann and Jens Kunstmann who shared with me their experience about the"PhD procedure" and gave me a lot of tips and tricks. THANKS A LOT!!! Among the PhD students my thanks go of course to Federico Paolucci, Benjamin Obert, Sofia-Michaela Souliou and Raquel Queiroz and Meng Wu for their kind friendship and company. At this point I want to thank also the people without which all my work at MPI would not have been materially possible. These people are Karl Roessmann, Armin Schuhmacher and Armin Burkhardt. They made things that are impossible to do for a normal human being like teaching german to a crazy italian guy..... The first challenge we had to face together was to find a proper name for my account at MPI. The straightforward one should have been l.ortenzi. Too boring! Then I asked for something more original: mandrache. That's cool! And it always brought me good luck. Unfortunately it was too long: man-dra-che.... Finally we got a perfect agreement: **mandrake**. THAT'S PERFECT!!! Indeed it is the name of a magician and ideally means:"the guy who is able to do things that common people cannot do". Well, I think they really made something special! After having thanked the IT guys (I hope in a proper way....) I would like to thank one of the most creative mind I have ever met in my life (well of course my thanks go to the person who possess this mind....): frau Regine Noack. Frau Noack thanks a lot! You are really great! This gives me the occasion to thank also all the people which were related to me and my work but not in a scientific way. These are all the people in the administration: Frank Gottschalk who took care, together with Elvira Hurst

of my contract, Brigitte King who took care of my registration in Büsnau and then in Stuttgart and then in Munich and so on... Moreover I want to thank Michael Eppard for his positive management. In particular I'm thankful to Frank for his nice friendship and also practical help (once we loaded together a large table in his small twingo... This was a miracle!) Finally, I want to thank Marion Vogel and Anette Schleehauf for their precious and kind help when I was almost desperate with flat searching and arranging trips, respectively. About these topics there are episodes that nobody will forget (ask Lilia for details).

Finally I would like to thank all the people that contributed to this thesis in way which won't appear in other document but this. These people were my friends and relatives. They contributed to this thesis because they contributed to the edification of my-self. I will group them by work and family context.

Among the friends I met at MPI there are Ove, Virginia, Kenyu, Sasha, Olle, Alaska, Marc and Leona, which i already thanked. Then comes Adolfo Avella. I know he already lost the hope of finding his name among the people I thank. HOW COULD YOU THINK THAT!!!!??? I really have to thank him for his patience and help! But also for the nice food he brought from his home town which made Büsnau into a nice and friendly place... My thanks also go to his wife Ester (nice name!) and his two kids Alfonso and Vincenzo which have the duty of showing him that what is in his mind is a small thing compared to the wonderful amount of possibilities and beauty of reality! I also thank Andreas Schnider for the nice discussions on non centrosymmetric superconductors and for having forgiven me all the time I promised him olive oil and never brought. SHAME ON ME!!! But you know: life is still long, and moreover you can come directly to me and pick it up. Last but of course not least, among the friends I met at MPI, there is George Jacheli. He is a kind and lovely person and I have many reason for thanking him. Among the most peculiar ones I thank him for having forgiven my bad pronunciation of greek letters like μ... Moreover I thank him for having invited my friend Alaska at his place for dinner without knowing him yet and for hosting me the all incoming month of November. Finally I thank him for the most important discovery I made in the last period: the fantastic georgian restaurant in Stoechack. I hope one day you will

come and visit me in Rome. In this way I can thank you also not only with words.

Among the friends I met out of MPI I have to thank Davide Bergomi, Davide Stricker, Benedetta Caggioni, Susanne Münkel, Michael Schliep and the families Schmidt, Zipp, Birke and Biba. These people offered me the first support when I came to Stuttgart and I did not know anybody and any single German word. In particular I thank Elmar and Micheil for coming to my PhD and Elmar once more for having taken such nice pictures! All these people are part of a great and mysterious friendship which helped me everyday to keep awake the soul and to focus my attention towards my real and deep desire. Thanks for your warm company! At this point I also want to thank Paolo Volpetti and Davide Arrigoni with whom I think the adventure of a friendship born abroad will continue in our land. I'm looking forward to seeing you soon! I also thank Bernardo Lo Sterzo for all the dinner he cooked for me, giving me the possibility to find something warm coming back from work and together with Caterina Palocci for having given me and Sara a possibility to open our family to guests. They were the precursor of another guest which would have came soon...

Now let's move to Munich where my family (and not only it) is. First of all let me thank Ilaria Zardo for the role of "big sister" that she always ascribed to herself in my respect and which I'm very grateful of. She offered me her unconditioned friendship which I really hardly tried during these 12 years... Grazie Ilaria perche' il fatto che ci sei mi spinge a non accontentarmi della soluzione banale ma a chiedermi cosa desidero sul serio. Vabe' il resto te lo dico a voce. Fortunately Sara appeared on my landscape and gentled my soul, offering to Ilaria a more pleasant person to face. A special thank goes of course also to her husband Hans Leonhard Prechtel, which she met in Germany and manages to stand my stormy and passionate friendship with his wife without spank us as one would do with kids. Thank also to their son Francesco Xaver who made me realize that I was going to become father of a small kid like him (Francesco Xaver is indeed just 5 month older than our Paolo). Let me here thank also the grandparents of francesco Xaver, Francesco and Rita and Jörg and Lilo. The firsts helped me when I was in Rome, the second supported us with friendship and things for Paolo. Overall I thank all of them for having accepted me,

Sara and Paolo as a part of Ilaria. It sounds strange I know, but I do not know any other words for describing our friendship but “belonging the ones to the others”.

The people I first met in Munich and first offered a place to stay during the weekends when I visited my fiancee Sara were Marco Anghileri, Christian Zucchetti and Vito Dantona. Now Christian is in USA and Marco married a beautiful austrian girl and they have a wonderful son, Matthias which is 15 days younger than Paolo. By chance Marco and Anna leave now close to us and share with us this new adventure of being fathers and mothers. Vito, thanks a lot for your discreet friendship and your silents full of mystery. Hoping to having you soon for dinner by us!

Since I got married I also got in deeper contact with my wife’s friends in Munich which sustained our family in several ways. First of all the “Paonni’s” (Matteo, Anna, Giorgia and Federica and Valentina) offered to me and Sara (and I think not only to us...) a great example of how a family should be. We spent a lot of time together and they invited us for lunch almost every Sunday. Matteo in particular was crucial in helping us with the renovation of our flat in Munich. Grazie mille per la vostra cordiale e familiare amicizia con voi la storia credo proprio che continuera’ in Italia, percio’ a presto! Also Enrico helped us with the works and together with his wife Malvina offered a us nice friendship and we could always count on them! Thanks a lot! dziękujęd!! He is italian and she is Polish and they leave in Germany: very international mixture! I think thiese things, together with the presence of international institutes (more than institutions...) help to build up Europe more then several good economical, political and cultural intentions....

Among the families I have already mentioned which are building up Europe, there are also Anna and Jan Cattani Scholz with their beautiful girls Francesca and Laura. I do not know if Europe is in good hands but for sure has solid foundations! I also would like to thank another couple of friends hat will soon get married and I wish them all the best for this: Roberta Caterino and Gordon Rinke. I thank Gordon for all the trips we joined from Stuttgart to Munich (he is in Kern’s group) and for the bavarian musical landscape we got the chance to discover every time we crossed the Baden Württemberg border, and the radio jumped on these fantastic bavarian stations. And now Roberta!!! Expecially in the last period I had the chance

to get knowing her as a very beautiful person! Especially for my wife Sara and my son Paolo she was always present and attentive. I think you know how precious you are for our family. At this point I also would like to thank also Tommaso Panni, Anna Miotello and Carlo Manara, Erica Berni, Sebastian, Simon, Sophie and Katarina Huegel, Isabel Otterbach, Thomas Mack, Lucia Bolzoni and Massiliano Pollini, Domenico Sammartano, Stefano Montanari and his wife Marcella for their kind vicinity and friendship during the new adventure of being father and ending my PhD. In particular I would like to thank Tommaso and Erica for having involved me in a new adventure which I think will continue also when I will move...

The presence of all these friends in Munich during Sara's pregnancy helped me to slip during the night and not get crazy.

I also would like to thank "old friends" like Francesca Lulli and Giovanni Marcotullio, Stefano and Rachele, Luigi, Marta, Marco and Daniele for coming from Italy just to visit me and Sara when she was at the hospital and I was finishing to write the thesis.... They sustained me and my family in such a delicate moment with kind and discrete friendship. THANKS A LOT!!!

Now it is time to thank my family which supported me from faraway and Sara's family who enjoyed with us Paolo's birth. Grazie Mamma che dal cielo mi hai sempre aiuato e sostenuto con segni discreti ma inconfondibili. Grazie anche per la vita donatami e per la furia dell'animo che da te ho ereditato. A volte mi manchi parecchio. Lascio al silenzioso dialogo con la tua presenza il resto delle cose che vorrei dirti in questo istante. Riposa in pace. Grazie anche a te papa'. Non credo che leggerai mai questo enorme incartamento in inglese che rappresenta il lavoro di quattro anni. Tuttavia sappi che ti sono grato, oltre che per la vita, anche per la semplicita' di cuore che mi hai trasmesso e l'attaccamento al lavoro che mi hai insegnato (e che difficilmente saro' in grado di imitare). Grazie anche a te fratello mio. Semplicemente per il fatto che ci sei. Grazie te ho imparato cosa significhi l'essere fratelli. Qualsiasi cosa tu faccia, ovunque tu vada, qualsiai cosa senti, pensi o vedi, c'e' uno che e' legato ontologicamente a te da sempre e lo sara' sempre. Ma soprattutto e' uno a cui tu sei legato. Che tu lo voglia o no, che tu lo riconosca o meno. Almeno come nostalgia. Spero di abbracciarti presto!

E adesso un salutino,
a un bravo cristianino
che e' il nonno di Paolino.
Egli vive lontanino
e venendo qui vicino
ha scoperto il tunisino.
Quando dopo un bel pranzino
egli prende il caffettino
non disdegna un buon grappino.
E' un pochino rotondino,
un tantino pelatino
sto parlando di Aladino!

Cari Anna e Aladino, grazie davvero per avermi accolto con cordiale benevolenza nella vostra famiglia. Spero che sarete nonni di tanti e tanti nipotini! Siete due persone eccezionali e due suoceri fantastici. Ma soprattutto grazie per esservi presi cura della mia famiglia in un momento in cui io proprio non potevo. Grazie anche a voi Dino e Wahida per aver rinunciato di buon cuore alla vostra parte di sottaceti, sottoli e affettati in favor mio e della mia famiglia. Grazie infinite anche a te Valeria per avermi fatto diventare zio (per la prima volta...) spero di saperti essere vicino come hanno fatto i miei zii con me. In particolare quelli piu' prossimi, penso a zio Terzo, zia Maria e zio Riziero. Grazie anche a voi, alle mie due cugine piu' "anziane", Sonia e Iole e alle loro famiglie perche' fin da piccino mi avete curato e accudito, facendo in modo che crescessi in un ambiente cordiale dove i rapporti familiari sono reali vincoli di cura reciproca. Parte di questo lavoro senza di voi non ci sarebbe stato. Infatti sapere che, dopo la morte di mamma, mio papa' sarebbe stato comunque in buone mani mi ha reso il cuore piu' leggero nella partenza e piu' sereno durante la permanenza in Germania. Grazie davvero tanto.

Finally this is my thank for you Sara, my wife. Cara, cordiale e (quasi) quotidiana presenza:

De' miei bollenti spiriti
il giovanile ardore
ella tempro' col placido

sorriso dell' amor, dell'amor!
Dal di che disse: vivere
io voglio, io voglio a te fedel,

dell'universo immemore
io vivo, io vivo quasi,
io vivo quasi in ciel.

Dal di che disse: vivere
io voglio a te fedel, si, si,
dell'universo immemore
io vivo, io vivo quasi,
io vivo quasi in ciel,
io vivo in ciel.

Dell'universo immemore
io vivo quasi in ciel,
ah si, io vivo quasi in ciel,

Io, io vivo quasi in ciel.

Grazie per addolcire il mio spirito senza afflosciarlo. E soprattutto grazie per tutto il sostegno materiale e morale che mi hai dato durante questi quattro anni. Per essere bella, brava, simpatica, intelligente (geniale direi!) e buona. Vederti diventare mamma e' una cosa che allarga il cuore. Percio' grazie anche a te Paolo che hai stravolto l'ordine (seppur precario) della nostra famiglia in un modo che, senza

saperlo, aspettavamo da sempre.

Many thanks to all of you!

Bibliography

[1] Yoichi Kamihara et al.

"Iron-Based Layered Superconductor: LaOFeP," Journal of the American Chemical Society **128**, 10012–10013 (2006).

[2] Yoichi Kamihara, Takumi Watanabe, Masahiro Hirano, and Hideo Hosono

"Iron-Based Layered Superconductor $LaO_{1-x}F_xFeAs$ ($x = 0.05 - 0.12$) with $T_c = 26$ K," Journal of the American Chemical Society **130**, 3296–3297 (2008).

[3] H. Luetkens et al.

"The electronic phase diagram of the $LaO_{1-x}F_xFeAs$ superconductor," Nature Materials **8**, 305–309 (2009).

[4] L. Boeri, O. V. Dolgov, and A. A. Golubov

"Is $LaFeAsO_{1-x}F_x$ an Electron-Phonon Superconductor?" Phys. Rev. Lett. **101**(2), 026403 (2008).

[5] I. I. Mazin, D. J. Singh, M. D. Johannes, and M. H. Du

"Unconventional Superconductivity with a Sign Reversal in the Order Parameter of $LaFeAsO_{1-x}F_x$," Phys. Rev. Lett. **101**(5), 057003 (2008).

[6] Kazuhiko Kuroki et al.

"Unconventional Pairing Originating from the Disconnected Fermi Surfaces of Superconducting $LaFeAsO_{1-x}F_x$," Phys. Rev. Lett. **101**(8), 087004 (2008).

[7] J. P. Carbotte

"Properties of boson-exchange superconductors," Rev. Mod. Phys. **62**(4), 1027–1157 (1990).

[8] W. L. McMillan

"Transition Temperature of Strong-Coupled Superconductors," Phys. Rev. **167**(2), 331–344 (1968).

[9] P. B. Allen and R. C. Dynes

"Transition temperature of strong-coupled superconductors reanalyzed," Phys. Rev. B **12**(3), 905–922 (1975).

[10] W. L. McMillan and J. M. Rowell

"Lead Phonon Spectrum Calculated from Superconducting Density of States," Phys. Rev. Lett. **14**(4), 108–112 (1965).

[11] B. Mitrović, H. G. Zarate, and J. P. Carbotte

"The ratio $\frac{2\Delta_0}{k_B T_c}$ within Eliashberg theory," Phys. Rev. B **29**(1), 184–190 (1984).

[12] S. Y. Savrasov and D. Y. Savrasov

"Electron-phonon interactions and related physical properties of metals from linear-response theory," Phys. Rev. B **54**(23), 16487–16501 (1996).

[13] Matteo Calandra and Francesco Mauri

"Theoretical Explanation of Superconductivity in C_6Ca," Phys. Rev. Lett. **95**(23), 237002 (2005).

[14] Lilia Boeri, Jens Kortus, and O. K. Andersen

"Three-Dimensional MgB_2-Type Superconductivity in Hole-Doped Diamond," Phys. Rev. Lett. **93**(23), 237002 (2004).

[15] Y. Kong, O. V. Dolgov, O. Jepsen, and O. K. Andersen

"Electron-phonon interaction in the normal and superconducting states of MgB_2," Phys. Rev. B **64**(2), 020501 (2001).

[16] J. Kortus et al.

"Superconductivity of Metallic Boron in MgB_2," Phys. Rev. Lett. **86**(20), 4656–4659 (2001).

[17] Tôru Moriya

"Spin Fluctuations in Itinerant Electron Magnetism," Springer, Berlin, (1985).

[18] P. Curie

"Lois expérimentales du magnétisme. Propriétés magnétiques des corps *à* diverses températures," Ann. de Chim et Phys. **5**, 289 (1895).

[19] P. Langevin

"Sur la théorie du magnétisme," J. Phys. Theor. Appl. **4**(1), 678 (1905).

[20] P. Weiss

"S*û*r L'hypothèse du champ moléculaire et la propriété ferromagnétique," J. Phys. Theor. Appl. **6**(1), 661 (1907).

[21] H. J. van Leeuwen

"Problèmes de la théorie électronique du magnétisme," J. de Phys. et le Rad. **2**(12), 361 (1921).

[22] P.A.M. Dirac

"Quantum Mechanics," Dover Books on Physics, DOVER PUBN Incorporated, (2001).

[23] F. Hund

"Linienspektren und periodisches System der Elemente," Struktur der Materie in Einzeldarstellungen, Berlin, (1927).

[24] W. Heitler and F. London

"Wechselwirkung neutraler Atome und homöpolare Bindung nach der Quantenmechanik," Zeitschrift für Physik A Hadrons and Nuclei **44**, 455–472 (1927).

[25] W. Heisenberg

"Zur Theorie des Ferromagnetismus," Zeitschrift für Physik **49**, 619–636 (1928).

[26] E. Ising

"Report on the theory of ferromagnetism," Zeitschrift Für Physik **31**, 253–258 (1925).

[27] L. Neél

"Propriétés magnétiques des ferrites - Ferrimagnetisme et Antiferromagnetisme," Annales de Physique **3**, 137 –198 (1948).

[28] F. Bloch

"Quantum mechanics of electrons in crystal lattices," Zeitschrift für Physik **52**(7-8), 555–600 (1928).

[29] J. C. Slater

"The Ferromagnetism of Nickel," Phys. Rev. **49**(7), 537–545 (1936).

[30] J. C. Slater

"The Ferromagnetism of Nickel. II. Temperature Effects," Phys. Rev. **49**(12), 931–937 (1936).

[31] N. F. Mott

"A discussion of the transition metals on the basis of quantum mechanics," Proceedings of the Physical Society **47**, 571 (1935).

[32] E. C. Stoner

"Collective electron specific heat and spin paramagnetism in metals," Proceedings of the Royal Society of London, Series A (Mathematical and Physical Sciences) **154**, 656–678 (1936).

[33] E. C. Stoner

"Collective electron ferromagnetism," Proceedings of the Royal Society of London, Series A (Mathematical and Physical Sciences) **165**, 0372–0414 (1938).

[34] E. P. Wohlfarth

"The Theoretical and Experimental Status of the Collective Electron Theory of Ferromagnetism," Rev. Mod. Phys. **25**(1), 211–219 (1953).

[35] J. C. Slater

"Magnetic Effects and the Hartree-Fock Equation," Phys. Rev. **82**(4), 538–541 (1951).

[36] Karlheinz Schwarz

"Optimization of the Statistical Exchange Parameter α for the Free Atoms H through Nb," Phys. Rev. B **5**(7), 2466–2468 (1972).

[37] P. Hohenberg and W. Kohn

"Inhomogeneous Electron Gas," Phys. Rev. **136**(3B), B864–B871 (1964).

[38] W. Kohn and L. J. Sham

"Self-Consistent Equations Including Exchange and Correlation Effects," Phys. Rev. **140**(4A), A1133–A1138 (1965).

[39] W. Kohn

"Nobel Lecture: Electronic structure of matter wave functions and density functionals," Rev. Mod. Phys. **71**(5), 1253–1266 (1999).

[40] O. Gunnarsson and B. I. Lundqvist

"Exchange and correlation in atoms, molecules, and solids by the spin-density-functional formalism," Phys. Rev. B **13**(10), 4274–4298 (1976).

[41] R. G*á*sp*á*r

"Über eine Approximation des Hartree-Fockschen Potentials Durch eine Universelle Potentialfunktion," Acta Physica Academiae Scientiarum Hungaricae **3**, 263–286 (1954).

[42] L. Hedin and B. I. Lundqvist

"Explicit local exchange−correlation potentials," Journal of Physics C: Solid State Physics **4**, 2064 (1971).

[43] U. von Barth and L. Hedin

"A local exchange-correlation potential for the spin polarized case. i," Journal of Physics C: Solid State Physics **5**, 1629 (1972).

[44] John P. Perdew and Yue Wang

"Accurate and simple analytic representation of the electron-gas correlation energy," Phys. Rev. B **45**(23), 13244–13249 (1992).

[45] O. Gunnarsson

"Band model for magnetism of transition metals in the spin-density-functional formalism," Journal of Physics F: Metal Physics **6**, 587 (1976).

[46] R. O. Jones and O. Gunnarsson

"The density functional formalism, its applications and prospects," Rev. Mod. Phys. **61**(3), 689–746 (1989).

[47] P. Walmsley et al.

"Quasiparticle Mass Enhancement Close to the Quantum Critical Point in $BaFe_2(As_{1-x}P_x)_2$," Phys. Rev. Lett. **110**(25), 257002 (2013).

[48] Kenichiro Hashimoto et al.

"Anomalous superfluid density in quantum critical superconductors," Proceedings of the National Academy of Sciences **110**, 3293–3297 (2013).

[49] K. Hashimoto et al.

"A Sharp Peak of the Zero-Temperature Penetration Depth at Optimal Composition in $BaFe_2(As_{1x}P_x)_2$," Science **336**, 1554–1557 (2012).

[50] A. G. Petukhov, I. I. Mazin, L. Chioncel, and A. I. Lichtenstein

"Correlated metals and the $LDA+U$ method," Phys. Rev. B **67**(15), 153106 (2003).

[51] P. Larson, I. I. Mazin, and D. J. Singh

"Magnetism, critical fluctuations, and susceptibility renormalization in Pd," Phys. Rev. B **69**(6), 064429 (2004).

[52] A. Aguayo, I. I. Mazin, and D. J. Singh

"Why Ni_3Al Is an Itinerant Ferromagnet but Ni_3Ga Is Not," Phys. Rev. Lett. **92**(14), 147201 (2004).

[53] Johnpierre Paglione and Richard L. Greene

"High−temperature superconductivity in iron-based materials," Nature Physics **6**, 645–658 (2010).

[54] David C. Johnston

"The puzzle of high temperature superconductivity in layered iron pnictides and chalcogenides," Advances in Physics **59**, 803–1061 (2010).

[55] G. R. Stewart

"Superconductivity in iron compounds," Rev. Mod. Phys. **83**(4), 1589–1652 (2011).

[56] D. J. Scalapino

"A common thread: The pairing interaction for unconventional superconductors," Rev. Mod. Phys. **84**(4), 1383–1417 (2012).

[57] I. I. Mazin et al.

"Problems with reconciling density functional theory calculations with experiment in ferropnictides," Phys. Rev. B **78**(8), 085104 (2008).

[58] E. G. Maksimov, I. I. Mazin, S. N. Rashkeev, and Yu A. Uspenski

"First-principles calculations of the optical properties of metals," Journal of Physics F: Metal Physics **18**, 833 (1988).

[59] L. Klein et al.

"Anomalous Spin Scattering Effects in the Badly Metallic Itinerant Ferromagnet $SrRuO_3$," Phys. Rev. Lett. **77**(13), 2774–2777 (1996).

[60] Y. Maeno et al.

"Superconductivity in a Layered Perovskite without Copper," Nature **372**, 532–534 (1994).

[61] A. S. Sefat et al.

"Renormalized behavior and proximity of $BaCo_2As_2$ to a magnetic quantum critical point," Phys. Rev. B **79**(2), 024512 (2009).

[62] I. I. Mazin and David J. Singh

"Ferromagnetic Spin Fluctuation Induced Superconductivity in $SrRu_2O_4$," Phys. Rev. Lett. **79**(4), 733–736 (1997).

[63] I. I. Mazin and D. J. Singh

"Electronic structure and magnetism in Ru-based perovskites," Phys. Rev. B **56**(5), 2556–2571 (1997).

[64] Gianluca Giovannetti et al.

"Proximity of iron pnictide superconductors to a quantum tricritical point," Nature Communications **2**, (2011).

[65] Johannes Ferber, Yu-Zhong Zhang, Harald O. Jeschke, and Roser Valentí

"Analysis of spin-density wave conductivity spectra of iron pnictides in the framework of density functional theory," Phys. Rev. B **82**(16), 165102 (2010).

[66] P. Hansmann et al.

"Dichotomy between Large Local and Small Ordered Magnetic Moments in Iron-Based Superconductors," Phys. Rev. Lett. **104**(19), 197002 (2010).

[67] Philipp Werner et al.

"Satellites and large doping and temperature dependence of electronic properties in hole-doped $BaFe_2As_2$," Nature Physics **8**, 331–337 (2012).

[68] Z. P. Yin, K. Haule, and G. Kotliar

"Kinetic frustration and the nature of the magnetic and paramagnetic states in iron pnictides and iron chalcogenides," Nature Materials **10**, 932–935 (2011).

[69] Tobias Schickling et al.

"Gutzwiller Theory of Band Magnetism in LaOFeAs," Phys. Rev. Lett. **108**(3), 036406 (2012).

[70] L. Boeri et al.

"Effects of magnetism and doping on the electron-phonon coupling in $BaFe_2As_2$," Phys. Rev. B **82**(2), 020506 (2010).

[71] Vladimir I. Anisimov, Jan Zaanen, and Ole K. Andersen

"Band theory and Mott insulators: Hubbard *U* instead of Stoner *I*," Phys. Rev. B **44**(3), 943–954 (1991).

[72] O.K. Andersen and L. Boeri

"On the multi-orbital band structure and itinerant magnetism of iron-based superconductors," Annalen der Physik **523**, 8–50 (2011).

[73] G. Rohringer, A. Toschi, A. Katanin, and K. Held

"Critical Properties of the Half-Filled Hubbard Model in Three Dimensions," Phys. Rev. Lett. **107**(25), 256402 (2011).

[74] V. L. Ginzburg and L. D. Landau

"On the theory of superconductivity," Zh. Eksp. Teor. Fiz. **20**, 1064 (1950).

[75] J. Bardeen, L. N. Cooper, and J. R. Schrieffer

"Microscopic Theory of Superconductivity," Phys. Rev. **106**(1), 162–164 (1957).

[76] J. Bardeen, L. N. Cooper, and J. R. Schrieffer
"Theory of Superconductivity," Phys. Rev. **108**(5), 1175–1204 (1957).

[77] Leon N. Cooper
"Bound Electron Pairs in a Degenerate Fermi Gas," Phys. Rev. **104**(4), 1189–1190 (1956).

[78] L. P. Gor'kov
"Microscopic derivation of the Ginzburg-Landau equations in the theory of superconductivity," Soviet Physics JETP-USSR **9**, 1364–1367 (1959).

[79] A.B. Migdal
"Interaction between electrons and the lattice vibrations in a normal metal," Zhurnal Eksperimental'noi i Teoreticheskoi Fiziki **34**(6), 1438–1446 (1958).

[80] G.M. Eliashberg
"Interaction between electrons and lattice vibrations in a superconductor," Zhurnal Eksperimental'noi i Teoreticheskoi Fiziki **38**(3), 966–976 (1960).

[81] D. J. Scalapino, J. R. Schrieffer, and J. W. Wilkins
"Strong-Coupling Superconductivity. I," Phys. Rev. **148**(1), 263–279 (1966).

[82] Dirk Manske
"Theory of Unconventional Superconductors (Cooper-Pairing Mediated by Spin Excitations)," Springer-Verlag Berlin Heidelberg, (2004).

[83] J. Nagamatsu et al.
"Superconductivity at 39 K in magnesium diboride," Nature **410**, 63–64 (2001).

[84] H. J. Choi et al.
"The origin of the anomalous superconducting properties of MgB_2," Nature **418**, 758–760 (2002).

[85] C Buzea and T Yamashita

"Review of the superconducting properties of MgB_2," Superconductor Science & Technology **14**, R115–R146 (2001).

[86] Oleg V. Dolgov et al.

"Thermodynamics of two-band superconductors: The case of MgB_2," Phys. Rev. B **72**(2), 024504 (2005).

[87] F. Bouquet et al.

"Specific Heat of $Mg^{11}B_2$: Evidence for a Second Energy Gap," Phys. Rev. Lett. **87**(4), 047001 (2001).

[88] Y. Wang, T. Plackowski, and A. Junod

"Specific heat in the superconducting and normal state (2-300 K, 0-16 T), and magnetic susceptibility of the 38 K superconductor MgB2: evidence for a multicomponent gap," Physica C: Superconductivity **355**, 179 –193 (2001).

[89] P. Szabó et al.

"Evidence for Two Superconducting Energy Gaps in MgB_2 by Point-Contact Spectroscopy," Phys. Rev. Lett. **87**(13), 137005 (2001).

[90] X. K. Chen et al.

"Evidence for Two Superconducting Gaps in MgB_2," Phys. Rev. Lett. **87**(15), 157002 (2001).

[91] T. Takahashi et al.

"High-Resolution Photoemission Study of MgB_2," Phys. Rev. Lett. **86**(21), 4915–4917 (2001).

[92] S. Tsuda et al.

"Evidence for a Multiple Superconducting Gap in MgB_2 from High-Resolution Photoemission Spectroscopy," Phys. Rev. Lett. **87**(17), 177006 (2001).

[93] H. Ding et al.

"Electronic structure of optimally doped pnictide $Ba_{0.6}$ $K_{0.4}Fe_2$ As_2 : a comprehensive angle-resolved photoemission spectroscopy investigation," Journal of Physics: Condensed Matter **23**, 135701 (2011).

[94] N. F. Berk and J. R. Schrieffer

"Effect of Ferromagnetic Spin Correlations on Superconductivity," Phys. Rev. Lett. **17**(8), 433–435 (1966).

[95] David Bohm and David Pines

"A Collective Description of Electron Interactions. I. Magnetic Interactions," Phys. Rev. **82**(5), 625–634 (1951).

[96] H. Rietschel and H. Winter

"Role of Spin Fluctuations in the Superconductors Nb and V," Phys. Rev. Lett. **43**(17), 1256–1260 (1979).

[97] H. Rietschel, H. Winter, and W. Reichardt

"Strong depression of superconductivity in VN by spin fluctuations," Phys. Rev. B **22**(9), 4284–4292 (1980).

[98] D. Glötzel, D. Rainer, and H.R. Schober

"Ab initio calculation of the superconducting transition temperature," Zeitschrift für Physik B Condensed Matter **35**, 317–326 (1979).

[99] D. Fay and J. Appel

"Coexistence of *p*-state superconductivity and itinerant ferromagnetism," Phys. Rev. B **22**(7), 3173–3182 (1980).

[100] F. Steglich et al.

"Superconductivity in the Presence of Strong Pauli Paramagnetism: $CeCu_2Si_2$," Phys. Rev. Lett. **43**(25), 1892–1896 (1979).

[101] Georg Knebel et al.

"Competition and/or coexistence of antiferromagnetism and superconductivity in $CeRhIn_5$ and $CeCoIn_5$," physica status solidi (b) **247**, 557–562 (2010).

[102] Tuson Park and J D Thompson

"Magnetism and superconductivity in strongly correlated $CeRhIn_5$," New Journal of Physics **11**, 055062 (2009).

[103] G. R. Stewart, Z. Fisk, J. O. Willis, and J. L. Smith

"Possibility of Coexistence of Bulk Superconductivity and Spin Fluctuations in UPt_3," Phys. Rev. Lett. **52**(8), 679–682 (1984).

[104] T. T. M. Palstra et al.

"Superconducting and Magnetic Transitions in the Heavy-Fermion System URu_2Si_2," Phys. Rev. Lett. **55**(24), 2727–2730 (1985).

[105] E. Bauer et al.

"Heavy Fermion Superconductivity and Magnetic Order in Noncentrosymmetric $CePt_3Si$," Phys. Rev. Lett. **92**(2), 027003 (2004).

[106] Lev P. Gor'kov and Emmanuel I. Rashba

"Superconducting 2D System with Lifted Spin Degeneracy: Mixed Singlet-Triplet State," Phys. Rev. Lett. **87**(3), 037004 (2001).

[107] M. W. Haverkort et al.

"Strong Spin-Orbit Coupling Effects on the Fermi Surface of Sr_2RuO_4 and Sr_2RhO_4," Phys. Rev. Lett. **101**(2), 026406 (2008).

[108] C. N. Veenstra et al., *Observation of strong spin-orbital entanglement in Sr_2RuO_4 by spin-resolved ARPES*, arXiv:1303.5444 [cond-mat.supr-con].

[109] J.G. Bednorz and K.A. Müller

"Possible high T_c superconductivity in the BaLaCuO system," Zeitschrift für Physik B Condensed Matter **64**, 189–193 (1986).

[110] Yoshiteru Maeno, T. Maurice Rice, and Manfred Sigrist

"The Intriguing Superconductivity of Strontium Ruthenate," Physics Today **54**, 42–47 (2001).

[111] K. Ishida et al.

"Spin-triplet superconductivity in Sr_2RuO_4 identified by O-17 Knight shift," Nature **396**, 658–660 (1998).

[112] Andrew Peter Mackenzie and Yoshiteru Maeno

"The superconductivity of Sr_2RuO_4 and the physics of spin-triplet pairing," Rev. Mod. Phys. **75**(2), 657–712 (2003).

[113] Patrick A. Lee, Naoto Nagaosa, and Xiao-Gang Wen

"Doping a Mott insulator: Physics of high-temperature superconductivity," Rev. Mod. Phys. **78**(1), 17–85 (2006).

[114] D. J. Singh and M.-H. Du

"Density Functional Study of $LaFeAsO_{1-x}F_x$: A Low Carrier Density Superconductor Near Itinerant Magnetism," Phys. Rev. Lett. **100**(23), 237003 (2008).

[115] D. N. Basov and Andrey V. Chubukov

"Manifesto for a higher T_c," Nature Physics **7**, 272–276 (2011).

[116] Christian Pfleiderer

"Superconducting phases of f-electron compounds," Rev. Mod. Phys. **81**(4), 1551–1624 (2009).

[117] Clifford W. Hicks et al.

"Limits on superconductivity-related magnetization in Sr_2RuO_4 and $PrOs_4Sb_{12}$ from scanning SQUID microscopy," Phys. Rev. B **81**(21), 214501 (2010).

[118] Yoshiteru Maeno et al.

"Evaluation of Spin-Triplet Superconductivity in Sr_2RuO_4," Journal of the Physical Society of Japan **81**, 011009 (2012).

[119] D. A. Wollman et al.

"Experimental determination of the superconducting pairing state in YBCO from the phase coherence of YBCO-Pb dc SQUIDs," Phys. Rev. Lett. **71**(13), 2134–2137 (1993).

[120] J. R. Kirtley et al.

"Symmetry of the order parameter in the high T_c superconductor $YBa_2Cu_3O_{7-\delta}$," Nature **373**, 225–228 (1995).

[121] C. C. Tsuei et al.

"Pairing Symmetry in Single-Layer Tetragonal $Tl_2Ba_2CuO_{\beta+\delta}$ Superconductors," Science **271**, 329–332 (1996).

[122] C. C. Tsuei and J. R. Kirtley

"Pairing symmetry in cuprate superconductors," Rev. Mod. Phys. **72**(4), 969–1016 (2000).

[123] D. J. Scalapino

"The case for $d_{x^2y^2}$ pairing in the cuprate superconductors," Physics Reports **250**, 329 –365 (1995).

[124] P. Phillips

"Mottness collapse and T-linear resistivity in cuprate superconductors.," Philos Trans A Math Phys Eng Sci **369**, 1574–98 (2011).

[125] H. F. Fong et al.

"Polarized and unpolarized neutron-scattering study of the dynamical spin susceptibility of $YBa_2Cu_3O_7$," Phys. Rev. B **54**(9), 6708–6720 (1996).

[126] H. He et al.

"Magnetic Resonant Mode in the Single-Layer High-Temperature Superconductor $Tl_2Ba_2CuO_{6+\delta}$," Science **295**, 1045–1047 (2002).

[127] H. He et al.

"Resonant Spin Excitation in an Overdoped High Temperature Superconductor," Phys. Rev. Lett. **86**(8), 1610–1613 (2001).

[128] Pengcheng Dai et al.

"The Magnetic Excitation Spectrum and Thermodynamics of High-Tc Superconductors," Science **284**, 1344–1347 (1999).

[129] P. Bourges et al.

"The Spin Excitation Spectrum in Superconducting $YBa_2Cu_3O_{6.85}$," Science **288**, 1234–1237 (2000).

[130] Ar. Abanov and Andrey V. Chubukov

"A Relation between the Resonance Neutron Peak and ARPES Data in Cuprates," Phys. Rev. Lett. **83**(8), 1652–1655 (1999).

[131] Z.-X. Shen et al.

"Anomalously large gap anisotropy in the a - b plane of $Bi_2Sr_2CaCu_2O_{8+\delta}$," Phys. Rev. Lett. **70**(10), 1553–1556 (1993).

[132] Andrea Damascelli, Zahid Hussain, and Zhi-Xun Shen

"Angle-resolved photoemission studies of the cuprate superconductors," Rev. Mod. Phys. **75**(2), 473–541 (2003).

[133] D. N. Basov and T. Timusk

"Electrodynamics of high-T_c superconductors," Rev. Mod. Phys. **77**(2), 721–779 (2005).

[134] G. Grüner and M. Dressel

"Electrodynamics Of Solids: Optical Properties Of Electrons In Matter," Cambridge University Press, United Kindom., (2002).

[135] D. N. Basov et al.

"Electrodynamics of correlated electron materials," Rev. Mod. Phys. **83**(2), 471–541 (2011).

[136] D. H. Lu et al.

"Electronic structure of the iron-based superconductor LaOFeP," Nature **455**, 81–84 (2008).

[137] Alaska Subedi, Lijun Zhang, D. J. Singh, and M. H. Du

"Density functional study of FeS, FeSe, and FeTe: Electronic structure, magnetism, phonons, and superconductivity," Phys. Rev. B **78**(13), 134514 (2008).

[138] A. V. Chubukov, M. G. Vavilov, and A. B. Vorontsov

"Momentum dependence and nodes of the superconducting gap in the iron pnictides," Phys. Rev. B **80**(14), 140515 (2009).

[139] H. Ding et al.

"Observation of Fermi-surfaceâĂŞdependent nodeless superconducting gaps in $Ba_{0.6}K_{0.4}Fe_2As_2$," EPL (Europhysics Letters) **83**, 47001 (2008).

[140] Zhao Lin et al.

"Multiple Nodeless Superconducting Gaps in $(Ba_{0.6}\ K_{0.4}\ )Fe_2\ As_2$ Superconductor from Angle-Resolved Photoemission Spectroscopy," Chinese Physics Letters **25**, 4402 (2008).

[141] Gang Mu et al.

"Low temperature specific heat of the hole-doped $Ba_{0.6}K_{0.4}Fe_2As_2$ single crystals," Phys. Rev. B **79**(17), 174501 (2009).

[142] J. D. Fletcher et al.

"Evidence for a Nodal-Line Superconducting State in LaFePO," Phys. Rev. Lett. **102**(14), 147001 (2009).

[143] Clifford W. Hicks et al.

"Evidence for a Nodal Energy Gap in the Iron-Pnictide Superconductor LaFePO from Penetration Depth Measurements by Scanning SQUID Susceptometry," Phys. Rev. Lett. **103**(12), 127003 (2009).

[144] C. T. Chen et al.

"Integer and half-integer flux-quantum transitions in a niobium-iron pnictide loop," Nature Physics **6**, 260–264 (2010).

[145] Xiaohang Zhang et al.

"Observation of the Josephson Effect in $Pb/Ba_{1-x}K_xFe_2As_2$ Single Crystal Junctions," Phys. Rev. Lett. **102**(14), 147002 (2009).

[146] Paul Seidel

"Josephson effects in iron based superconductors," Superconductor Science and Technology **24**, 043001 (2011).

[147] K. Hashimoto et al.

"Line nodes in the energy gap of superconducting $BaFe_2(As_{1-x}P_x)_2$ single crystals as seen via penetration depth and thermal conductivity," Phys. Rev. B **81**(22), 220501 (2010).

[148] T. Hanaguri, S. Niitaka, K. Kuroki, and H. Takagi

"Unconventional s-Wave Superconductivity in Fe(Se,Te)," Science **328**, 474–476 (2010).

[149] K. Matan, R. Morinaga, K. Iida, and T. J. Sato

"Anisotropic itinerant magnetism and spin fluctuations in $BaFe_2As_2$: A neutron scattering study," Phys. Rev. B **79**(5), 054526 (2009).

[150] R. Osborn, S. Rosenkranz, E. A. Goremychkin, and A. D. Christianson

"Inelastic neutron scattering studies of the spin and lattice dynamics in iron arsenide compounds," Physica C- Superconductivity and its Applications **469**, 498–506 (2009).

[151] A. D. Christianson et al.

"Unconventional superconductivity in $Ba_{0.6}K_{0.4}Fe_2As_2$ from inelastic neutron scattering," Nature **456**, 930–932 (2008).

[152] D. S. Inosov et al.

"Normal-state spin dynamics and temperature-dependent spin-resonance energy in optimally doped $BaFe_{1.85}Co_{0.15}As_2$," Nature Physics **6**, 178–181 (2010).

[153] M. M. Qazilbash et al.

"Electronic correlations in the iron pnictides," Nature Physics **5**, 647–650 (2009).

[154] N. Barišić et al.

"Electrodynamics of electron-doped iron pnictide superconductors: Normal-state properties," Phys. Rev. B **82**(5), 054518 (2010).

[155] J. J. Tu et al.

"Optical properties of the iron arsenic superconductor $BaFe_{1.85}Co_{0.15}As_2$," Phys. Rev. B **82**(17), 174509 (2010).

[156] D. Wu et al.

"Eliashberg analysis of optical spectra reveals a strong coupling of charge carriers to spin fluctuations in doped iron-pnictide $BaFe_2As_2$ superconductors," Phys. Rev. B **82**(14), 144519 (2010).

[157] J. Yang et al.

"Optical Spectroscopy of Superconducting $Ba_{0.55}K_{0.45}Fe_2As_2$: Evidence for Strong Coupling to Low-Energy Bosons," Phys. Rev. Lett. **102**(18), 187003 (2009).

[158] A. Charnukha et al.

"Eliashberg approach to infrared anomalies induced by the superconducting state of $Ba_{0.68}K_{0.32}Fe_2As_2$ single crystals," Phys. Rev. B **84**(17), 174511 (2011).

[159] A. Charnukha et al.

"Superconductivity—induced optical anomaly in an iron arsenide," Nature Communications **2**, (2011).

[160] David Pines and David Bohm

"A Collective Description of Electron Interactions: II. Collective *vs* Individual Particle Aspects of the Interactions," Phys. Rev. **85**(2), 338–353 (1952).

[161] David Bohm and David Pines

"A Collective Description of Electron Interactions: III. Coulomb Interactions in a Degenerate Electron Gas," Phys. Rev. **92**(3), 609–625 (1953).

[162] Takeo Izuyama, Duk Joo Kim, and Ryogo Kubo

"Band Theoretical Interpretation of Neutron Diffraction Phenomena in Ferromagnetic Metals," Journal of the Physical Society of Japan **18**, 1025–1042 (1963).

[163] J. R. Schrieffer, X.-G. Wen, and S.-C. Zhang

"Spin-bag mechanism of high-temperature superconductivity," Phys. Rev. Lett. **60**(10), 944–947 (1988).

[164] J. R. Schrieffer, X. G. Wen, and S. C. Zhang

"Dynamic spin fluctuations and the bag mechanism of high-T_c superconductivity," Phys. Rev. B **39**(16), 11663–11679 (1989).

[165] E. E. Salpeter and H. A. Bethe

"A Relativistic Equation for Bound-State Problems," Phys. Rev. **84**(6), 1232–1242 (1951).

[166] P. Monthoux and D. Pines

"Spin-fluctuation-induced superconductivity in the copper oxides: A strong coupling calculation," Phys. Rev. Lett. **69**(6), 961–964 (1992).

[167] P. Monthoux and D. Pines

"$YBa_2Cu_3O_7$: A nearly antiferromagnetic Fermi liquid," Phys. Rev. B **47**(10), 6069–6081 (1993).

[168] A. J. Millis, Hartmut Monien, and David Pines

"Phenomenological model of nuclear relaxation in the normal state of $YBa_2Cu_3O_7$," Phys. Rev. B **42**(1), 167–178 (1990).

[169] P. Monthoux, A. V. Balatsky, and D. Pines

"Toward a theory of high-temperature superconductivity in the antiferromagnetically correlated cuprate oxides," Phys. Rev. Lett. **67**(24), 3448–3451 (1991).

[170] P. Monthoux, A. V. Balatsky, and D. Pines

"Weak-coupling theory of high-temperature superconductivity in the antiferromagnetically correlated copper oxides," Phys. Rev. B **46**(22), 14803–14817 (1992).

[171] A. J. Millis

"Nearly antiferromagnetic Fermi liquids: An analytic Eliashberg approach," Phys. Rev. B **45**(22), 13047–13054 (1992).

[172] Ar. Abanov and Andrey V. Chubukov

"Spin-Fermion Model near the Quantum Critical Point: One-Loop Renormalization Group Results," Phys. Rev. Lett. **84**(24), 5608–5611 (2000).

[173] Ar. Abanov, Andrey V. Chubukov, and J. Schmalian

"Quantum-critical theory of the spin-fermion model and its application to cuprates: Normal state analysis," Advances in Physics **52**, 119–218 (2003).

[174] P. Monthoux, D. Pines, and G. G. Lonzarich

"Superconductivity without phonons," Nature **450**, 1177–1183 (2007).

[175] Walter Metzner and Dieter Vollhardt

"Correlated Lattice Fermions in $d = \infty$ Dimensions," Phys. Rev. Lett. **62**(3), 324–327 (1989).

[176] Antoine Georges and Gabriel Kotliar

"Hubbard model in infinite dimensions," Phys. Rev. B **45**(12), 6479–6483 (1992).

[177] G. Kotliar et al.

"Electronic structure calculations with dynamical mean-field theory," Rev. Mod. Phys. **78**(3), 865–951 (2006).

[178] A. Georges, G. Kotliar, K. Werner, and M. J. Rozenberg

"Dynamical mean-field theory of strongly correlated fermion systems and the limit of infinite dimensions," Rev. Mod. Phys. **68**(1), 13–125 (1996).

[179] C. Wetterich

"Exact evolution equation for the effective potential," Physics Letters B **301**, 90 –94 (1993).

[180] C. Honerkamp, M. Salmhofer, N. Furukawa, and T. M. Rice

"Breakdown of the Landau-Fermi liquid in two dimensions due to umklapp scattering," Phys. Rev. B **63**(3), 035109 (2001).

[181] W. Metzner et al.

"Functional renormalization group approach to correlated fermion systems," Rev. Mod. Phys. **84**(1), 299–352 (2012).

[182] S. Graser et al.

"Determining gap nodal structures in Fe-based superconductors: Theory of the angle dependence of the low-temperature specific heat in an applied magnetic field," Phys. Rev. B **77**(18), 180514 (2008).

[183] A. V. Chubukov, D. V. Efremov, and I. Eremin

"Magnetism, superconductivity, and pairing symmetry in iron-based superconductors," Phys. Rev. B **78**(13), 134512 (2008).

[184] L. Benfatto et al.

"Multiple gaps and superfluid density from interband pairing in a four-band model of the iron oxypnictides," Phys. Rev. B **78**(14), 140502 (2008).

[185] L. Benfatto, E. Cappelluti, and C. Castellani

"Spectroscopic and thermodynamic properties in a four-band model for pnictides," Phys. Rev. B **80**(21), 214522 (2009).

[186] Kazuhiko Kuroki et al.

"Pnictogen height as a possible switch between high-T_c nodeless and low-T_c nodal pairings in the iron-based superconductors," Phys. Rev. B **79**(22), 224511 (2009).

[187] V. Cvetkovic and Z. Tesanovic

"Multiband magnetism and superconductivity in Fe-based compounds," EPL (Europhysics Letters) **85**, 37002 (2009).

[188] G. A. Ummarino, M. Tortello, D. Daghero, and R. S. Gonnelli

"Three-band $s_{\pm}$ Eliashberg theory and the superconducting gaps of iron pnictides," Phys. Rev. B **80**(17), 172503 (2009).

[189] Fa Wang et al.

"Functional Renormalization-Group Study of the Pairing Symmetry and Pairing Mechanism of the FeAs-Based High-Temperature Superconductor," Phys. Rev. Lett. **102**(4), 047005 (2009).

[190] Ronny Thomale et al.

"Functional renormalization-group study of the doping dependence of pairing symmetry in the iron pnictide superconductors," Phys. Rev. B **80**(18), 180505 (2009).

[191] A. F. Kemper et al.

"Sensitivity of the superconducting state and magnetic susceptibility to key aspects of electronic structure in ferropnictides," New Journal of Physics **12**, 073030 (2010).

[192] Ronny Thomale, Christian Platt, Werner Hanke, and B. Andrei Bernevig

"Mechanism for Explaining Differences in the Order Parameters of FeAs-Based and FeP-Based Pnictide Superconductors," Phys. Rev. Lett. **106**(18), 187003 (2011).

[193] Hiroaki Ikeda, Ryotaro Arita, and Jan Kuneš

"Phase diagram and gap anisotropy in iron-pnictide superconductors," Phys. Rev. B **81**(5), 054502 (2010).

[194] Takashi Miyake, Kazuma Nakamura, Ryotaro Arita, and Masatoshi Imada

"Comparison of *Ab initio* Low-Energy Models for LaFePO, LaFeAsO, $BaFe_2As_2$, LiFeAs, FeSe, and FeTe: Electron Correlation and Covalency," Journal of the Physical Society of Japan **79**, 044705 (2010).

[195] L. Ortenzi, E. Cappelluti, L. Benfatto, and L. Pietronero

"Fermi-Surface Shrinking and Interband Coupling in Iron-Based Pnictides," Phys. Rev. Lett. **103**(4), 046404 (2009).

[196] Markus Aichhorn et al.

"Dynamical mean-field theory within an augmented plane-wave framework: Assessing electronic correlations in the iron pnictide LaFeAsO," Phys. Rev. B **80**(8), 085101 (2009).

[197] T. Takayama et al.

"Strong Coupling Superconductivity at 8.4 K in an Antiperovskite Phosphide $SrPt_3P$," Phys. Rev. Lett. **108**(23), 237001 (2012).

[198] I.A. Nekrasov and M.V. Sadovskii

"Electronic structure of new multiple band Pt-pnictide superconductors APt3P," JETP Letters **96**, 227–230 (2012).

[199] Hui Chen, Xiaofeng Xu, Chao Cao, and Jianhui Dai

"First-principles calculations of the electronic and phonon properties of APt_3P (A = Ca, Sr, and La): Evidence for a charge-density-wave instability and a soft phonon," Phys. Rev. B **86**(12), 125116 (2012).

[200] I. I. Mazin

"Superconductivity and magnetism in CuBiSO from first principles," Physical Review B **81**, (2010).

[201] P. G. Niklowitz et al.

"Spin-fluctuation-dominated electrical transport of Ni_3Al at high pressure," Phys. Rev. B **72**(2), 024424 (2005).

[202] Stefano Baroni, Stefano de Gironcoli, Andrea Dal Corso, and Paolo Giannozzi

"Phonons and related crystal properties from density-functional perturbation theory," Rev. Mod. Phys. **73**(2), 515–562 (2001).

[203] Satomi Kakiya et al.

"Superconductivity at 38 K in Iron-Based Compound with Platinum–Arsenide Layers $Ca_{10}(Pt_4As_8)(Fe_{2-x}Pt_xAs_2)_5$," Journal of the Physical Society of Japan **80**, 093704 (2011).

[204] Takayuki Kawamata et al.

"Crystal Structure of New Pt-Doped Fe Pnictide Superconductors," Journal of the Physical Society of Japan **80**, 073710 (2011).

[205] Masatoshi Sato et al.

"Magnetic Excitation Spectra of Superconducting Ca–Fe–Pt–As System," Journal of the Physical Society of Japan **80**, 093709 (2011).

[206] Kazutaka Kudo, Yoshihiro Nishikubo, and Minoru Nohara

"Coexistence of Superconductivity and Charge Density Wave in $SrPt_2As_2$," Journal of the Physical Society of Japan **79**, 123710 (2010).

[207] Kazutaka Kudo et al.

"Breakdown of Chemical Scaling for Pt-Doped $CaFe_2As_2$," Journal of the Physical Society of Japan **81**, 035002 (2012).

[208] Xiyu Zhu et al.

"Superconductivity induced by doping platinum in $BaFe_2As_2$," Phys. Rev. B **81**(10), 104525 (2010).

[209] Yoshihiro Nishikubo, Kazutaka Kudo, and Minoru Nohara

"Superconductivity in the Honeycomb-Lattice Pnictide SrPtAs," Journal of the Physical Society of Japan **80**, 055002 (2011).

[210] Jun Goryo, Mark H. Fischer, and Manfred Sigrist

"Possible pairing symmetries in SrPtAs with a local lack of inversion center," Phys. Rev. B **86**(10), 100507 (2012).

[211] Suk Joo Youn et al.

"Role of strong spin-orbit coupling in the superconductivity of the hexagonal pnictide SrPtAs," Phys. Rev. B **85**(22), 220505 (2012).

[212] R. Hoffmann and C. Zheng

"Making and breaking bonds in the solid state: the thorium chromium silicide ($ThCr_2Si_2$) structure," Journal of Physical Chemistry **89**(20), 4175–4181 (1985).

[213] S. Arsenijevi

"Signatures of quantum criticality in the thermopower of $Ba(Fe_{1-x}Co_x)_2As_2$," Phys. Rev. B **87**(22), 224508 (2013).

[214] Jia Shuang et al.

"Ferromagnetic quantum critical point induced by dimer-breaking in $SrCo_2(Ge_{1-x}P_x)_2$," Nature Physics **7**(3), 207–210 (2011).

[215] Manfred Sigrist and Kazuo Ueda

"Phenomenological theory of unconventional superconductivity," Rev. Mod. Phys. **63**(2), 239–311 (1991).

[216] Mark H. Fischer, Florian Loder, and Manfred Sigrist

"Superconductivity and local noncentrosymmetricity in crystal lattices," Phys. Rev. B **84**(18), 184533 (2011).

[217] T. Takayama

, Private communication (2013).

[218] Chang-Jong Kang, Kyo-Hoon Ahn, Kwan-Woo Lee, and Byung Il Min

"Electron and Phonon Band-Structure Calculations for the Antipolar $SrPt_3P$ Antiperovskite Superconductor: Evidence of Low-Energy Two-Dimensional Phonons," Journal of the Physical Society of Japan **82**, 053703 (2013).

[219] C. W. Chu et al.

"Superconductivity above 150 K in $HgBa_2Ca_2Cu_3O_{8+\delta}$ at high pressures," Nature **365**, 323–325 (1993).

[220] Cao Wang et al.

"Thorium doping induced superconductivity up to 56 K in $Gd_{1-x}Th_xFeAsO$," EPL (Europhysics Letters) **83**, 67006 (2008).

[221] G. Wu et al.

"Superconductivity at 56 K in samarium doped SrFeAsF," Journal of Physics: Condensed Matter **21**, 142203 (2009).

[222] M. Tegel, D. Bichler, and D. Johrendt

"Synthesis, crystal structure and superconductivity of LaNiPO," Solid State Sciences **10**, 193 –197 (2008).

[223] T. Mine et al.

"Nickel-based phosphide superconductor with infinite-layer structure, BaNi2P2," Solid State Communications **147**, 111 –113 (2008).

[224] Fong-Chi Hsu et al.

"Superconductivity in the PbO-type structure α-FeSe," Proceedings of the National Academy of Sciences **105**, 14262–14264 (2008).

[225] A. Ubaldini, E. Giannini, C. Senatore, and D. van der Marel

"BiOCuS: A new superconducting compound with oxypnictide-related structure," Physica C−Superconductivity and its Applications **470**, S356–S357 (2010).

[226] Hidenori Hiramatsu et al.

"Crystal structures, optoelectronic properties, and electronic structures of layered oxychalcogenides MCuOCh (M = Bi, La; Ch = S, Se, Te): Effects of electronic configurations of M_3+ ions," Chemistry of Materials **20**, 326–334 (2008).

[227] Anand Pal, H. Kishan, and V. P. S. Awana

"Synthesis and Structural Details of BiOCu1-xS: Possible New Entrant in a Series of Exotic Superconductors?" Journal of Superconductivity and Novel Magnetism **23**, 301–304 (2010).

[228] F. Yndurain

"Coupling of magnetic moments with phonons and electron−phonon interaction in $LaFeAsO_{1-x}F_x$," EPL **94**, (2011).

[229] A. I. Coldea et al.

"Fermi Surface of Superconducting LaFePO Determined from Quantum Oscillations," Phys. Rev. Lett. **101**(21), 216402 (2008).

[230] T. M. McQueen et al.

"Intrinsic properties of stoichiometric LaFePO," Phys. Rev. B **78**(2), 024521 (2008).

[231] Yoshimitsu Kohama et al.

"Possible Unconventional Superconductivity in Iron-Based Layered Compound LaFePO: Study of Heat Capacity," Journal of the Physical Society of Japan **77**, 094715 (2008).

[232] S. V. Streltsov, M. A. Korotin, V. I. Anisimov, and D. I. Khomskii

"Band versus localized electron magnetism in $CaCrO_3$," Phys. Rev. B **78**(5), 054425 (2008).

[233] D. J. Singh and I. I. Mazin

"Superconductivity and electronic structure of perovskite $MgCNi_3$," Phys. Rev. B **64**(14), 140507 (2001).

[234] I. I. Mazin and D. J. Singh

"Spin fluctuations and the magnetic phase diagram of $ZrZn_2$," Phys. Rev. B **69**(2), 020402 (2004).

[235] M. Shimizu

"Itinerant Electron Magnetism," Reports on Progress in physics **44**, 329–409 (1981).

[236] F. Marsiglio and J. P. Carbotte

"Strong-coupling corrections to Bardeen-Cooper-Schrieffer ratios," Phys. Rev. B **33**(9), 6141–6146 (1986).

[237] Carlo Di Castro

"Critical Phenomena," University Lecture (2007).

[238] Daniel J. Amit

"Field Theory, the Renormalization Group, and Critical Phenomena," World Scientific, (1984).

[239] L. D. Landau, "On the theory of phase transitions," in: *Theory of phase transformations 1*, vol. 7, 1937, p. 19.

[240] Leo P. Kadanoff et al.

"Static Phenomena Near Critical Points: Theory and Experiment," Rev. Mod. Phys. **39**(2), 395–431 (1967).

[241] Kenneth G. Wilson

"Renormalization Group and Critical Phenomena. II. Phase-Space Cell Analysis of Critical Behavior," Phys. Rev. B **4**(9), 3184–3205 (1971).

[242] Kerson Huang

"Statistical Mechanics," John Wiley & Sons, (1987).

[243] W. M. Lomer

"Electronic Structure of Chromium Group Metals," Proceedings of the Physical Society **80**, 489 (1962).

[244] A.R. Mackintosh and O.K. Andersen, "The electronic structure of transition metals," in: *Electrons at the Fermi surface*, ed. by (Cambridge University press) M. Springford, 1980, pp. 149–224.

[245] L. J. Sham and W. Kohn

"One-Particle Properties of an Inhomogeneous Interacting Electron Gas," Phys. Rev. **145**(2), 561–567 (1966).

[246] L. H. Thomas

"The calculation of atomic fields," Mathematical Proceedings of the Cambridge Philosophical Society **23**(05), 542–548 (1927).

[247] E. Fermi

"Eine statistische Methode zur Bestimmung einiger Eigenschaften des Atoms und ihre Anwendung auf die Theorie des periodischen Systems der Elemente," Zeitschrift für Physik **48**, 73–79 (1928).

[248] E. Wigner

"Effects of the electron interaction on the energy levels of electrons in metals," Trans. Faraday Soc. **34**(0), 678–685 (1938).

[249] D. Ceperley

"Ground state of the fermion one-component plasma: A Monte Carlo study in two and three dimensions," Phys. Rev. B **18**(7), 3126–3138 (1978).

[250] D. M. Ceperley and B. J. Alder

"Ground State of the Electron Gas by a Stochastic Method," Phys. Rev. Lett. **45**(7), 566–569 (1980).

[251] John P. Perdew, Kieron Burke, and Matthias Ernzerhof

"Generalized Gradient Approximation Made Simple [Phys. Rev. Lett. 77, 3865 (1996)]," Phys. Rev. Lett. **78**(7), 1396–1396 (1997).

[252] Ole Krogh Andersen

"Total Magnetic energy and Stoner," Private notes (2008-2009).

[253] O.K. Andersen et al.

"Magnetic ground state properties of transition metals," Physica B+C **86 - 88, Part 1**, 249 –256 (1977).

[254] U K Poulsen, J Kollar, and O K Andersen

"Magnetic and cohesive properties from canonical bands (for transition metals)," Journal of Physics F: Metal Physics **6**, L241 (1976).

[255] "Proceedings of the International School of Physics "Enrico Fermi"," in: *Course LXXXIX. Highlights of Condensed-Matter Theory*, ed. by F. Bassani, F. Fumi, and M.P. Tosi, Amsterdam, 1985, pp. 59–176, ISBN: 0-444-86976-X.

[256] S. Doniach and S. Engelsberg

"Low-Temperature Properties of Nearly Ferromagnetic Fermi Liquids," Phys. Rev. Lett. **17**(14), 750–753 (1966).

[257] G. Vignale and K. S. Singwi

"Spin-flip electron-energy-loss spectroscopy in itinerant-electron ferromagnets: Collective modes versus Stoner excitations," Phys. Rev. B **32**(5), 2824–2834 (1985).

[258] W. F. Brinkman and S. Engelsberg

"Spin-Fluctuation Contributions to the Specific Heat," Phys. Rev. **169**(2), 417–431 (1968).

[259] M. Eschrig

"The effect of collective spin−1 excitations on electronic spectra in high T_c superconductors," Advances in Physics **55**, 47–183 (2006).

[260] Manfred Sigrist

"Introduction to Unconventional Superconductivity.," AIP Conference Proceedings **789**, 165 –243 (2005).

[261] John A. Hertz

"Quantum critical phenomena," Phys. Rev. B **14**(3), 1165–1184 (1976).

[262] A. J. Millis

"Effect of a nonzero temperature on quantum critical points in itinerant fermion systems," Phys. Rev. B **48**(10), 7183–7196 (1993).

[263] D. J. Singh I. I. Mazin and A. Aguayo

"Proceedings of the NATO ARW on Physics of Spin in Solids," Materials, Methods and Applications, (2004).

[264] A. J. Leggett

"A theoretical description of the new phases of liquid ^{3}He," Rev. Mod. Phys. **47**(2), 331–414 (1975).

[265] A. Z. Solontsov and D. Wagner

"Zero-point spin fluctuations and the magnetovolume effect in itinerant-electron magnetism," Phys. Rev. B **51**(18), 12410–12417 (1995).

[266] S. N. Kaul

"Spin-fluctuation theory for weak itinerant-electron ferromagnets: revisited," Journal of Physics: Condensed Matter **11**, 7597 (1999).

[267] Aya Ishigaki and Tôru Moriya

"On the Theory of Spin Fluctuations around the Magnetic Instabilities: Effects of Zero-Point Fluctuations," Journal of the Physical Society of Japan **67**, 3924–3935 (1998).

[268] K. K. Murata and S. Doniach

"Theory of Magnetic Fluctuations in Itinerant Ferromagnets," Phys. Rev. Lett. **29**(5), 285–288 (1972).

[269] J. Callaway and C. S. Wang

"Transverse magnetic susceptibility in the local exchange approximation," Journal of Physics F: Metal Physics **5**, 2119 (1975).

[270] S. Y. Savrasov

"Linear Response Calculations of Spin Fluctuations," Phys. Rev. Lett. **81**(12), 2570–2573 (1998).

[271] Erich Runge and E. K. U. Gross

"Density-Functional Theory for Time-Dependent Systems," Phys. Rev. Lett. **52**(12), 997–1000 (1984).

[272] E. K. U. Gross and Walter Kohn

"Local density-functional theory of frequency-dependent linear response," Phys. Rev. Lett. **55**(26), 2850–2852 (1985).

[273] J. B. Staunton et al.

"Incommensurate and Commensurate Antiferromagnetic Spin Fluctuations in Cr and Cr Alloys from *Ab Initio* Dynamical Spin Susceptibility Calculations," Phys. Rev. Lett. **82**(16), 3340–3343 (1999).

[274] S. Lounis, A. T. Costa, R. B. Muniz, and D. L. Mills

"Dynamical Magnetic Excitations of Nanostructures from First Principles," Phys. Rev. Lett. **105**(18), 187205 (2010).

[275] S. Lounis, A. T. Costa, R. B. Muniz, and D. L. Mills

"Theory of local dynamical magnetic susceptibilities from the Korringa-Kohn-Rostoker Green function method," Phys. Rev. B **83**(3), 035109 (2011).

[276] W. Kohn and N. Rostoker

"Solution of the Schrödinger Equation in Periodic Lattices with an Application to Metallic Lithium," Phys. Rev. **94**(5), 1111–1120 (1954).

[277] J. Korringa

"On the calculation of the energy of a Bloch wave in a metal," Physica **13**, 392 –400 (1947).

[278] G. Vignale and K. S. Singwi

"Effective two-body interaction in Coulomb Fermi liquids," Phys. Rev. B **32**(4), 2156–2166 (1985).

[279] G. Vignale and Walter Kohn

"Current-Dependent Exchange-Correlation Potential for Dynamical Linear Response Theory," Phys. Rev. Lett. **77**(10), 2037–2040 (1996).

[280] Zhixin Qian and Giovanni Vignale

"Spin Dynamics from Time-Dependent Spin-Density-Functional Theory," Phys. Rev. Lett. **88**(5), 056404 (2002).

[281] Giovanni Onida, Lucia Reining, and Angel Rubio

"Electronic excitations: density-functional versus many-body Green's-function approaches," Rev. Mod. Phys. **74**(2), 601–659 (2002).

[282] Paweł Buczek, Arthur Ernst, Patrick Bruno, and Leonid M. Sandratskii

"Energies and Lifetimes of Magnons in Complex Ferromagnets: A First-Principle Study of Heusler Alloys," Phys. Rev. Lett. **102**(24), 247206 (2009).

[283] Paweł Buczek, Arthur Ernst, and Leonid M. Sandratskii

"Standing Spin Waves as a Basis for the Control of Terahertz Spin Dynamics: Time Dependent Density Functional Theory Study," Phys. Rev. Lett. **105**(9), 097205 (2010).

[284] Paweł Buczek, Arthur Ernst, and Leonid M. Sandratskii

"Interface Electronic Complexes and Landau Damping of Magnons in Ultrathin Magnets," Phys. Rev. Lett. **106**(15), 157204 (2011).

[285] Paweł Buczek, Arthur Ernst, and Leonid M. Sandratskii

"Different dimensionality trends in the Landau damping of magnons in iron, cobalt, and nickel: Time-dependent density functional study," Phys. Rev. B **84**(17), 174418 (2011).

[286] F. Essenberger et al.

"Paramagnons in FeSe close to a magnetic quantum phase transition: *Ab initio* study," Phys. Rev. B **86**(6), 060412 (2012).

[287] L. D. Landau, in: *Collected Papers*, Oxford: Pergamon Press, 1965, p. 546.

[288] A. A. Abrikosov

"On the magnetic properties of Suprconductors of the second group," Soviet Physics JETP-USSR **5**, 1174–1183 (1957).

[289] Michael Tinkham

"Introduction to Superconductivity: Second Edition (Dover Books on Physics) (Vol i)," Dover Publications, (2004).

[290] I. I. Mazin

"Intercalant-Driven Superconductivity in YbC_6 and CaC_6," Phys. Rev. Lett. **95**(22), 227001 (2005).

[291] A. Sanna et al.

"Anisotropic gap of superconducting CaC_6: A first-principles density functional calculation," Phys. Rev. B **75**(2), 020511 (2007).

[292] L. N. Oliveira, E. K. U. Gross, and W. Kohn

"Density-Functional Theory for Superconductors," Phys. Rev. Lett. **60**(23), 2430–2433 (1988).

[293] T. Kreibich and E. K. U. Gross

"Multicomponent Density-Functional Theory for Electrons and Nuclei," Phys. Rev. Lett. **86**(14), 2984–2987 (2001).

[294] M. Lüders et al.

"*Ab initio* theory of superconductivity. I. Density functional formalism and approximate functionals," Phys. Rev. B **72**(2), 024545 (2005).

[295] M. A. L. Marques et al.

"*Ab initio* theory of superconductivity. II. Application to elemental metals," Phys. Rev. B **72**(2), 024546 (2005).

[296] P. Cudazzo et al.

"Electron-phonon interaction and superconductivity in metallic molecular hydrogen. I. Electronic and dynamical properties under pressure," Phys. Rev. B **81**(13), 134505 (2010).

[297] P. Cudazzo et al.

"Electron-phonon interaction and superconductivity in metallic molecular hydrogen. II. Superconductivity under pressure," Phys. Rev. B **81**(13), 134506 (2010).

[298] Oleg V. Dolgov, Igor I. Mazin, David Parker, and Alexander A. Golubov

"Interband superconductivity: Contrasts between Bardeen Cooper Schrieffer and Eliashberg theories," Phys. Rev. B **79**(6), 060502 (2009).

[299] Alaska Subedi, Luciano Ortenzi, and Lilia Boeri

"Electron-phonon superconductivity in $A\mathrm{Pt}_3\mathrm{P}$ (A =Sr, Ca, La) compounds: From weak to strong coupling," Phys. Rev. B **87**(14), 144504 (2013).

[300] K. Hippler, S. Sitta, P. Vogt, and H. Sabrowsky

"Structure of $\mathrm{Na}_3\mathrm{OCl}$," Acta Crystallographica Section C **46**, 736–738 (1990).

[301] H. Padamsee, J.E Neighbor, and C.A. Shiffman

"Quasiparticle phenomenology for thermodynamics of strong-coupling superconductors," Journal of Low Temperature Physics **12**, 387–411 (1973).

[302] Z. Hiroi, S. Yonezawa, Y. Nagao, and J. Yamaura

"Extremely strong-coupling superconductivity and anomalous lattice properties in the β-pyrochlore oxide KOs_2O_6," Phys. Rev. B **76**(1), 014523 (2007).

[303] B. Lachal, A. Junod, and J. Muller

"Heat capacity analysis of a large number of Chevrel-type superconductors," Journal of Low Temperature Physics **55**, 195–232 (1984).

[304] J. J. Hopfield

"Angular Momentum and Transition-Metal Superconductivity," Phys. Rev. **186**(2), 443–451 (1969).

[305] H. Suhl, B. T. Matthias, and L. R. Walker

"Bardeen-Cooper-Schrieffer Theory of Superconductivity in the Case of Overlapping Bands," Phys. Rev. Lett. **3**(12), 552–554 (1959).

[306] Neil W. Ashcroft and David N. Mermin

"Solid state physics," Toronto: Thomson Learning, (1976).

[307] Paolo Giannozzi et al.

"QUANTUM ESPRESSO: a modular and open-source software project for quantum simulations of materials," Journal of Physics: Condensed Matter **21**, 395502 (19pp) (2009).

[308] O. Krogh Andersen

"Linear methods in band theory," Phys. Rev. B **12**(8), 3060–3083 (1975).

[309] P. Blaha et al.

"WIEN2K, an Augmented Plane Wave + Local Orbitals Program for Calculating Crystal Properties," Wien, Austria: Karlheinz Schwarz, Techn. Universität Wien, Austria, (2001).

[310] David Vanderbilt

"Soft self-consistent pseudopotentials in a generalized eigenvalue formalism," Phys. Rev. B **41**(11), 7892–7895 (1990).

[311] Luciano Ortenzi et al.

"Competition between electron-phonon coupling and spin fluctuations in superconducting hole-doped CuBiSO," Phys. Rev. B **83**(10), 100505 (2011).

[312] A. Yu. Ignatov, S. Y. Savrasov, and T. A. Tyson

"Superconductivity near the vibrational-mode instability in $MgCNi_3$," Phys. Rev. B **68**(22), 220504 (2003).

[313] G. Santi, S. B. Dugdale, and T. Jarlborg

"Longitudinal Spin Fluctuations and Superconductivity in Ferromagnetic $ZrZn_2$ from *Ab Initio* Calculations," Phys. Rev. Lett. **87**(24), 247004 (2001).

[314] H. Rosner et al.

"Superconductivity near Ferromagnetism in $MgCNi_3$," Phys. Rev. Lett. **88**(2), 027001 (2001).

[315] I. R. Shein and A. L. Ivanovskii

"Electronic band structure and inter-atomic bonding in tetragonal BiOCuS as a parent phase for novel layered superconductors," Solid State Communications **150**, 640–643 (2010).

[316] DJ Scalapino

"Superconductivity and spin fluctuations," Journal of low Temperature Physics **117**, 179–188 (1999).

[317] O. V. Dolgov et al.

"Critical Temperature and Enhanced Isotope Effect in the Presence of Paramagnons in Phonon-Mediated Superconductors," Phys. Rev. Lett. **95**(25), 257003 (2005).

[318] Peter E. Blöchl, O. Jepsen, and O. K. Andersen

"Improved tetrahedron method for Brillouin-zone integrations," Phys. Rev. B **49**(23), 16223–16233 (1994).

[319] L. Benfatto, E. Cappelluti, L. Ortenzi, and L. Boeri

"Extended Drude model and role of interband transitions in the midinfrared spectra of pnictides," Phys. Rev. B **83**(22), 224514 (2011).

[320] A. Lucarelli et al.

"Charge dynamics of Co-doped $BaFe_2$ As_2," New Journal of Physics **12**, 073036 (2010).

[321] S. Lebégue

"Electronic structure and properties of the Fermi surface of the superconductor LaOFeP," Phys. Rev. B **75**(3), 035110 (2007).

[322] Verónica Vildosola et al.

"Bandwidth and Fermi surface of iron oxypnictides: Covalency and sensitivity to structural changes," Phys. Rev. B **78**(6), 064518 (2008).

[323] A. Carrington et al.

"Quantum oscillation studies of the Fermi surface of LaFePO," Physica C: Superconductivity **469**, 459 –468 (2009).

[324] K. Terashima et al.

"Fermi surface nesting induced strong pairing in iron-based superconductors," Proceedings of the National Academy of Sciences **106**, 7330–7333 (2009).

[325] M. Yi et al.

"Unconventional electronic reconstruction in undoped (Ba, Sr)Fe_2As_2 across the spin density wave transition," Phys. Rev. B **80**(17), 174510 (2009).

[326] S. V. Borisenko et al.

"Superconductivity without Nesting in LiFeAs," Phys. Rev. Lett. **105**(6), 067002 (2010).

[327] A. Yamasaki et al.

"Electron correlation in the Fee superconductor studied by bulk-sensitive photoemission spectroscopy," Phys. Rev. B **82**(18), 184511 (2010).

[328] A. Tamai et al.

"Strong Electron Correlations in the Normal State of the Iron-Based $FeSe_{0.42}Te_{0.58}$ Superconductor Observed by Angle-Resolved Photoemission Spectroscopy," Phys. Rev. Lett. **104**(9), 097002 (2010).

[329] C. Putzke et al.

"de Haas-van Alphen Study of the Fermi Surfaces of Superconducting LiFeP and LiFeAs," Phys. Rev. Lett. **108**(4), 047002 (2012).

[330] B. J. Arnold et al.

"Nesting of electron and hole Fermi surfaces in nonsuperconducting $BaFe_2P_2$," Phys. Rev. B **83**(22), 220504 (2011).

[331] H. Shishido et al.

"Evolution of the Fermi Surface of $BaFe_2(As_{1-x}P_x)_2$ on Entering the Superconducting Dome," Phys. Rev. Lett. **104**(5), 057008 (2010).

[332] J. G. Analytis et al.

"Fermi Surface of $SrFe_2P_2$ Determined by the de Haas-van Alphen Effect," Phys. Rev. Lett. **103**(7), 076401 (2009).

[333] Amalia I. Coldea et al.

"Topological Change of the Fermi Surface in Ternary Iron Pnictides with Reduced c/a Ratio: A de Haas - van Alphen Study of $CaFe_2P_2$," Phys. Rev. Lett. **103**(2), 026404 (2009).

[334] M. Yi et al.

"Electronic structure of the $BaFe_2As_2$ family of iron-pnictide superconductors," Phys. Rev. B **80**(2), 024515 (2009).

[335] L. X. Yang et al.

"Electronic Structure and Unusual Exchange Splitting in the Spin-Density-Wave State of the $BaFe_2As_2$ Parent Compound of Iron-Based Superconductors," Phys. Rev. Lett. **102**(10), 107002 (2009).

[336] L. Benfatto and E. Cappelluti

"Effects of the Fermi-surface shrinking on the optical sum rule in pnictides," Phys. Rev. B **83**(10), 104516 (2011).

[337] S. Engelsberg and J. R. Schrieffer

"Coupled Electron-Phonon System," Phys. Rev. **131**(3), 993–1008 (1963).

[338] Anil Khurana

"Electrical conductivity in the infinite-dimensional Hubbard model," Phys. Rev. Lett. **64**(16), 1990–1990 (1990).

[339] Antoine Georges, Gabriel Kotliar, Werner Krauth, and Marcelo J. Rozenberg

"Dynamical mean-field theory of strongly correlated fermion systems and the limit of infinite dimensions," Rev. Mod. Phys. **68**(1), 13–125 (1996).

[340] Lev P. Gor'kov Aleksej A. Abrikosov and Igor E. Dzyaloshinskii

"Methods of Quantum Field Theory in Statistical Physics," (Prentice-Hall, Englewood), (1963).

[341] F. Marsiglio, M. Schossmann, and J. P. Carbotte

"Iterative analytic continuation of the electron self-energy to the real axis," Phys. Rev. B **37**(10), 4965–4969 (1988).

[342] Shulga S. V., O. V. Dolgov, and E. G. Maksimov

"Electronic states and optical spectra of {HTSC} with electron-phonon coupling," Physica C: Superconductivity **178**, 266 –274 (1991).

[343] R. Abt, C. Ambrosch-Draxl, and P. Knoll

"Optical response of high temperature superconductors by full potential LAPW band structure calculations," Physica B: Condensed Matter **194-196, Part 2**, 1451 –1452 (1994).

[344] C. Ambrosch-Draxl and J. O. Sofo

"Linear optical properties of solids within the full-potential linearized augmented planewave method," Computer Physics Communications **175**, 1–14 (2006).

[345] L. Ortenzi, I. I. Mazin, P. Blaha, and L. Boeri

"Accounting for spin fluctuations beyond local spin density approximation in the density functional theory," Phys. Rev. B **86**(6), 064437 (2012).

[346] Y. Takahashi and T. Moriya

"Quantitative aspects of the theory of weak itinerant ferromagnetism," Journal of the Physical Society of Japan **54**, 1592–1598 (1985).

[347] G. G. Lonzarich and L. Taillefer

"Effect of spin fluctuations on the magnetic equation of state of ferromagnetic or nearly ferromagnetic metals," Journal of Physics C−Solid state Physics **18**, 4339–4371 (1985).

[348] N. Buis, J. J. M. Franse, and P. E. Brommer

"The magnetic properties of Ni3Al under high pressures," Physica B+C **106**, 1 –8 (1981).

[349] Myung-Hwan Whangbo, Changhoon Lee, and Juergen Koehler

"Transition-metal anions in solids and their implications on bonding," Angewandte Chemie - International Edition **45**, 7465–7469 (2006).

[350] Myung-Hwan Whangbo, Changhoon Lee, and Juergen Koehler

"Metal Anions in Metal-Rich Compounds and Polar Intermetallics," European Journal of Inorgamic Chemistry, 3841–3847 (2011).

[351] N. R. Bernhoeft, G. G. Lonzarich, P. W. Mitchell, and D. McK Paul

"Magnetic excitations in Ni_3Al at low energies and long wavelengths," Phys. Rev. B **28**(1), 422–424 (1983).

[352] O. K. Andersen and O. Jepsen

"Advances in theory of one - electron energy - states," Physica B & C **91**, 317–328 (1977).

[353] Genrich L. Krasko

"Metamagnetic behavior of fcc iron," Phys. Rev. B **36**(16), 8565–8569 (1987).

[354] Tôru Moriya and Arisato Kawabata

"Effect of Spin Fluctuations on Itinerant Electron Ferromagnetism," Journal of the Physical Society of Japan **34**, 639–651 (1973).

[355] FD Murnaghan

"The compressibility of media under extreme pressures," Proceedings of the national Academy of Science of the United States of America **30**, 244–247 (1944).